Function and pharmacology of TRPM3 ion channel

Jacqueline Naylor

Submitted in accordance with the requirements for the degree of Doctor of Philosophy

The University of Leeds
Institute of Membrane and Systems Biology

January 2008

Acknowledgments

I would like to thank my supervisor David Beech for his guidance and support.

I would also like to thank my fellow lab members, the Rao Boys and Team Lippiat for all of their help and encouragement. A special thankyou to Alex D, Fanning, Jing, Alex C and Alan Bateson for teaching me everything I know.

Thankyou also to everyone in Target Validation at AstraZeneca R&D Charnwood for a valuable and enjoyable 3 months, and in particular to my supervisor Clare Jones.

Finally I would like to thank my mum and sister for all of their love and support throughout the past 3 years.

My work was supported by the BBSRC and AstraZeneca.

Abstract

For many ion channels there are few, if any, pharmacological agents, and even fewer showing specificity. In this study, a set of pharmacological tools were developed to investigate TRPM3, a widely expressed transient receptor potential (TRP) channel for which no functional role has yet been identified.

Human TRPM3 was first expressed in HEK 293 cells and shown to be activated by hypo-osmotic challenge or sphingosine, consistent with previous reports. In addition, TRPM3 was activated by pregnenolone sulphate. Hydrophobicity analysis of the TRPM3 amino acid sequence revealed a short and reasonably unique peptide in the 3rd extracellular loop (E3) region, to which polyclonal antiserum (TM3E3) was produced. Extracellular application of TM3E3 inhibited TRPM3 function with a high degree of specificity, having no effect on TRPM2 or example members of other sub-types of mammalian TRP, TRPC5 or TRPV4. The data validate E3-targeting as an approach for production of isoform-specific channel blockers and reveal a specific agent for blocking TRPM3.

The cellular and tissue functions of TRPM3 were also investigated. RT-PCR and immunocytochemistry demonstrated TRPM3 expression in human saphenous vein smooth muscle cells, where sphingosine- and pregnenolone sulphate-induced calcium responses were also apparent. These calcium responses could be selectively blocked by TM3E3. Furthermore, TRPM3 activators inhibited matrix metalloproteinase and interleukin-6 secretion, indicating a protective function for TRPM3 in vascular smooth muscle cells. Medium throughput screening systems were employed to screen a library of compounds for further TRPM3 modulators with vascular relevance. Cholesterol, antidepressants, antipsychotics, calmodulin inhibitors, and PIP_2 all inhibited TRPM3, whereas nifedipine and elevated temperature activated the channel. TRPM3 appears to be regulated by a large number of different chemicals and mechanisms.

In summary, TRPM3 has constitutive, protective, activity which can be suppressed by a multitude of compounds, including known vascular disease factors such as cholesterol.

Table of Contents

Figures and Tables

Chapter 1.

Chapter 2.

Chapter 3.

Chapter 5.

DHL acid	Dihydrolipoic acid
DHS	D-*erythro*-dihydro-sphingosine
DIDS	4,4′-Diisothiocyanatostilbene-2,2′-disulfonic acid disodium salt
DiHETE	Dihydroxy-Eicosa-5,8,11,17-Tetraenoic Acid
DMEM	Dulbecco's modified Eagle's medium
DMS	D-*erythro*-N,N-dimethyl-sphingosine
DMSO	Dimethylsulphoxide
dNTP	Deoxyribonucleotide triphosphate
E3	3rd extracellular loop
ECGC	Epigallocatechin-3-gallate
EDTA	Ethylenediaminetetraacetic acid
ELISA	Enzyme-linked immunosorbant assay
ER	Endoplasmic reticulum
ET-18-OCH_3	1-O-Octadecyl-2-O-methyl-*sn*-glycero-3-phosphorylcholine
EtBr	Ethidium bromide
FA	Flufenamic acid
FCS	Foetal calf serum
Gd^{3+}	Gadolinium
GPCR	G-protein coupled receptors
H_2O_2	Hydrogen peroxide
HAMA	Human anti-murine Antibody
HRP	Horseradish peroxidase
Ig	Immunglobin
IP_3	Inositol 1,4,5-triphospate
IP_3R	Inositol 1,4,5-triphospate receptor
La^{3+}	Lanthanum
LB	Luria-Bertani
LB-amp	Luria-Bertani-amplicillin
LDL	Low-density lipoprotein
LGIC	Ligand-gated ion channel
LHRH	Luteinizing hormone releasing hormone
LIMA	Left internal mammary artery
L-NAME	N^G-Nitro-L-arginine methyl ester
LPA	L-α-lysophosphatidic acid
LPC	Lysophosphatidylcholine

LPI	Lysophosphatidylinositol
LT	Leukotriene
mAEA	methanandamide
MCH	Melanin concentrating hormone
ML-9	1-(5-chloronaphthalene-1-sulphonyl)homopiperazine
MLCK	Myosin light chain-kinase
MMP	Matrix metalloproteinases
mβCD	methyl β-cyclodextrin
NAADP	Nicotinic acid adenine dinucleotide phosphate
NAPA	N-acetylprocainamide
NCX	Na^+/Ca^{2+} exchanger
NMDA	N-methyl-D-aspartate
ORF	Open reading frame
PAF	Platelet-activating factor
PB	Phosphate buffer
PBS	Phosphate buffered saline
PCR	Polymerase chain reaction
4αPDD	4α-phorbal-12,13-didecanoate
PG	Prostaglandin
15d-PGJ_2	15-deoxy-$\Delta^{12,14}$-Prostaglandin J_2
PIP_2	Phosphatidylinositol 4,5-bisphosphate
PKA	Protein kinase A
PKC	Protein kinase C
PLA_2	Phospholipase A_2
PLC	Phospholipase C
PMCA	Plasma membrane Ca^{2+}-ATPase
3-PPP	3-phenyl-1-pyrolidin-1-yl-propenone
Preg	Pregnenolone
PregS	Pregnenolone sulphate
Prog	Progesterone
PUFA	Polyunsaturated fatty acids
QX222	Lidocaine N-methyl chloride
QX314	Lidocaine N-ethyl bromide
Rev 5901	α-Pentyl-3-[2-quinolinylmethoxy]benzyl alcohol
RNAi	RNA interference

ROC	Receptor-operated channel
RR	Ruthenium red
RSCH23390	R(+)-7-Chloro-8-hydroxy-3-methyl-1-phenyl-2,3,4,5-tetrahydro-1H-3-benzazepine
RTX	Resiniferatoxin
RyR	Ryanodine receptor
S1P	Sphingosine-1-phosphate
SAC	Stretch-activated channel
SBS	Standard bath solution
SDS-PAGE	SDS polyacrylamide gel electrophoresis
SERCA	Sarco(endo)plasmic reticulum Ca^{2+}-ATPase
siRNA	Small interfering RNA
SK&F 96365	l-β-[3-(*p*-methoxyphenyl)-propyloxy]-*p*-methoxyphenetyl-imidazole
SM	Sphingomyelin
SMOC	Second messenger-operated channel
SNAP	(±)-*S*-nitroso-*N*-acetylpenicillamine
SOC	Store-operated channel
SOCE	Store-operated channel Ca^{2+} entry
SPC	Sphingosylphosphorylcholine
SPH	D-*erythro*-sphingosine
SR	Sarcoplasmic reticulum
TEA	Tetraethylammonium
Tg	Thapsigargin
TNFα	Tumour necrosis factor α
TPA	12-*O*-tetradecanoylphorbol 13-acetate
TRH	Thyrotropin releasing factor
TRP	Transient Receptor Potential
TX B_2	Thromboxane B_2
U-46619	9,11-dideoxy-9α,11α-methanoepoxy Prostaglandin $F_{2\alpha}$
VGCC	Voltage-gated Ca^{2+} channel
W-7	N-(6-aminohexyl)-5-chloro-1-naphthalenesulfonamide hydrochloride
YFP	Yellow fluorescent protein

Publications and Communications

Publications

Xu, S.Z., Muraki, K., Zeng, F., Li, J., Sukumar, P., Shah, S., Dedman, A.M., Flemming, P.K., McHugh, D., **Naylor, J.**, Cheong, A., Bateson, A.N., Munsch, C.M., Porter, K.E., Beech, D.J. (2006) A sphingosine-1-phosphate-activated calcium channel controlling vascular smooth muscle cell motility. *Circulation Research*, **98**(11):1381-9.

Kumar, B., Dreja, K., Shah, S.S., Cheong, A., Xu, S.Z., Sukumar, P., **Naylor, J.**, Forte, A., Cipollaro, M., McHugh, D., Kingston, P.A., Heagerty, A.M., Munsch, C.M., Bergdahl, A., Hultgardh-Nilsson, A., Gomez, M.F., Porter, K.E., Hellstrand, P., Beech, D.J. (2006) Upregulated TRPC1 channel in vascular injury in vivo and its role in human neointimal hyperplasia. *Circulation Research*, **98**(4):557-63.

Flemming, P.K., Dedman, A.M., Xu, S.Z., Li, J., Zeng, F., **Naylor, J.**, Benham, C.D., Bateson, A.N., Muraki, K., Beech, D.J. (2006) Sensing of lysophospholipids by TRPC5 calcium channel. *Journal of Biological Chemistry*, **281**(8):4977-82.

Xu, S.Z., Sukumar, P., Zeng, F., Li, J., Jairaman, A., English, A., **Naylor, J.**, Ciurtin, C., Majeed, Y., Milligan, C.J., Bahnasi, Y.M., Al-Shawaf, E., Porter, K.E., Jiang, L., Emery, P., Sivaprasadarao, A., Beech, D.J. (2008) TRPC channel activation by extracellular thioredoxin. *Nature,* **451**(7174):69-72.

Naylor, J., Milligan, C.J., Zeng, F., Majeed, Y., Harper, S., Jones, C., Beech, D.J. E3-targeted blocking antibody to TRPM3 calcium channel. *(In preparation)*.

Naylor, J., Li, J., Zeng, F., Majeed, Y., Sukumar, P., Kumar, B., Munsch, C.M., Harteneck, C., Porter, K.E., Jones, C., Beech, D.J. TRPM3 is a novel cholesterol-inhibited calcium channel of vascular smooth muscle cells. *(In preparation)*.

Naylor, J., Jones, C., Beech, D.J. Pharmacology of TRPM3 calcium channel. *(In preparation)*.

Communications

J. Naylor. Opposite Temperature Sensitivities of TRPC5 and TRPM2. *Postgraduate Symposium*, University of Leeds. June 2005.

J. Naylor, J. Li, F. Zeng, K.E. Porter, C. Jones, S. Harper, D.J. Beech. Characterisation of the sphingosine-regulated TRPM3 calcium channel using a novel and specific blocker. *NCRG 14th annual meeting*, University of Leeds. January 2006.

J. Naylor, J. Li, F. Zeng, D.J. Beech. Peptide-Specific Antibody as a Tool to Evaluate TRPM3 Ion Channel Function. *FASEB*, San Francisco, U.S. April 2006.

J. Naylor. Peptide Specific Antibodies as Tools to Evaluate TRP Ion Channel Function*. *Postgraduate Symposium*, University of Leeds. June 2006.
* Awarded 'Best 2nd Year Talk'.

J. Naylor, J. Li, F. Zeng, K.E. Porter, D.J. Beech. Development of a Specific Blocker for TRPM3 Ion Channel. *Biochemical Society Focused Meeting; 'Cell and Molecular Biology of TRP Channels'*, University of Bath. September 2006.

J. Naylor. Functional TRPM3 in Vascular Smooth Muscle cells*. *Postgraduate Symposium*, University of Leeds. June 2006.
* Awarded 'Best Presentation in Bioenterprise'.

J. Naylor, J. Li, C.J. Milligan, F. Zeng, P. Sukumar, B. Kumar, K.E. Porter, C. Jones, D.J. Beech. Functional TRPM3 Channel in Human Saphenous Vein Smooth Muscle Cells. *LifeSciences (joint meeting of the Biochemical Society, the British Pharmacological Society and the Physiological Society)*, SECC, Glasgow. July 2007.

J. Naylor, J. Li, CJ Milligan, F Zeng, KE Porter, DJ Beech. TRPM3 channel expression and block in vascular smooth muscle cells. *FASEB*, San Diego, U.S. April 2008.

Chapter 1
Introduction

Vascular system

The cardiovascular system comprises the heart and blood vessels, and is essential for maintaining organ function and blood pressure. Blood pressure refers to the force exerted on the blood by contraction of the heart, and is regulated by factors such as the resistance of blood vessels. The heart circulates blood around the body's vascular network via the systemic or pulmonary circulation. The systemic circulation carries oxygenated blood away from the heart and around the body, and returns deoxygenated blood to the right side of the heart. The role of the pulmonary circulation is to oxygenate the blood. Deoxygenated blood is carried to the lungs, oxygenated, and returned to the left side of the heart.

Vascular physiology

Blood vessels are divided into 3 main groups; arteries, veins and capillaries. Arteries carry blood away from heart, and are subjected to the greatest hydrostatic pressure. As a result their vessel walls are thicker and more complex than veins, although they both share common physiological features. With the exception of capillaries, blood vessels are comprised of 3 major layers; tunica intima, tunica media, and tunica adventitia (Figure 1.1). The tunica intima, a single layer of endothelial cells, lines the vessel lumen and protects the tunica media from the shear stress of the blood flow. Vascular smooth muscle cells (VSMC) are the predominant cell type in the tunica media, and are arranged circumferentially to the vessel lumen to allow for contraction necessary to regulate the diameter of the vessel. The tunica adventitia forms the outer layer, and is primarily comprised of connective tissues which provide support for the tunica media, plus a network of much smaller vessels termed the vasa vasorum. The vasa vasorum supply blood to the outer tissues of large blood vessels, and in larger vessels will also extend to the tunica media. Also present are small nerve fibres which innervate the smooth muscle of the tunica media. Conversely, capillaries have very thin vessel walls that are only one endothelial cell layer thick, ideal to allow gas exchange between the blood and surrounding tissues.

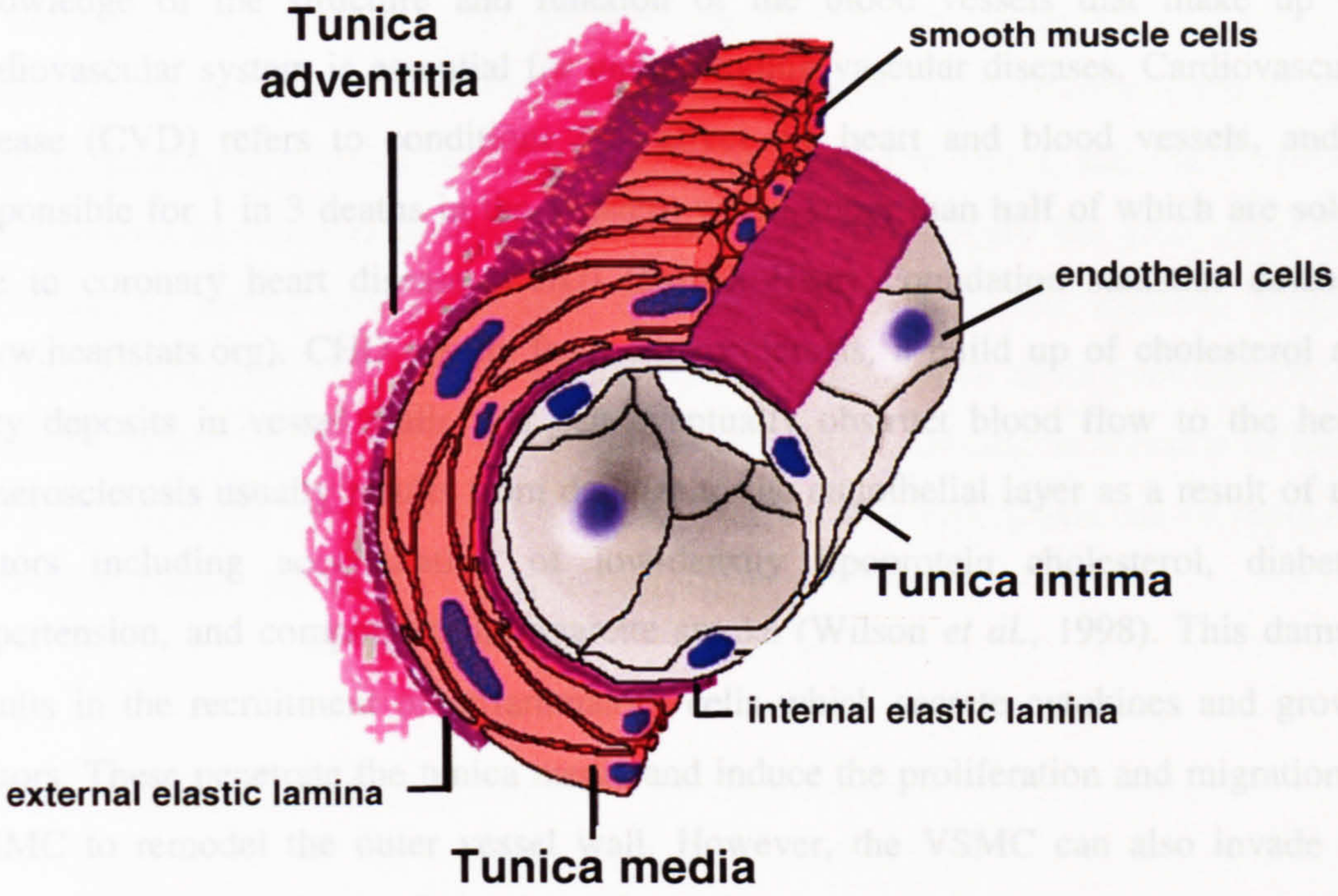

Figure 1.1. General structure of an artery or vein The schematic depicts the 3 major layers; the tunica intima, tunica media and tunica adventitia plus separating layers of elastic connective tissue (reproduced from www.lab.anhb.uwa.edu.au).

Vascular disease

Knowledge of the structure and function of the blood vessels that make up the cardiovascular system is essential for understanding vascular diseases. Cardiovascular disease (CVD) refers to conditions that affect the heart and blood vessels, and is responsible for 1 in 3 deaths in the Western world, more than half of which are solely due to coronary heart disease (CHD) (British Heart Foundation statistics database www.heartstats.org). CHD results from atherosclerosis, a build up of cholesterol and fatty deposits in vessel walls that can eventually obstruct blood flow to the heart. Atherosclerosis usually results from damage to the endothelial layer as a result of risk factors including accumulation of low-density lipoprotein cholesterol, diabetes, hypertension, and components in cigarette smoke (Wilson *et al.*, 1998). This damage results in the recruitment of inflammatory cells which secrete cytokines and growth factors. These penetrate the tunica media and induce the proliferation and migration of VSMC to remodel the outer vessel wall. However, the VSMC can also invade the lumen. This results in the formation of a lesion comprised of a lipid core which is protected from the circulating blood by a layer of VSMC, referred to as an atherosclerotic plaque. The plaque obstructs the blood vessel, causing a general narrowing that may restrict blood flow. If coronary vessels are obstructed, the reduced oxygen supply to the heart muscle can cause angina. As atherosclerosis progresses, factors secreted by the VSMC themselves can have a dual effect on the atherosclerotic plaque; In particular matrix-degrading metalloproteinases (MMPs) can interact with the extracellular matrix and stabilise plaque structures, forming a fibrous cap. Alternatively prolonged exposure to these secreted factors can weaken the fibrous cap tissue and cause it to rupture (Newby, 2007). The rupture of a plaque structure exposes the lipid core to the circulating blood and can induce the formation of a blood clot. If the blood clot creates a sudden complete block of the vessel, the result is myocardial infarction.

Depending on the progression of cardiovascular disease, treatments may be as simple as a lifestyle change, lipid-lowering drugs such as statins, or antihypertensive and antiplatelet drugs. Severe cases where blood flow is restricted will require physical intervention, usually balloon angioplasty. A balloon attached to a catheter is inserted into the partially blocked vessel and inflated to push the plaque against the wall of the artery, thus widening the vessel and restoring normal blood flow. Often a small stent is inserted in the narrowed area to support the damaged vessel wall and keep the artery

open. In more severe cases where there are several regions of occlusion, or even complete block, coronary artery bypass surgery is performed. This involves bypassing the damaged coronary artery with a graft, commonly the great saphenous vein or the left internal mammary artery, to provide an alternative route for blood flow. Each of these surgical techniques will inadvertently cause damage to the vessel, and the artery will reseal around an inserted stent, or in the case of bypass surgery the graft has a 50% likelihood of failure within 10 years (British Heart Foundation statistics database www.heartstats.org). The primary mechanism for this is once again proliferation and migration of the VSMC, triggered by the vascular injury, leading to invasion of lumen in a process known as neointimal hyperplasia. Neointimal hyperplasia can be replicated in cultured human saphenous vein (Figure 1.2).

Vascular smooth muscle cells

VSMC phenotypic switching

One state of the VSMC is a differentiated and contractile phenotype. In this state, the cells proliferate at a slow rate, and their primary function is the regulation of blood vessel diameter, thus regulating vascular tone and blood pressure. During blood vessel growth or in response to vascular injury, VSMC can revert to an undifferentiated or synthetic phenotype and display a dramatic increase in proliferation and migration to form new tunica media and repair vascular injury. This phenotypic switching can result from exposure to growth factors, and also atherogenic factors such as lipids, inflammatory mediators, mechanical trauma and reactive oxygen species. The result is upregulation of genes that encode proteins required for cell-cycle progression, and downregulation of genes necessary for the contractile machinery of the cell (Owens *et al.*, 2004).

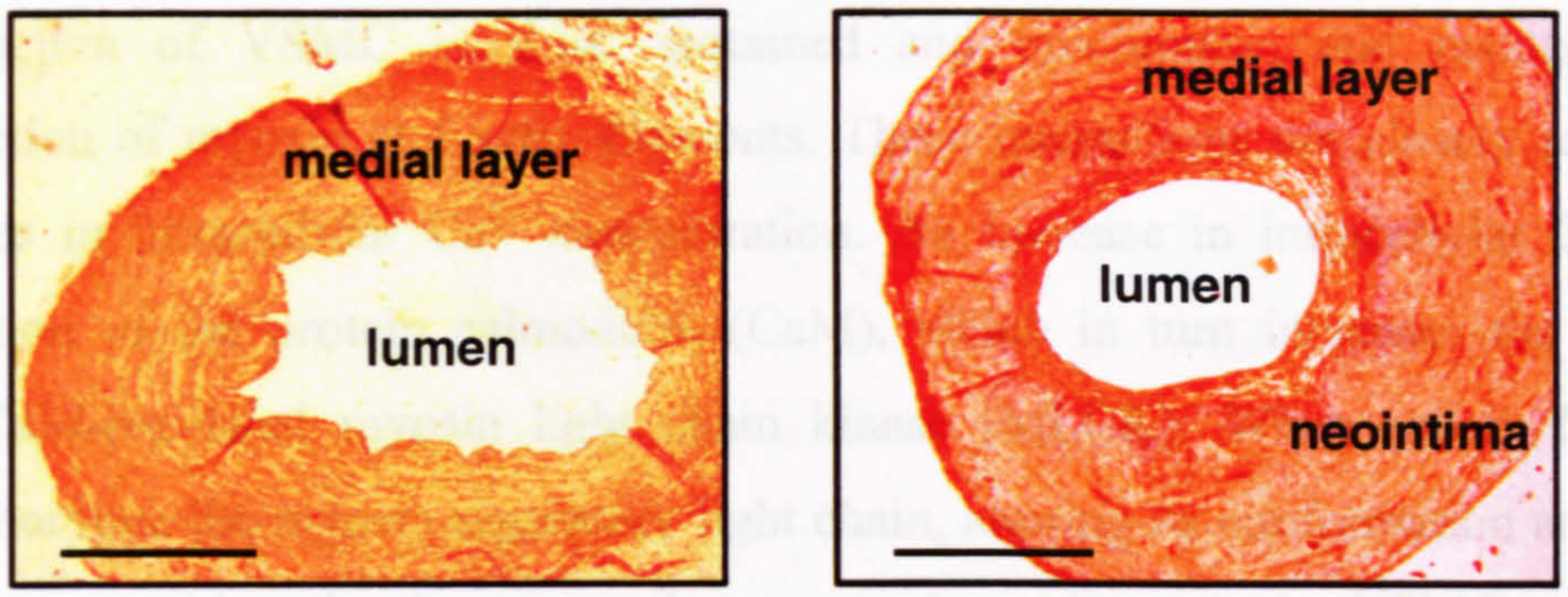

Figure 1.2. Model for neointimal hyperplasia in cultured saphenous vein Immunocytochemistry of saphenous vein section before (left hand panel) and 2 weeks after organ culture. Sections were stained orange for smooth muscle α-actin. Vein was obtained with consent from a patient undergoing coronary artery bypass surgery. Scale bar 1 mm. Reproduced with permission from (Cheong *et al.*, 2005).

VSMC contraction

Contraction of VSMC is slow, sustained and involuntary, and results from the interaction of myosin and actin filaments. These interactions are closely regulated by changes in intracellular Ca^{2+} concentration. An increase in intracellular Ca^{2+} causes activation of the protein calmodulin (CaM), which in turn increases the activity of Ca^{2+}/CaM-regulated myosin light chain kinase (MLCK). When active, MLCK can phosphorylate the myosin regulatory light chain, altering its conformation and allowing it to interact with actin, thus promoting contraction. Alternatively, VSMC contraction is caused by a Ca^{2+} independent mechanism which involves sensitisation of the contractile apparatus to Ca^{2+} (Somlyo *et al.*, 2000). Activation of cell-surface receptors activates the monomeric G protein RhoA, which binds GTP and translocates to the cell membrane where it activates Rho kinase. Rho kinase then phosphorylates myosin light chain phosphatase rendering it inactive, and unable to dephosphorylate myosin. This increases the Ca^{2+} sensitivity of smooth muscle myofilaments, allowing MLCK contraction to dominate.

Calcium signaling

The concentration of free Ca^{2+} in the cytosol is responsible for a multitude of cellular processes, including the regulation of transmitter release, muscle contraction, gene transcription, cell proliferation and cell death (Berridge *et al.*, 2000). Intracellular Ca^{2+} is closely regulated by Ca^{2+} permeable ion channels, exchangers and receptors located in both the plasma and intracellular membranes (Figure 1.3). Cytosolic Ca^{2+} is removed from the intracellular environment either by extrusion from the cell by the Na^{+}/Ca^{2+}exchanger and the plasma membrane Ca^{2+}-ATPase, or by uptake into intracellular stores by the endoplasmic (or muscle-specific sarcoplasmic) reticulum Ca^{2+}-ATPase. Intracellular Ca^{2+} is increased by release from stores through ryanodine and inositol-1,4,5-triphosphate (IP_3) receptors. Alternatively, Ca^{2+} can enter the cell by crossing the plasma membrane via a multitude of differentially-activated Ca^{2+}-permeable cation channels.

Extrusion of Ca^{2+}

Differences in electrical charge and ionic concentration between the intra and extracellular environments result in an electrochemical gradient across the plasma membrane which determines the direction an ion will move. The gradient for Ca^{2+} ions is maintained by the extrusion of Ca^{2+} from the cell by two main systems; the plasma membrane Ca^{2+}-ATPase (PMCA) and the Na^{+}/Ca^{2+} exchanger (NCX). Together these proteins keep intracellular levels in the nM range, creating a driving potential for Ca^{2+} influx into cells.

PMCA has 10 putative transmembrane domains which form 4 main units, including both N and C-terminal units, a phospholipid-interacting site, and a catalytic site. CaM binding to the intracellular C terminus regulates the activity of the protein, and increases its affinity for Ca^{2+} (Guerini, 1998). The extrusion of Ca^{2+} by PMCA is powered by the hydrolysis of ATP, which binds to the catalytic site and transfers a phosphate group to the protein, producing a phosphorylated intermediate. The exact mechanism of Ca^{2+} transport is unclear, but 2 Ca^{2+} ions are transferred for every ATP molecule hydrolysed. Although PMCA has a low transport rate, it has a high affinity for Ca^{2+}. This allows the pump to respond to very small changes in Ca^{2+}, thus maintaining a low basal level of Ca^{2+}. The existence of 4 PMCA genes and their alternative splicing produces functionally distinct isoforms which are differentially expressed in various cell types (Strehler *et al.*, 2001).

The NCX is driven by the movement of Na^{+} down its electrochemical gradient into the cell. Excess Na^{+} must then removed by the Na^{+}/K^{+}-ATPase in order to maintain the gradient. Despite having a lower affinity for Ca^{2+}, the NCX has a much faster transport rate, and is more efficient than PMCA for removing a large number of Ca^{2+} ions quickly. The protein comprises 9 transmembrane domains with an external N terminus and internal C terminus, but the exact structure-function relationships required for binding and transport of Ca^{2+} ions is not understood (Shigekawa *et al.*, 2001). For 3 Na^{+} entering the cell, one Ca^{2+} is extruded against its electrochemical gradient.

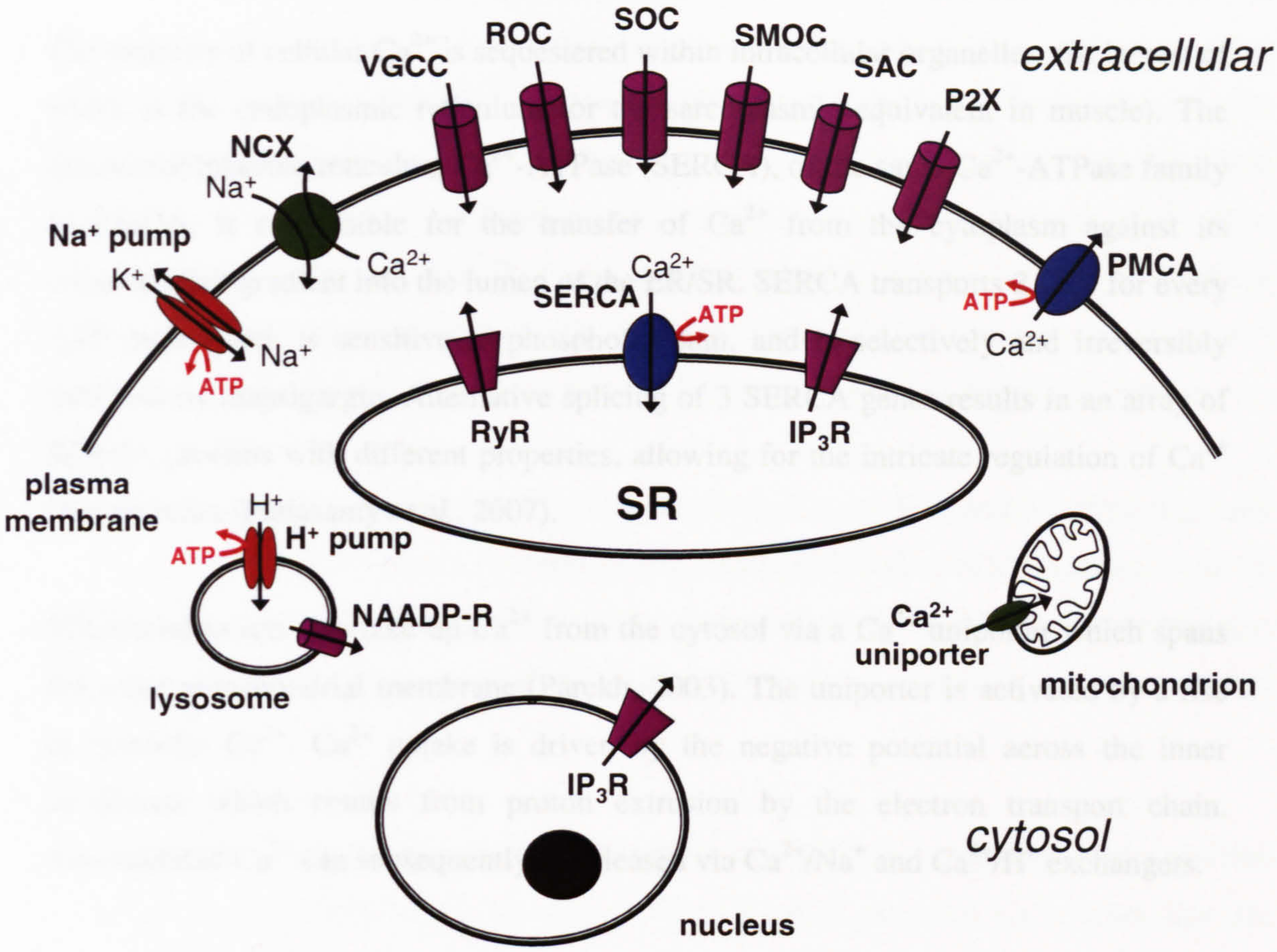

Figure 1.3. Summary of proteins involved in membrane transport of Ca^{2+} Proteins shown include: NCX, Na^+/Ca^{2+} exchanger; Na^+ pump, Na^+/K^+-ATPase; VGCC, voltage-gated Ca^{2+} channel; ROC, receptor-operated Ca^{2+} channel; SOC, store-operated Ca^{2+} channel; SMOC, second messenger-operated Ca^{2+} channel; SAC, stretch-activated channel; PMCA, plasma membrane Ca^{2+}-ATPase; SERCA, sarco(endo)plasmic reticulum Ca^{2+}-ATPase; RyR, ryanodine receptor; IP_3R, inositol 1,4,5-phosphate receptor; NAADP-R, NAADP-sensitive Ca^{2+} release channel. SR represents sarcoplasmic reticulum, the muscle equivalent of the endoplasmic reticulum (ER).

Ca^{2+} uptake by intracellular stores

The majority of cellular Ca^{2+} is sequestered within intracellular organelles, the largest of which is the endoplasmic reticulum (or the sarcoplasmic equivalent in muscle). The sarco(endo)plasmic reticulum Ca^{2+}-ATPase (SERCA), of the same Ca^{2+}-ATPase family as PMCA, is responsible for the transfer of Ca^{2+} from the cytoplasm against its concentration gradient into the lumen of the ER/SR. SERCA transports 2 Ca^{2+} for every ATP hydrolysed, is sensitive to phospholambam, and is selectively and irreversibly inhibited by thapsigargin. Alternative splicing of 3 SERCA genes results in an array of SERCA proteins with different properties, allowing for the intricate regulation of Ca^{2+} sequestration (Periasamy *et al.*, 2007).

Mitochondria can also take up Ca^{2+} from the cytosol via a Ca^{2+} uniporter which spans the inner mitochondrial membrane (Parekh, 2003). The uniporter is activated by a rise in cytosolic Ca^{2+}. Ca^{2+} uptake is driven by the negative potential across the inner membrane which results from proton extrusion by the electron transport chain. Accumulated Ca^{2+} can subsequently be released via Ca^{2+}/Na^{+} and Ca^{2+}/H^{+} exchangers.

Ca^{2+} release from intracellular stores

IP_3 and ryanodine receptors (IP_3R and RyR) are the principal intracellular Ca^{2+} channels responsible for the release of Ca^{2+} from intracellular stores. Located in the ER membrane, both receptors exist as tetramers, with large N termini projected into the cytoplasm. In addition, both receptors are sensitive to Ca^{2+}, thus are termed Ca^{2+}-induced Ca^{2+}-release channels (CICR), and will release a large amount of Ca^{2+} from stores in response to a small Ca^{2+} influx across the plasma membrane. However both receptors are inhibited by high concentrations of Ca^{2+}. Furthermore, the receptors are regulated by CaM binding and phosphorylation by PKC and PKA (Nadif Kasri *et al.*, 2002).

Ca^{2+} is released form stores when IP_3, an important second messenger produced by the phosphoinositide signalling system, binds to the IP_3R and increases its affinity for Ca^{2+}. Receptor activation and the subsequent Ca^{2+} transport requires the binding of both IP_3 and Ca^{2+}. The IP_3R protein consists of 6 transmembrane domains that form the Ca^{2+}

pore, plus a cytoplasmic N terminal IP_3 binding domain, and also a regulatory domain containing PKA-dependant phosphorylation sites and nucleotide binding sites. Several antagonists have been characterised, including heparin which competitively inhibits IP_3R by interacting directly with the IP_3 binding site, caffeine which interacts with nucleotide binding sites, and polyamines and tetraalkyl ammonium cations which interact with the transmembrane Ca^{2+} channel domain and block Ca^{2+} flow (Michelangeli *et al.*, 1995). IP_3Rs are also expressed in the nucleus, in an organelle continuous with the nuclear envelope termed the nucleoplasmic reticulum (Echevarria *et al.*, 2003). These nuclear IP_3Rs are responsible for nuclear IP_3-induced Ca^{2+} release.

The RyR displays high affinity for the plant alkaloid ryanodine, and the physiologically relevant cyclic ADP ribose (Sharma *et al.*, 2000). Although similar in structure to the IP_3R, the RyR is much bigger, and can be distinguished by its different pharmacology; it activated by caffeine, and inhibited by ruthenium red and high concentrations of ryanodine.

Nicotinic acid adenine dinucleotide phosphate (NAADP) is a signalling nucleotide that regulates intracellular Ca^{2+} via release from NAADP-sensitive Ca^{2+} stores that are separate from IP_3- and cADPR-sensitive ER/SR stores. NAADP-induced Ca^{2+} release is dependent on a proton gradient, which is maintained by a lysosomal, ATP-dependent proton pump. This suggests the channel responsible for this Ca^{2+} release is located in the lysosome. A likely candidate is TRPML1, a member of the TRP superfamily that is predominantly expressed in lysosomes (Zhang *et al.*, 2007).

Voltage-gated Ca^{2+} channels

Voltage-gated ion channels open in response to membrane depolarisation to allow the passage of ions. There are 6 types of voltage-dependent Ca^{2+} channels (VGCC); those that are high voltage-activated and require large depolarisations to activate, including long lasting L-, neuronal N-, P-, Q- and R-type, and transient T-type channels that are low voltage-activated channels, activated by small depolarisations. Individual channel types can be distinguished by their sensitivity to various toxins. L-type channels are selectively inhibited by dihydropyridines such as nifedipine, N-type channels are

blocked by ω-conotoxin GVIA, and P/Q-type channels are blocked by ω-agatoxins. The R-type channels are resistant to all of these toxins.

The dihydropyridine-sensitive L-type VGCC has been well characterised, and in addition to inhibition by dihydropyridines, is also sensitive to block by classical Ca^{2+} antagonists such as phenyalkamines and bexothiazapines. The protein exists as a complex of 5 subunits, the pore-forming α_1-subunit, plus regulatory auxiliary β-, γ- and $\alpha_2\delta$-subunits. The α_1-subunit resembles other voltage-gated ion channels, with a tetrameric association of 4 domains, each with 6 transmembrane domains designated S1-S6. Positively charged lysine and arginine residues in the S4 in each of the 4 domains collectively form the voltage sensor, whereas negatively charged residues in the pore loops between S5 and S6 are responsible for the Ca^{2+} selectivity of the channels (Dolphin, 2006). The α_1-subunit also contains the binding site for dihydropyridines in a hydrophobic region on its extracellular surface.

The auxiliary β-subunit contains mainly hydrophilic residues and is not glycosylated, thus is presumed to be intracellular. Interactions between the α_1- and β-subunits modulate channel gating and trafficking of the channel complex to the plasma membrane. The α_2-subunit is extracellular, and is linked via disulfide bonds to the transmembrane δ-subunit. These 2 subunits are believed to increase current amplitude and activation rate. The role of the γ-subunit is not known, but it is believed to form 4 transmembrane segments.

Ligand-gated ion channels

Ligand-gated ion channels (LGIC) are transmembrane ion channels that are opened or closed in response to the binding of an extracellular ligand mediator. LGIC that are permeable to Ca^{2+} include the ionotropic glutamate receptor N-methyl-D-aspartate (NMDA), and ATP-gated P2X receptors.

NMDA receptors are expressed in the CNS at glutamatergic synapses where they mediate synaptic transmission. The channels are unusual in that they are both ligand-gated and voltage-dependent. Functional receptors are comprised of a heterodimer of 2 subunits, NR1 and NR2, and alternative splicing and differential expression of these

subunits allows for multiple receptor isoforms with varying properties. NMDA receptor ligand-activation requires the binding of both an agonist (glutamate or other structurally-related amino acids), and a coagonist (glycine or D-serine). NMDA receptors are not voltage-gated channels; instead, depolarisation regulates the inhibitory effect of external Mg^+ (MacDonald *et al.*, 1990).

P2X receptors are cation-permeable LGIC activated by extracellular ATP. There are 7 genes that encode P2X subunits, $P2X_1$-$P2X_7$, and these can exist in multiple spliced forms (North, 2002). Each subunit comprises 2 transmembrane domains, intracellular N- and C-termini, and a large extracellular loop containing conserved lysine residues to which ATP binds. The transmembrane domains of a single subunit are insufficient to form an ion conducting pore, therefore functional channels exist as homo- or heterotrimeric structures (Roberts *et al.*, 2006).

Stretch-activated channels

Mechanosensitive, or stretch-activated channels (SAC), are non-selective cation channels that are activated by stretch of the plasma membrane. Originally discovered in chick skeletal muscle, SAC have subsequently been identified in a range of different cell types (Kalapesi *et al.*, 2005). Examples of SAC include the two-pore domain K^+ channels TREK and TRAAK (Maingret *et al.*, 2000), and members of the TRP cation channel superfamily (Pedersen *et al.*, 2007). The exact mechanism for SAC activation is not yet understood; mechanosensitivity may be directly modulated via SAC associations with the actin cytoskeleton, or alternatively membrane stretch may activate PLC or PLA_2 to stimulate cellular signalling cascades, intermediates of which could activate SAC. Ultimately SAC activation can result in depolarisation of the membrane, causing activation of VGCC.

Second-messenger-operated channels

Second-messenger-operated channels (SMOC) are activated by various second messengers produced as a result of signalling cascades. An example of SMOC are the cyclic nucleotide gated (CNG) channels. CNG channels were first identified in

photoreceptors and olfactory sensory neurons, where they are gated by second messengers produced by visual and olfactory signalling cascades, such as cGMP and cAMP respectively (Bradley *et al.*, 2005).

Receptor-operated channels

Receptor-operated channels (ROC), such as homologues of the *Drosophila* TRP family, are activated as a result of the stimulation of G-protein coupled receptors (GPCR) such as M2 and M3 muscarinic receptors and the α_1-adrenergic receptor. Ligand activation of a GPCR induces a conformational change which allows the exchange of GDP for GTP on the associated G_α subunit. This allows G_α to dissociate from the $G_{\beta\gamma}$ subunit in order to activate signalling cascades. A common GPCR signalling cascade involves the activation of PLC, which then hydrolyses PIP_2 into DAG and IP_3, and subsequently activates ROC. In addition, IP_3 production activates the IP_3R and thus causes an increase in Ca^{2+} release form stores, thereby activating store-operated channels (SOC).

Store-operated Ca^{2+} channels

Stimulation of plasma membrane receptors to generate IP_3 not only depletes intracellular Ca^{2+} stores, but also causes a sustained Ca^{2+} influx across the plasma membrane. This sustained Ca^{2+} influx is referred to as capacitative Ca^{2+} entry or store-operated Ca^{2+} entry (SOCE), and results from the opening of plasma membrane Ca^{2+} channels in response to the emptying of ER stores (Berridge, 1995). Extracellular Ca^{2+} entry in response to Ca^{2+} release from stores occurs through store operated Ca^{2+} channels (SOC). Inhibition of SERCA by thapsigargin, which blocks the reuptake of Ca^{2+} into the ER, can induce SOCE, suggesting SOC are activated by the process of store depletion, not by the Ca^{2+} that is released from the stores (Thastrup *et al.*, 1989). Homologues of the *drosophila trp* gene family are believed to encode SOC (Birnbaumer *et al.*, 1996).

There are several theories for how SOCE occurs. The conformational coupling theory suggests that IP_3Rs can translocate from the ER membrane to associate with SOC in the plasma membrane, resulting in direct refilling of Ca^{2+} stores. Alternatively, there may

be a separate Ca^{2+} sensing protein that can detect luminal store depletion, translocate to the plasma membrane, and interact with SOC. A likely candidate is suggested to be stromal interaction molecule (STIM1), which senses ER luminal Ca^{2+} and transduces information directly to the plasma membrane (Hewavitharana *et al.*, 2007). A third hypothesis is that a diffusible Ca^{2+} influx factor is produced by the stores in response to Ca^{2+} depletion, which diffuses to the plasma membrane to activate SOC. Finally, SOCE may result from the fusion of vesicles containing SOC with the plasma membrane (Rosado *et al.*, 2005).

Ca^{2+} homeostasis in VSMC

Smooth muscle contraction is initiated by an increase in intracellular Ca^{2+} concentration, thus VSMC express a plethora of Ca^{2+} channels to closely regulate Ca^{2+} homeostasis. In general, contraction requires the activation of GPCR, resulting in the stimulation of PLC by the Gα subunit, the production of IP_3, and the release of Ca^{2+} from IP_3-dependent Ca^{2+} stores. This store release will also activate SOC in the plasma membrane. In addition, Ca^{2+}-permeable ROC are activated, and in combination with ATP-activated P2X receptors, the cation movement into the cell depolarizes the plasma membrane and activates VGCC. All of these combined events allow for the large increase in intracellular Ca^{2+} that is necessary to cause smooth muscle contraction.

Of the 6 VGCC, only L-type and T-type channels are expressed in VSMC. L-type channels are well characterised as regulators of the Ca^{2+} entry necessary for VSM contraction and vasoconstirction, and the vasodilatory and anti-hypertensive properties of dihydropyridines result from inhibition of L-type VGCC expressed in smooth muscle. T-type channels contribute less to vasoconstriction, and instead are suggested to regulate the cell cycle, thus controlling gene expression necessary for cell growth and division (Cribbs, 2006). Furthermore, T-type channels are upregulated, and L-type Ca^{2+} channels are downregulated in proliferating VSM, suggesting that proliferating SMC require transient voltage-dependent Ca^{2+} influx.

Non-voltage gated channels are also expressed in VSM. ATP can regulate smooth muscle activity via $P2X_1$ and $P2X_4$, which are widely expressed in vascular smooth muscle (Lewis *et al.*, 2001). $P2X_1$ causes smooth muscle contraction (Banks *et al.*,

2006), and $P2X_4$ regulates vascular tone (Yamamoto *et al.*, 2006). Although little is known about the function of CNG channels in VSM, they are reportedly expressed in freshly isolated smooth muscle, and may play a regulatory role in VSMC (Cheng *et al.*, 2003). SOCE has been implicated in contraction, proliferation and gene transcription in smooth muscle, suggesting SOC play an important role in regulating intracellular Ca^{2+} in VSM. Finally, Ca^{2+}-permeable SAC are reportedly expressed in mesenteric, coronary, bladder and cerebral arteries (Welsh *et al.*, 2002; Wu *et al.*, 2001). Ca^{2+} influx through Ca^{2+} channels can also occur in cells in the absence of any stimulus. This Ca^{2+} leak is believed to occur through distinct channels referred to as leak channels.

Reports dating back to the late 1970s suggested ROC and SOC in VSM were formed by a novel and distinct Ca^{2+} channel (Bolton, 1979; Van Breemen *et al.*, 1978). It is now apparent that a likely candidate for this novel Ca^{2+} channel are members of the TRP channel superfamily, many of which have now been identified as ROC, SOC, SMOC and SAC (Beech *et al.*, 2004). TRP channels are suggested to be responsible for nonselective cation current in VSM (Walker *et al.*, 2001), and specifically have been demonstrated to have a functional relevance; TRPC6 and TRPV2 are suggested to form SAC (Muraki *et al.*, 2003; Welsh *et al.*, 2002), TRPC1 is a candidate for a native SOC in smooth muscle (Xu *et al.*, 2001), and furthermore Ca^{2+} leak channels are suggested to be TRP channels in smooth muscle (Beech *et al.*, 2004).

Transient receptor potential (TRP) channels

The Transient Receptor Potential (TRP) channels form a diverse superfamily of cation channels, and were originally identified in *Drosophila melanogaster* as the genes responsible for visual transduction (Montell *et al.*, 1989). Photoreceptors in the *trp* mutant displayed a transient, rather than sustained, response to light stimulation, thus termed the transient receptor potential. This response was characterized by a reduction in Ca^{2+} entry, indicative of a defect in the activation of a cation channel. TRP channels are now recognised as the largest known family of ion channels, with 28 mammalian TRP channels identified thus far. Despite sharing a common putative 6 transmembrane domain structure and permeability to cations, TRP channels are activated by a huge diversity of signals, including both external stimuli and changes in local intracellular environment.

Based on sequence homology, TRP channels are divided into seven subfamilies; canonical or classical (TRPC), vanilloid receptor-related (TRPV), and melastatin-related (TRPM), as well as the more distantly related polycystins (TRPP), mucolipidins (TRPML), ankyrin (TRPA) and NOMPC (TRPN) (Figure 1.4).

TRP structure

TRP protein conformation is believed to resemble that of classical voltage-gated ion channels, in particular K^+ channels for which the structure is well characterised. Intracellular N and C termini are connected to 6 transmembrane domains designated S1-S6, and the S5-S6 linker forms the pore. TRP channels are also presumed to function as tetramers. In contrast to voltage-gated channels, TRP channels are not believed to be voltage activated, as the majority of family members lack the necessary positive residues on S4. However, voltage-modulation of TRP channels has been demonstrated (Nilius *et al.*, 2005b). Negatively charged residues that form selectivity filters in the pore loop of ion channels are often absent in TRP channels, therefore they tend to be non-selective cation channels. However, some family members, such as TRPV6, display high selectivity for Ca^{2+}.

There are also common structural features conserved between the different subfamilies (figure 1.5). These include coiled coil domains in the N- and C-termini of TRPC, TRPM and TRPA, plus a number of N-terminal ankyrin repeats that range from zero in TRPM, TRPP and TRPML, to as many as 14 in TRPA1 (Clapham, 2003). There is also a highly conserved C-terminal sequence that immediately follows S6, termed the TRP domain. In TRPC, the TRP domain contains the sequence EWKFAR which is referred to as the TRP box, but this is less conserved in TRPV and TRPM (Clapham, 2003). C-terminal CaM binding domains are present in TRPV, TRPM and TRPC, but have not yet been identified in other family members.

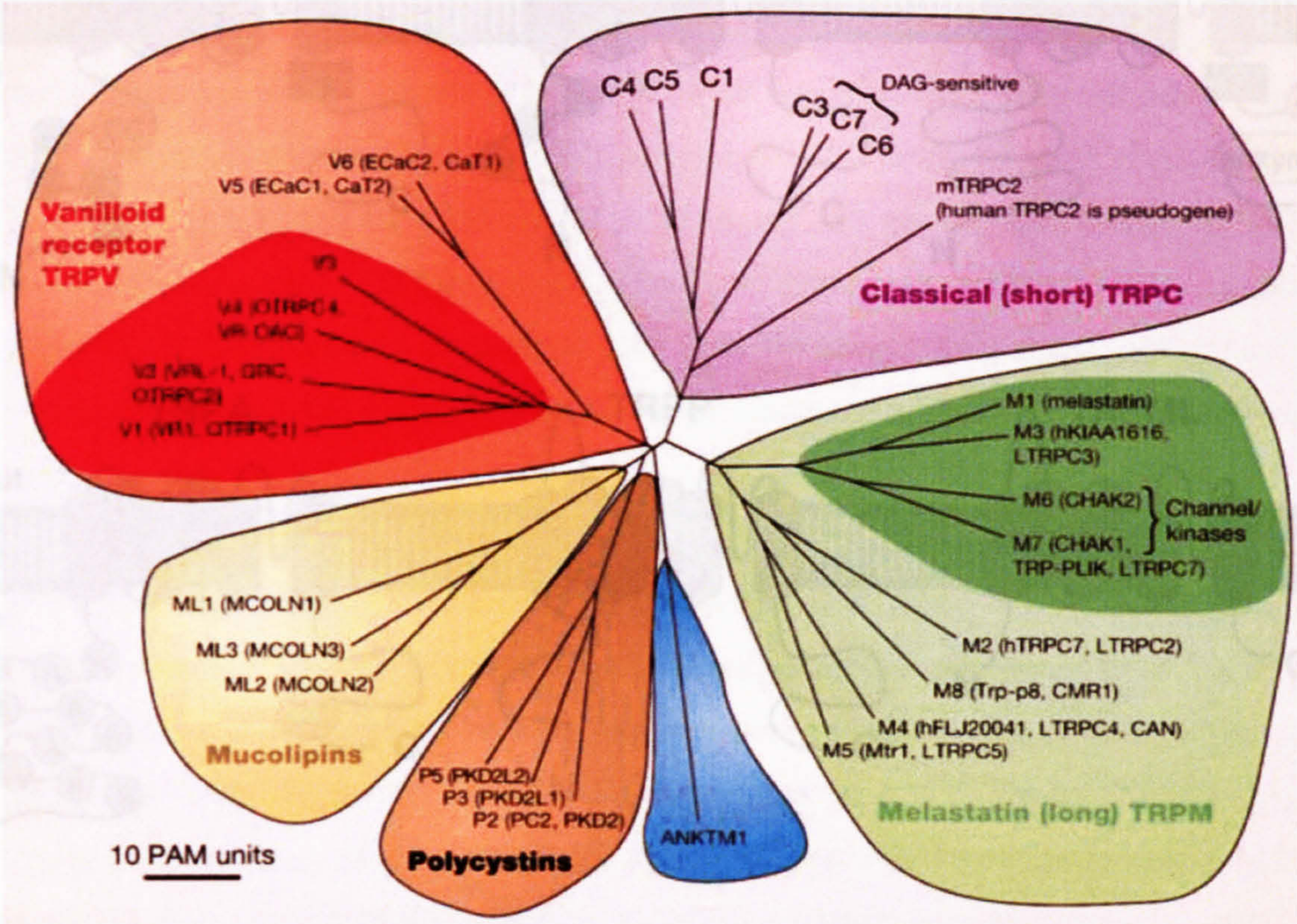

Figure 1.4. Mammalian TRP family tree The evolutionary distance is shown by the total branch lengths in point accepted mutations (PAM) units, which is the mean number of substitutions per 100 residues. Figure and legend reproduced from (Clapham, 2003).

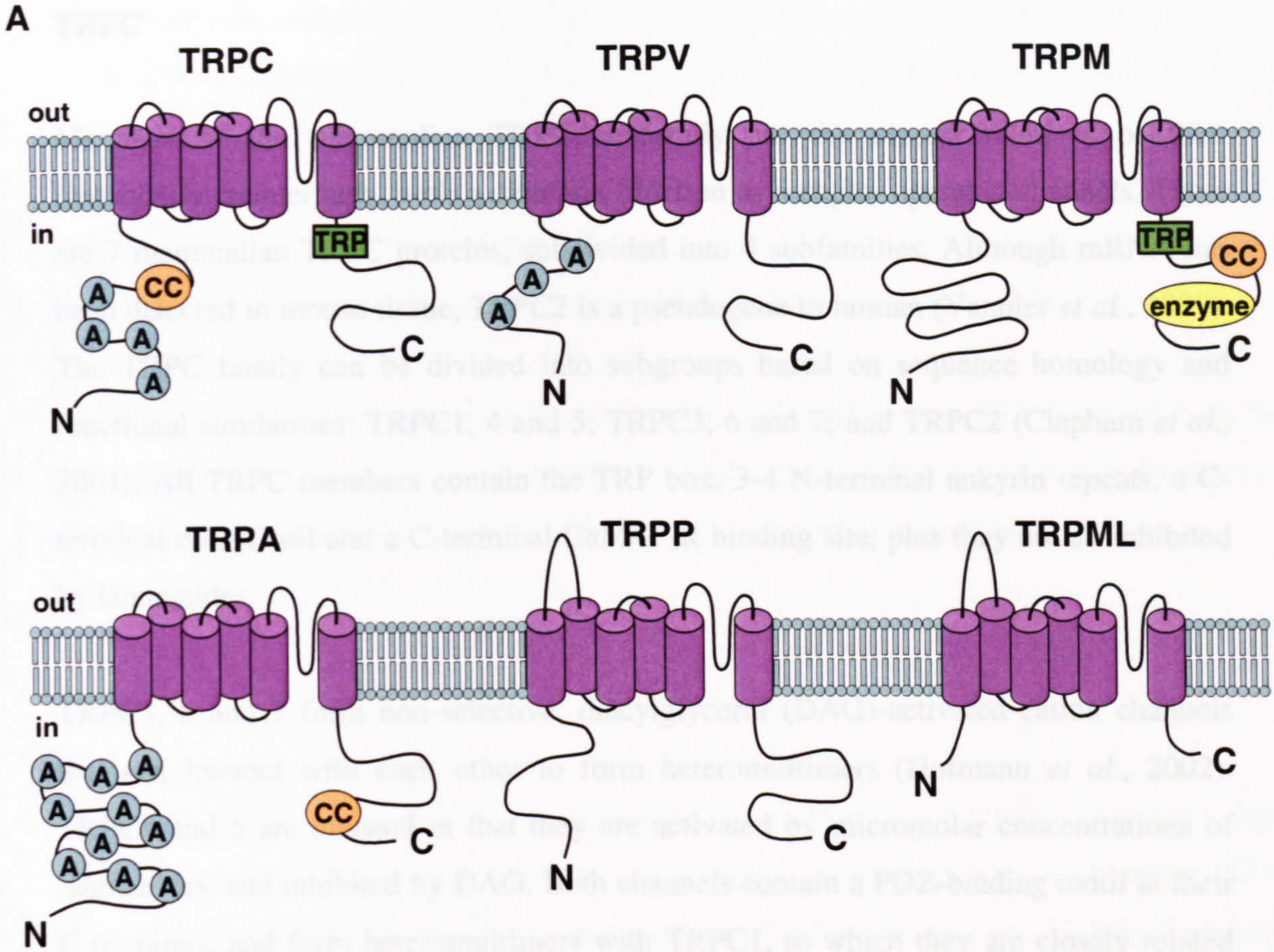

Figure 1.5. Mammalian TRP superfamily TRP channels contain 6 TM domains plus a pore loop. **A.** The six mammalian subfamilies. Domains indicated include: A, Ankyrin repeats; CC, coiled-coil domain; TRP, TRP domain; enzyme, protein kinase domain (TRPM6/7) or ADP-ribose pyrophosphatase domain (TRPM2). **B.** Putative TRP channel tetramer forming homo- or heteromeric channels. S5-S6 linkers (blue) line the pore.

TRPC

Members of the mammalian TRPC subfamily are the closest relatives of their *Drosophila* counterparts, with a common function as receptor operated channels. There are 7 mammalian TRPC proteins, subdivided into 4 subfamilies. Although mRNA has been detected in mouse tissue, *TRPC2* is a pseudogene in human (Vannier *et al.*, 1999). The TRPC family can be divided into subgroups based on sequence homology and functional similarities; TRPC1, 4 and 5; TRPC3, 6 and 7; and TRPC2 (Clapham *et al.*, 2001). All TRPC members contain the TRP box, 3-4 N-terminal ankyrin repeats, a C-terminal coiled coil and a C-terminal CaM/IP_3R binding site, plus they are all inhibited by lanthanides.

TRPC3, 6 and 7 form non-selective, diacylglycerol (DAG)-activated cation channels that can interact with each other to form heteromultimers (Hofmann *et al.*, 2002). TRPC4 and 5 are unusual in that they are activated by micromolar concentrations of lanthanides, and inhibited by DAG. Both channels contain a PDZ-binding motif at their C terminus, and form heteromultimers with TRPC1, to which they are closely related (Strubing *et al.*, 2001). TRPC1, TRPC3, TRPC4 and TRPC7 are reported to form SOC, but the store-operation of TRPC5 is controversial. TRPC5 is predominantly expressed in brain tissue, and is activated by many different signals within a single cell including receptor stimulation, lanthanides and lysophospholipids (Flemming *et al.*, 2006; Zeng *et al.*, 2004)

TRPV

The TRPV family has 6 members, and is named after founding member TRPV1, which is activated by the inflammatory vanilloid, capsaicin. All TRPV family members contain N-terminal ankyrin repeats and the TRP domain; however the TRP box is less conserved than in TRPC and TRPM families.

TRPV1-4 are non-selective cation channels capable of activation by multiple stimuli, commonly heat. Referred to as 'thermoTRPs', heat-activated TRPV channels play a role in thermosensation. TRPV1 is well characterised, and known to be activated by many different stimuli including noxious chemicals (capsaicin, endocannabinoids,

anandamide, camphor, piperine and allicin), PIP_2 and heat (≥43°C) (Venkatachalam *et al.*, 2007). Activation is enhanced by exposure to low pH. TRPV2 and TRPV4 are both sensitive to hypotonic shock, presumably as a result of cell swelling. Specifically the stretch activation of TRPV4 is believed to occur through PLA_2-mediated arachadonic acid and subsequent metabolites (Watanabe *et al.*, 2003). TRPV3 is also activated by arachadonic acid and menthol (Hu *et al.*, 2006; Macpherson *et al.*, 2006).

TRPV5 and TRPV6 are not activated by heat, and unlike other TRPV members, show high selectivity for Ca^{2+}. Their activity is regulated following insertion into the plasma membrane, and form heteromers with each other (Hoenderop *et al.*, 2003).

TRPP

There are 2 TRPP channels characterised thus far; TRPP1 and TRPP2. Although they form non-selective cation channels, they share little homology with other TRP members, and TRPP1 contains a much larger 1st extracellular loop. TRPP2 is mainly localised in intracellular membranes and complexes to TRPP1 in order to translocate to the plasma membrane to form cation channels (Qian *et al.*, 2003). TRPP1 putatively contains 11 TM domains, however the structural similarity of the first 6 domains means it is classed as TRPP channel. Two additional TRPP homologues, TRPP3 and TRPP5, have been identified in mammals. TRPP3 is localized to a taste receptor cells in the tongue, and mice lacking TRPP3 do not display taste responses to sour stimuli (Ishimaru *et al.*, 2006). The function of TRPP5 is unknown.

TRPML

Named after the founding member mucolipin-1, there are 3 mammalian TRPML proteins. TRPML1 and TRPML2 reside in the lysosomal membrane as a result of lysosomal targeting signals, and TRPML3 localises to the ER membrane. Only TRPML1 has been shown to form a non-selective cation channel, and is reported to regulate lysosomal Ca^{2+} release. TRPML1 is also reported to be permeable to monovalent cations, and may allow proton flux to regulate acidity of the lysosome.

Furthermore, TRPML is a likely candidate for the lysosomal NAADP-activated Ca^{2+} channel (Zhang *et al.*, 2007).

TRPA

The single mammalian TRPA channel, TRPA1, was previously referred to as ANKTM1 due to the presence of multiple N terminal ankyrin repeats. TRPA1 is a further example of the ability of TRP to be stimulated by a multiplicity of signals. It is activated by pungent compounds including isothiocyanates, allicin, cinnemaldehyde, acrolein, tetrahydrocannabinol, plus components of wasabi and horseradish, products of PLC stimulation, and noxious cold. TRPA1 is suggested to act as the mechanosensitive transduction channel of vertebrate hair cells, which functions as a 'gating spring' formed by the multiple ankyrin repeats (Corey *et al.*, 2004).

TRPN

Studies in *Drosophila* demonstrated that loss-of-function mutations in the *no mechanoreceptor potential C (nompC)* gene abolished mechanosensory signalling (Walker *et al.*, 2000). This suggests that the *nompC* gene encodes an ion channels necessary for mechanosensory transduction, and now referred to as TRPN channel. TRPN channels are not present in mammals. They contain several conserved TRP features, including the TRP box, plus N terminal ankyrin repeats. Similar to TRPA1, the presence of ankyrin repeats suggests they are likely to be mechanically gated.

TRPM

The TRPM subfamily contains 8 members that are further divided into 4 subgroups of pairs which display significant sequence homology; TRPM1 and TRPM3, TRPM2 and TRPM8, TRPM4 and TRPM5, and TRPM6 and TRPM7. All members are relatively long proteins that contain conserved features such as the TRP box. However, a 'TRPM homology region' of approximately 700 amino acids replaces the N-terminal ankyrin repeats. TRPM members have multiple protein forms as a result of alternative splicing

events. The founding member melastatin (TRPM1), for which the family is named, has been shown to be downregulated in melanoma cell lines (Duncan *et al.*, 2001). There are no known activators for the TRPM1 channel, and it is believed to be constitutively active.

TRPM2 is a widely expressed, non-selective cation channel that can be activated by hydrogen peroxide (H_2O_2), ADP-ribose (ADPR), arachadonic acid and tumour necrosis factor α (TNFα). It contains a C-terminal Nudix enzymatic domain, homologous to human NUDT9 ADPR hydrolase, which functions as an ADPR pyrophosphatase (Nagamine *et al.*, 1998). This domain is unique to TRPM2, and binds intracellular ADPR (Perraud *et al.*, 2001). Intracellular Ca^{2+} sensitises the channel to ADPR (McHugh *et al.*, 2003). Ca^{2+} influx resulting from activation by TNFα or H_2O_2 leads to cell death, thus TRPM2 is believed to be a cell fate modulator (Hara *et al.*, 2002). Recently, TRPM2 has been reported to be activated by warm temperatures via direct heat-evoked channel gating, and ADPR-induced activity is potentiated at increased temperatures (Togashi *et al.*, 2006). The closely related TRPM8 also exhibits temperature-dependant gating, and can be regulated by both cold stimuli and the cooling agents menthol and icilin (Peier *et al.*, 2002). TRPM8 activity is regulated by PIP_2 binding to regions in the TRP box, suggesting regulation of many TRP channels by PIP_2 may depend on this highly conserved region (Rohacs *et al.*, 2005).

Unlike other members of the TRP family, TRPM4 and TRPM5 are impermeable to Ca^{2+}, and instead are selective for monovalent cations (Nilius *et al.*, 2005a). They are also directly gated by intracellular Ca^{2+} and regulated by PIP_2. TRPM4 is expressed as two splice variants, a smaller, constitutively active TRPM4a variant, plus a longer and Ca^{2+}-activated TRPM4b variant. TRPM5 is also sensitive to temperature change, and is activated by heat in the range of 15–35°C (Talavera *et al.*, 2005).

TRPM6 and TRPM7 have C terminal enzymatic activity in the form of an α-kinase domain, and are thought to be involved in magnesium homeostasis (Runnels *et al.*, 2002). Both are selective for divalent cations, and are inhibited by intracellular Mg^{2+}. Furthermore the 2 related channels can coassemble to form multimeric structures (Chubanov *et al.*, 2004). TRPM7 activity is regulated by pH, ATP, lipids, and translocation, and the channel is upregulated following a decrease in extracellular pH (Venkatachalam *et al.*, 2007).

TRPM3

TRPM3 forms non-selective cation channels, and shares significant sequence homology with TRPM1. While endogenous protein is primarily expressed in the brain, mRNA has also been detected in human kidney, brain, spinal cord, liver, testis, ovaria and pancreas (Grimm *et al.*, 2003; Lee *et al.*, 2003a). Although present in human and bovine kidney, TRPM3 is not expressed in the same tissue in mouse, suggesting species and tissue-specific expression of the protein (Grimm *et al.*, 2003). Overexpression of the protein in HEK 293 cells shows it is primarily located at the plasma membrane, indicating a functional membrane-spanning channel (Grimm *et al.*, 2003).

The TRPM3 gene is alternatively spliced to encode functionally distinct splice variants, all of which are constitutively active cation channels. The human variant $hTRPM3_{1325}$, which encodes a protein of 1325 amino acids, was originally reported to be activated by a reduction in extracellular osmolarity, presumably as a result of cell swelling (Grimm *et al.*, 2003). Subsequently lipid activators of $hTRPM3_{1325}$ were described; specifically intermediates in sphingolipid metabolism including D-*erythro*-sphingosine (SPH) and the related analogues N,N-dimethyl-D-*erythro*-sphingosine (DMS) and dihydro-D-*erythro*-sphingosine (DHS) (Grimm *et al.*, 2005). The effect appears specific, as additional lipid activators were ineffective, and SPH did not activate other TRP family members. In addition, activation occurred independently of PKC, IP_3R and Ca^{2+} store depletion. It is not clear from this study whether SPH activates the TRPM3 channel directly, and it is possible that activation is the result of SPH-induced cell swelling. A further 6 human variants have been identified, designated hTRPM3a-f (Lee *et al.*, 2003a). These variants possess much shorter N termini, and as a result lack the TRPM homology region present in other TRPM proteins. The variant hTRPM3a is comprised of 1555 amino acids, and is reported to form a store-operated channel, showing enhanced Ca^{2+}entry when stores are first depleted by thapsigargin or carbachol (Lee *et al.*, 2003a). The increased Ca^{2+} in hTRPM3a-expressing cells is small, and furthermore SPH-activation of $hTRPM3_{1325}$ is not influenced by thapsigargin, suggesting store depletion may not be a predominant regulatory mechanism of $TRPM3_{1325}$ (Grimm *et al.*, 2005).

A further 5 variants have been identified in mouse, mTRPM3α1-5 (Oberwinkler *et al.*, 2005). A single splicing event creates a longer pore region in TRPM3α1, and

comparison with TRPM3α2 demonstrated a change in the cation selectivities (Oberwinkler *et al.*, 2005). Both variants are inhibited by Mg^{2+}. Splice variants with a shorter pore ($hTRPM3_{1325}$ and mTRPM3α2) are permeable to divalent cations, however TRPM3α1 exhibited no inward current in the presence of high extracellular divalent cations (Grimm *et al.*, 2005; Oberwinkler *et al.*, 2005). Alternative splicing is likely to be a method to regulate activation and functional properties of expressed TRPM3 channels.

The physiological function of TRPM3 is unknown, but the ability of $TRPM3_{1325}$ to respond to changes in extracellular osmolarity, together with its localisation to the kidney, suggests a role for the channel in renal Ca^{2+} homeostasis. Interestingly TRPM3 mRNA is downregulated in renal tumours, so perhaps reduced TRPM3 expression plays a role in tumorigenesis (Lee *et al.*, 2003a). Northern blot analysis shows a high expression of TRPM3 in epithelial cells of the choroid plexus, the area of the brain responsible for the production of cerebrospinal fluid (Oberwinkler *et al.*, 2005).

TRP channels in disease

Mutations in TRP channels are linked to several human diseases. Autosomal dominant polycystic kidney disease (ADPKD) results from mutations in the *PKD2* gene, which encodes polycystin-2 (TRPP2) (Kottgen, 2007). ADPKD is characterised by the replacement of healthy renal tissue with fluid filled cysts. The gene encoding TRPML1 is mutated in mucolipidosis type IV (MLIV), a lysosomal storage disorder characterised by large intracellular lysosomes (Qian *et al.*, 2005). The exact roles of TRPP and TRPML channels in the progression of ADPKD and MLIV have yet to be elucidated. TRPC6 and TRPM6 are also associated with kidney disease. Mutations in the TRPC6 gene are linked to focal segmental glomerulosclerosis (Huber *et al.*, 2006), while mutation of the gene encoding TRPM6 results in hypomagnesemia with secondary hypocalcemia, presumably as a result of defective Mg^{2+} homeostasis (Walder *et al.*, 2002). Ca^{2+} and Mg^{2+} deficiency is also linked to guamanian amyotrophic lateral sclerosis and parkinsonism dementia, and a *TRPM7* variant produces a protein with a missense mutation associated with these disease states (Hermosura *et al.*, 2005).

In addition to abnormalities that result from gene mutation, the expression of certain TRP genes can also be correlated to human disease, specifically cancer. Both TRPV6

and TRPM8 are upregulated in prostate cancers (Tsavaler *et al.*, 2001; Wissenbach *et al.*, 2004). Northern blot analysis indicated TRPM8 was also upregulated in breast colon, lung and skin cancers (Tsavaler *et al.*, 2001). Conversely TRPM1 is downregulated in malignant melanomas, suggesting it in fact functions as a tumour suppressor protein (Duncan *et al.*, 2001).

Evidence for TRP expression in VSM

Members of TRPC, TRPV, TRPM and TRPP are all expressed in vascular smooth muscle, but for many the physiological function of the channel in the vasculature has yet to be elucidated (Dietrich *et al.*, 2006).

All TRPM channels, except TRPM1, are expressed in the vasculature (Yang *et al.*, 2006). The PKC-dependent regulation of TRPM4 activity regulates myogenic tone (Earley *et al.*, 2004), and TRPM6 and TRPM7 are required for Mg^{2+} homeostasis in A7R5 smooth muscle cell line (He *et al.*, 2005). Furthermore TRPM7 is highly expressed in VSM, and when the blood vessel endothelium is damaged, the shear stress of blood flow results in the translocation and accumulation of TRPM7 at the plasma membrane, suggesting a role in the pathological response to vessel injury (Oancea *et al.*, 2006).

TRPC1 forms a SOC in vascular smooth muscle (Xu *et al.*, 2001), and is present in both contractile and proliferative VSMC (Beech, 2005). Specifically, TRPC1 is linked to the excessive proliferation of VSMC that results in neointimal hyperplasia (Kumar *et al.*, 2006). TRPC4 is also implicated in store-mediated regulation of VSMC proliferation (Zhang *et al.*, 2004), while TRPC5 is implicated in S1P-induced VSMC migration (Xu *et al.*, 2006b). TRPC3 and TRPC6 are involved in both receptor-mediated and pressure-induced vasoconstriction, suggesting they play a role in regulating myogenic tone and blood pressure (Inoue *et al.*, 2006). TRPC7 is also a ROC in the vasculature, and is predicted to have similar functions to TRPC6 (Maruyama *et al.*, 2006).

TRPP1 and TRPP2 are also expressed in the vasculature, where they are suggested to form homo- and heteromultimeric complexes with TRPC1 (Tsiokas *et al.*, 1999). Patients with polycystic kidney disease, which results from mutations in *TRPP* genes,

display thinning of arterial walls which can lead to internal bleeding. Furthermore SOC Ca^{2+} entry is reduced in TRPP2 knockout mice, and as these mice develop haemorrhaging the suggestion is that TRPP2 is necessary for maintaining the structural integrity of vessels (Kim *et al.*, 2000).

The function of TRPV channels in VSM is less well characterised. TRPV mRNA is expressed in rat aorta and pulmonary artery, and the established TRPV4 activator 4αPDD evoked Ca^{2+} responses in blood vessels, suggesting TRPV4 protein is expressed and functional (Yang *et al.*, 2006). Furthermore TRPV4 is suggested to form a Ca^{2+} signalling complex with RyR and Ca^{2+}-activated K^+ channels in VSM, which is responsible for arterial contraction (Earley *et al.*, 2005). TRPV2 expression has been confirmed in mouse aortic myocytes where it is activated by hypotonic stimulation, suggesting it forms a stretch-activated channel in VSM (Muraki *et al.*, 2003).

In summary, several TRP family members are demonstrated to be expressed, and to have functional roles, in VSM. In order to improve understanding of the role of these multifunctional channels in vascular biology and disease, further investigation is needed to characterise their activation mechanisms, endogenous modulators, and putative interactions with other proteins and signalling complexes. The development of selective pharmacological agents as tools will allow for the investigation and characterisation of existing and novel TRP channels in the vasculature.

Pharmacological agents as channel blockers

Channel blockers are molecules that bind to an ion channel and inhibit the flow of ions through its pore. They may do this directly, or through changing the conformation of the protein to its closed state. Specific inhibitors are essential to characterise ion channels, determine their physiological roles and produce new drugs. Traditionally, ion channel blockers were naturally occurring substances such as toxins. Synthetic ion channel blockers have also proved useful, for example the use of nifedipine was central to distinguishing between VGCC types. Novel channel blockers can be identified through screening vast chemical libraries using high throughput systems.

As well as inhibiting channel function by directly blocking the pore, recent methods can inhibit function by reducing channel expression. One example is small interfering RNA (siRNA), in which small, double stranded sections of RNA interfere with the expression of a gene's complementary DNA through involvement in the RNA interference (RNAi) pathway. siRNA can be transiently transfected or recombinantly expressed in the desired cell type. A drawback is that siRNA has varying effects in different cell types, and can induce non-specific effects such as triggering an immune response. A solution may be to convert siRNA into naturally occurring microRNAs.

TRP channel blockers

There are many existing TRP antagonists that have been used to investigate TRP channel function. A summary of TRP channel agonists and antagonists is presented in Tables 1.1 & 1.2.

Lanthanide ions (Gd^{3+}, La^{3+}) block Ca^{2+} permeable cation channels, and have been used to characterise channels of the TRP family (Halaszovich *et al.*, 2000). Although known to inhibit many TRP family members, micromolar concentrations of lanthanides activate TRPC4 and TRPC5 (Zeng *et al.*, 2004). Although the exact mechanism of inhibition is not understood, Gd^{3+} has been postulated to interact with the lipid membrane to antagonize mechanosensitive channels (Hamill *et al.*, 1996). The imidazole SKF96365 is a known inhibitor of both receptor-mediated and store-operated Ca^{2+} entry, and blocks all TRPC family members except TRPC4, and also TRPV2 (Halaszovich *et al.*, 2000; Inoue *et al.*, 2001).

2-Aminoethoxydiphenylborate (2-APB) inhibits store-operated calcium channels and several TRP isoforms (Xu *et al.*, 2005a). The mechanism by which 2-APB regulates TRP channels is complicated by the fact that inhibition is not a common feature as several TRP channels are unaffected by 2-APB, and interestingly, 2-APB stimulates TRPV1, TRPV2 and TRPV3 (Chung *et al.*, 2004). Inhibition is concentration-dependent, occurs from the extracellular side of plasma membrane only, and exhibits slight voltage-dependence, suggesting that 2-APB disrupts cation flow through the channels either by entering the electric field, or by modulating channel gating (Xu *et al.*,

2005a). It is not known whether stimulation by 2-APB occurs at the same 2-APB binding site, or via a distinct site.

Ruthenium red is a non-selective ryanodine receptor antagonist which blocks all TRPV family members, plus TRPA1 and TRPM6 (Dray *et al.*, 1990; Nagata *et al.*, 2005; Voets *et al.*, 2004b), and also Ca^{2+}-activated K^+ channels (Wu *et al.*, 1999). Ruthenium red is a highly charged inorganic cation and is suggested to block L-type Ca^{2+} channels in guinea-pig isolated ventricular heart cells by interacting with negatively charged pore residues that are involved in Ca^{2+} permeation (Malecot *et al.*, 1998). In TRPV1, inhibition by ruthenium red is dependent upon 4 acidic residues in the pore region of the channel that form a ring of negative charge (Garcia-Martinez *et al.*, 2000). Specifically, mutation of an aspartate residue reduced sensitivity of the channel to ruthenium red blockade, and reduced its permeability to divalent cations. This suggests a direct interaction of the aspartate residue with both divalent cations and ruthenium red, presumably because the spatial arrangement of acidic carboxyl groups creates a high affinity binding site for cationic molecules in the pore. However, the mutation of the aspartate residue did not completely prevent the inhibitory effect of ruthenium red, indicating a contribution of other amino acid residues from the pore region of the channel.

Extracellular application of the non-steroidal anti-inflammatory agent flufenamic acid (FA) inhibits ADPR-induced current in TRPM2-expressing cells (Hill *et al.*, 2004a). This action is not selective, as FA also inhibits TRPM4 and TRPM5, plus TRPC3 TRPC7 and TRPC5, while increasing TRPC6 currents (Inoue *et al.*, 2001; Lee *et al.*, 2003b; Tesfai *et al.*, 2001; Ullrich *et al.*, 2005). Commonly used to treat rheumatoid arthritis, FA also targets chloride channels, voltage activated Na^+ channels, voltage activated K^+ channels, and $GABA_A$ receptors (Naziroglu *et al.*, 2007). Prolonged application of FA produced irreversible inhibition of TRPM2, suggesting a conformational change in the TRPM2 protein occurs, rather than direct binding and blockade of the pore. The imidazole antifungal agents clotrimazole (1-[(2-chlorophenyl) diphenylmethyl]-1H-imidazole) and econazole (1-[2-[4-chlorophenyl) methoxy]-2-(2,4-dichlorophenyl) ethyl]-1H-imidazole) have also been described as TRPM2 blockers (Hill *et al.*, 2004b). Again these agents are irreversible and non specific, as econazole has also been shown to inhibit TRPV5 (Nilius *et al.*, 2001).

In addition, both ADPR-induced currents and H_2O_2-induced Ca^{2+}-entry can be inhibited by the PLA_2 inhibitor *N*-(*p*-amylcinnamoyl)anthranilic acid (ACA) (Kraft *et al.*, 2006). Other PLA_2 inhibitors and intracellularly applied ACA were ineffective, suggesting that the block is independent of PLA_2 inhibition. ACA also inhibited both menthol-induced TRPM8 current and AlF_4^--induced TRPC6 current, proving it is not selective. Inhibition by ACA was accelerated by decreasing pH therefore it would appear that ACA, a weak acid at higher pH7.4, is more effective in its uncharged state. Inhibition is likely to be due to modulation of channel gating as channel open probability was reduced and the block was not voltage dependent (Kraft *et al.*, 2006).

TRPC6 is also inhibited by the myosin light chain kinase (MLCK) inhibitor, 1-(5-chloronaphthalene-1-sulphonyl)homopiperazine (ML-9). Inhibition occurs regardless of which side of membrane it is applied, and is independent of MLCK as other MLCK inhibitors had no effect. ML-9 also inhibits TRPC5 but activates TRPC7 (Shimizu *et al.*, 2006).

Polyamines including putrescine, spermidine, spermine, and the synthetic polyamine philanthotoxin-343 (PhTX-343) cause irreversible, dose-dependent block of TRPM7 The voltage-dependence of the inhibition indicates a blocking site within the electric field of the ion channel, accessible from the extracellular side only, thus causing disruption of cation flow through the pore (Kerschbaum *et al.*, 2003). Spermine also blocks TRPM5 and the long splice variant TRPM4b (Nilius *et al.*, 2004a; Ullrich *et al.*, 2005).

The TRPV1 antagonists capsazepine, BCTC, and iodo-resiniferatoxin (I-RTX) are suggested to share the same binding pocket with the potent agonists capsaicin and resiniferatoxin (RTX) at transmembrane domains 2–3 of TRPV1 (Jordt *et al.*, 2002; Valenzano *et al.*, 2003). These compounds are similar in that they share a relatively polar aromatic head group linked to a hydrophobic tail group. However, capsazepine can also inhibit proton activation of the channel, suggesting a more general disruption of channel gating (Tominaga *et al.*, 1998). N-(4-tertiarybutylphenyl)-4-(3-cholorphyridin-2-yl)tetrahydropyrazine-1(2H)-carboxamide (BCTC) and iodo-resiniferatoxin (I-RTX), an analogue of the potent TRPV1 activator resiniferatoxin (RTX), also inhibit TRPV1 (Bevan *et al.*, 1990). Many of these agents are non-specific, and BCTC, thio-BCTC and capsazepine have been shown to block the TRPM8 menthol

response, while I-RTX and capsazepine had no effect (Behrendt *et al.*, 2004). Residues necessary for binding these antagonists may be conserved between these two channels, as the predicted capsaicin binding region of TRPV1 shares 36% sequence homology with the equivalent region in TRPM2.

The epithelial Na^+ channel blocker amiloride also inhibits TRPC6, TRPC7, TRPA1, TRPML1 and TRPP2 (Nagata *et al.*, 2005). Amiloride and its analogues block by interacting with an extracellular part of the channel that is outside of the electric field of the pore (Rusch *et al.*, 1994). TRPC members TRPC3, TRPC5 and TRPC6 can be inhibited by the Na^+/Ca^{2+} exchange inhibitor KB-R7943, although the mechanism for this block is not established (Kraft, 2007).

It is clear that existing TRP antagonists lack specificity, and cannot distinguish between members of the same TRP subfamily, or even between different ion channels. However, the differential modulation of different TRP members by compounds such as lanthanides, 2-APB and FA can be exploited, and it is possible to use a combination of non-specific blockers in order to identify some TRP isoforms in native cells. For further, specific characterisation of these channels, selective tools must be developed.

Name	Agonists	Antagonists
TRPC1	Store depletion, membrane stretch	Gd^{3+}, La^{3+}, SKF96365, 2-APB
TRPC2	DAG	
TRPC3	Store depletion, DAG	Gd^{3+}, La^{3+}, SKF96365, 2-APB, KB-R7943
TRPC4	Store depletion, CaM antagonists	La^{3+}(mM), 2-APB
TRPC5	Gd^{3+}& La^{3+}(μM), S1P, LPC, protons, store depletion	La^{3+} (mM), SKF96365, 2-APB, CaM antagonists, KB-R7943, ML-9
TRPC6	AlF_4^-, DAG, flufenamic acid, PIP_3	Gd^{3+}, La^{3+}, SKF96365, 2-APB, amiloride, ACA, KB-R7943, ML-9
TRPC7	Store depletion, DAG, ML-9	La^{3+}, SKF96365, amiloride
TRPV1	Heat (43°C), PIP_2, vanilloids, anandamide, camphor, piperine, allicin, ethanol, eicosanoids, nicotine, protons, 2-APB	BCTC, capsazepine, ruthenium red
TRPV2	Heat (52°C), cell swelling, 2-APB	La^{3+}, SKF96365, ruthenium red
TRPV3	Heat (>33°C), PUFAs, menthol, camphor, 2-APB	Ruthenium red
TRPV4	Constitutively active; heat (>27°C), cell swelling, 4αPDD, PMA, epoxyeicosatrienoic acids	Gd^{3+}, La^{3+}, ruthenium red
TRPV5	Constitutively active	Gd^{3+}, La^{3+}, ruthenium red, econazole
TRPV6	Constitutively active; store depletion, 2-APB potentiates	La^{3+}, ruthenium red
TRPA1	Cold (17°C), icilin, isothiocyanates, allicin, cinnemaldehyde, acrolein, cannaboids, membrane stretch, DAG, PUFAs	Gd^{3+}, ruthenium red, menthol, gentamicin, amiloride
TRPML	Constitutively active; activity enhanced by Ca^{2+}, pH, NAADP	Amiloride
TRPP2	Constitutively active; activity enhanced by Ca^{2+}, PIP_2	Gd^{3+}, La^{3+}, amiloride, 2-APB, activity suppressed by TRPP1
TRPP3	Constitutively active; activity enhanced by Ca^{2+}	Gd^{3+}, La^{3+}, flufenamic acid

Name	Agonists	Antagonists
TRPM1	Constitutively active	Gd^{3+}, La^{3+}
TRPM2	Intracellular ADPR, NAD, Ca^{2+}, arachadonic acid, H_2O_2	Flufenamic acid, econazole, clotrimazole, ACA
TRPM3	Constitutively active; activity enhanced by store depletion, cell swelling, sphingolipids	Gd^{3+}, La^{3+}, Mg^{2+}, 2-APB
TRPM4	Ca^{2+}, voltage modulated, PIP_2	Intracellular nucleotides, flufenamic acid, spermine
TRPM5	Heat (15-30°C), Ca^{2+}, voltage modulated, PIP_2	Flufenamic acid, spermine, H^+
TRPM6	Constitutively active	Mg^{2+}, ruthenium red
TRPM7	ATP, protons, activation of PKA, PIP_2	Mg^{2+}, La^{3+}, spermine, H^+, 2-APB
TRPM8	Cold (<26°C), menthol, icilin, PIP_2	La^{3+}, BCTC, capsazepine, ACA, 2-APB

Table 1.1. Pharmacology and regulation of TRP channels Mechanisms of action discussed further in main text.

Antibodies as channel blockers

Antibodies are immunoglobin proteins of the immune system that recognise and neutralise foreign objects, known as antigens. They are synthesised and secreted by plasma cells derived from immune system B cells as part of the humoral immune response. B cells can recognise and engulf an antigen, and present MHC molecules on their surface to attract a matching T cell. T cells then secrete cytokines to activate the B cells, causing them to proliferate and differentiate into antibody secreting plasma cells. When the secreted antibodies bind the target antigen, they mark it for destruction by killer T cells.

Antibody structure

Antibodies are Y-shaped, and consist of 4 polypeptide chains connected by disulphide bonds. There are 2 identical heavy chains (~50 kDa) and 2 identical light chains (~25 kDa), divided into constant and variable regions (Figure 1.6). The variable regions form the antigen-binding site, and are responsible for the antibody's specificity. The antigen-binding sites are identical, and are each complementary to a small area on the surface of the antigen molecule. They are formed from several loops of polypeptide chain that can be mutated to change the amino acid sequence, without changing the basic antibody structure, allowing for huge diversity. The constant regions determine immune function, and are used to divide antibodies into 5 major classes, IgA, IgD, IgE, IgG and IgM. Following exposure to antigen, IgM are produced, and after ~10 days, IgG are produced. This is referred to as the primary immune response. If the immune system is exposed to the antigen for a second time, B cells will remember the antigen, and launch a secondary immune response.

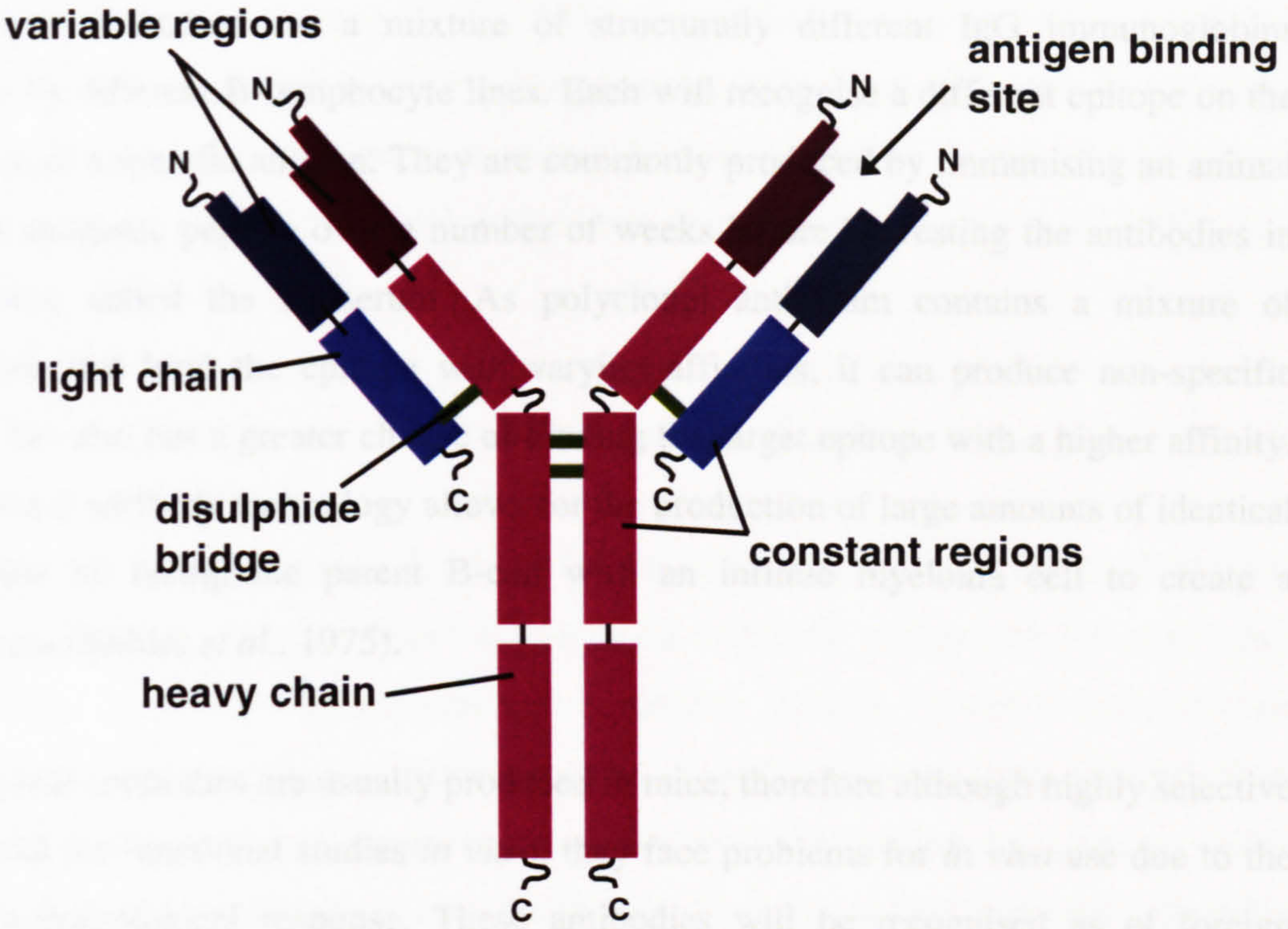

Figure 1.6. Structure of immunoglobulin type G (IgG) The 'Y' shaped IgG molecule consists of 2 'heavy' chains composed of 4 domains, and 2 'light' chains composed of 2 domains. The N-terminal variable regions of both the heavy and light chains form the antigen binding sites.

Polyclonal and monoclonal antibodies

Polyclonal antibodies are a mixture of structurally different IgG immunoglobins secreted by different B-lymphocyte lines. Each will recognise a different epitope on the sequence of a specific antigen. They are commonly produced by immunising an animal with an antigenic peptide over a number of weeks before harvesting the antibodies in the serum, called the antiserum. As polyclonal antiserum contains a mixture of antibodies that bind the epitope with varying affinities, it can produce non-specific effects, but also has a greater chance of binding the target epitope with a higher affinity. Monoclonal antibody technology allows for the production of large amounts of identical antibodies by fusing the parent B-cell with an infinite myeloma cell to create a hybridoma (Kohler *et al.*, 1975).

Monoclonal antibodies are usually produced in mice, therefore although highly selective and useful for functional studies *in vitro*, they face problems for *in vivo* use due to the host's immunological response. These antibodies will be recognised as of foreign origin, and provoke a human anti-murine Antibody (HAMA) immune response in human subjects. This would result in rapid destruction and removal of the antibodies, probably long before they exerted their intended effect. The host response can be reduced through the use of chimeric antibodies, produced by transgenic fusion of immunoglobin genes to produce an IgG molecule with variable regions from the host animal, and human constant domains. Antibodies that are completely human in origin are much more difficult to obtain. However, recent developments have allowed for the production of humanised antibodies, which are produced by combining only the mouse complementarity-determining region with a human IgG molecule, to further reduce HAMA. Such antibodies are produced by selection from phage-display libraries of human antibody fragments, or from the immunisation of transgenic mice (Brekke et al., 2003). Another approach is the use of 'intrabodies', where DNA encoding an antibody is delivered into the cell, however this method faces problems of cellular delivery common with techniques such as siRNA (Lobato et al., 2003).

Antibodies are large, poorly soluble, and unstable unless stored correctly. The solubility of antibodies can be improved by cleaving the protein into Fab and Fv fragments. However, these antibody fragments are less immunogenic, less stable, and are prone to proteolysis and aggregation. The solution to this problem may be the use of nanobodies,

fragments of antibodies discovered in camels that contain only the heavy chain, yet have evolved to be fully functional, stable, and display a strong affinity for their target antigen (Hamers-Casterman *et al.*, 1993). Nanobodies show potential as novel agents for the treatment of certain cancers. Nanobodies can be fused with specific enzymes and targeted to cancer cell receptors in mice, where they function to convert a pro-drug to a toxic chemical that kills any cells in the immediate vicinity (Revets *et al.*, 2005).

Antibodies in disease

Autoimmune disease results from the failure of the host to recognise 'self' molecules, thus inducing an immune response against its own cells and tissues. Examples include rheumatoid arthritis, myasthenia gravis, coeliac disease, diabetes mellitus type 1, psoriasis, systemic lupus erythematosus, multiple sclerosis and Graves' disease. Myasthenia gravis is a neuromuscular disease characterised by muscle weakness. Weakness is typically caused by antibodies directed against nicotinic acetylcholine receptors at the post-synaptic neuromuscular junction. These antibodies cause inhibition of acetylcholine-induced muscle contraction, either by preventing ACh binding, or by marking the receptor for internalisation. While myasthenia gravis is an autoimmune disease and features antibodies directed against 'self' proteins, there is no known causative pathogen. A second category of myasthenia gravis results from autoantibodies targeted against muscle specific kinase (MuSK) a tyrosine kinase receptor involved in the formation of the neuromuscular junction. Antibodies inhibit MuSK binding its ligand, agrin.

Antibodies as tools

Antibodies can be engineered to recognise any number of surface-expressed proteins, allowing for their use in a multitude of experimental procedures. Commonly, purified antibodies are used to detect proteins present in a particular lysate using ELISA or Western blotting methods, or to examine protein localisation and expression in different cell and tissue types using immunohistochemistry. In addition, the high specificity an antibody displays for its target antigen, plus the ability to eliminate the antigen from the body, makes antibodies attractive as biological tools and therapeutic agents. Such

therapeutic antibodies can selectively block the action of a molecule, target specific cells, and even deliver other agents to target cells so they can exert their effect (Brekke et al., 2003). More recently, antibodies have been recognised as specific ion channel blockers, and have demonstrated functions for these particular channel proteins (Dallas et al., 2005).

Antibodies targeted to particular ionotropic neurotransmitter receptor subunits have been shown to modulate the function of the receptor. In particular, antibodies targeted to extracellular regions of neuronal nicotinic acetylcholine receptors, and $P2X_2$ or $P2X_4$ in rat neurones, inhibit ACh- and ATP-evoked currents respectively. Conversely, extracellularly targeted antibodies to $P2X_7$ and $GABA_A$ receptors increased the maximum current amplitude evoked by agonist application (Ekema *et al.*, 2001; Kim *et al.*, 2001). Antibodies targeted to the extracellular N-terminus of STIM1 in the plasma membrane inhibited Ca^{2+} entry via arachidonic acid-regulated Ca^{2+}-selective channels, suggesting a role for STIM1 in the plasma membrane that is independent of store-operated Ca^{2+} entry (Mignen *et al.*, 2007). A polyclonal antibody targeted to the C-terminal functional domain of TRPML1 inhibited channel activity, and was used to demonstrate TRPML1 forms a lysosomal NAADP-sensitive Ca^{2+} release channel (Zhang *et al.*, 2007).

E3 targeted antibodies

Antibodies targeted to the 3rd extracellular loop (E3) of ion channels function as highly selective blockers of Ca^{2+} flux and current through the channel, and can be used to elucidate physiological function of the protein. Currently there are 8 E3-targeted antibodies. The first study to develop a specific antibody-blocker demonstrated that polyclonal antibodies targeted to the voltage-gated K^+ channels $K_v1.2$ and $K_v3.1$ inhibited whole cell currents, and established that $K_v1.2$ in particular is functional in neuronal cells (Zhou *et al.*, 1998). Polyclonal antibodies have also proven successful as inhibitors of the voltage gated Na^+ channel, $Na_v1.5$, plus the TRP channel TRPV1 (Klionsky *et al.*, 2006; Xu *et al.*, 2005b). There are fewer studies where monoclonal antibodies have been successful as channel blockers. Monoclonal antibodies demonstrated specific inhibition of the voltage-gated K^+ channel hEag1, implicating a function for the channel in modulating tumour cell growth (Gomez-Varela *et al.*, 2007).

Furthermore, E3-targeted antibodies have been used to elucidate physiological roles for TRP channels expressed in the vasculature. T1E3, directed against the E3 of TRPC1, initially revealed a role for TRPC1 as a store-operated Ca^{2+} channel of vascular smooth muscle (Xu *et al.*, 2001). Further studies shown TRPC1 upregulation as a feature in the SMC proliferation that underlies neointimal hyperplasia, a key player in occlusive vascular disease (Kumar *et al.*, 2006). Importantly, T1E3 significantly reduced neointimal growth in cultured human vein sections, suggesting that such selective TRPC1 blockers have potential in the prevention of vascular failure. A second anti-TRPC1 antibody targeted to a different sequence in E3 is commercially available (Alomone Laboratories, Israel). This antibody is also an effective blocker of the TRPC1 channel, and has been shown to inhibit Ca^{2+} entry in platelets, suggesting TRPC1 is necessary for the normal response of platelets to agonists that induce SOCE (Rosado *et al.*, 2002). The blockade of TRPC5 current using the E3-targeted T5E3 antibody proved a functional role for the channel in SOCE in rabbit pial arterioles, and in a separate study by the same authors suggested a role for TRPC5 in VSMC motility (Xu *et al.*, 2006a; Xu *et al.*, 2006b).

Aims of the thesis:

1. To develop an isoform-specific blocker of TRPM3 to use in functional experiments.

2. To determine the expression and function of TRPM3 in vascular smooth muscle.

3. To identify novel modulators of the TRPM3 channel.

Chapter 2

Materials and Methods

General Solutions

Solutions were prepared in MilliQ water and adjusted to pH 7.4 using 4 M NaOH unless otherwise stated. Solutions used in cell culture or microbiology were sterilised by autoclaving prior to use.

Standard bath solution: 130 mM NaCl, 5 mM KCl, 10 mM HEPES, 8 mM D-glucose, 1.2 mM $MgCl_2$ and 1.5 mM $CaCl_2$. Osmolarity is kept between 290 and 310 mOsm with mannitol.

Balanced salt solution: 125 mM NaCl, 5.4 mM KCl, 16 mM $NaHCO_3$, 0.8 mM $MgCl_2$, 5.5 mM D-glucose, 20 mM HEPES, 0.75 mM NaH_2PO_4, 1.8 mM $CaCl_2$, 0.1% BSA.

Phosphate Buffered Saline: 2.5 mM Na_2HPO_4, 9 mM NaH_2PO_4 and 154mM NaCl.

PBS/Tween-20: 0.05 % Tween-20 in PBS.

Chemicals

General salts were purchased from Sigma, UK.

Compound stocks were stored at -20°C unless otherwise stated. Thapsigargin (Calbiochem) was stored at a stock concentration of 1 mM in DMSO. Adenosine 5'-triphosphate disodium salt (Sigma, UK) was stored at a stock concentration of 100 mM in H_2O. Verapamil hydrochloride (Sigma, UK) was stored at a stock concentration of 10 mM in H_2O. D-*erythro*-sphingosine C18 (Sigma, UK or Matreya, US), D-*erythro*-

dihydro-sphingosine (Sigma, UK) and D-*erythro*-N,N-dimethyl-sphingosine (Calbiochem) were stored at stock concentrations of 20 mM and 100 mM in ethanol. Glucosylsphingosine (psychosine) from bovine brain (Sigma, UK) was stored at a stock concentration of 50 mM in methanol. Pregnenolone sulphate (Sigma, UK) was stored as a stock concentration of 100 mM in DMSO. Progesterone, 5β-pregnan-3α-OL-20-one (pregnanolone), 5α-pregnan-3α-OL-20-one and 5-pregnan-3β-OL-20-one (all Sigma, UK) were stored as stock concentrations of 25 mM and 50 mM in DMSO. 3β-hydroxy-5α-pregnan-20-one (isoallopregnanolone, Sigma, UK) was stored as a stock concentration of 25 mM in MeOH. (±)-*S*-nitroso-*N*-acetylpenicillamine (Calbiochem) and N^G-Nitro-L-arginine methyl ester hydrochloride (Sigma, UK) were stored at stock concentrations of 100 mM in DMSO. 5-cholesten-3β-ol-7-one (7-ketocholesterol, Sigma, UK) and 7-β-hydroxycholesterol (Sigma, UK) were stored at stock concentrations of 50 mM in ethanol. Water soluble cholesterol (Sigma, UK) and methyl β-cyclodextrin (Sigma, UK) were added to recording solutions directly just before use. Hydrogen peroxide (Sigma, UK) was supplied as a 30% (w/w) solution and stored at 4°C. Gadolinium and carbachol were stored at stock concentrations of 100 mM in water at room temperature. 4α-phorbal-12,13-didecanoate (Calbiochem) was stored at a stock concentration of 50 mM in DMSO. L-α-lysophosphatidylcholine C16:0 (Sigma, UK) and L-α-lysophosphatidylinositol C16:0 soybean extract (Avanti Lipids, US) were stored at stock concentrations of 50 mM in methanol. Tumour necrosis factor-α (TNFα, human) (Sigma, UK) and 12-*O*-tetradecanoylphorbol 13-acetate (TPA), (Sigma, UK) were stored at stock concentrations of 10 μg ml^{-1} and 1 mM respectively, in H_2O.

The final concentration of vehicle in solutions was never more than 0.1%. For dose response curves, stock concentrations were further diluted in vehicle before addition to the bath solution at 1:1000 to keep the final vehicle concentration constant.

High-throughput compound screen

The following chemicals were stored at stock concentrations of 10-100 mM at -20°C. All were purchased by AstraZeneca from Sigma, UK, unless otherwise described:

Lipid screen (10 mM stocks in ethanol) - D-*erythro*-sphingosine, dihydro-D-*erythro*-sphingosine, sphingomyelin (bovine brain), L-*threo*-Dihydrosphingosine,

sphingosylphosphorylcholine[#], sphingosine-1-phosphate[†], N,N-dimethyl-D-*erythro*-sphingosine [#], C2 ceramide[†], C8 ceramide[†], C8 ceramide-1-phosphate[†], carbacyclin, palmitic acid, α-lipoic acid, stearic acid, 1-O-Octadecyl-2-O-methyl-*sn*-glycero-3-phosphorylcholine, methanandamide, arachadoinc acid[†], L-α-Lysophosphatidylcholine (egg yolk), platelet-activating factor 16[#], lyso-platelet activating factor 16[#], platelet-activating factor 16 antagonist[#], platelet-activating factor 18[#], lyso-platelet activating factor 18[#], ginkolide A[#], hepoxillin A3[#], Rev 5901[†], Rev 5901 paraisomer[†], misoprostol, leukotriene B_4[†], leukotriene C_4[†], leukotriene D_4[†], leukotriene E_4[†], prostaglandin A_2[†], prostaglandin B_2[†], prostaglandin D_2[†], prostaglandin E_1[†], prostaglandin E_2[†], prostaglandin $F_{2\alpha}$[†], prostaglandin I_2[†], prostaglandin K_1[†], 15-deoxy-$\Delta^{12,14}$-Prostaglandin J_2 (15d-PGJ_2)[†], 9,11-dideoxy-9α,11α-methanoepoxy Prostaglandin $F_{2\alpha}$ (U-46619)[†], carbocyclic thromboxane A_2[†], thromboxane B_2[†], carbaprostacyclin[†], sulprostone[†], AH6809[†], BW245C[†], trans-BTP Dioxolane[†], L-α-lysophosphatidic acid[†], 8(S),15(S)-Dihydroxy-Eicosa-5,8,11,17-Tetraenoic Acid (DiHETE)[†], 5(S),15(S)-DiHETE[†], 5(S), 6(R)-DiHETE[†], 15(S)-DiHETE[†], 12(R)-DiHETE[†].

[#] purchased from Calbiochem, UK.

[†] purchased from the Cayman Chemical Company.

Lipid screen (10 mM stocks in DMSO) - Cholesterol, cholesterol esterase, lipase, ß-cyclodextrin, oleic acid, linoleic acid, dihydrolipoic acid, lipase, phosphatidylinositol 4,5-bisphosphate disodium salt.

Peptide screen (10 mM stocks in DMSO) - Angiotensin II acetate (human), endomorphin I, luteinizing hormone releasing hormone acetate salt (human), melanin concentrating hormone (rat), bradykinin acetate, Substance P acetate salt hydrate, [Arg^8]-vasotocin acetate salt, [Arg^8]-vasopressin, bombesin acetate hydrate , oxytocin acetate salt hydrate, thyrotropin releasing factor (Calbiochem).

Small molecule screen (100 mM stocks in DMSO) - 1-(4-methanesulphonamidophenoxy)-3-(N-methyl-3-4-dichlorophenethylamino)-2-propanol benzoic acid salt (AM 92016), amiloride hydrochloride, 4-aminopyridine, amiodarone hydrochloride, 2-aminoethyl diphenylborinate, amitriptyline hydrochloride, anandamide, antozoline hydrochloride, benzocaine, benzyl isothiocyanate, bepridil hydrochloride, bisindolylmaleimide I, bupivacaine, calmidazolium chloride, canrenoic acid potassium salt, capsaicin, carbamazepine, chloroquine diphosphate, (+)-

chlorpheniramine maleate, chlorpromazine hydrochloride, chromanol, cinnamaldehyde, citalopram hydrobromide, clotrimazole, 1-benzyl-4-pentylimino-1,4-dihydroquinoline hydrochloride (CP 339818), dexamethasone, 4,4′-Diisothiocyanatostilbene-2,2′-disulfonic acid disodium salt hydrate (DIDS), 5,5-diphenylhydantoin, diphenhydramine, doxepin hydrochloride, epigallocatechin-3-gallate, erythromycin, ethosuximide, felodipine, flecainide acetate, fluoxetine hydrochloride, fluspirilene, fluvoxamine maleate, gabapentin, haloperidol, imipramine hydrochloride, indapamide, ketoconazole, lamotrigine, lidocaine, linopirdine, loperamide hydrochloride, menthol, mepivacaine, (±)-methoxyverapamil hydrochloride, mexiletene hydrochloride, mibefradil dihydrochloride, N-(6-aminohexyl)-5-chloro-1-naphthalenesulfonamide hydrochloride, N-acetylprocainamide hydrochloride, nicardipine hydrochloride, nicotine, nifedipine, niflumic acid, nimodipine, nisoldipine, nitrendipine, nortriptyline, papaverine hydrochloride, perhexiline maleate salt, 3-phenyl-1-pyrolidin-1-yl-propenone, procainamide, propafenone hydrochloride, quinidine sulphate, QX222, QX314, R(+)-SCH-23390 hydrochloride, RCL R41,038-1, riluzole, ruthenium red, l-*β*-[3-(*p*-methoxyphenyl)-propyloxy]-*p*-methoxyphenetyl-1H-imidazole-hydrochloride (SK&F 96365), (±)-solatol hydrochloride, spironolactone, SR 33805, (±)-sulpiride, tetraethylammonium chloride, thioridazine hydrochloride, tocainide, triamterene, venlafaxine, verapamil, vinpocetine.

β-cyclodextrin and methyl β-cyclodextrin were stored at stock concentrations of 10 mM in 1 M NaOH at room temperature. When added to bath solution, the pH was adjusted back to 7.4 with 1 M HCl.

The final concentration of vehicle in solutions was never more than 0.5%. For dose response curves, stock concentrations were further diluted in vehicle before addition to bath solution at 1:1000 to keep the final vehicle concentration constant.

TRPM3 cDNA and transformation of competent cells

Luri-Bertani (LB) medium: 1% tryptone, 0.5% yeast extract, 170 mM NaCl, pH 7.0.

LB-amp Agar plates: 1% agar in LB medium supplemented with 50 μg ml^{-1} ampicillin.

Transformation of competent cells

When bacterial cells are treated with calcium chloride they take up water, swell and become competent. Competent cells are capable of absorbing foreign DNA, which they then replicate along with their own, in a process called transformation. TRPM3 cDNA (GenBank accession number AJ505026) was kindly provided by the Harteneck laboratory (Berlin, Germany) as a TRPM3-YFP fusion construct subcloned in the TOPOpcDNA3.1/V5 expression vector (Invitrogen). The coding sequence of YFP was subcloned in-frame by using *Not*I and *Avr*II restriction sites (Grimm *et al.*, 2003). For transformation, approximately 20 ng of plasmid DNA was added to 100 μl of ice-thawed XL-GOLD Supercompetent cells (Stratagene), gently mixed, and incubated on ice for 30 minutes. The cell mixture was heat shocked at 42°C for 45 seconds to induce DNA uptake, followed by further incubation on ice for 1 minute. The mixture was then streaked onto LB-amp plates and incubated overnight at 37°C to allow the growth of bacterial colonies. The pcDNA3.1 vector contains the ampicillin resistance (amp^r) gene which encodes β-lactamase, an enzyme that detoxifies ampicillin by catalysing the hydrolysis of an integral β-lactam ring. This allowed for selection of successfully transformed bacteria containing pcDNA3.1 that were able to grow on the LB-amp plates. A single colony was selected in order to isolate DNA from transformed bacterial cells.

DNA preparation

5 ml aliquots of LB media supplemented with 50 μg ml^{-1} ampicillin were inoculated with a single colony transformed with TRPM3 plasmid DNA as described, and incubated overnight at 37°C, 200 rpm. The resulting cultures were used immediately for

small-scale DNA preparation using a Plasmid Mini Kit (Qiagen) or diluted 1:100 in LB-medium for large-scale DNA preparations according to manufacturer's instructions. The mini-prep construct was analysed by restriction mapping and sequenced in forward and reverse directions to confirm the DNA in the preparation was TRPM3 before large-scale preparation using the Endofree Plasmid Maxi Kit (Qiagen). The EndoFree Plasmid Maxi Kit has an extra endotoxin removal step to remove lipopolysaccharides. Such endotoxins are present in bacterial lysates and can affect transfection of the plasmid DNA by competing for transfection reagent. The maxi-prep DNA was sequenced fully before storage at -20°C.

Restriction mapping of DNA

Restriction enzymes can be used to specifically cleave phosphodiester bonds within DNA at a particular sequence of bases. Restriction enzymes *Sca*I and *Nde*I (New England Biolabs) were used in conjunction with the manufacturers recommended buffers (NE buffers 3 and 4 respectively) to cleave DNA. An individual 10 µl reaction comprised TRPM3 DNA (1.5 µg), buffer (1 µl), and restriction enzyme (1 µl) and were incubated for 1 hour at 37°C. *Sca*I was predicted to cleave DNA twice (both the vector and TRPM3) to produce 2 DNA fragments approximately 6.6 kb and 4.3 kb. *Nde*I was predicted to cleave once to produce a single DNA fragment approximately 10.0 kb. Restriction enzyme DNA digests were analysed by agarose gel electrophoresis and were as predicted, confirming the mini-prep DNA was TRPM3.

Agarose gel electrophoresis

TAE buffer:	40 mM TRIS base, 1.14% v/v glacial acetic acid, 0.1mM ethylenediaminetetraacetic acid (EDTA).
2% Agarose-EtBr gel:	0.5 g electrophoresis grade agarose in 25 ml 1 x TAE; the mixture was heated in a microwave until dissolved, and 2 µl ethidium bromide (EtBr) was added before pouring.

DNA samples were analysed by separation alongside a marker lane on a 2% agarose gel containing ethidium bromide. Ethidium bromide intercalates base pairs of DNA and fluoresces when exposed to UV light, allowing visualisation of the DNA. Samples were mixed with 6 x blue/orange loading dye and gels were run at 100 V in an electrophoresis tank (BioRad) containing 1 x TAE buffer. A Benchtop 100bp DNA ladder (Promega), consisting of 11 fragments ranging in size from 100-1000bp in 100bp increments, was included for comparison. The DNA fragments were viewed using a Bio-Rad gel documentation system and Quantity One software (Bio-Rad). The quantity and size of the DNA was estimated by comparison with the intensity and distance travelled by the marker bands.

Automated DNA sequencing

DNA sequencing was performed in forward and reverse directions using universal primers on the mini- and maxi-prep products by Lark Technologies using a high throughput PE Biosystems Sequencer (Applied Biosystems).

Cell culture

Cells were maintained in Dulbecco's Modified Eagle's Medium (DMEM)-F12 + Glutamax-1 (Gibco) supplemented with 10% foetal calf serum (FCS) and 100 units ml^{-1} penicillin-streptomycin (PenStrep), at 37°C in a 5% CO_2 incubator. PenStrep is a broad spectrum bacteriostatic and bacteriocidal with activity against both gram negative and gram positive organisms, and was used in cell culture to prevent infection of the cell media. Cells were grown to confluence (never more than 80%) before passage. Cells were detached from the surface of cell culture flasks (Sarstedt, US) using Trypsin-EDTA solution (Sigma, UK), resuspended in prewarmed media at the appropriate cell density, and transferred to fresh culture flask(s).

Human saphenous vein (HSV) was obtained with local research ethical committee approval. HSV smooth muscle cells were kindly prepared by Dr K. Porter. These primary cells were maintained in DMEM-F12 with 10% FCS and 1% PenStrep and discarded after passage 4.

For long term storage cells were stored under liquid N_2. Cells detached by Trypsin-EDTA were resuspended in an equal volume of cell freezing medium (Sigma) and aliquoted in 1 ml volumes into CryoTube freezing Vials (Nunc, Denmark). Vials were stored at -80°C for 24 hours before transfer into a liquid nitrogen storage container. When required, cells were thawed quickly at 37°C and resuspended in prewarmed media.

Stable cell lines

CHO K1 cells stably expressing human TRPV4 (a kind gift from AstraZeneca) were maintained in Ham's F12 (Gibco) in the presence of 1 mg ml^{-1} G418 (Sigma). G418 is an aminoglycoside antibiotic, similar in structure to neomycin, that blocks polypeptide synthesis in both prokaryotic and eukaryotic cells. It was used for the selection of TRPV4 expressing cells as the CHO-TRPV4 cell line contained the neomycin gene that conferred resistance.

For the stable expression of human TRPM3, human TRPC5 and human TRPM2, the T-REx expression system (Invitrogen, UK) was employed. T-REx is a HEK 293 cell line that stably expresses the tetracycline repressor protein from the blasticidin resistant plasmid pcDNA6/TR, under the control of the human cytomegalovirus (CMV) promoter. These cells can additionally be transfected with a second, zeocin resistant plasmid containing the gene that expresses the protein of interest. This second gene is repressed by the binding of the tetracycline repressor protein. When tetracycline (tet) is present in the cell culture media, it binds the tetracycline repressor protein and stops repression of transcription, allowing rapid expression of the gene of interest. TRPM3 (Genbank accession number AJ505026) minus the YFP tag, or TRPC5 (accesssion number AF0544568) channel DNA was subcloned into the pcDNA4 vector and transfected into T-REx 293 cells (Invitrogen) by F. Zeng (Zeng *et al.*, 2004). The tetracycline-inducible TRPM2 cell line was kindly provided by A. Scharenberg (McHugh *et al.*, 2003). Tetracycline-inducible cell lines (TRPM3, TRPM2 and TRPC5) were maintained in the presence of 250 µg ml^{-1} Zeocin™ (InvivoGen) and 10 µg ml^{-1} Blasticidin S (InvivoGen). To induce TRP channel expression, cells were incubated with 1 µg ml^{-1} tetracycline (Sigma, UK) for 24-72 hours prior to experiments.

For FLIPR experiments, a tetracycline-inducible stable TRPM2 cell line was kindly provided by AstraZeneca. TRPM2 expression was induced by 1 μg ml^{-1} doxycycline (dox), a synthetic derivative of tetracycline, for 24 hours prior to experiments.

Transfection

Preparation of poly-L-lysine coverslips

Sterile glass coverslips were transferred into a 24 well plate and overlaid with 200 μl of 100 μg ml^{-1} poly-L-lysine (Sigma) for 1 hour at 37°C. Coverslips were washed 3 times with PBS and allowed to air dry before use.

Quantification of TRPM3 DNA

The concentration of the EndoFree maxi-preparation of TRPM3 DNA was determined as 1 μg μl^{-1} using a UV 1101 Biotech photometer (WPA, Cambridge, UK).

Transient transfection

Wild-type HEK 293 cells were plated onto poly-L-lysine coated coverslips in a 24-well plate with a final volume of 0.5 ml DMEM and grown to ~80% confluency. TRPM3 cDNA (1 μg) or empty vector was mixed with 36 μl of FuGENE® 6 Transfection Reagent (Roche, UK) and 564 μl OPTIMEM® serum free medium, and incubated for half an hour at room temperature to allow DNA-liposomes to form. The DNA:FuGENE complex (20 μl) was then added directly to cell media within each well. Functional studies were carried out 48 hours after transfection on successfully transfected cells identified by their YFP-fluorescence at an excitation wavelength of 480nm.

Peptide-specific antibody design

Hydropathy Analysis

Hydrophilicity analysis was performed using Lasergene software (DNAStar) to identify transmembrane and surface regions of the TRPM3 protein. The Kyte-Doolittle hydropathy plot uses a 'hydropathy scale', in which each amino acid is given a score between -4.5 and 4.5 (where 4.5 is the most hydrophilic), in order to compare the hydrophilic and hydrophobic properties of the amino acid side chains within a protein (see table). In addition, the computer program assigns a 'window size'; this corresponds to the number of amino acids whose hydrophobicity scores will be averaged in order to produce a smoothed plot, the default window size being 9 amino acids. The computer program calculates an average hydrophobicity score for each assigned window, and these averages are plotted in a Kyte-Doolittle plot in which the y axis represents the hydrophobicity score, and the x axis represents the amino acid position within the protein sequence (Kyte *et al.*, 1982). Although this method only gives a prediction of a protein structure, this was sufficient to identify the amino acid sequence of the putative 3rd extracellular loop of TRPM3.

Antibody generation

TM3E3 polyclonal antiserum was prepared in rabbit to peptide [C]LFPNEEPSWKLA, a region corresponding to the 3rd extracellular loop (E3) of TRPM3 (Figure 2.1). E3 targeting is emerging as a widely reliable method for the design of subtype-specific blocking antibodies for an array of ion channels. The N-terminal cysteine residue of the peptide is not present in the native protein sequence, but was included in order to conjugate the peptide to a carrier protein, keyhole limpet hemocyanin (KLH). KLH is used to increase the antigenicity of a synthesised peptide in order to stimulate an immune response. E3 is considered a good target for antibody production as it is not thought to be glycosylated in the native protein, nor will it have any complicated secondary structure, allowing for good access of the antibody. The antigenic peptide was injected into New Zealand white rabbits initially as a stable emulsion with complete Freund's adjuvant (CFA) (Sigma-Genosys). CFA allows for the slow release of the antigen so it is more readily trapped by macrophages, and contains inactivated

mycobacteria that stimulate both the humoral and cell-mediated immune response. Following the initial immunisation, rabbits were immunised once a week with antigen using incomplete Freund's adjuvant (IFA), which does not contain mycobacteria, for 4 weeks before antiserum collection (Sigma-Genosys). Antiserum refers to the blood from the immunized host that has had red blood cells and clotting proteins removed. Typically antisera contain between 5 and 10 mg ml^{-1} of IgG, with approximately 0.1 mg ml^{-1} of specific antibody (information provided by Sigma-Genosys). Serum taken before the initial injection was retained for use as a negative control (preimmune). Antisera were aliquoted and stored at -20°C or -80 °C for longer periods of time.

Antibody Dialysis

Manufacturers supply custom-made antisera in buffers that contain 0.1% sodium azide to extend the shelf life and protect against bacterial growth; however this can prevent the use of the antibody in some assays. For example, sodium azide is a metabolic poison so may interfere with assays involving cell culture. To remove sodium azide and other small molecules, anti-sera were dialysed against PBS. Dialysis membranes (Scientific Laboratory Supplies Ltd, UK) were cut into 10 cm lengths and boiled for 10 minutes in 0.1 M $NaHCO_3$. Membranes were then washed in distilled water (dH_2O), and boiled for a second time. Finally, membranes were washed in dH_2O and stored at 4°C in 25% ethanol. For antibody dialysis, membranes were removed from ethanol storage and left to soak in PBS until flexible, and then checked for leaks by filling with a small volume of PBS and clamping both ends. The tubing was then filled with 1 ml of preimmune or TM3E3 antiserum, clamped, and placed into a beaker filled with PBS at a volume 500 times that of the sample (500 ml PBS). Samples were left for 48 hours at 4°C, as low temperatures improve antibody stability, with gentle stirring to allow exchange. During this dialysis period, the buffer was changed a total of 3 times. Dialysed samples were aliquoted to sterile eppendorfs and stored at –20°C.

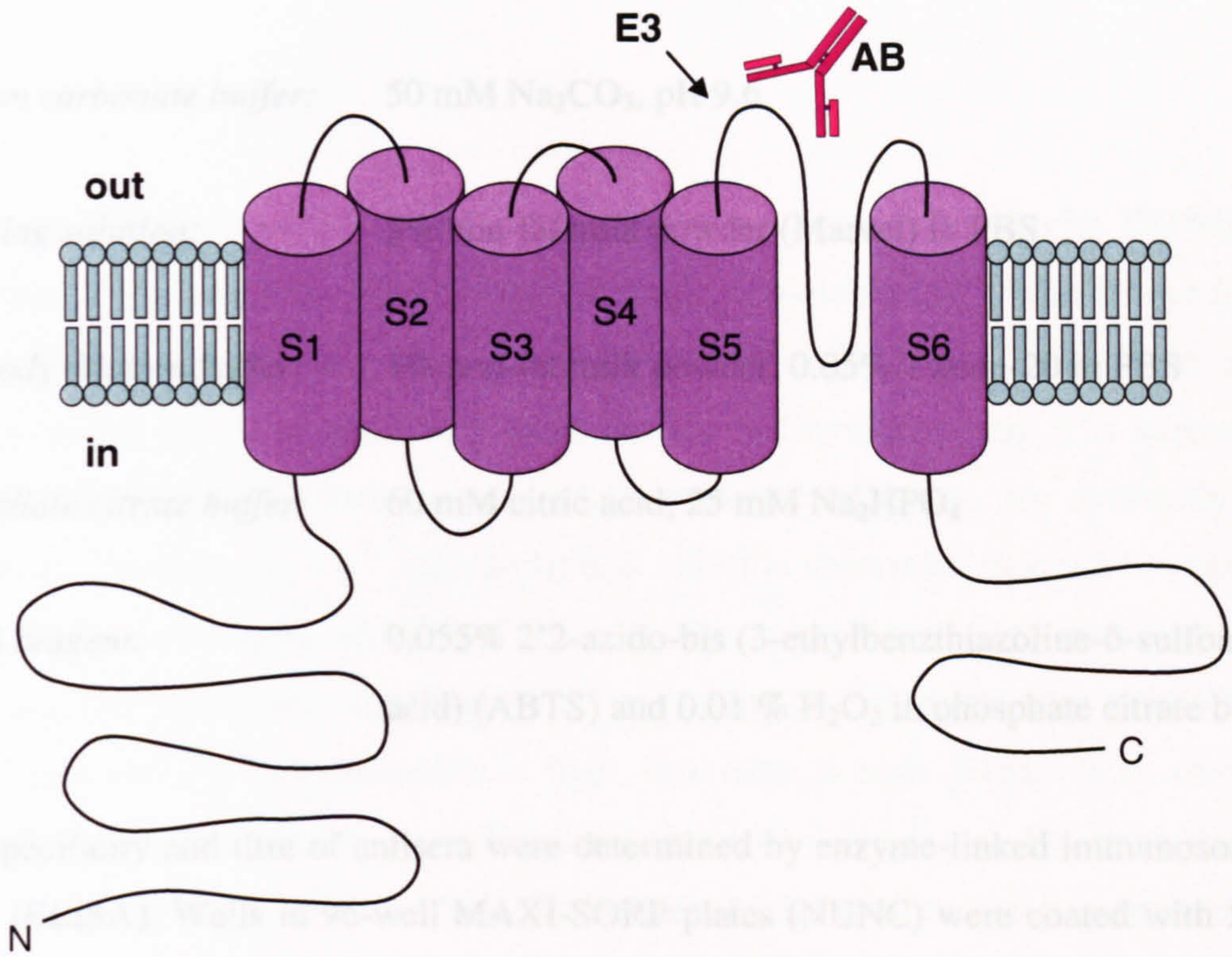

Figure 2.1. E3 Targeting Schematic of an antibody targeted to the 3rd extracellular loop of an ion channel. S1-S6 refer to the 6 transmembrane domains, and the N- and C-termini are indicated by N and C respectively. E3 donates the 3rd extracellular loop, and AB the E3-targetted antibody (not to scale).

Enzyme linked immunosorbant assay

Sodium carbonate buffer: 50 mM Na_2CO_3, pH 9.6

Blocking solution: 5% non-fat milk powder (Marvel) in PBS

Antibody dilution buffer: 1% non-fat milk powder, 0.05% Tween-20 in PBS

Phosphate citrate buffer: 60 mM citric acid, 25 mM Na_2HPO_4

ABTS reagent: 0.055% 2'2-azido-bis (3-ethylbenzthiazoline-6-sulfonic acid) (ABTS) and 0.01 % H_2O_2 in phosphate citrate buffer

The specificity and titre of antisera were determined by enzyme-linked immunosorbant assay (ELISA). Wells in 96-well MAXI-SORP plates (NUNC) were coated with 50 µl of antigenic peptide diluted to 4 µg ml^{-1} in sodium carbonate buffer. No-peptide (NP) control wells were left blank, and plates were incubated overnight at 4°C to allow peptide to adsorb to the well surface. The following day, wells were washed 3 times with PBS/Tween to remove unbound peptide. Blocking solution (300 µl) was added to each well for 1 hour at 37°C to block non-specific adsorption of other proteins to the plate. Following a further PBS/Tween wash, serial dilutions of preimmune and TM3E3 antisera were made in antibody dilution buffer (1:500, 1:1000, 1:2000, 1:4000, 1:8000, 1:16000, 1:32000) and added to corresponding wells. Each dilution was assayed in duplicate. Plates were incubated for 2 hours at 37°C to allow antibody present in the diluted serum samples to specifically bind to its antigenic peptide. Wells were again washed with PBS/Tween, leaving antibody-antigen complexes attached to the well surface. A secondary, enzyme-linked antibody directed against the host animal's immunoglobin, was then applied. Horseradish peroxidase (HRP)-conjugated goat anti-rabbit IgG (Abcam) was added to each well (50 µl) and incubated for 1 hour at 37°C. After a final wash with PBS/Tween, 50 µl of the ABTS reagent was added to each well and plates were incubated for 30 min at room temperature in the dark. This allowed ABTS, the substrate for HRP, to be oxidised in the presence of H_2O_2. Oxidation caused a permanent colour change due to the formation of a green reaction product. The absorbance at 405 nm for each well was read on a plate reader, the intensity of which was directly related to the amount of antibody bound to the surface-bound peptide.

Calcium Imaging

Microscope-based System

Cells were split onto poly-L-lysine coated coverslips and transfected with TRPM3 24-48 hours before recording. The UV-light excitable, ratiometric Ca^{2+} indicator dye fura-2 (Calbiochem) was used to measure intracellular calcium. Fura-2 is supplied as an acetoxymethyl ester that can easily pass into the cell cytosol where it is cleaved by endogenous, non-specific esterases to produce free carboxyl groups that covalently bind Ca^{2+} ions. Upon binding Ca^{2+}, fura-2 displays a shift in absorption that can be observed at excitation wavelengths of 340 and 380 nm. This spectral shift is proportional to the Ca^{2+} concentration. When intracellular Ca^{2+} concentration is low, the ratio of 340/380 is low. When the Ca^{2+} concentration is high, this ratio is high (Figure 2.2). Cells on coverslips were incubated in a non-CO_2 incubator with 4 μM fura-2 AM at 37 °C for 1 hour in standard bath solution (SBS). Exclusion of CO_2 from this step is necessary as SBS is not bicarbonate-buffered, and the diffusion of CO_2 into the buffer would have resulted in acidity. Cells were then washed for half an hour in SBS at room temperature before coverslips were fixed onto the recording chamber with vacuum grease and placed onto the microscope stage. Solutions were continuously perfused over cells in the recording chamber during recordings using a standard perfusion system with a 4 ml min^{-1} flow rate. Fluorescence within cells was observed using an inverted microscope (Zeiss, Germany) through a 40x Fluar oil-immersion objective (numerical aperture, NA = 1.30) with excitation light at 340 and 380 nm provided by a xenon arc lamp, the wavelength of which was controlled by a monochromator (Till photonics, Germany). Emitted light at 510 nm was collected via an emission filter and Fura-2 images were captured every 10 seconds by a CCD camera (Hamamatsu, Japan), for the two excitation wavelengths of 340 and 380 nm, allowing a ratio image to be produced. Imaging was controlled using Openlab 2 software (Image Processing and Vision Company Ltd, UK). Recordings were made alternately from test and control cells at room temperature and analysed offline by selecting regions of interest (ROI). Changes in Ca^{2+} are displayed as changes in the ratio of the emission recorded for both 340 and 380 excitation ($\Delta R_{340/380}$) for Fura-2.

For antibody experiments, anti-sera at the desired dilution were present for 2 hours in the cell culture media, during loading and washing stages, but not during recording.

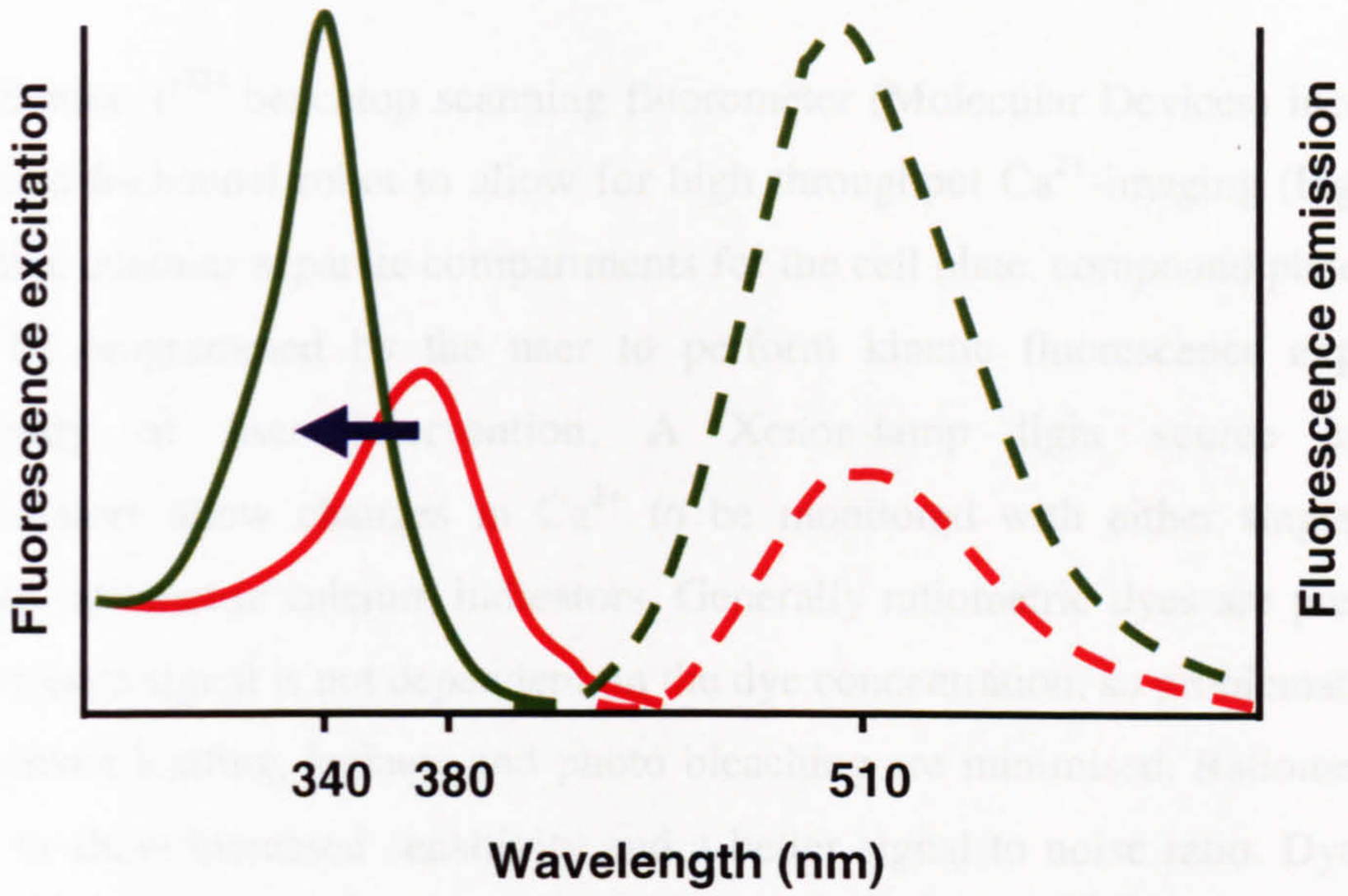

Figure 2.2. Excitation spectrum for Fura-2 Excitation spectra are shown for 340 nm (green) and 380 nm (red) for Fura-2, with emission spectra denoted as a dashed line. The spectrum shifts to the left (shown by arrow) when Ca^{2+} is increased. This spectral shift is proportional to the change in Ca^{2+} concentration.

FlexStation II^{384}

The FlexStation II^{384} benchtop scanning fluorometer (Molecular Devices) incorporates an integrated 8-channel robot to allow for high throughput Ca^{2+}-imaging (Figure 2.3). The machine contains separate compartments for the cell plate, compound plate and tips and can be programmed by the user to perform kinetic fluorescence experiments independently of user intervention. A Xenon-lamp light source and dual monochromators allow changes in Ca^{2+} to be monitored with either single or dual wavelength ratiometric calcium indicators. Generally ratiometric dyes are preferred as the fluorescence signal is not dependent on the dye concentration, so problematic effects such as uneven loading, leakage and photo bleaching are minimised. Ratiometric dyes also tend to show increased sensitivity and a better signal to noise ratio. Dye loading can be improved with pluronic acid (Invitrogen), a non-ionic, surfactant polyol that facilitates the solubilisation of calcium dyes and prevents compartmentalisation. Stable cell lines were cultured in 96-well, poly-D Lysine coated, black walled, clear-bottomed plates (BD Bioscience or Corning), and primary cells were plated into CellBIND (Corning) 96-well plates. Cells in each well were loaded with 50 µl of 4 µM Fura-2 AM in SBS and incubated in the dark at 37°C for 1 hour. Cells were washed for half an hour in 100 µl of SBS, and then filled with SBS so that the final volume of recording buffer in each well was 200 µl. Compound addition to cells resulted in a 1:5 dilution; therefore compound plates (Greiner) were made up at 5 times the required final concentration. Fluorescence emission was recorded every 10 seconds for 340 and 380 nm excitation, with compound addition after at least 1 minute to provide a baseline for analysis. Responses were displayed as the change in the excitation ratio ($\Delta R_{340/380}$), as calculated by SoftMax Pro® software.

Where indicated, thapsigargin (1 µM), verapamil (10 µM) or methyl β-cyclodextrin (10 mM) was present in the bath solution during the washing step. For experiments performed in the absence of extracellular Ca^{2+}, $CaCl_2$ was omitted from standard bath solution, and replaced with 0.4 mM EGTA. For antibody experiments, anti-sera at the desired dilution were present for 2 hours in the cell culture media, during loading and washing stages, but not during recording. For cholesterol enrichment experiments, cholesterol (1 mM) was present during fura-2 loading and for an hour long wash step at 37°C. The TRP channel inhibitors 2-APB (75 µM) and gadolinium (100 µM) were present during the washing step and throughout recordings in the loading buffer.

Figure 2.3. A high throughput fluorimeter Photograph of FlexStation II^{384} benchtop fluorimeter. The cell culture plate (bottom drawer), compound plate (centre) and tips (top) are inserted into the machine, which then performs fluorescent measurements as instructed by SoftMax Pro software. Reproduced from www.moleculardevices.com.

FLIPR

In addition to the FlexStation, a second fluorometric imaging plate reader, the FLIPR system (Molecular Devices), was also used for the high throughput analysis of calcium responses (AstraZeneca). In contrast to the FlexStation, the FLIPR can record fluorescence from each well of a 96-well plate simultaneously; however due to the absence of a xenon light source, can only be used with single wavelength calcium indicators. Unlike ratiometric calcium dyes, for single wavelength indicators the intensity of the fluorescence recorded is dependent on the Ca^{2+} concentration.

Stable TRPM3 cells were cultured in 96-well, poly-D Lysine coated, black walled, clear-bottomed plates (BD Bioscience) for analysis with a FLIPR (Molecular Devices). Cells were counted using a COULTER® A^{c}·T™ Hematology Analyzer and plated at 50,000 cells per well unless otherwise indicated. Tet+ and Tet- cells were included within the same plate for direct comparison. Cells were loaded with 4.5 μM Fluo-4 AM (Sigma) in the presence of 2.5 mM probenecid (Sigma) and 0.01% pluronic acid (Molecular Probes) to facilitate dye loading. Although fluo-4 AM is lipophilic and readily passes across membranes, it will form micelles in aqueous media that can impede its passage. Dye dispersion was enhanced by 0.01% pluronic acid (F-127), a non-ionic detergent that prevents micelle formation, and retention with the addition of 2.5 mM probenecid, an organic anion transport inhibitor that prevents the removal of dye from the cytoplasm (Di Virgilio *et al.*, 1990). Prolonged loading in the presence of pluronic acid decreases dye loading (Maruyama *et al.*, 1989) and was avoided. Cells were washed 3 times with 100 μl SBS, then filled with a final volume of 50 μl. Compound addition (50 μl) to cells resulted in a 1:2 dilution; therefore compound plates were made up at double the required final concentration.

Before recordings, a signal test was performed to indicate loading efficiency, and wells displaying poor loading were disregarded. Fluorescence emission at 516 nm was recorded for an excitation wavelength of 488 nm using one of 2 protocols; Fluorescence measurements for single addition protocols consisted of a baseline of 5 points taken every 2 seconds, followed by compound addition at 10 seconds, a 1st interval of 60 readings every second (total 1 min), followed by a 2nd interval of 60 readings every 5 seconds (total 5 min). For 2 addition protocols, fluorescence measurements consisted of

a baseline of 5 points taken every 2 seconds, followed by test compound addition at 10 seconds, a 1st interval of 15 readings every 2 seconds and a 2nd interval of 40 readings every 5 seconds (total 4 min), followed by second 5 point baseline reading, then addition of the positive control PregS at 4.2 minutes with a 1st interval of 60 readings every second (total 1 min) and a 2nd interval of 20 readings every 5 seconds (total 1.7 min). Total runtime was 6.8 minutes (Figure 2.4).

When necessary, cells were exposed to β-cyclodextrin or methyl β-cyclodextrin in the bath solution for a half hour wash step before the addition of recording buffer. For antibody experiments, anti-sera at the desired dilution were present for 2 hours in the cell culture media, during loading and washing stages, but not during recording.

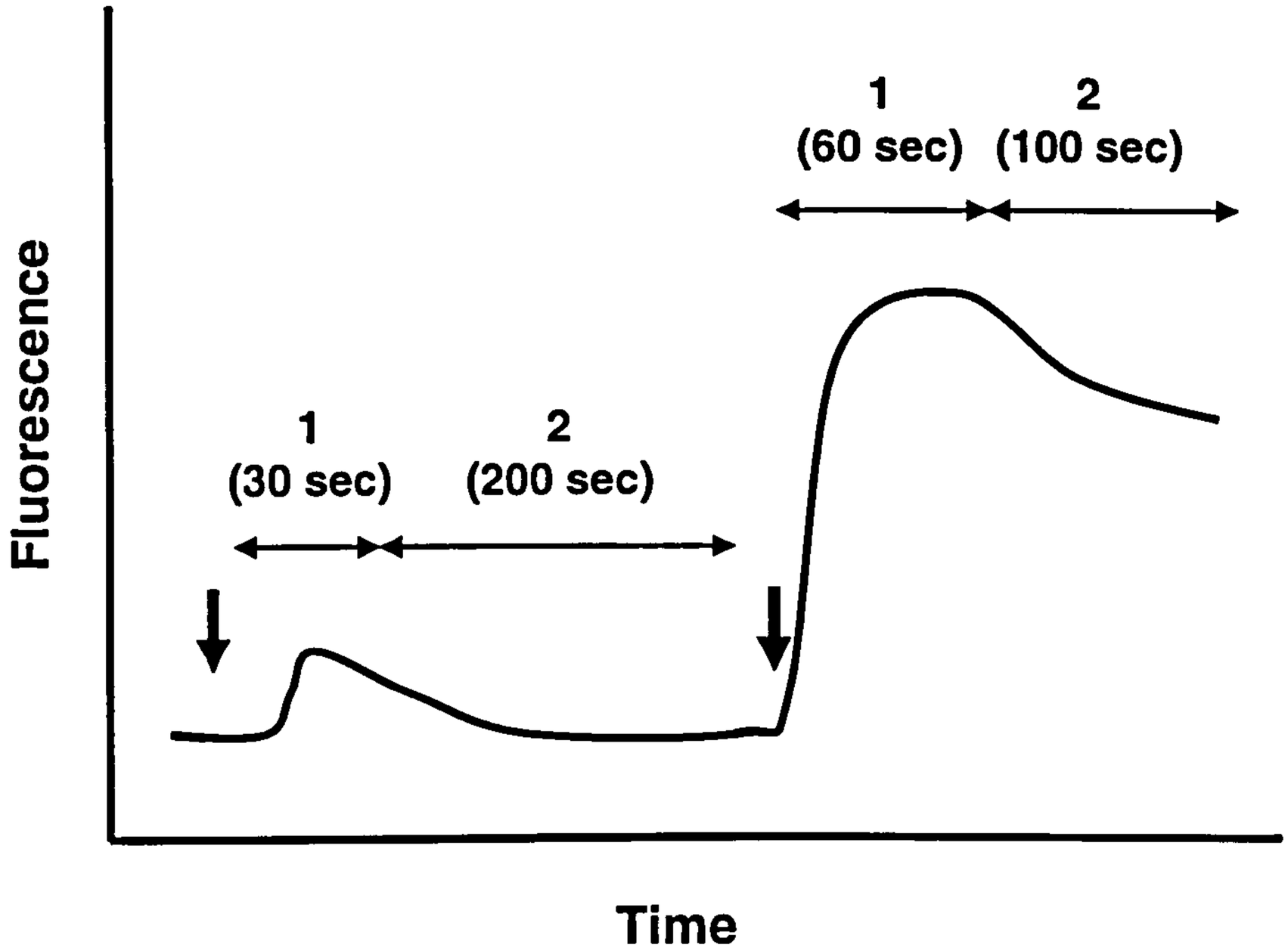

Figure 2.4. FLIPR 2-addition protocol Initial baseline recording indicated in red. Blue arrows signify time point of test compound and PregS positive control addition. Recordings were divided into 2 intervals (indicated as 1 and 2).

Patch Clamping

Internal solution:	75 mM CsCl, 10 mM NaCl, 70 mM CsF, 2 mM $MgCl_2$, 10 mM EGTA, 10 mM HEPES, pH 7.2 with KOH. Osmolarity is adjusted to 320 mOsm with mannitol.
Pipette solution:	135 mM CsCl, 1 mM EGTA, 2 mM $MgCl_2$ 10 mM HEPES, 5 mM NaATP and 0.1 mM Na_2GTP, pH 7.2 with CsOH. Osmolarity is adjusted to 290 mOsm with mannitol.
External K^+ solution:	160 mM NaCl, 4.5 mM KCl, 1 mM $MgCl_2$, 2 mM $CaCl_2$, 5 mM D-Glucose monohydrate, 10 mM HEPES, pH 7.4 with NaOH. Osmolarity is adjusted to 340 mOsm with mannitol.
Seal enhancer:	105 mM NaCl, 4.5 mM KCl, 1 mM $MgCl_2$, 40 mM $CaCl_2$, 5 mM D-Glucose monohydrate, 10 mM HEPES, pH 7.4 with NaOH. Osmolarity is adjusted to 340 mOsm with mannitol.

Cell preparation

Planar patch clamp recordings were made using a benchtop NPC-1 Port-a-patch and the automated higher throughput NPC-16 Patchliner (Nanion, Germany). TRPM3 cells were incubated with tetracycline 24 hours prior to experiments, and grown to 70% confluence in a 10 cm culture dish (Starstedt, US). The cell media was removed and cells were washed with PBS before being gently detached with trypsin. Fresh, prewarmed media was added and the cell solution was agitated to disperse cell clumps. The cell solution was then centrifuged for 2 min at 100g to form a cell pellet. The supernatant was removed, and the pellet resuspended in external K^+ solution. After a second centrifugation step, supernatant was discarded and the pellet resuspended in 300 µl external K^+ solution.

Port-a-Patch

The Port-a-Patch allows for patch clamp recording using planar patch clamp chips under the control of HEKA software (Brueggemann *et al.*, 2004). For Port-a-Patch recordings, internal solution was applied to the inside face of the chip, and SBS to the outer face. The chip was then screwed into place and covered with a Faraday cap. Cell solution (5 µl) was applied to the surface of the chip, and the software instructed to apply negative pressure in order to attract a single cell to the aperture in the chip, so that it was exposed to both external and internal solution (Figure 2.5 A). Seal enhancer solution was added to encourage formation of a gigaseal (seal resistance >1 GΩ). A stronger suction pulse was then applied to rupture the cell membrane to achieve whole cell. The software was then paused, the chip was unscrewed (with the cell still attached), and the internal solution replaced with pipette solution. The chip was replaced and the programme was restarted to maintain whole cell configuration. For experiments, solution exchange was performed by direct addition of test solution using a pipette, and removal of the previous solution. This addition/removal step was repeated 3 times to ensure sufficient exchange. Recordings were made using an EPC-10 amplifier (HEKA electronic). Data were acquired using Patchmaster software and analysed using Fitmaster software (HEKA). Data were sampled at 1 kHz. Currents were measured during voltage ramps from -100 mV to +100 mV for 1s every 10s from a holding potential of 0 mV. (Figure 2.5 B).

Patchliner

Voltage-clamp recordings were performed on a NPC-16 Patchliner (Nanion Technologies), a high throughput planar patch clamp technique that allows parallel investigation of 8 cells within separate compartments on the same chip (Bruggemann *et al.*, 2006). Unlike the Port-a-Patch, the whole experiment is automated. Cells and solutions are transferred by a robotic pipettor into the chip, and old solutions are decanted, allowing for fast and efficient exchange of both the external and internal solutions. Patchliner experiments were kindly performed by C. Milligan, using the same software parameters as for Port-a-Patch.

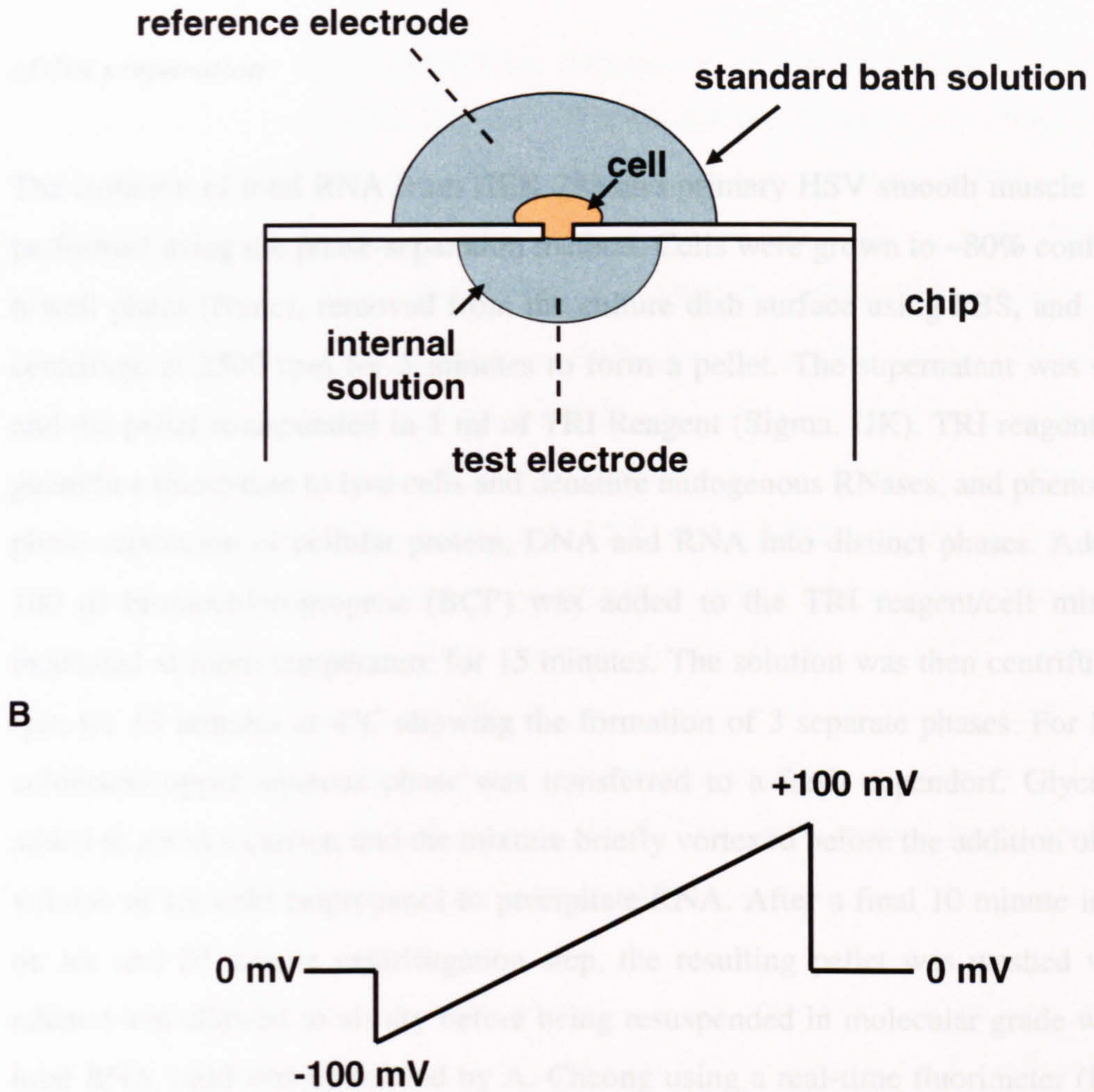

Figure 2.5. Planar patch clamp set-up The benchtop NPC-1 Port-a-patch is capable of automated patch clamp recordings. **A**. Schematic of planar patch clamp chip. The default configuration for a cell is cell attached. The application of negative pressure, or suction, is required to achieve whole-cell. **B**. Ramp protocol used for whole cell voltage clamp recordings for both Port-a-Patch and Patchliner. Cells were held at 0 mV. Hyperpolarisation to -100 mV was followed by a ramp to +100 mV before returning to 0 mV.

Polymerase Chain Reaction (PCR)

cDNA preparation

The isolation of total RNA from HEK 293 and primary HSV smooth muscle cells was performed using the phase-separation method. Cells were grown to ~80% confluency in 6-well plates (Nunc), removed from the culture dish surface using PBS, and spun in a centrifuge at 2500 rpm for 5 minutes to form a pellet. The supernatant was discarded and the pellet resuspended in 1 ml of TRI Reagent (Sigma, UK). TRI reagent contains guanidine thiocynate to lyse cells and denature endogenous RNases, and phenol to assist phase separation of cellular protein, DNA and RNA into distinct phases. Additionally 100 µl bromochloropropane (BCP) was added to the TRI reagent/cell mixture and incubated at room temperature for 15 minutes. The solution was then centrifuged at 13 rpm for 15 minutes at 4°C allowing the formation of 3 separate phases. For RNA, the colourless upper aqueous phase was transferred to a fresh eppendorf. Glycogen was added to act as a carrier, and the mixture briefly vortexed before the addition of an equal volume of ice cold isopropanol to precipitate RNA. After a final 10 minute incubation on ice and 20 minute centrifugation step, the resulting pellet was washed with 75% ethanol and allowed to air dry before being resuspended in molecular grade water. The total RNA yield was quantified by A. Cheong using a real-time fluorimeter (Roche) to perform a Ribogreen assay (Molecular Probes, UK). Ribogreen dye associates with nucleic acids and emits at a wavelength of 530 nm following excitation at 470 nm. The resulting fluorescence values can be used to quantify total RNA in a sample by comparison with a standard calibration curve.

Oligo dT Reverse Transcription

The RNA isolated from HEK 293 or HSV SMC as described was transcribed using AMV-reverse transcriptase (Promega) to produce cDNA. RNA (1 µg) was combined with primer (0.5 µg), 25 mM dNTPs (final concentration 0.63 mM each), 30 U AMV-reverse transcriptase plus 5X reaction buffer, and made up to 40 µl with molecular grade water. The mixture was incubated at 42°C for 1 hour, followed by heat inactivation at 94°C for 5 min.

Primer design

Forward and reverse primers were designed to be complementary to the target DNA sequence for individual human TRPM3 splice variants according to sequences deposited in Genbank under the following accession numbers: $TRPM3_{1325}$ (AJ505026); TRPM3a (AF536748); TRPM3b (AF536749); TRPM3c (AF536750); TRPM3d (AF536751); TPRM3e (AF536752); and TRPM3f (AF536753). Primers specific for variant $TRPM3_{1325}$ were directed to the unique N-terminal region ($TRPM3_{1325}$), while primers spanning exon 4 of the TRPM3 gene were designed to identify the TRPM3f variant (TRPM3f). A primer pair spanning exons 11-12 & 14-15 was intended to give 4 products of similar sizes, relating to TRPM3b, TRPM3e, TRPM3d and all remaining variants (TRPM3bed). Primers spanning a 12 amino acid sequence that is only present in the TRPM3c variant were designed to identiy the TRPM3c variant (TRPM3c) (Figure 2.6). It was not possible to design primers specific for variant TRPM3a due to the absence of any splice-specific, unique regions. Primers directed to human β-actin cDNA (Genbank accession number BC004251) were created by A. Dedman. Primer sequences and predicted products are given in Table 2.1.

Primers were chosen to avoid high GC content, were predicted to have low secondary structure content, and had a melting point (T_m) close to 60°C. A nucleotide-nucleotide BLAST search of the *homo sapien* database (www.ncbi.nlm.nih.gov/BLAST) was performed to ensure primers were specific for TRPM3. Primers were synthesised by Sigma-Genosys and stored in stock solution of 100 mM in water at -20°C. Working stocks of 20 mM were stored at 4°C.

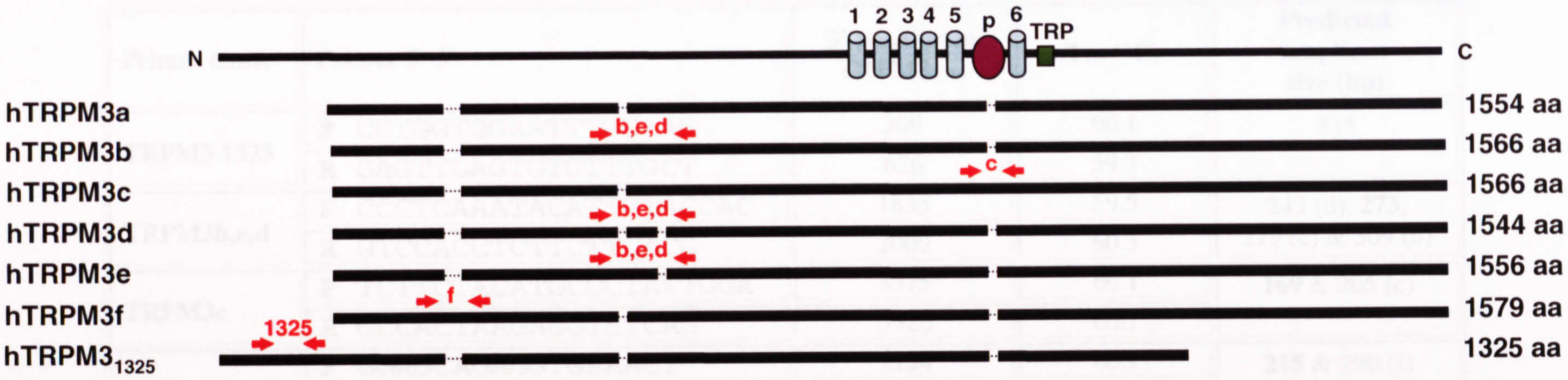

Figure 2.6. TRPM3 splice variant-specific primer design Schematic representation of TRPM3 protein depicting transmembrane domains 1-6, pore region and TRP homology domain. Human variants hTRPM3a-f and hTRPM3$_{1325}$ are aligned, and the number of amino acid residues in each is given on the right hand side. Primers are indicated in red. Primer pair 1325 directed to N-terminal region of hTRPM3$_{1325}$, primer pair f spans exon 4, primer pair b,e,d spans exons 11-12 & 14-15, and primer pair c spans 12 amino acid residues that are only present in hTRPM3c.

Primer name	Primer 5'-3'	5' position in $TRPM3_{1325}$	Tm (°C)	Predicted amplicon size (bp)
TRPM3 1325	**F** CCTGGTGGAATTTGGAAG	309	60.1	335
	R GAGTTGAGTGTGTTTGCT	626	59.3	
TRPM3b,e,d	**F** CCCTCAAATACATTGTACCAC	1835	59.5	243 (d), **273**, 279 (e) & 309 (b)
	R GTCCACCTCTTCTTCACG	2009	60.3	
TRPM3c	**F** TCTTCTACATGCCCTATTGGA	3375	60.1	**169** & 205 (c)
	R GCCACTAAGAGGTSTCAG	3526	60.1	
TRPM3f	**F** GGAGCAGAGGTGAAACT	1154	60.7	**215** & 290 (f)
	R CCAAAGGCCAGGATGTC	1352	60.7	
Primer name	**Primer 5'-3'**	**5' position in β-actin**	**Tm (°C)**	**Predicted amplicon size (bp)**
β-actin	**F** TCGAGCAAGAGATGGC	729	58.5	194
	R TGAAGGTAGTTTCGTTGGATG	899	60.1	

Table 2.1. List of primers used for amplification of TRPM3 and β-actin during solution RT-PCR F, forward primer, R, reverse primer and Tm, melting temperature. Where two or more predicted amplicon sizes are given the value in bold represents the product size expected for the $TRPM3_{1325}$ variant. Additional predicted amplicon sizes represent the various splice variants as indicated.

Conventional (solution) PCR

PCR allows for amplification of a single DNA strand through a series of cycles using specific primers. Each cycle consists of a high temperature denaturation step to allow separation of the double stranded DNA, an annealing step in which primers can anneal to their target DNA sequence, and a final extension step in which the 3' end of each primer is extended. Extension is catalysed by a thermostable DNA polymerase that incorporates dNTPs into the new DNA strand. DNA amplification is exponential, as primers can bind both template DNA and the newly formed PCR products to yield further PCR products. A 10 µl PCR reaction consisted of 1 µl template cDNA, 0.5 µM of both forward and reverse primers, 0.25 U *Taq* DNA polymerase (Promega) and supplied buffer, 1.5 mM $MgCl_2$ as a catalyst, and 250 µM dNTPs, made up to 10 µl with PCR grade water. A standard protocol of denaturation at 94°C for 30 seconds, annealing for 45 seconds (at a temperature 5°C below T_m), and elongation at 72°C for 45 seconds for 40 cycles was performed on a PCR block thermocycler (Eppendorf).

PCR products were analysed by agarose gel electrophoresis alongside a DNA ladder as described previously. Where necessary, separated PCR product bands were visualised using a UV transilluminator and single bands excised using a sterile scalpel blade. Individual PCR products were cleaned using the QIAquick Gel Extraction. (Qiagen) as per manufacturer's instructions. The resulting product was used as the template for a subsequent PCR reaction to provide sufficient DNA for sequencing, which was performed in house (Astbury Building, University of Leeds).

Western blotting

Resolving gel (6%):

H_2O	5.3 ml
30% acrylamide mix	2 ml
1.5 M TRIS (pH 8.8)	2.5 ml
10% SDS	100 µl
10% ammonium persulphate	100 µl
TEMED	8 µl

Stacking gel (5%):

H_2O	1.4 ml
30% acrylamide mix	330 µl
0.5 M TRIS (pH 6.8)	250 µl
10% SDS	20 µl
10% ammonium persulphate	20 µl
TEMED	2 µl

SDS sample buffer:	100 mM TRIS-HCL (pH 6.8), 4% sodium dodecyl sulphate (SDS) and 20% glycerol
Running buffer:	25 mM TRIS, 192 mM glycine and 0.1% SDS (w/v).
Transfer buffer:	0.068 mM TRIS, 77.2 mM glycine, SDS (0.037%), and methanol (25%).

Protein extraction

HEK-TRPM3 cells were grown to confluence on a 6 well plate (NUNC), removed from the incubator and left on ice. Media was aspirated and cells washed with ice cold PBS. Cells were then lysed using 100 µl ice cold sample buffer containing a protease inhibitor cocktail (Roche Diagnostics) as per manufacturer's instruction. Samples were then transferred into eppendorfs and left on a heat block set at 100°C for 5 minutes before protein quantification and storage at -20°C.

Protein quantification

The concentration of protein in samples was determined using the *DC* Protein Assay (Bio-Rad). The colorimetric assay consists of 2 steps in which the protein in the sample reacts with an alkaline copper tartrate solution and then reduces a Folin reagent to produce blue reduced species with maximum absorbance at 750 nm. Comparisons with a standard curve comprised of several dilutions of a BSA protein standard allow determination of the protein concentration within a sample.

Western blotting

Western blotting can be used to detect a single protein within a cell lysate by incorporating SDS polyacrylamide gel electrophoresis (SDS-PAGE) to separate proteins on the basis of their molecular weight. SDS is an anionic detergent that denatures protein and applies an overall negative charge by binding to polypeptide chains via a hydrophobic tail. Proteins can be further denatured using a suitable reducing agent to reduce disulfide linkages. When an electric charge is applied across an SDS-PAGE gel, proteins of a similar molecular weight will migrate the same distance towards the positive electrode, regardless of their secondary structure. Larger proteins will take longer to migrate through the gel, as they encounter more resistance due to their size. Negatively charged proteins resolved on the SDS-PAGE gel can then be transferred onto a special membrane using electrophoresis and detected using specific antibodies.

Protein samples were thawed on ice then combined with bromophenol blue (0.1%) and the reducing agent dithiothreitol (DTT, 100 mM). In addition, samples were heated to 100°C to ensure complete denaturation of protein. Protein (20µg) was then loaded alongside markers (Bio-Rad) onto an SDS-PAGE gel composed of a 6% resolving gel and 5% stacking gel. Electrophoresis was carried out for one hour at 200V in running buffer to allow full separation of proteins within the sample. Protein gels were then transferred onto Immobilon-P polyvinylidene fluoride (PDVF) membrane (Millipore), pre-soaked in 100% methanol for 1 minute and transfer buffer for 5 minutes, for 1 hour at 0.03 A using a Trans-Blot® SD semi-dry transfer cell (Bio-Rad). Membranes were washed for 1 minute in 100% methanol and allowed to air dry before being incubated in 5% non-fat milk (Marvel) in PBS tween overnight at 4°C to block non-specific binding

sites. The membrane was then transferred into a primary antibody solution (1:2000 dilution in 5% milk/PBS tween) for 1 hour at RT. The membrane was washed x3 in PBS tween and incubated with a horse radish peroxidise (HRP)-conjugated goat anti-rabbit secondary antibody (diluted 1:20000 in 5% milk/PBS tween) for 1 hour at RT. The membrane was washed a further 3x in PBS tween before being developed using the ECL plus kit (Amersham Biosciences). ECL solution was applied evenly to the surface of membrane and incubated for 1 minute in the dark to allow chemiluminescene to develop before excess solution was drained. Exposure of the developed blot to photographic paper (Kodak) for 1-5 minutes was used to detect chemiluminescence, followed by 4 minutes in developing solution to develop the film, a brief wash, and 5 minutes in fixing solution (Photosol). After a final brief wash, blots were allowed to dry before being scanned and analysed using ImageJ software (http://rsb.info.nih.gov/ij/).

Immunofluorescence staining

Antibody diluting solution: PBS, 1% bovine serum albumin (BSA) and 0.1% sodium azide

Cells were split onto poly-L-lysine coated coverslips 48 hours prior to experiments. For HEK-TRPM3 staining, cells were induced with tetracycline 48 hours prior to experiments. Cells were washed 3 times with PBS before fixing with 2% paraformaldehyde (PFA) for 5 minutes. Permeabilisation was not necessary as TM3E3 targets an extracellular epitope. Cells were washed 3 times with PBS and transferred into blocking solution (1% BSA) for 30 minutes to block non-specific binding sites. Following the blocking stage cells were incubated overnight at 4°C in the primary antibody, TM3E3, diluted 1:1000 in antibody diluting solution. Antibody pre-adsorbed to its antigenic peptide (prepared 24 hours prior to experiments), or exclusion of the primary antibody were used as negative controls. The next day cells were washed 3 times in PBS and then incubated in a 1:40 dilution of the secondary antibody, FITC-conjugated goat anti-rabbit IgG (Abcam), for 1 hour at room temperature. After a final wash step with PBS, coverslips were mounted cell-side down onto glass slides using DAPI Hard-Set mounting medium (VectaShield). Slides were stored at 4°C until viewed by laser-scanning confocal microscopy.

Confocal Microscopy

Confocal microscopy provides a high resolution image from light emitted from a single plane through a specimen. Images were taken using a Zeiss LSM 510-META laser scanning inverted confocal microscope controlled by Zeiss LSM imaging software, with an oil-immersed 63x (NA = 1.40) or 40x objective lens (NA = 1.30), or an air-exposed 20x objective lens (NA = 0.80). FITC (494 nm excitation, 519 nm emission) was excited using argon laser fitted with 488 nm filters. DAPI (excitation 360 nm, emission 460 nm) was excited using a diode laser fitted with 405 nm filters.

Immunohistology Staining

Immunohistology staining of human saphenous vein sections was performed by S. Piruthivi. Briefly, tissue samples in paraffin wax were prepared using a Leica ASP 300 automated tissue processing unit (Leica Microsystems, UK). For immunohistology investigation, sections 8 µm thick were mounted onto polylysine slides (VWR International, UK). Samples were dewaxed and rehydrated, and immunostaining was performed using the rabbit ABC kit (Vector Laboratories Ltd, UK). Primary antibody or the preadsorbed peptide control was added overnight at 4°C. The following day slides were incubated with biotinylated secondary antibody was for 30 minutes. Following application of ABC solution, sections were saturated with DAB solution for 5-10 minutes to allow colour development. Tissue sections were then dehydrated and mounted in DPX.

Gelatin Zymography

Separating gel buffer:	1.5 M Tris-base (pH 8.8)
Stacking gel buffer:	0.5 M Tris-base (pH 6.8)
2 x non reducing sample buffer:	20 mM TRIS (pH 6.8), 45 % glycerol, 10% SDS and 0.025% bromophenol blue
5 x running buffer:	25 mM TRIS, 200 mM glycine, 0.1% (w/v) SDS. Stock solution diluted 1:5 with dH_20 before use.
Washing buffer:	2.5% Triton X-100
10 x incubation buffer:	50 mM Tris-base (pH 7.6), 10% $CaCl_2.2H_2O$, 50 M NaCl and 0.005% Brij-35. Stock solution diluted 1:5 with dH_20 before use.
Coomassie brilliant blue:	25% methanol, 10% glacial acetic acid and 0.02% Coomassie blue R-250

Matrix metalloproteinases (MMPs) are responsible for the degradation of extracellular matrix molecules. MMP-2 and MMP-9 are more commonly known as gelatinases due to their role as gelatin degrading proteases.

Cell treatment

Cells were serum starved for 48 hours before a 48-hour treatment with conditioned media (0.4% serum) containing 100 nM phorbol ester (TPA), plus SPH or PregS alone, or in the presence of TM3E3 or peptide control. Non-treated 0.4% serum media was included as a negative control. Media was removed and centrifuged at 5000 rpm for 5 minutes to pellet any cell debris. The supernatant was collected and snap frozen in liquid N_2 before storage at –20°C.

Gelatin Zymography

Gelatin Zymography uses SDS polyacrylamide gel electrophoresis (SDS-PAGE) to separate gelatinase matrix metalloproteinases (MMPs) on the basis of their molecular weight. It is important that proteins are not reduced as their native structure and activity is important to the method. Media samples were defrosted on ice and mixed 1:1 with 2 x non-reducing sample buffer. Samples were then run on a 7.4% acrylamide gel, containing 1.0 mg ml^{-1} gelatin, at 120 V for 105 minutes alongside conditioned medium from HT-1080 cells. This media was used as a positive control to indicate the position of MMP-2 at 72 kDa, and of MMP-9 at 92 kDa. Gels were removed from glass plates and washed with 2.5 % Triton X-100 for 1 hour to remove SDS and to allow fractionated proteins to renature. Incubation at 37°C for 6½ hours allowed for the digestion of gelatin at the location of gelatinase bands in the gel. MMP proteins were detected as bands of clear lysis on a blue background following staining with Coomassie brilliant blue for 1 hour at room temperature on a rocking platform. Gels were scanned into the computer to allow analysis of band density using ImageJ software.

Colorimetric sandwich ELISA

MMP-9 secretion was further investigated using the Quantikine ELISA Kit (R&D Systems, UK). The kit measures total MMP-9, i.e. both active and pro forms of the MMP-9 protein. Briefly, microplates were supplied pre-coated with a monoclonal antibody specific for MMP-9. Conditioned media samples prepared for zymography experiments were applied to wells and MMP-9 present was able to bind to the surface-bound antibody. A secondary, HRP-conjugated polyclonal antibody against MMP-9 was added, followed by addition of a substrate solution. The resulting colour change was proportional to the amount of MMP-9 in samples. Plates were read at A_{450} nm using a plate reader with correction set to 540 nm (to allow for background readings in the plate). Samples were assayed in duplicate. MMP-9 concentration within samples was determined by comparison with a standard curve.

Additionally, the secretion of interleukin-6 (IL-6), a cytokine known to influence MMP-9 secretion, was measured using a PeliKine-compact™ ELISA kit (Sanquin,

Netherlands). Briefly, 96-well MAXI-SORP plates (NUNC) were coated with an antibody against human IL-6 overnight at 4°C. When conditioned media was applied, any IL-6 present was able to bind to the surface-bound antibody. In turn, a secondary biotinylated sheep antibody was added, which bound to the IL-6-antibody complex. Addition of HRP-conjugated streptavidin followed by a substrate solution caused a colour change directly related to the concentration of IL-6 present in the sample. The colour change was read at A_{450} nm using a plate reader. As the IL-6 concentration present in media samples was high, samples were diluted 1:100 in dH_2O before ELISA analysis, and assayed in duplicate. IL-6 concentration within samples was determined by comparison with a standard curve.

Data Analysis

Data were analysed and presented using the Origin 7 Software package. For conventional Ca^{2+}-imaging using the microscope based system, 'n/N' represents the number of coverslips/total number of individual cells. For FlexStation and FLIPR experiments, 'n/N' represents the number of independent experiments/the number of individual wells. For experiments performed on HSV smooth muscle cells, each independent experiment was performed on cells obtained from different patients.

If a representative trace is shown, error bars represent the standard error of the mean (SEM), where the mean (μ) is given by:

$$\mu = \frac{\Sigma x}{N}$$

And SEM is given by:

$$SEM = \frac{\sigma}{\sqrt{N}}$$

Where N is the sample size (i.e. the number of individual wells or cells measured) and x is the value of each sample, and σ is the standard deviation. For all other cases, SEM is calculated using n, the number of independent experiments.

Dose response curves were produced using the Hill equation:

$$y = V_{max} \frac{x^n}{k^n + x^n}$$

Where V_{max} is the maximum response to an agonist, x is the concentration of the agonist, k is the EC_{50} for half-maximal response to the agonist, and *n* is the slope of the curve, referred to as the Hill coefficient.

The statistical significance is determined by analysing the probability (p) that an experimental result occurred by chance. The reliability of such an observation is represented by the p-value. The higher the p-value, the greater the probability the result occurred simply by chance. Statistical significance was investigated using a two-tailed student's t test, which is derived from the normal distribution, and significant difference is given by $p<0.05$.

Sequence alignment

Protein and DNA sequences were obtained from Genbank (www.ncbi.nlm.nih.gov/) and aligned with each other or with sequencing results using ClustalW software (www.ebi.ac.uk/Tools/clustalw/). This allowed for the identification of conserved regions within the protein sequence of TRP family members, and also to check the results of the DNA sequencing used to identify PCR products.

Chapter 3

Development of an externally-acting specific blocker of TRPM3

Although there is currently an abundance of drugs commercially available for use as ion channel modulators, many are nonselective, and lack the ability to differentiate between structurally related proteins. TRP ion channel antagonists have also proven to be non-specific, blocking not only members of the same subfamily, but also a broad range of calcium channels. The generation of peptide-specific antibodies is emerging as a reliable method for the design of subtype specific channel blockers. Antibodies targeted to extracellular regions of ion channels, most commonly the third extracellular loop, have proven to be selective blockers for a variety of ion channels.

The first instance of a rational method to develop specific channel blockers used polyclonal antibodies to inhibit whole-cell currents relating to the voltage-gated K^+ channels $K_v1.2$ and $K_v3.1$, and established that $K_v1.2$ contributes to endogenous neuronal cell currents (Zhou *et al.*, 1998). When applied to TRP channels, such antibody design revealed a role for TRPC1 as a store-operated Ca^{2+} channel of vascular smooth muscle (Xu *et al.*, 2001), and demonstrated a physiological relevance for TRPC5 in rabbit arterioles (Xu *et al.*, 2006a). Polyclonal antibodies have also been used to inhibit both proton and chemical activation of TRPV1 (Klionsky *et al.*, 2006), and to block Na^+ current through the voltage gated Na^+ channel, $Na_v1.5$ (Xu *et al.*, 2005b). More recently, the first study to use monoclonal antibodies has shown specific inhibition of the voltage-gated K^+ channel hEag1, and suggested a function for the channel in modulating tumour cell growth (Gomez-Varela *et al.*, 2007).

The development of such selective inhibitors for TRP channels in particular does not appear to be complicated by their diverse methods of activation, which range from both intra and extracellular ligands to changes in pH or temperature. Lipid-mediated regulation is a common mechanism for the activation of the TRP superfamily, and lipid-regulated currents have been identified for a number of TRP channel family members. Lipids are a diverse range of naturally occurring compounds, and include fatty acids, their naturally occurring derivatives, esters and amides, and functionally or biosynthetically related compounds, such as alcohols and cholesterol. The major

structural compounds of cell membranes are sphingolipids. The reversible hydrolysis of sphingomyelin, the most abundant sphingolipid in human plasma, to ceramide occurs via the sphingomyelin pathway (Auge *et al.*, 1996). Several intermediates of this pathway, including sphingosine-1-phosphate, sphingosylphosphorylcholine and sphingosine, are common lipid mediators involved in many cell-signalling pathways, including acting as modulators of TRP channels (Xu *et al.*, 2006b). The TRPM3 splice variant $TRPM3_{1325}$ is activated by D-*erythro*-Sphingosine (SPH) and its analogues (Grimm *et al.*, 2005). TRPM3 is a relatively newly discovered member of the TRPM subfamily, and its function remains elusive. Studies by means of over-expression demonstrate non-specific inhibition of TRPM3 by the TRP channel blockers gadolinium (Gd^{3+}) and 2-aminoethoxydiphenylborate (2-APB) (Grimm *et al.*, 2005; Xu *et al.*, 2005a). However, a subtype specific channel blocker would prove a useful tool for further characterisation of the channel, and enable investigations into native channel expression and physiological function.

The aim of this study was to use E3 targeting (Xu *et al.*, 2005b) to design and develop an antibody as a selective inhibitor for the TRPM3 ion channel. Western blotting and immunocytochemistry were necessary to confirm the antibody was able to specifically bind the epitope expressed by the channel. Calcium imaging was used to ascertain the inhibitory effect of the antibody in live cells against known activators of TRPM3, and to explore its selectivity. The development of a stable TRPM3 cell line allowed for the use of high throughput technologies to further characterise the channel, and led to the discovery of a novel activator of TRPM3.

TRPM3 expression in HEK 293 cells

TRPM3 cDNA clone (a gift from C. Harteneck) contains yellow fluorescent protein (YFP) fused to the 3' end of the TRPM3 ORF. After transfection, the fusion construct is expressed by host cells as TRPM3 protein with a C-terminal YFP tag, resulting in specifically labelled protein in live cells. Western blotting with a TRPM3 specific antibody confirmed that transfection with the YFP-tagged cDNA causes a marked increase in TRPM3 protein levels (Grimm *et al.*, 2003).

In order to study the effect of a peptide-specific antibody as a blocker for TRPM3, the channel was over-expressed in HEK 293 cells. Cells loaded with the ratiometric calcium indicator dye, fura-2, were visible at an excitation wavelength of 380 nm. Successfully transfected cells expressing YFP-tagged human TRPM3 were identified by their YFP-fluorescence at 480 nm (Figure 3.1). Following extensive optimisation of the method, transfection efficiency was typically 30%. The identification of transfected cells allowed for regions of interest to be selected in order to minimise background signals and measurements from non-transfected cells, and gave an indication of the location and distribution of tagged protein within the cell.

The data show that TRPM3 can be successfully transfected into HEK 293 cells to give a roughly equal distribution of the protein throughout the cell.

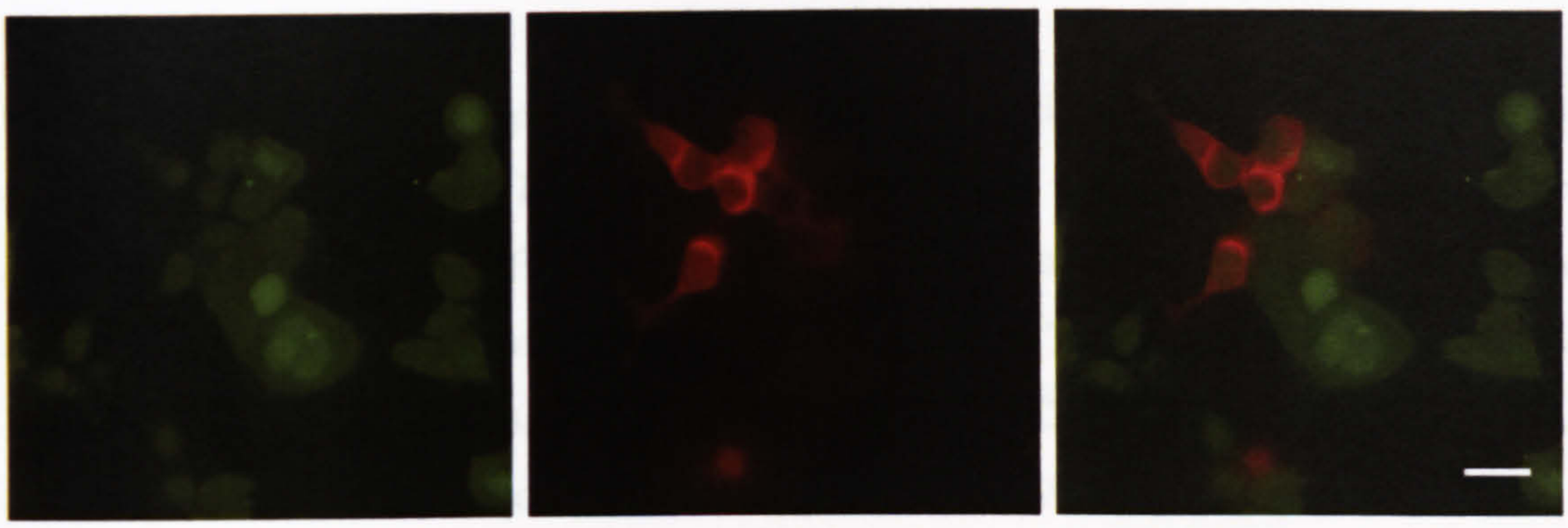

Figure 3.1. TRPM3 expression in HEK 293 cells The YFP tag allows for the identification of successfully transfected cells. **A.** Fura-2 loaded cells visible at excitation wavelength 380 nm. **B.** In the same cells, TRPM3-expressing cells were identified by their YFP fluorescence at 480 nm excitation. **C.** Merged image. Scale bar represents 10 μm.

SPH increases intracellular Ca^{2+} in TRPM3-expressing cells

Fluorescence microscopy experiments using the ratiometric Ca^{2+} dye fura-2 were used to investigate Ca^{2+} entry in TRPM3-expressing cells. This was necessary to confirm the channel identified by its YFP-tag was both functional and expressed at the plasma membrane. Known modulators of TRPM3 were tested on TRPM3-YFP-transfected and YFP-transfected control cells, including the sphingolipid D-*erythro*-sphingosine (SPH), an intermediate in the sphingomyelin pathway (Figure 3.2 A).

SPH is reported to activate TRPM3 independently of PKC or depletion of intracellular Ca^{2+} stores (Grimm *et al.*, 2005). In this study, SPH (20 μM) caused a significant increase in intracellular Ca^{2+} in HEK-TRPM3 cells within 2 min of application (Figure 3.2 B). Ethanol (the solvent for SPH) was kept constant at 0.1% in recording solutions throughout experiments and failed to elicit a significant Ca^{2+} signal in the absence of SPH. The response to SPH in control HEK-YFP cells was much less, and the mean data show that after 5 min the Ca^{2+} response in HEK-TRPM3 cells was 7 times larger than that in HEK-YFP cells (Figure 3.2 C).

The data suggest that TRPM3 protein can be successfully exogenously expressed at the plasma membrane, and serves as a functional calcium channel in HEK 293 cells, in agreement with previous reports.

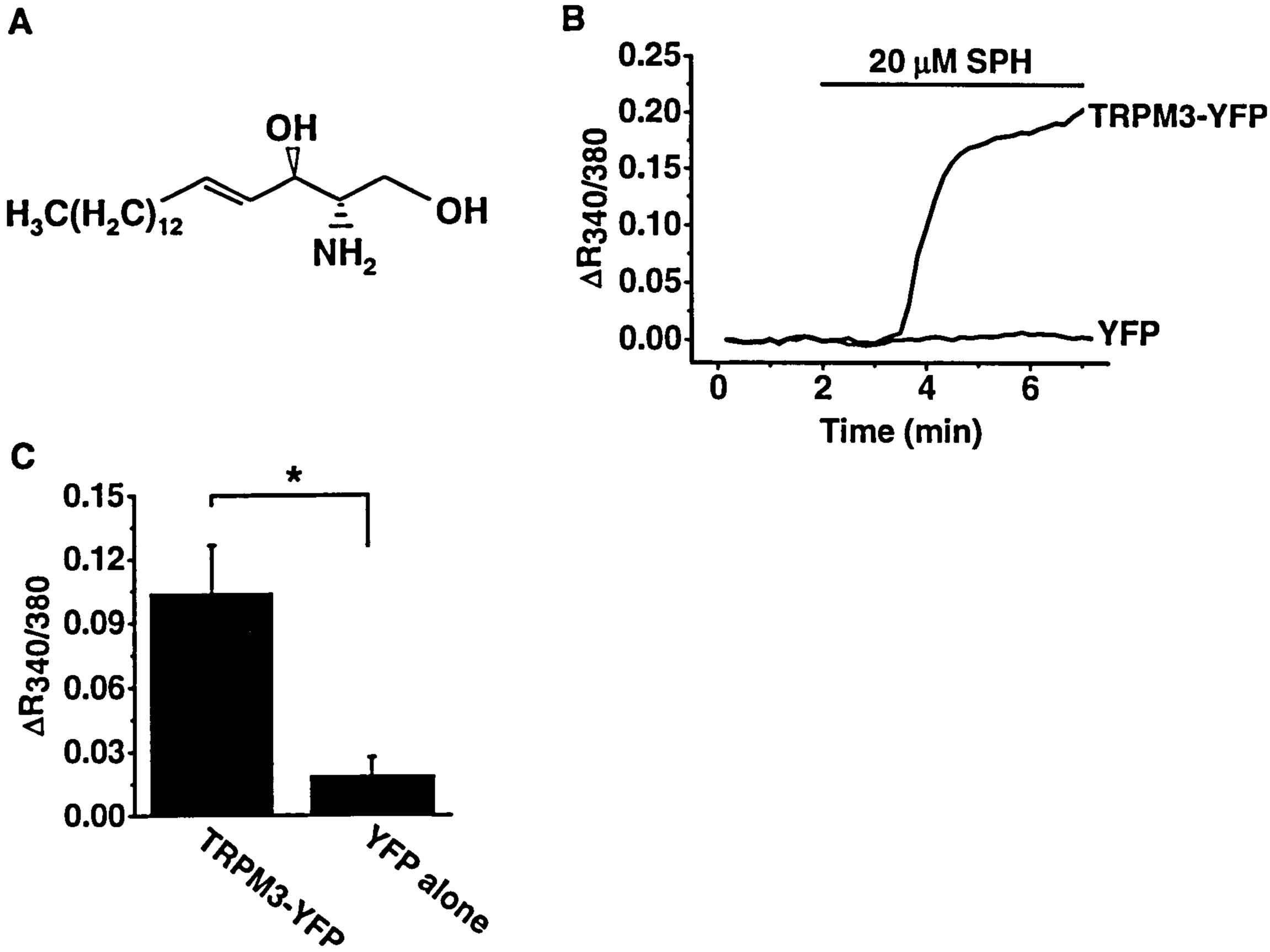

Figure 3.2. D-*erythro*-sphingosine (SPH) increases Ca^{2+} signals in TRPM3-expressing cells Ca^{2+} signals were measured as the 340/380 nm ratio of emission in fura-2 loaded HEK 293 cells. Cells were transfected with TRPM3 or YFP as a control. Ethanol (vehicle) was present throughout recordings. **A.** Structure of SPH. **B.** Representative traces from single cells. SPH causes an increase in Ca^{2+} in TRPM3-YFP-expressing cells compared to YFP-expressing control cells (grey trace). **C.** Mean data (±SEM) showing a significant increase in Ca^{2+} 5 min after SPH application (TRPM3 n/N=6/28, YFP n/N=3/16).

An analogue of SPH increases Ca^{2+} in HEK-TRPM3

The SPH precursor D-*erythro*-dihydrosphingosine (DHS) is a sphingosine kinase inhibitor and prevents the conversion of SPH to sphingosine-1-phosphate. DHS, also an intermediate in the sphingomyelin pathway, is a saturated analogue of SPH, lacking the double bond at position 4 (Figure 3.3 A). Esterification of DHS results in the formation of ceramide, which is then converted to SPH by ceramidases (Auge *et al.*, 1996).

DHS has previously been shown to activate TRPM3 (Grimm *et al.*, 2005). Likewise, I found that DHS (20 μM) caused a significant increase in Ca^{2+} entry in TRPM3-expressing cells within 2 min of application (Figure 3.3 B). DHS also caused a small increase in Ca^{2+} entry in HEK-YFP cells. However, the mean data indicate that after 5 min the response in HEK-TRPM3 cells was 3 times larger than that of HEK-YFP (Figure 3.3 C).

The data provide further evidence that the TRPM3 protein is functional when over-expressed in HEK 293 cells, and confirm the results of (Grimm *et al.*, 2005).

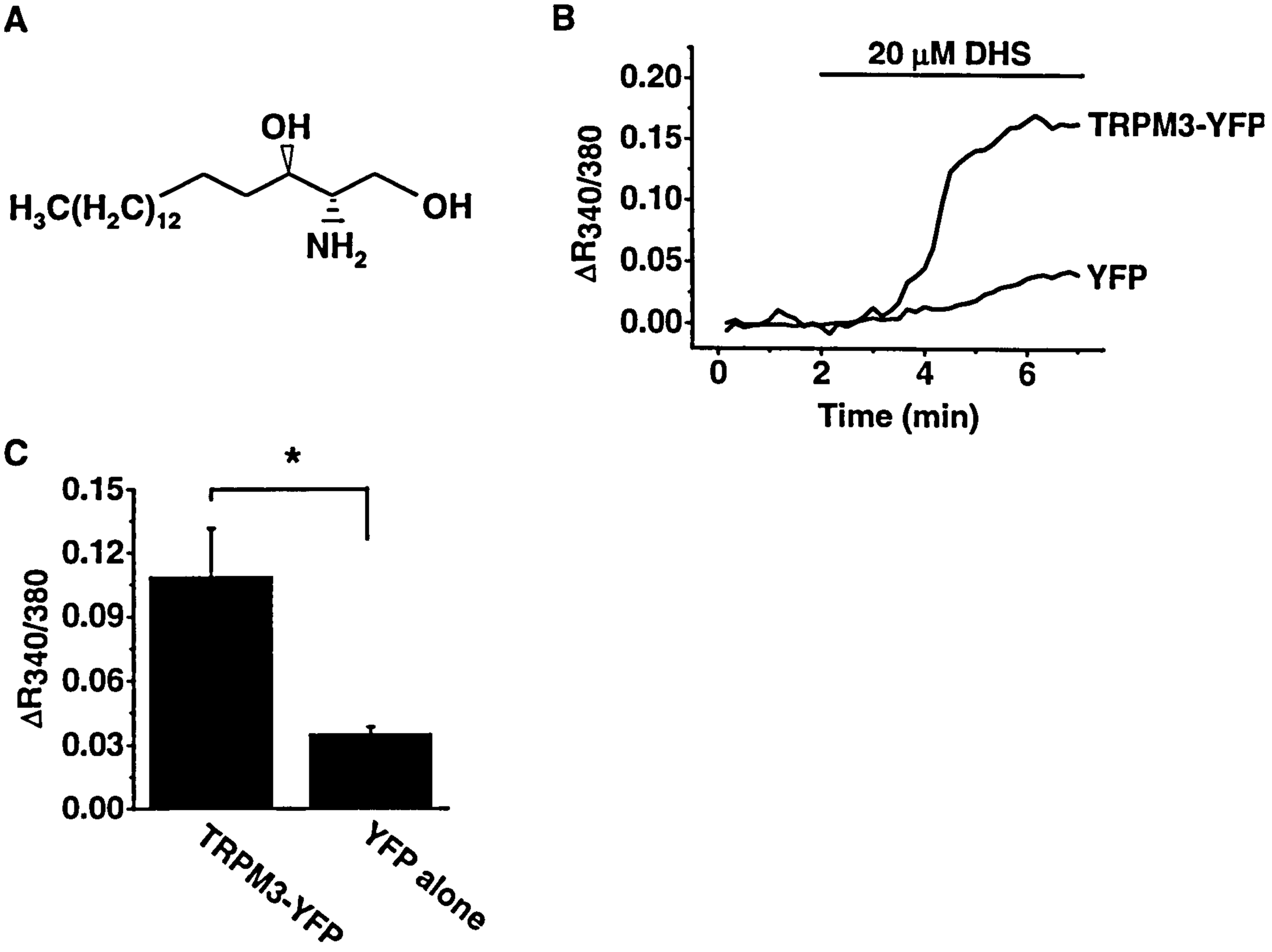

Figure 3.3. D-*erythro*-dihydro-sphingosine (DHS) also increases Ca^{2+} signals in TRPM3 expressing cells Ca^{2+} signals were measured as the 340/380 nm ratio of emission in fura-2 loaded HEK 293 cells. Cells were transfected with TRPM3 or YFP as a control. Ethanol (vehicle) was present throughout recordings. **A.** Structure of DHS. **B.** Representative traces from single cells. DHS causes an increase in Ca^{2+} in TRPM3-expressing cells compared to YFP-expressing control cells (grey trace). **C.** Mean data (±SEM) showing a significant increase in Ca^{2+} 5 min after DHS application (TRPM3 n/N=3/22, YFP n/N=3/19).

Hypotonic shock also activates TRPM3

Reducing extracellular osmolarity is also reported to activate TRPM3 (Grimm *et al.*, 2003). Activation is believed to be the result of cell swelling, leading to stretch of the membrane, which suggests volume-regulated activity of the channel.

Replacing bath solution with hypotonic solution in order to decrease the osmolarity from 300 to 200 mOsm caused a significantly larger Ca^{2+} signal in TRPM3-expressing cells than YFP-control cells (Figure 3.4 A). In contrast to the Ca^{2+} response to the lipid activators, SPH and DHS, the Ca^{2+} response to hypotonic shock was transient and had faster onset. Hypotonic shock also induced Ca^{2+} entry in HEK-YFP cells; however the response was slower and not statistically significant at the time points indicated. After 2 min, the response in HEK-TRPM3 was 4 times larger than that of HEK-YFP (Figure 3.4 B).

In summary, hypotonic solution causes small but significant activation of over-expressed TRPM3.

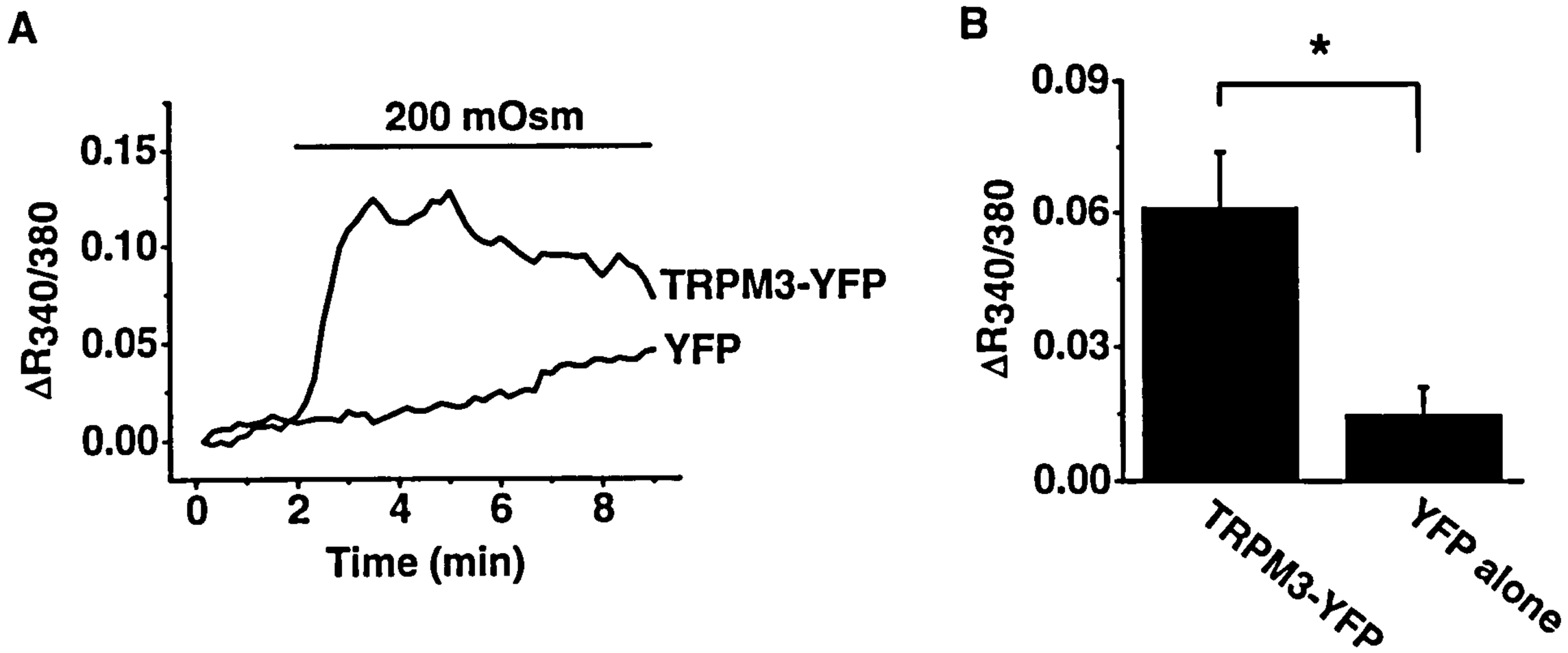

Figure 3.4. Hypotonic solution activates TRPM3 Ca^{2+} signals were measured as the 340/380 nm ratio of emission in fura-2 loaded HEK 293 cells. Cells were transfected with TRPM3 or YFP as a control. **A.** Representative traces from single cells. Switching bath solution osmolarity from 300 to 200 mOsm causes an increase in Ca^{2+} in TRPM3-expressing cells larger than the Ca^{2+} increase in YFP-expressing control cells (grey trace). **B.** Mean data (±SEM) showing a significant increase in Ca^{2+} 2 min after 200 mOsm application (TRPM3 n/N=5/22, YFP n/N=3/21).

Hydrophilicity analysis of the TRPM3 amino acid sequence

Kyte-Doolittle analysis maps the hydrophobic and hydrophilic nature of amino acids within a protein sequence in order to locate surface exposed and membrane embedded regions of the protein (Kyte *et al.*, 1982). Such hydrophilicity analysis allowed for the determination of the location and sequence of a region likely to be the 3rd extracellular loop (E3) of TRPM3 (Figure 3.5). This sequence is conserved for all reported human TRPM3 splice variants, and for several species including human, rat and mouse, and was used to engineer a peptide for peptide-specific antibody generation. The peptide [C]LFPNEEPSWKLA was conjugated to keyhole limpet hemacyanin via the N-terminal cysteine residue, which is not present in the native protein sequence, and used to immunise rabbits to induce an immune response (Sigma-Genosys). Anti-sera containing anti-peptide polyclonal antibodies, TM3E3, were harvested. Preimmune sera taken before the initial injection were retained as a control.

Alignment of the amino acid sequence from the third extracellular loop of TRPM subfamily members indicates TRPM3 shares ~70% sequence homology in this region with its closest relative, TRPM1 (Figure 3.6). In addition, the alignment shows that only 9 residues in the peptide sequence used for antibody design are conserved between TRPM3 and TRPM1, and even less for other family members. A BLAST search performed using the peptide sequence indicated that, excluding TRPM3 splice variants, no other proteins contain this specific peptide sequence.

In summary, the third extracellular loop of TRPM3 is a good target for antibody design. The unique peptide sequence of this region suggests that the polyclonal antibodies directed against it will specifically bind the TRPM3 protein.

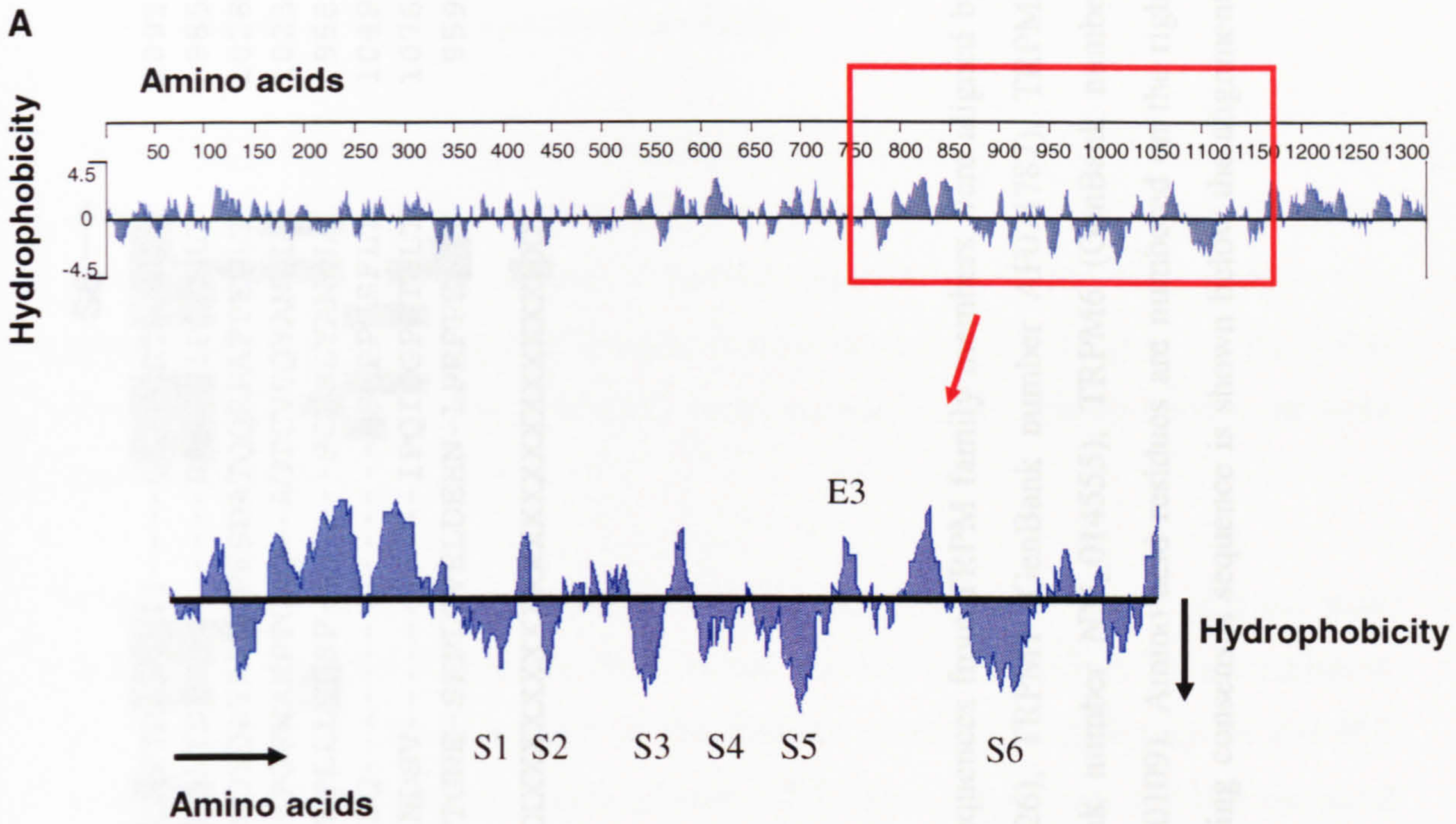

Figure 3.5. Hydrophilicity Analysis Kyte-Doolittle plot of amino acid sequence for TRPM3 produced using Lasergene software (DNAStar). S1-S6 refer to the predicted 6 transmembrane domains. E3 donates the 3rd extracellular loop.

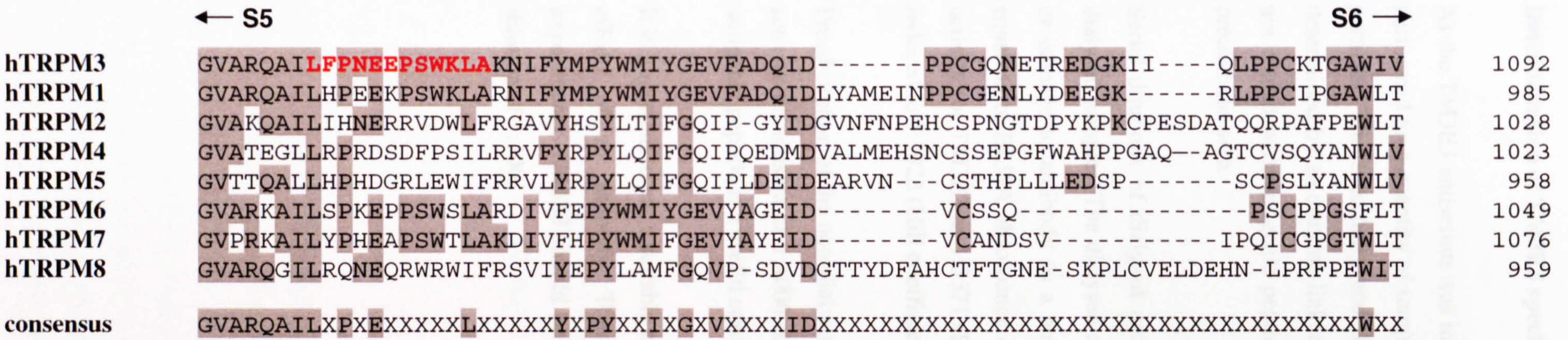

Figure 3.6. Sequence alignment of TRPM subfamily 3rd extracellular loop Amino acid sequences from TRPM family members were aligned by ClustalW software using published sequence data of TRPM3 (GenBank number AJ505026), TRPM1 (GenBank number AF071787), TRPM2 (GenBank number AJ878416), TRPM4 (GenBank number AY297045), TRPM5 (GenBank number NM_014555), TRPM6 (GenBank number AF448232), TRPM7 (GenBank number NM_017672) and TRPM8 (GenBank number AY090109). Amino acid residues are numbered on the right hand side, and those conserved in the majority of compared sequences are shaded. The resulting consensus sequence is shown below the alignment. TM3E3 peptide sequence is shown in red.

Determination of TM3E3 specificity and titre

As the TM3E3 antiserum was intended for use in cell culture experiments, dialysis was performed on a quantity of sample to remove sodium azide preservative and other small particles. The specificity and titre of TM3E3 antisera before and after dialysis was determined by an enzyme-linked immunosorbant assay (ELISA) (Figure 3.7 A). Wells not coated with antigenic peptide (NP) were included as a negative control, as were preimmune sera.

Serial dilutions of dialysed antiserum samples were compared to the original, non-dialysed samples. The dialysed antibody serum was less potent, possibly due to dilution or damage to antibody as a result of the dialysis procedure. Application of the Hill equation to ELISA absorbance data (Figure 3.7 B) gave the dilution for half maximal activity for TM3E3 as 1:3571 (Hill coefficient 1.50), and for dialysed TM3E3 this was reduced to 1:1923 (Hill coefficient 1.42).

Preadsorption of the non-dialysed antibody to its antigenic peptide significantly reduced activity of antisera at 1:4000 dilution (Figure 3.7 C) indicating pre-adsorption to the antigenic peptide is a useful control for preventing the antibody binding its epitope.

It is important to use a suitable concentration of antibody in order to reduce non-specific effects of an antibody. Therefore, based on the ELISA result, for functional experiments, TM3E3 should be used at a dilution of 1:4000, and dialysed TM3E3 at a dilution of 1:500.

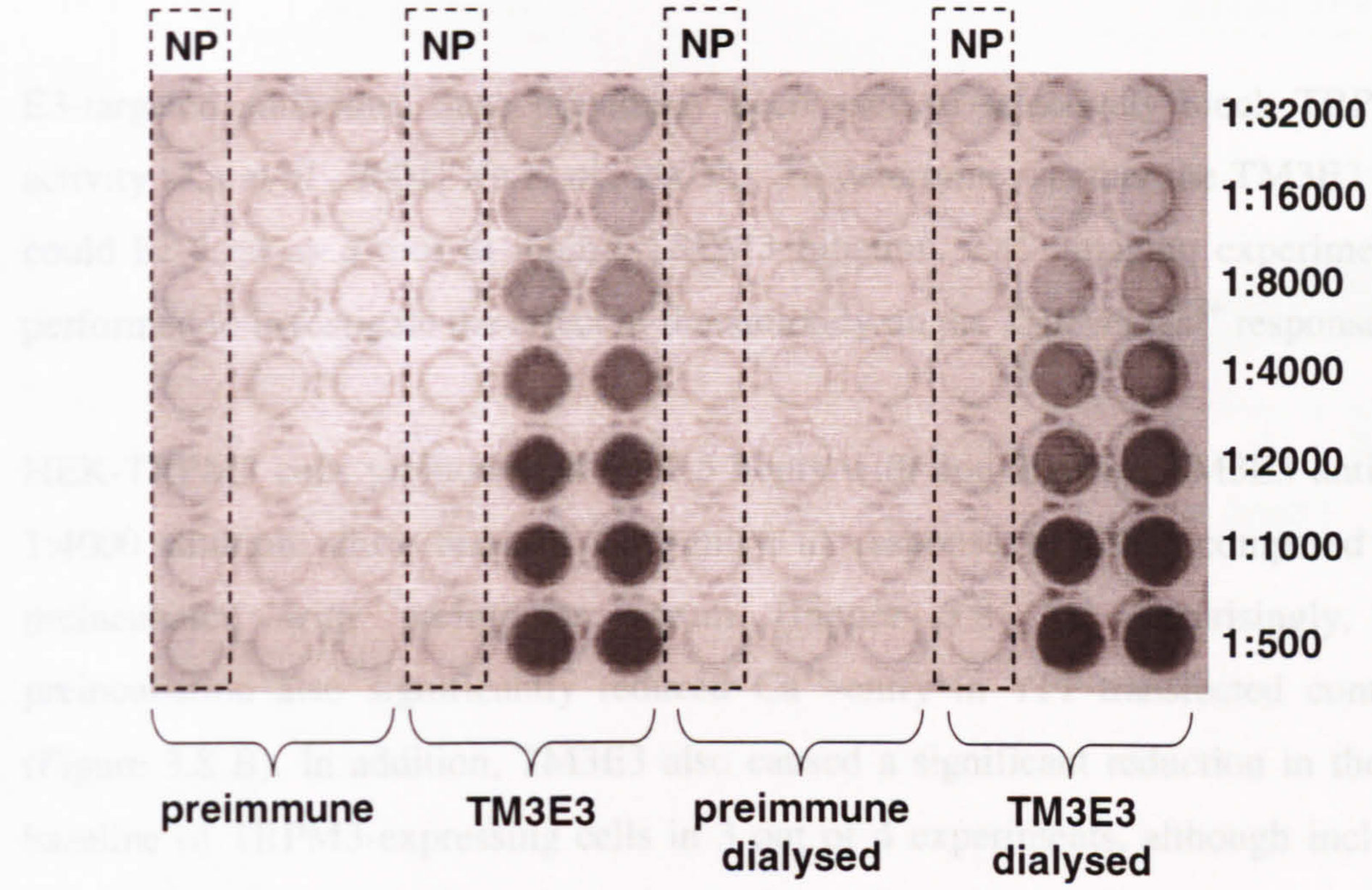

Figure 3.7. Antibody specificity and titre ELISAs were performed on antisera before and after dialysis. The amount of antibody bound to wells was determined by reading the absorbance at 405 nm (A_{405}). **A.** Image of ELISA plate layout; NP denotes no peptide control wells. **B**. Hill plot fitted to original (TM3E3) and dialysed (TM3E3d) antisera activity to calculate the concentration for half maximal activity. **C**. Mean data (±SEM) from duplicate readings in a single plate for TM3E3 with and without preadsorption to the antigenic peptide.

TM3E3 blocks SPH-activation of TRPM3

E3-targeted antibodies have previously been used to selectively block TRP channel activity (Xu *et al.*, 2001; Xu *et al.*, 2005b). To determine whether the TM3E3 antibody could be used as a tool to inhibit TRPM3 function, Ca^{2+} imaging experiments were performed to investigate the effect of the antibody on the TRPM3 Ca^{2+} response.

HEK-TRPM3 cells preincubated for 3.5 hours with non-dialysed TM3E3 antiserum at 1:4000 dilution show reduced Ca^{2+}-entry in response to SPH, compared to cells preincubated with preimmune serum (Figure 3.8 A). Surprisingly, TM3E3 preincubation also significantly reduced Ca^{2+}-entry in YFP-transfected control cells (Figure 3.8 B). In addition, TM3E3 also caused a significant reduction in the starting baseline of TRPM3-expressing cells in 3 out of 4 experiments, although including all the data led to a lack of statistical significance. No change in baseline was evident for YFP-expressing cells. This trend indicates that the antibody can also block constitutive activity of TRPM3.

The mean data indicate that TM3E3 inhibited SPH-induced Ca^{2+} entry in HEK-TRPM3 by ~47%, and in HEK-YFP by ~80% (Figure 3.8 C).

In summary, an antibody targeted to the 3rd extracellular loop of TRPM3 inhibits constitutive TRPM3 activity, and SPH-induced Ca^{2+}-entry, through native TRPM3 channels and channels over-expressed in HEK 293 cells.

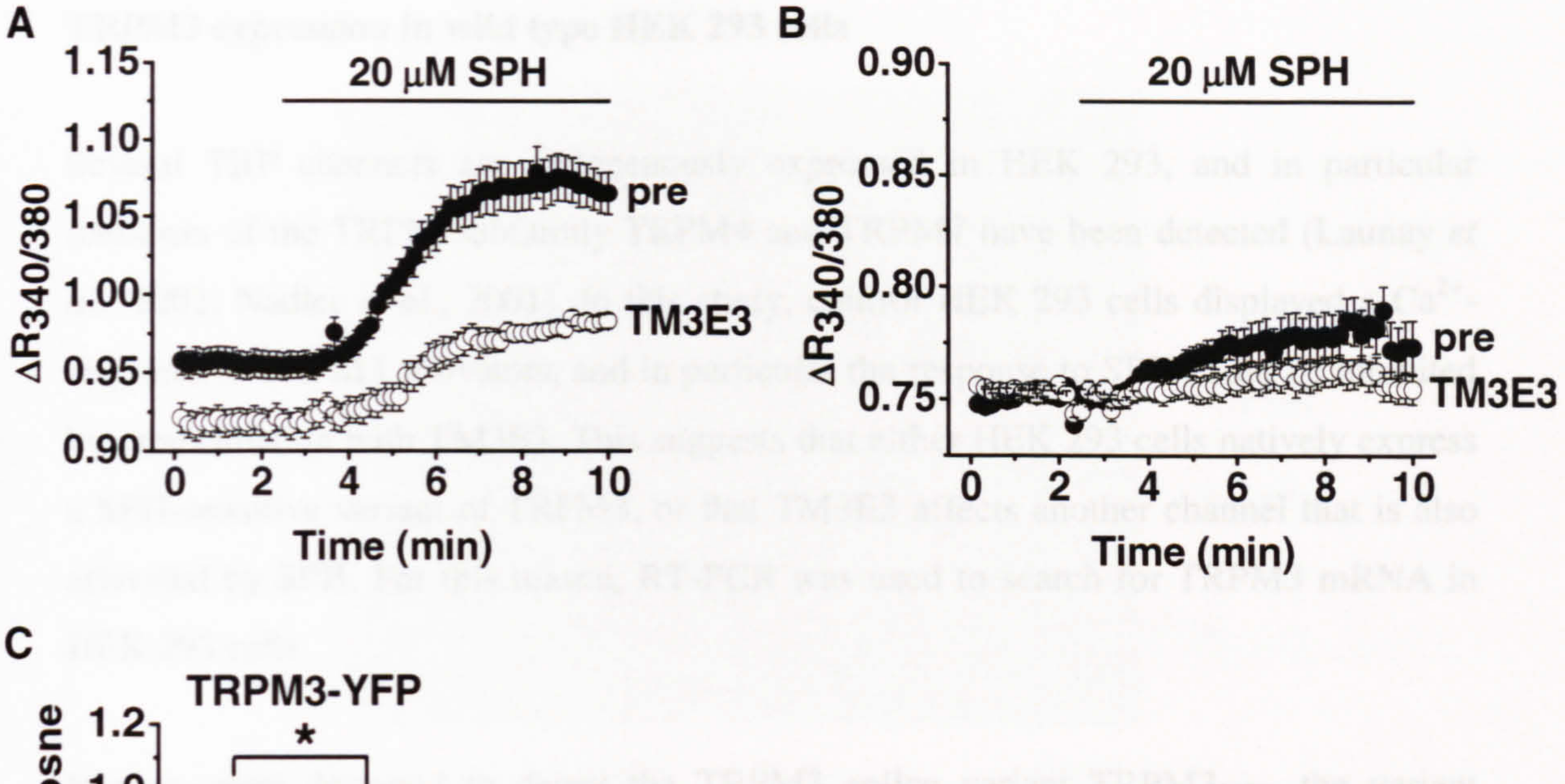

Figure 3.8. TM3E3 inhibits SPH-activation of TRPM3 Ca^{2+} signals were measured as the 340/380 nm ratio of emission in fura-2 loaded HEK 293 cells. Cells were transfected with TRPM3 or YFP as a control. Ethanol (vehicle) was present throughout experiments. **A.** Representative mean data (±SEM) showing Ca^{2+}-entry induced by SPH is inhibited by preincubation of HEK-TRPM3 with TM3E3, compared to preincubation with preimmune serum (pre) (pre n/N=3/29, TM3E3 n/N=3/22). **B.** Representative mean data (±SEM) showing effect of TM3E3 on YFP-expressing control cells (pre n/N=3/29, TM3E3 n/N=3/39). **C.** Mean data (±SEM) normalised to HEK-TRPM3 maximum preimmune response 6 min after SPH addition (TRPM3-YFP: TM3E3 n/N=11/85, pre n/N=11/90, YFP alone: TM3E3 n/N=3/39, pre n/N=3/30).

TRPM3 expression in wild type HEK 293 cells

Several TRP channels are endogenously expressed in HEK 293, and in particular members of the TRPM subfamily TRPM4 and TRPM7 have been detected (Launay *et al.*, 2002; Nadler *et al.*, 2001). In this study, control HEK 293 cells displayed a Ca^{2+}-response to TRPM3 activators, and in particular the response to SPH could be inhibited by preincubation with TM3E3. This suggests that either HEK 293 cells natively express a SPH-sensitive variant of TRPM3, or that TM3E3 affects another channel that is also activated by SPH. For this reason, RT-PCR was used to search for TRPM3 mRNA in HEK 293 cells.

Primers were designed to detect the TRPM3 splice variant $TRPM3_{1325}$, the variant reportedly activated by SPH and hypotonic stimulation and used in this study. As TRPM3 is highly expressed in brain (Lee *et al.*, 2003a), human brain cDNA was included as a positive control for TRPM3 expression. Primers directed against β-actin were used to probe HEK 293 cDNA as a second positive control. β-actin is one of 6 different actin isoforms that contribute to the actin cytoskeleton, and high levels are expressed by most cell lines. PCR products were resolved by agarose gel electrophoresis.

PCR amplified a 335 bp product corresponding to TRPM3 from both HEK 293 and brain cDNA using the $TRPM3_{1325}$ primer pair (Figure 3.9). The β-actin primer pair amplified a 194 bp product from HEK 293 cDNA, as predicted.

In summary, solution PCR amplification revealed TRPM3 mRNA is present in HEK 293 cells, which could account for the Ca^{2+}-responses to TRPM3 activators that were observed in control cells.

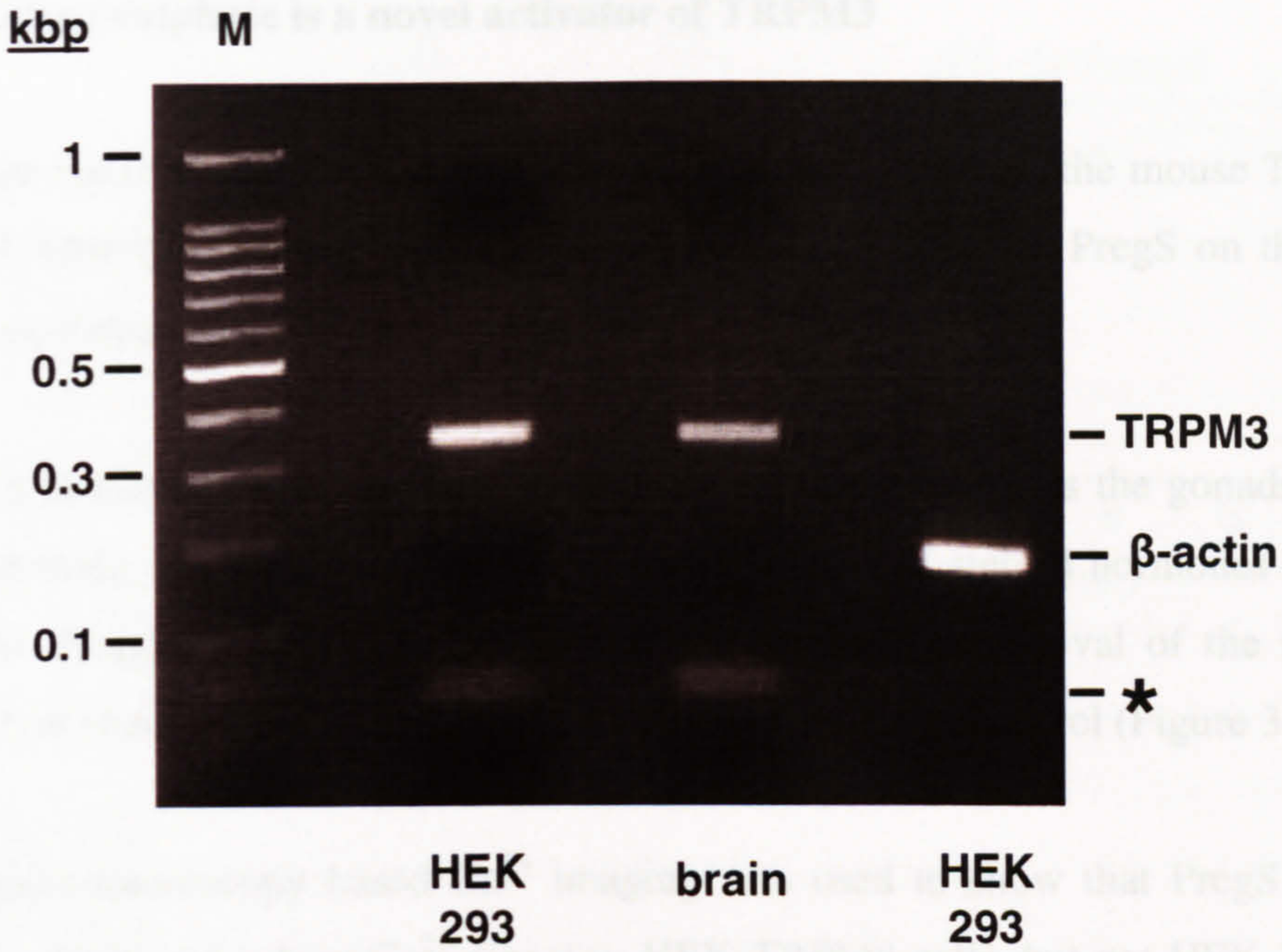

Figure 3.9. TRPM3 expression in HEK 293 cells DNA gel stained with ethidium bromide. PCR was performed using primers designed to amplify reverse transcribed TRPM3 mRNA from human brain or HEK 293 cDNA. M depicts 100 bp marker. Low molecular weight bands designated by * are most likely a consequence of the extension of self-annealed primers (primer dimers).

Pregnenolone sulphate is a novel activator of TRPM3

It has been reported that pregnenolone sulphate (PregS) activates the mouse TRPM3α2 variant (J. Oberwinkler, personal communication). The effect of PregS on the human $TRPM3_{1325}$ variant was therefore examined.

PregS is a neurosteroid endogenous to mammalian tissues such as the gonads, adrenal gland and brain, and is a precursor for the biosynthesis of steroid hormones (Gibbs *et al.*, 2006). PregS itself is synthesized from cholesterol by removal of the non-polar hydrocarbon chain, and is therefore similar in structure to cholesterol (Figure 3.10 A).

Fluorescence-microscopy based Ca^{2+} imaging was used to show that PregS (25 μM) activated a large and robust Ca^{2+} signal in HEK-TRPM3 cells, but not HEK-YFP cells (Figure 3.10 B). Compared to Ca^{2+} responses induced by other TRPM3 activators, the response to PregS was rapid, sustained and of much greater magnitude. After 2 min, responses in HEK-TRPM3 were 20 times larger than the YFP-control response, confirming PregS is a novel and strong activator of human TRPM3.

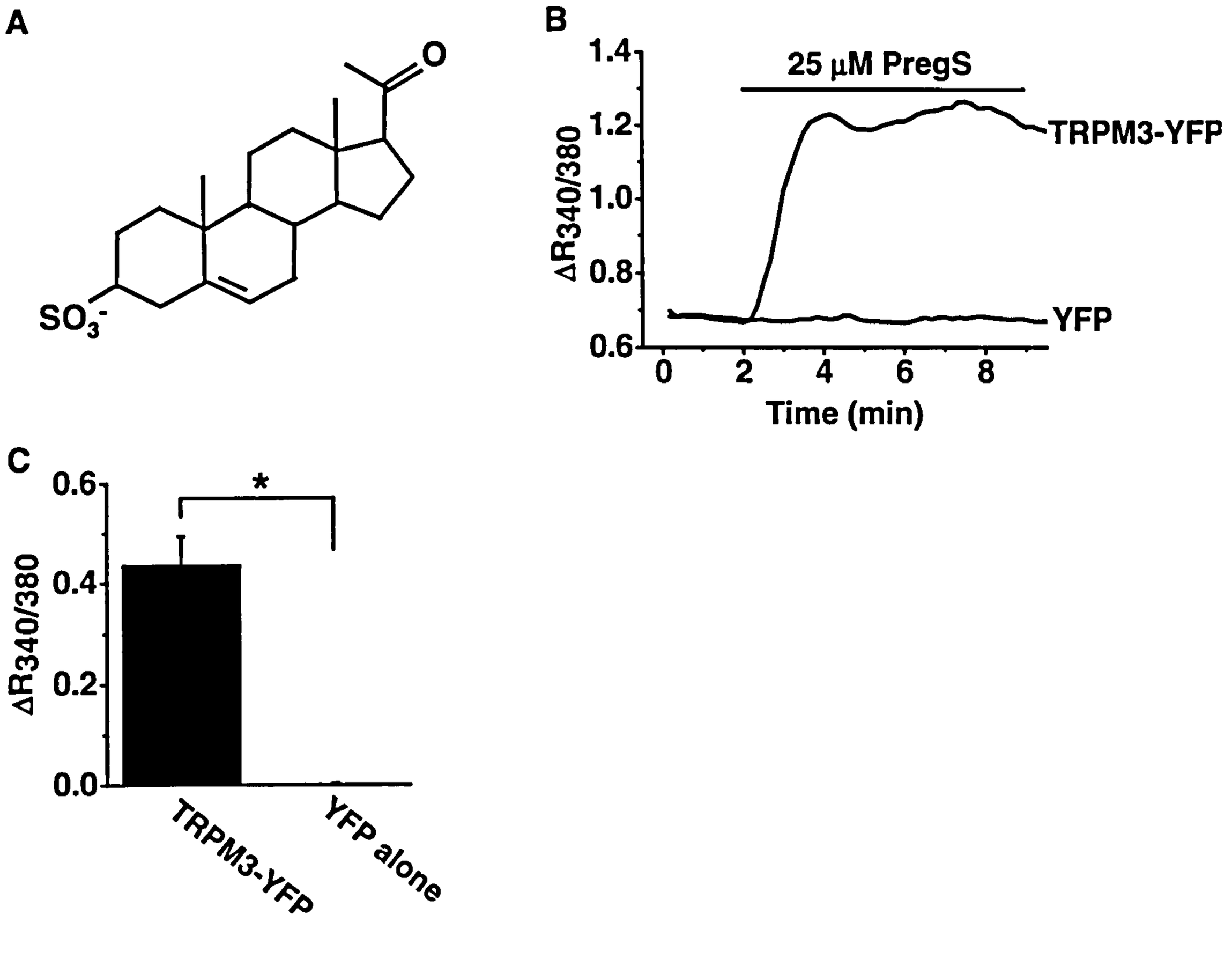

Figure 3.10. Pregnenolone sulphate (PregS) increases Ca^{2+} signals in TRPM3-expressing cells Ca^{2+} signals were measured as the 340/380 nm ratio of emission in fura-2 loaded HEK 293 cells. Cells were transfected with TRPM3 or YFP as a control. DMSO (vehicle) was present throughout recordings. **A.** Structure of PregS. **B.** Representative traces from single cells. PregS (25 μM) causes an increase in Ca^{2+} in TRPM3-expressing cells compared to YFP-expressing control cells (grey trace). **C.** Mean data (±SEM) showing a significant increase in Ca^{2+} 2 min after PregS application (TRPM3 n/N=3/26, YFP n/N=3/50).

A tetracycline-inducible stable TRPM3 cell line

A tetracycline-inducible TRPM3-expression system in HEK 293 cells was developed by F. Zeng to allow for the high-throughput analysis of TRPM3 Ca^{2+} signals. The YFP-tag was removed for this system. An inducible system is ideal for identification of specific TRPM3 responses as opposed to endogenous cell activity, as TRPM3-expressing and control cells come from the same population of cells.

To determine whether the TRPM3-specific antibody TM3E3 could specifically detect its target antigen in tetracycline-induced (tet+) cells, and to demonstrate a marked increase in protein expression compared to non-induced cells, western blotting was performed. Dialysed TM3E3 was used at a dilution of 1:4000. The calculated molecular weight for TRPM3 is 157 kDa, and published western blot data give an apparent molecular mass of 160 kDa (Grimm *et al.*, 2003). In this study, TM3E3 recognised a protein of approximately 150 kDa (Figure 3.11 A). This 150 kDa band was absent following pre-incubation of TM3E3 with 10 μM of the antigenic peptide. Line scan analysis of individual lanes shows other low molecular weight bands detected by TM3E3 were not completely blocked by pre-incubation with peptide, indicating these bands are not related to TRPM3 (Figure 3.11 B).

TRPM3 expression was further confirmed using immunocytochemistry. The nuclear staining agent DAPI was used to locate cells. Dialysed TM3E3 at a dilution of 1:4000 was able to detect TRPM3 in tetracycline-induced (tet+) cells (Figure 3.12), and no staining was observed when the primary antibody was omitted or when TM3E3 was preadsorbed to its antigenic peptide. Additionally, there was a small amount of faint staining observed in non-induced (tet-) control cells, consistent with native expression.

In summary, TM3E3, an antibody targeted to the 3rd extracellular loop of TRPM3, binds TRPM3 protein. In addition, the data confirm that tetracycline-induction causes a clear increase in TRPM3 protein levels.

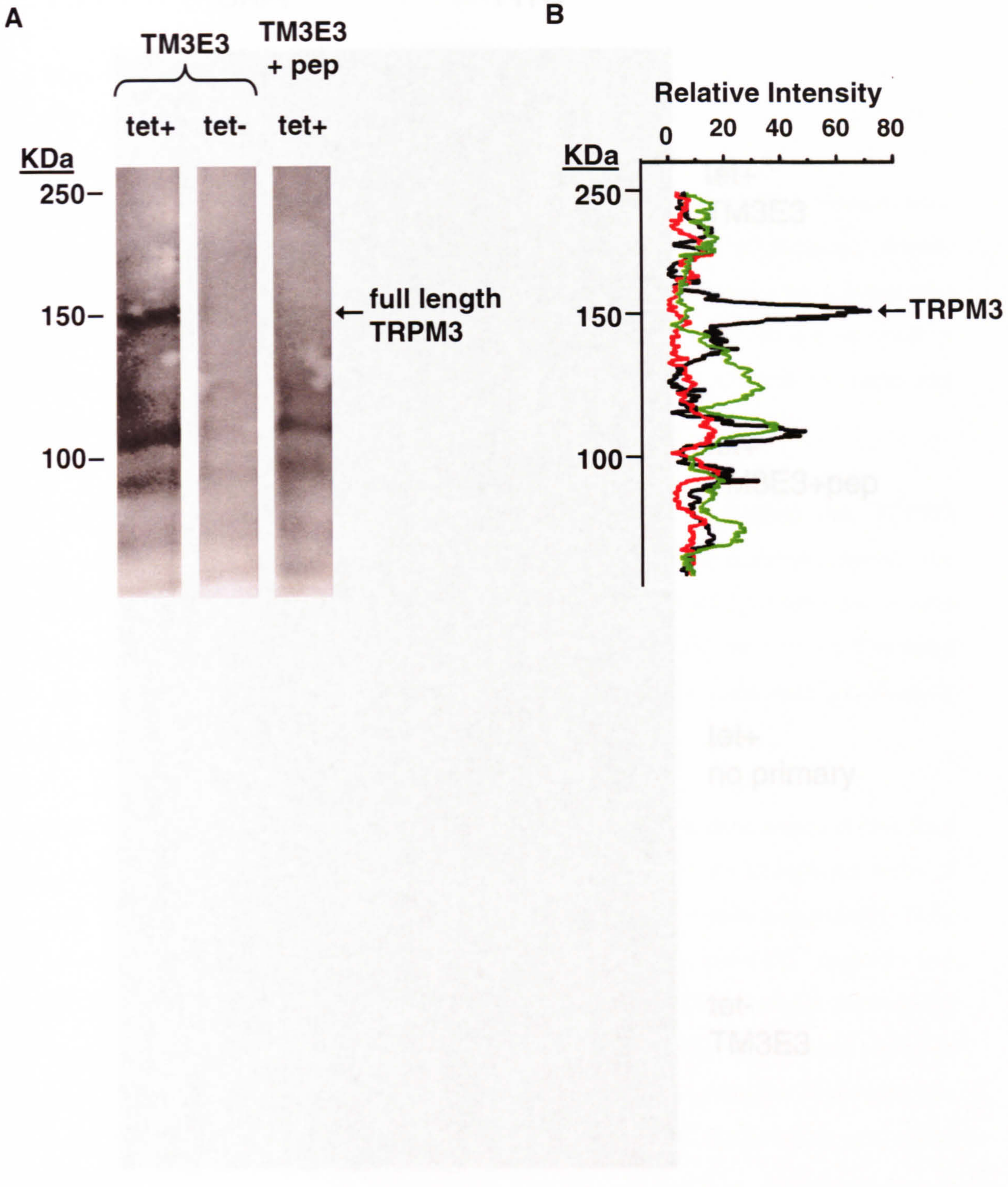

Figure 3.11. Detection of TRPM3 protein Western blotting on lysates of tetracycline-induced (tet+) or non-induced (tet-) HEK-TRPM3 cells. **A.** Lysates were blotted with dialysed TM3E3 antibody or TM3E3 preadsorbed to its antigenic peptide (TM3E3 + pep) as a negative control. **B.** Line scan analysis of individual western blot lanes shows TRPM3 signal present in tet+ lane (black line) is not present in peptide-adsorbed (green line) or tet- (red trace) control lanes.

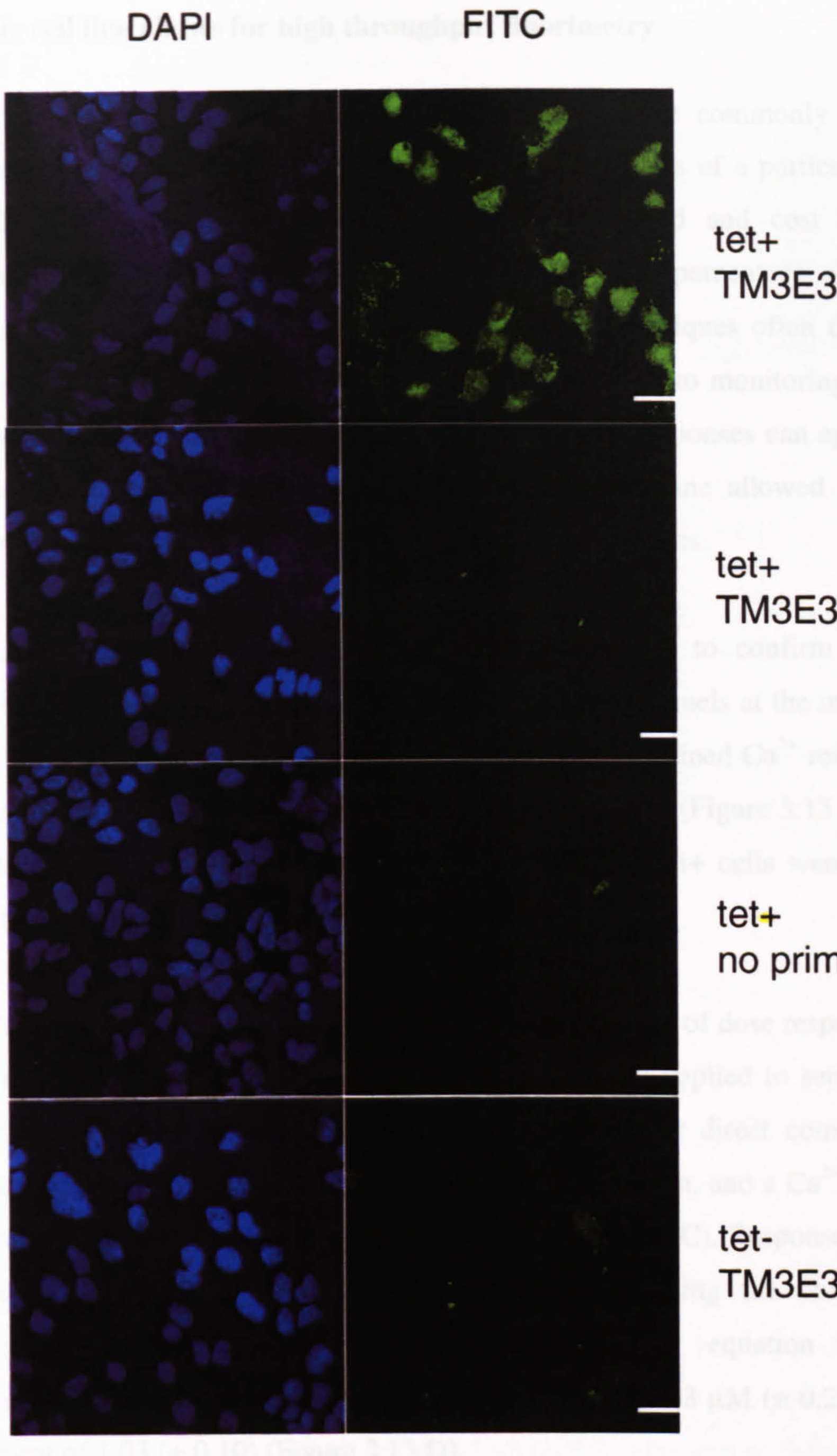

Figure 3.12. Immunofluorescence detection of TRPM3 Immunocytology performed on non-permeabilised, tetracycline-induced (tet+) or non-induced (tet-) HEK-TRPM3 cells. Cells were co-stained with DAPI and TM3E3 antibody plus a FITC conjugated secondary antibody. For negative controls, TM3E3 was preadsorbed to its antigenic peptide (TM3E3 + pep) or primary antibody was omitted. Scale bar represents 20μm.

A stable cell line allows for high throughput fluorimetry

High throughput technologies such as the FlexStation are commonly used in drug discovery to screen large compound libraries for modulators of a particular protein or physiological function. Although such systems are rapid and cost effective, the downside is they require large numbers of cells, a high percentage of which must express the protein of interest. Standard transfection techniques often do not display sufficient efficiency of expression. As the user is restricted to monitoring a population of cells rather than selecting regions of interest, cellular responses can appear small or undetectable. The development of a stable TRPM3 cell line allowed for rapid and efficient channel expression, ideal for high-throughput systems.

FlexStation fluorimetry of fura-2 loaded cells was used to confirm that TRPM3 expression induced by tetracycline produced functional channels at the membrane. The TRPM3 activator PregS (25 μM) activated a rapid and sustained Ca^{2+} response in cells expressing TRPM3 (tet+) but not in non-induced cells (tet-) (Figure 3.13 A). The mean data show that after 1 min, PregS-induced responses in tet+ cells were significantly larger than tet- cells (Figure 3.13 B).

The FlexStation also enables fast and accurate determination of dose response data for a given agonist. Different concentrations of agonist can be applied to separate wells of test and control cells within the same plate, allowing for direct comparison. Dose response data were produced in this way for PregS activation, and a Ca^{2+} response was activated by concentrations of PregS $\geq$ 0.3 μM (Figure 3.13 C). Responses increased in magnitude with higher concentrations of PregS, indicating the channel displays concentration-dependant activation. Fitting of the Hill equation indicated the concentration for half maximal activation, the EC_{50}, was 1.83 μM (± 0.23), with a Hill coefficient of 1.03 (± 0.10) (Figure 3.13 D).

The robust Ca^{2+} signals in response to PregS activation of TRPM3 were ideal for FlexStation fluorimetry. It is evident that PregS can activate TRPM3 in a concentration dependent manner, and when combined with a stable cell line, is a valuable tool for high throughput screening.

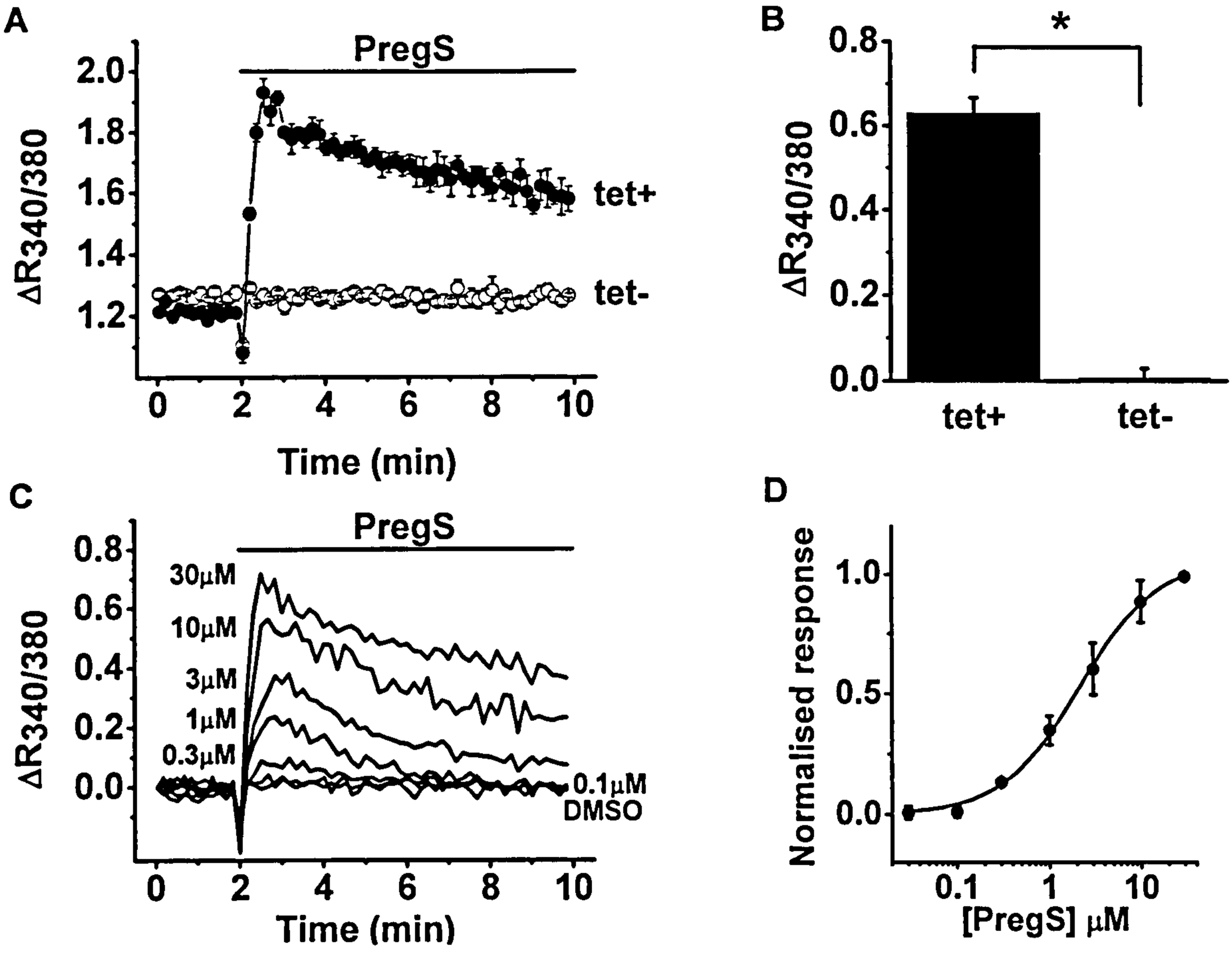

Figure 3.13. PregS increases Ca^{2+} signals in tet+ TRPM3 cells Ca^{2+} signals were measured as the 340/380 nm ratio of emission in fura-2 loaded HEK 293 cells. Cells were induced by incubation with tetracycline (tet+). Cells not treated with tetracycline were included as a control (tet-). DMSO (vehicle) was present throughout recordings. **A.** Mean data from 6 wells within a single plate. PregS (25 μM) causes an increase in Ca^{2+} in tet+ TRPM3 compared to tet- (open circles). **B.** Mean data (±SEM) showing significant increase in Ca^{2+} 1 min after PregS application (tet+ n/N=3/12, tet- n/N=3/12). **C.** Single trace representatives show dose-dependant activation of TRPM3 expressing cells in response to PregS (0.1-30 μM). **D.** Mean dose response data (±SEM) taken 1 min after application from 3 independent experiments, analysed using the Hill equation.

Pregnenolone sulphate does not activate TRPC5 or TRPM2

To determine the specificity of TRPM3 activation by PregS, its effect on other stable, tetracycline-inducible TRP cell lines was also investigated using fura-2 loaded cells and high-throughput Ca^{2+} fluorimetry. TRPM2 and TRPC5 stable cell lines were induced by tetracycline (tet+), and non-induced cells (tet-) were included in the same 96-well plate as controls.

The lanthanide gadolinium (Gd^{3+}) is a non-specific cation channel modifier that exerts dual effects on TRP channels in that it can be either excitatory or inhibitory. It is recognised as a TRPC5 channel activator at micromolar concentrations (Jung *et al.*, 2003). Gd^{3+} (100 μM) caused a significant increase in Ca^{2+} influx in tet+ TRPC5 cells, but PregS (25 μM) had no effect (Figure 3.14 A). The mean data show neither Gd^{3+} nor PregS caused any Ca^{2+} increase in non-induced cells (tet-) (Figure 3.14 C).

TRPM2 plays an important role in cell death induced by oxidative-stress, and can be activated by hydrogen peroxide (H_2O_2) (Wehage *et al.*, 2002). H_2O_2 (1 mM) caused a significant increase in Ca^{2+} entry in tet+ TRPM2 cells, yet again PregS (25 μM) had no effect (Figure 3.14 B). The mean data show neither H_2O_2 nor PregS caused a Ca^{2+} response in tet- control cells (Figure 3.14 C).

In addition, PregS failed to elicit Ca^{2+} responses in TRPV4-expressing cells (C. Jones, AstraZeneca, personal communication).

The data indicate PregS cannot activate TRPC5, TRPM2 and TRPV4, and may be a relatively specific activator for TRPM3.

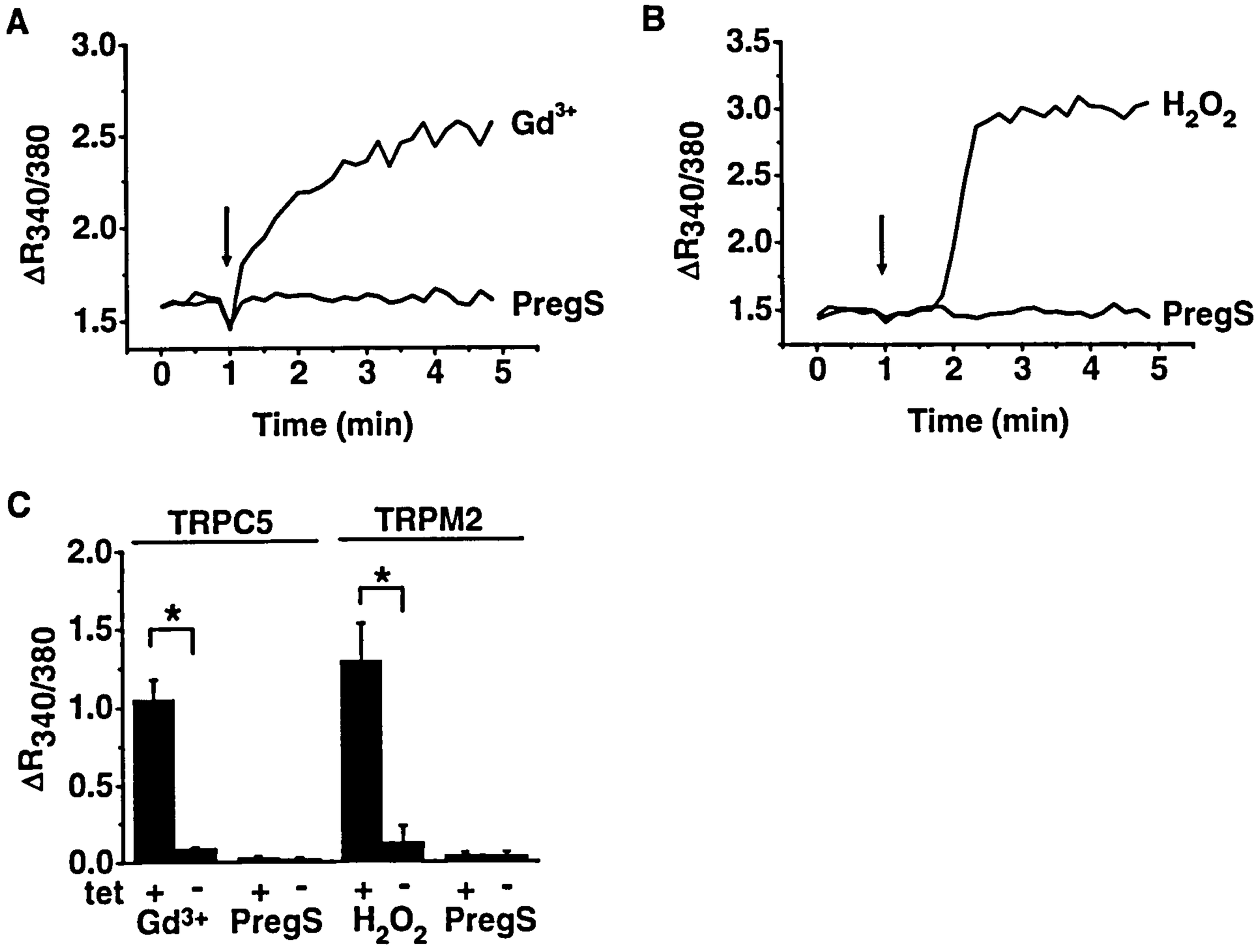

Figure 3.14. PregS does not activate other TRP family members Ca^{2+} signals were measured as the 340/380 nm ratio of emission in fura-2 loaded HEK 293 cells. For PregS application, DMSO (vehicle) was constant throughout experiments. Traces correspond to data from a single well, representative of 6 wells within one plate (n/N=1/6). Arrow indicates time point of compound addition. **A.** Tetracycline-induced TRPC5 with PregS (25 μM) or positive control (100 μM Gd^{3+}) addition. **B.** Tetracycline-induced tet+ TRPM2 with PregS (25 μM) or positive control (1 mM H_2O_2) addition. **C.** Mean data (±SEM) from 3 plates normalised to maximum response for positive control at 4 min after application (n/N=3/12).

Characterisation of PregS-induced Ca^{2+} responses

Recognised TRP channel inhibitors were used to further characterise the PregS-induced TRPM3 response. Fura-2 loaded cells were preincubated for half an hour with inhibitors before analysis using high-throughput fluorimetry.

Although known to activate TRPC5, gadolinium (Gd^{3+}) is also useful as a blocker of most TRP channels, including TRPM3 (Lee *et al.*, 2003a). Gd^{3+} (100 μM) completely inhibited PregS-induced Ca^{2+}-influx in tetracycline-induced (tet+) TRPM3 cells (Figure 3.15 A). The mean data indicate that at 1 min after PregS application, Gd^{3+} inhibited the PregS response in tet+ cells by 100%, but did not affect non-induced (tet-) cells (Figure 3.15 C).

2-aminoethoxydiphenylborate (2-APB) was initially introduced as an inhibitor of the IP_3 receptor; however it has become established as a blocker of store-operated Ca^{2+} entry (Bootman *et al.*, 2002). More recently it has emerged as an inhibitor of several TRP family members, including TRPM3 (Xu *et al.*, 2005a). 2-APB (75 μM) inhibits Ca^{2+}-responses evoked by PregS (25 μM) in tet+ cells (Figure 3.15 B). The mean data show that at 1 min after PregS application, 2-APB inhibited PregS-induced Ca^{2+} responses by approximately 70%, with no significant effect in non-induced (tet-) cells (Figure 3.15 C).

To investigate if PregS causes Ca^{2+} influx across the membrane through TRPM3 channels, rather than leading to Ca^{2+} release from stores, cells were exposed to thapsigargin (Tg). Tg empties intracellular Ca^{2+} pools by inhibiting the sarcoplasmic reticulum Ca^{2+}-ATPase (SERCA), thus preventing refilling of Ca^{2+} stores following depletion. A 30 min preincubation with Tg (1 μM) reduced the amplitude of the response to PregS, but the overall response was the same as the control. The mean data show that the baseline ratio in both tet+ and tet- cells was increased in cells exposed to Tg, which is likely to be the result of activation of endogenous store-operated channels in this cell type (Figure 3.16 B). The mean data also show a significant reduction in the amplitude of the PregS response in TRPM3-expressing cells (Figure 3.16 C).

To further investigate the relationship between intracellular Ca^{2+} stores and the PregS response, experiments were performed in the absence of extracellular Ca^{2+}. In the

absence of Ca^{2+} the PregS response was completely absent, demonstrating PregS causes Ca^{2+}influx (Figure 3.17 A & B). As a positive control, CCh was applied, and was seen to elicit a Ca^{2+} response, demostrating availability of stores for Ca^{2+} release (Figure 3.17 C).

In summary, the PregS response is due to TRPM3-mediated Ca^{2+} influx across the plasma membrane and does not involve Ca^{2+} release.

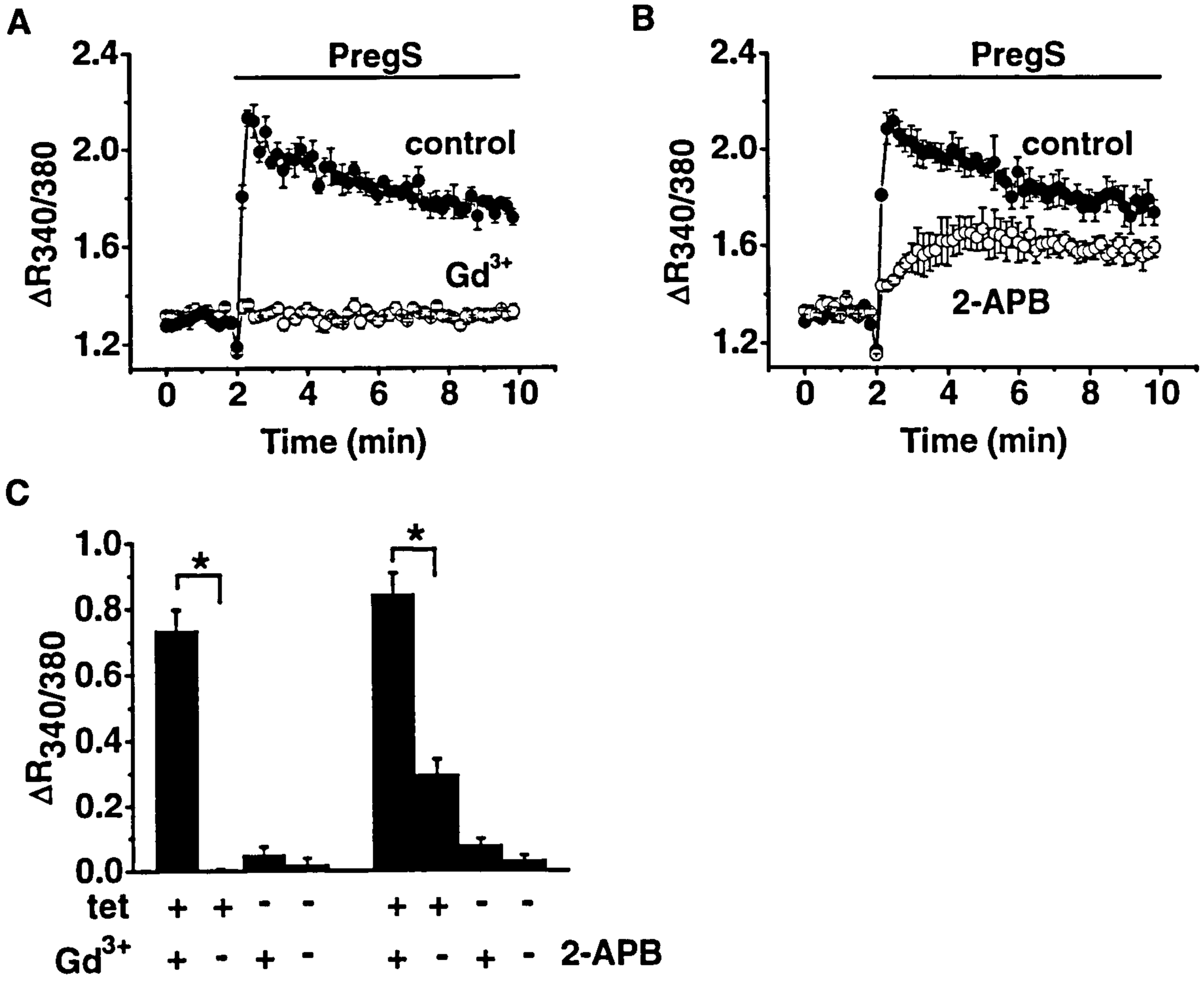

Figure 3.15. Characterisation of the PregS response Ca^{2+} signals were measured as the 340/380 nm ratio of emission in fura-2 loaded HEK 293 cells. Traces are representative mean data (±SEM) from 6 wells within a single plate. DMSO (vehicle), Gd^{3+} and 2-APB were present for the duration of recordings. **A.** Gd^{3+} (100 μM) completely inhibited the Ca^{2+} response. **B.** 2-APB also causes significant inhibition of the Ca^{2+} response. **C.** Mean data (±SEM) from 3 independent experiments taken 1 min after PregS application, with (n/N=3/9) and without inhibitors (n/N=3/9).

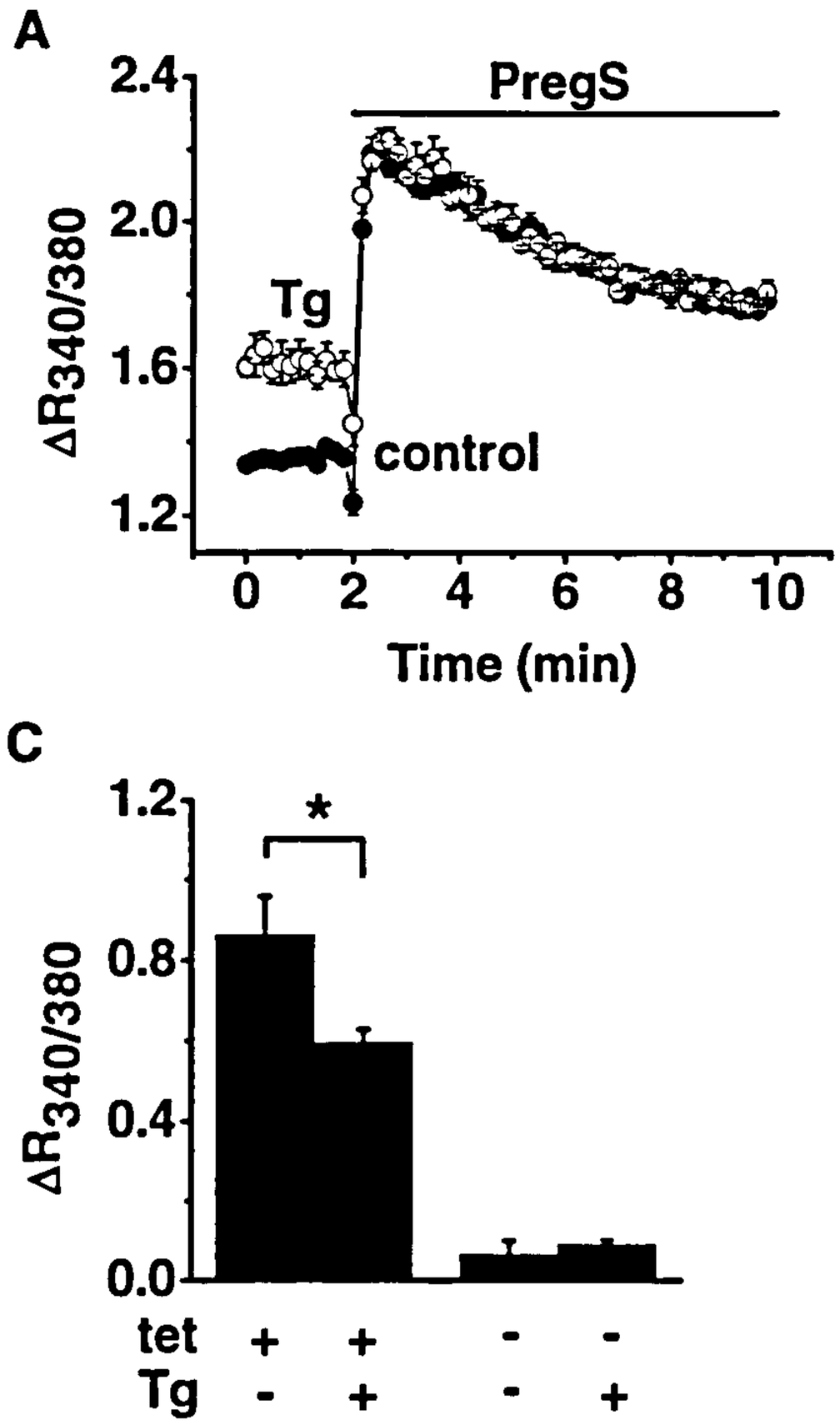

Figure 3.16. Effect of thapsigargin on the PregS response Ca^{2+} signals were measured as the 340/380 nm ratio of emission in fura-2 loaded HEK 293 cells. Traces are representative mean data (±SEM) from 6 wells within a single plate. DMSO (vehicle) was present throughout recordings. **A.** Preincubation for ½ hour with Tg (1 μM) increases the baseline Ca^{2+} ratio. **B.** Mean data (±SEM) showing change in baseline. **C.** Baseline subtracted mean data (±SEM) from 3 independent experiments taken 1 min after PregS application, with (n/N=3/9) and without Tg (n/N=3/9) preincubation.

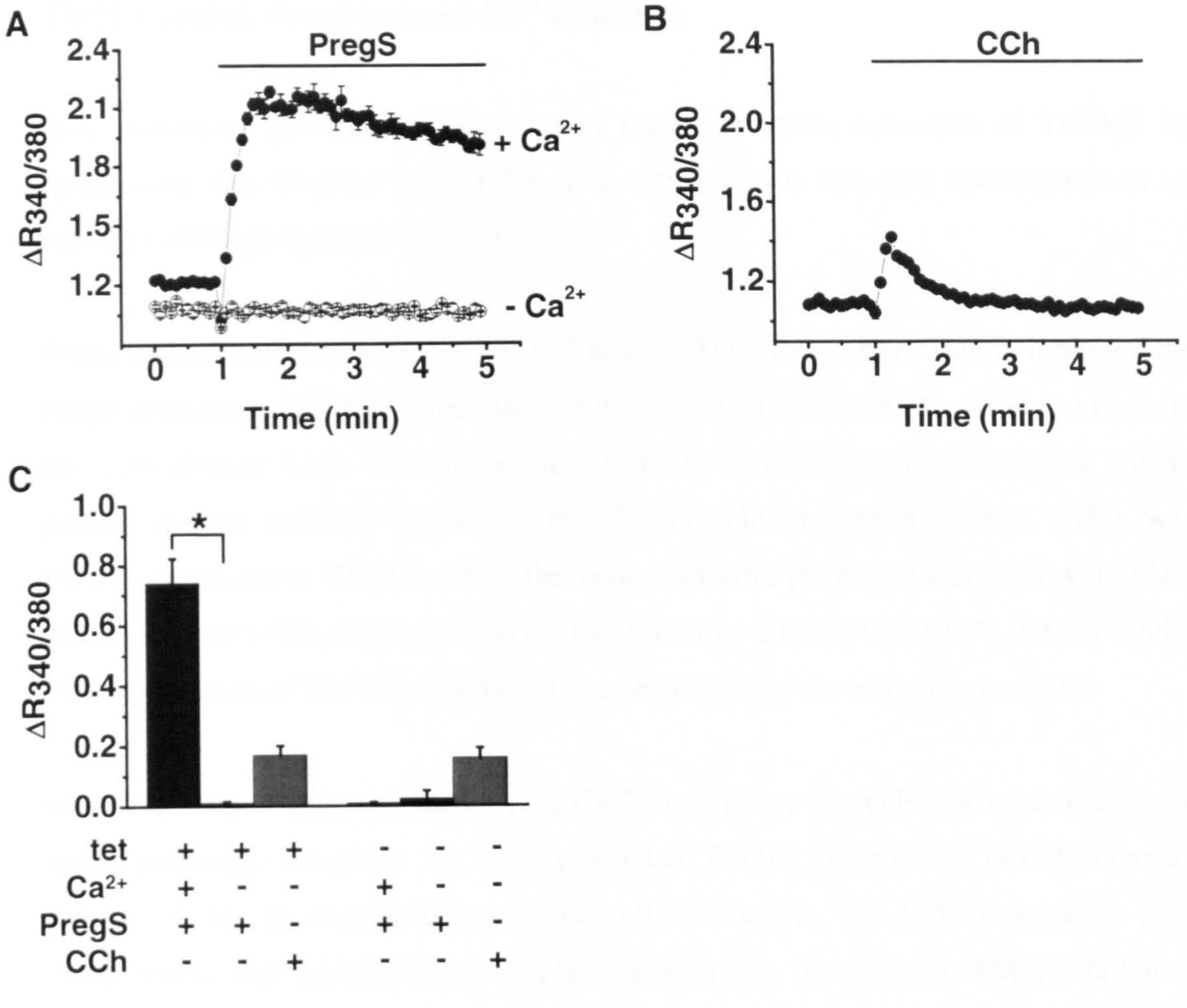

Figure 3.17. The PregS response does not involve Ca^{2+} release from stores Ca^{2+} signals were measured as the 340/380 nm ratio of emission in fura-2 loaded HEK 293 cells. DMSO (vehicle) was present throughout recordings. **A**. Representative mean data (±SEM) from 3 wells within a single plate. PregS (25 μM) does not elicit a Ca^{2+} response in the absence of extracellular Ca^{2+}. **B.** Mean data (±SEM) from 3 independent experiments (n/N=3/9) taken 30 seconds after PregS application.

TM3E3 inhibits PregS-induced Ca^{2+} responses

Data previously presented in this chapter showed that the activation of TRPM3 by sphingosine was blocked by TM3E3. The antibody was therefore investigated as an inhibitor of PregS-induced Ca^{2+} entry.

Preincubation with non-dialysed TM3E3 at a 1:4000 dilution significantly inhibited the PregS response in TRPM3-expressing cells by an average of 26.1%, with no effect on tet- cells (Figure 3.18). To explore the selectivity of E3-targeted antibodies, a second peptide specific antibody targeted to the 3rd extracellular loop of TRPC1, T1E3, was directly compared to TM3E3 within the same microtitre plate. Preincubation with T1E3 at a dilution of 1:500, determined as the most suitable dilution by ELISA, did not inhibit PregS activation of TRPM3, nor did it have any effect on tet- cells (Figure 3.18).

HEK 293 cells display an increase in Ca^{2+} in response to ATP due to activation of native purinergic receptors. To explore whether TM3E3 inhibits the TRPM3 channel directly, or has an overall effect on the cell as a whole, the ATP response in cells preincubated with preimmune or TM3E3 antisera was investigated. TM3E3 failed to inhibit the endogenous ATP-induced Ca^{2+}-reponse in tet- cells (Figure 3.19 A and B). In addition, the mean data (Figure 3.19 B) confirm that ATP applied to tet+ cells does not cause a significant difference in the Ca^{2+} response in tet+ cells, suggesting ATP cannot activate TRPM3.

To further confirm specificity of the antibody, the blocking ability of TM3E3 was examined for other TRP family members. TM3E3 did not inhibit H_2O_2-induced Ca^{2+} responses in TRPM2, (Figure 3.20 A), Gd^{3+} activation of TRPC5 (Figure 3.20 B), or 4αPDD activation of TRPV4 (Figure 3.20 C).

The data strengthen the idea that E3-targetted antibody design can be used to generate a highly specific ion channel blocker.

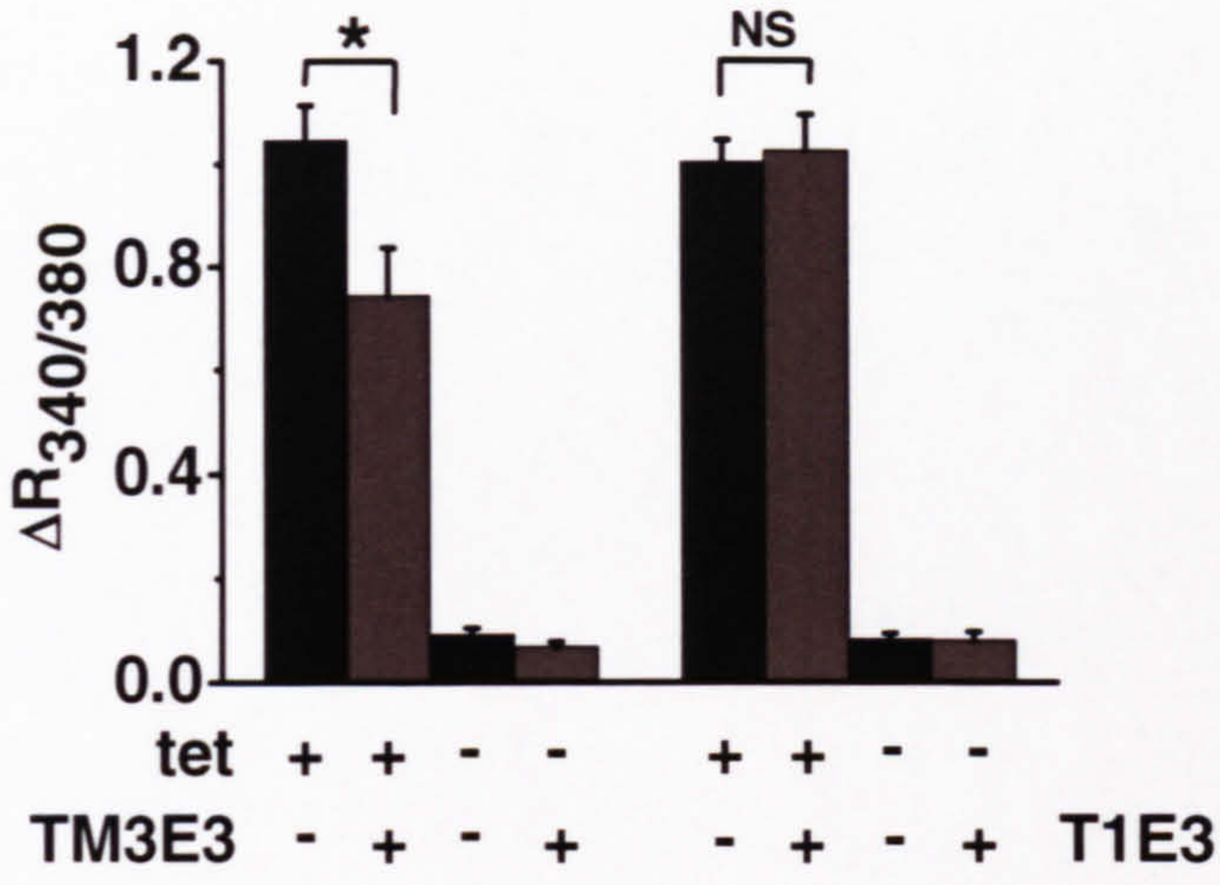

Figure 3.18. TM3E3, but not T1E3, inhibits PregS activation of TRPM3 Ca^{2+} signals were measured as the 340/380 nm ratio of emission in fura-2 loaded HEK 293 cells. Cells were induced by incubation with tetracycline (tet+); non-induced cells (tet-) were included as a control. Mean data (±SEM) from 3 individual experiments taken 30 seconds after PregS application. Cells preincubated with antibody are indicated by grey bars. Preimmune controls are indicated by black bars. PregS (25 μM) caused an increase in Ca^{2+} in tet+ TRPM3 that was inhibited by preincubation with TM3E3 compared to preimmune control. Within the same plate, the PregS response was not inhibited by preincubation with the anti-TRPC1 antibody, T1E3 compared to its preimmune control. For each test group n/N=3/18.

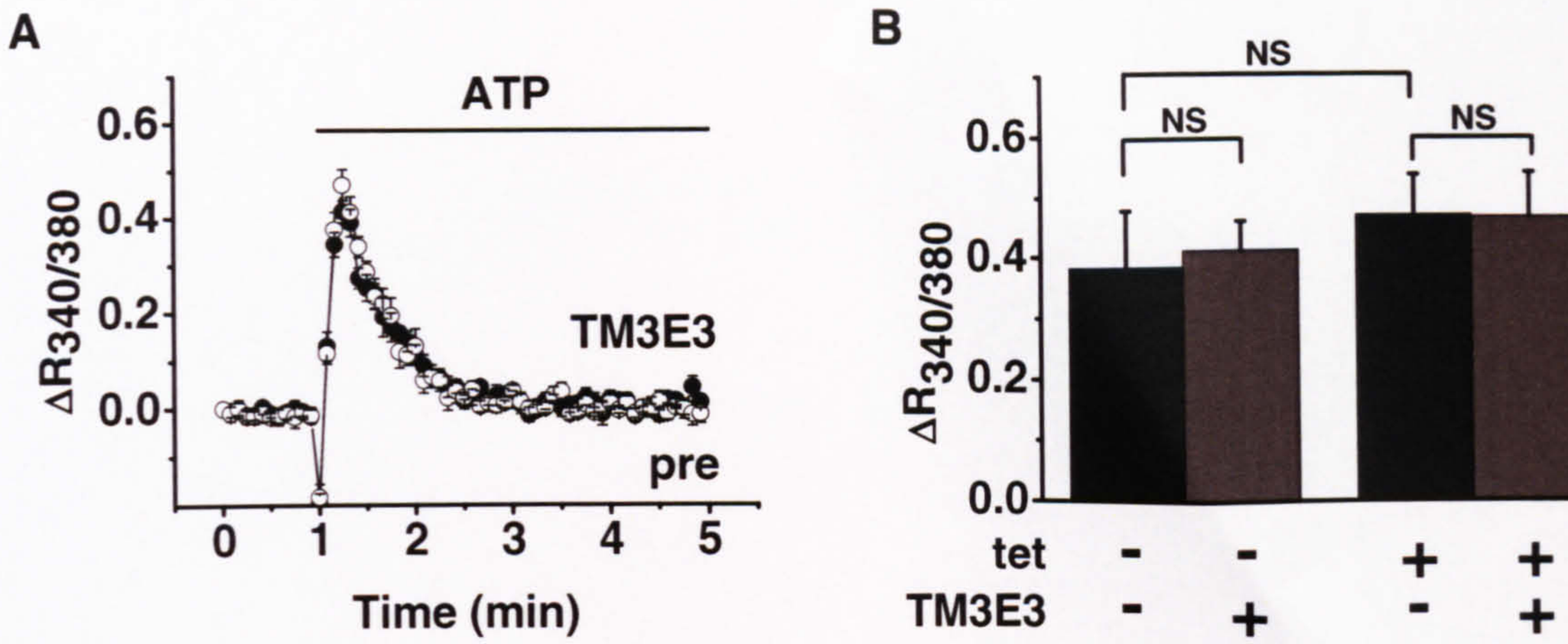

Figure 3.19. TM3E3 does not inhibit the native ATP response Ca^{2+} signals were measured as the 340/380 nm ratio of emission in fura-2 loaded HEK 293 cells. Traces are representative mean data (±SEM) from 6 wells within a single plate. **A**. ATP (10 μM) caused an increase in Ca^{2+} in tet- TRPM3 that was not inhibited by preincubation with TM3E3 (open circles) compared to preimmune control (closed circles). **B**. Mean data (±SEM) taken 15 seconds after ATP application, for 3 individual experiments for tet- and tet+ TRPM3 cells preincubated with preimmune (black bars) or TM3E3 antisera (grey bars). For each test group, n/N=3/18.

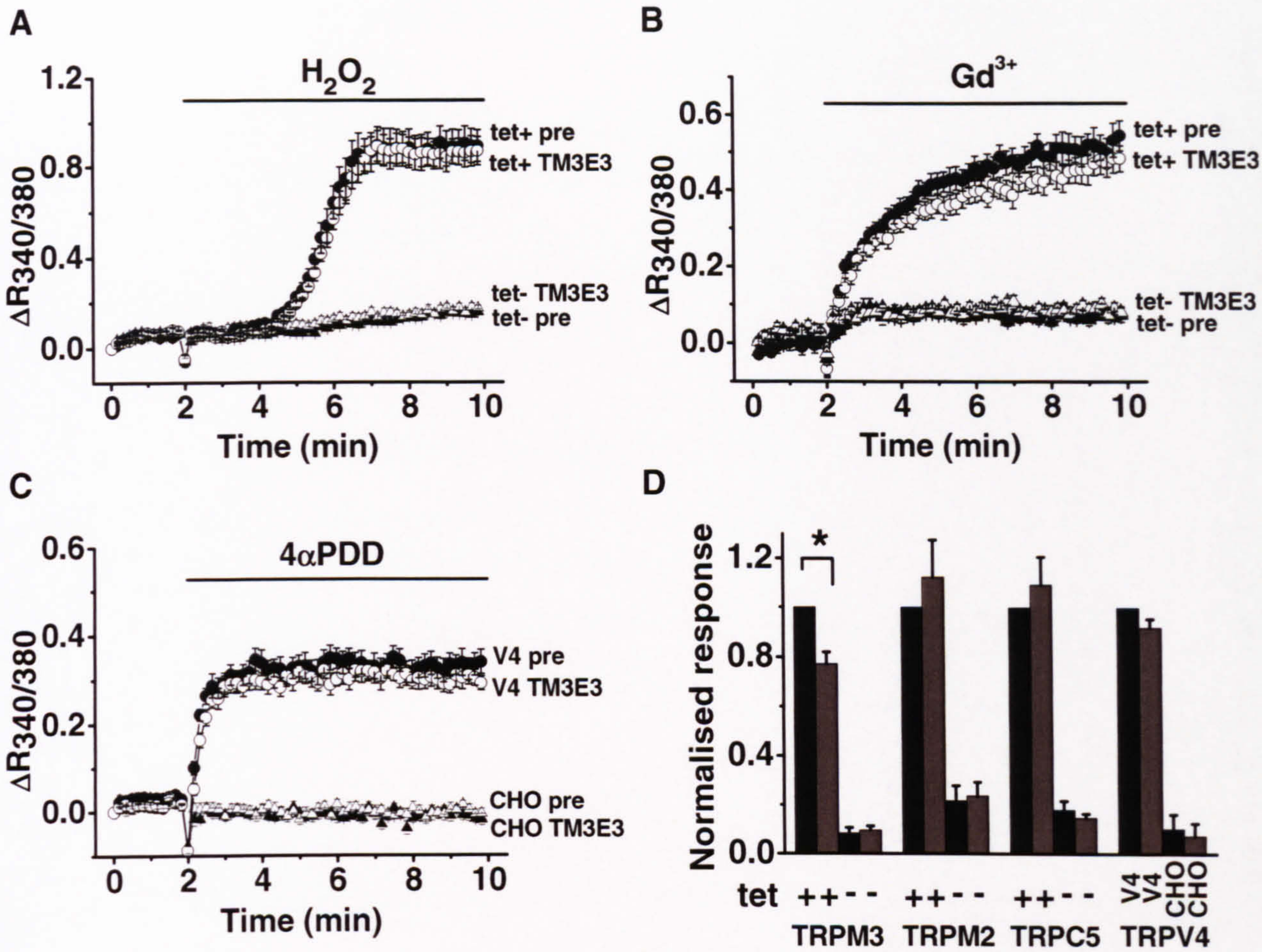

Figure 3.20. Specificity of TM3E3 Ca^{2+} signals were measured as the 340/380 nm ratio of emission in fura-2 loaded HEK 293 cells. TRPM2 and TRPC5 cells were induced by incubation with tetracycline (tet+), non-induced cells (tet-) were included as a control. For TRPV4, the parent CHO cell line was included as a control. Traces are representative mean data (±SEM) from one independent experiment. **A**. H_2O_2 (1 mM) caused an increase in Ca^{2+} in tet+ TRPM2 (closed circles) that was not inhibited by TM3E3 (open circles). **B**. Gd^{3+} 100 μM) caused an increase in Ca^{2+} in tet+ TRPC5 (closed circles) that was not inhibited by TM3E3 (open circles). **C.** 4αPDD (10 μM) caused an increase in Ca^{2+} in TRPV4 (closed circles) that was not inhibited by preincubation with TM3E3 (open circles). **D**. Mean data (±SEM) from 3 independant experiments for each cell type, normalised to maximum response to agonist. Cells were preincubated with preimmune (black bars) or TM3E3 antisera (grey bars). TRPM3 n/N=5/25, TRPM2 n/N=3/34, TRPC n/N=3/34, TRPV4 n/N=3/27.

TRPM3 inhibition by dialysed TM3E3

As mentioned previously, TM3E3 antisera were dialysed to remove preservative and other small molecules. Analysis by ELISA confirmed dialysis decreased the amount of antibody in samples, reducing the EC_{50} for dialysed TM3E3 activity to 1:500. It was therefore necessary to ensure the dialysed antibody was still effective at blocking the TRPM3 channel.

Dialysed TM3E3 at a dilution of 1:500 effectively inhibited PregS activation of TRPM3, and had no effect on non-induced cells (Figure 3.21 A). Mean dose response data for 4 dilutions of the antibody indicate only dilutions of 1:1000 and 1:500 caused significant block of the PregS response (Figure 3.21 B). Analysis of the dose response data using the Hill equation gives an extrapolated IC_{50} for dialysed antibody inhibition as 1:454 dilution (Figure 3.21 C).

The data suggest that in order to achieve a significant inhibitory effect using the dialysed antibody, it must be used at a 1:500 dilution.

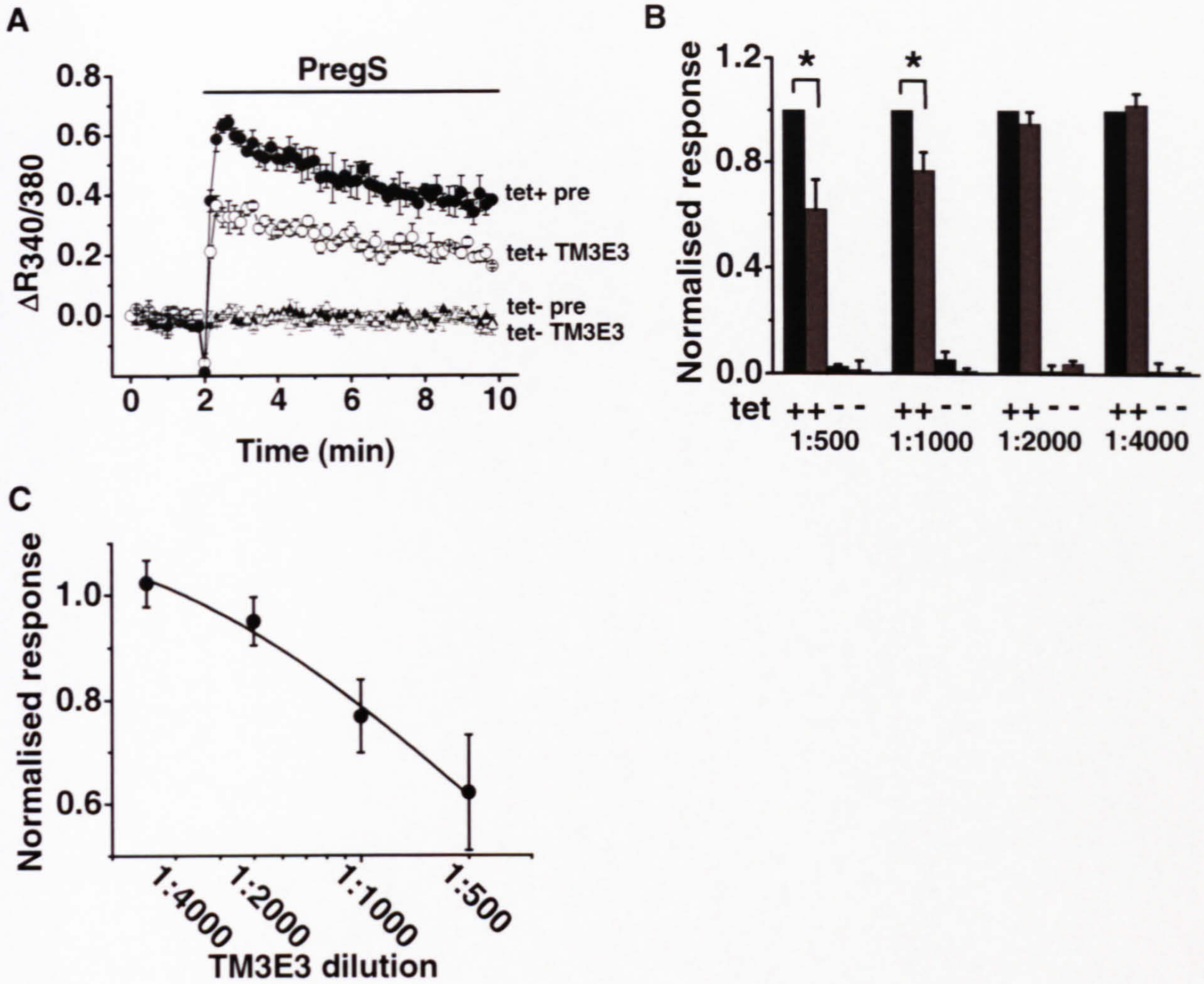

Figure 3.21. Dialysed antibody dose response Ca^{2+} signals were measured as the 340/380 nm ratio of emission in fura-2 loaded HEK 293 cells. TRPM3 cells were induced by incubation with tetracycline (tet+), non-induced cells (tet-) were included as a control. **A**. PregS (25 μM) caused an increase in Ca^{2+} in tet+ TRPM3 that is inhibited by preincubation with dialysed TM3E3 at 1:500 dilution (open circles) compared to dialysed preimmune control (closed circles) n/N=1/3. **B**. Mean data (±SEM) from 3 independant experiments for cells preincubated with TM3E3 (grey bars) or preimmune antisera (black bars). Data are normalised to maximum Ca^{2+} response in preimmune-treated tet+ cells 1 min after PregS application (n/N=3/12). **C**. Mean data (±SEM) for TM3E3 block of tet+ PregS response analysed using the Hill equation.

PregS activated currents in TRPM3-expressing cells

To further investigate whether the antibody had direct blocking effect on the channel, electrophysiology was performed. This also served to further characterise the effect of PregS on the TRPM3 channel, and to build confidence that PregS effects are TRPM3 mediated.

The Port-a-patch benchtop system was used to perform whole-cell recordings using a voltage ramping protocol to investigate the current-voltage (I-V) relationship of TRPM3. Cells were held at 0 mV, followed by a step to -100 mV with a 200 ms ramp up to +100 mV, before returning to 0 mV. Series resistance was never greater than 20 MΩ.

PregS (25 μM) applied to TRPM3-expressing cells led to the rapid development of a TRPM3-like current (Figure 3.22 A). The I-V was linear (Figure 3.22 B), and revealed a non rectifying current, with PregS activation shifting the reversal potential to an average value of -13.6 (±9.1) mV. This is consistent with the activation of a non-selective cation channel as described in the literature for TRPM3 (Grimm *et al.*, 2005).

Whole cell-voltage clamp was also performed using the Patchliner, an automated, planar patch clamp device. Experiments using the same ramping protocol as designed on the Port-a-patch show that PregS did not activate current in tet- cells (Figure 3.22 C and D). The overall increase in current at both -80mV and +80 mV was 10 times larger in tet+ cells than for tet- cells, 3 minutes after PregS application (Figure 3.22 E).

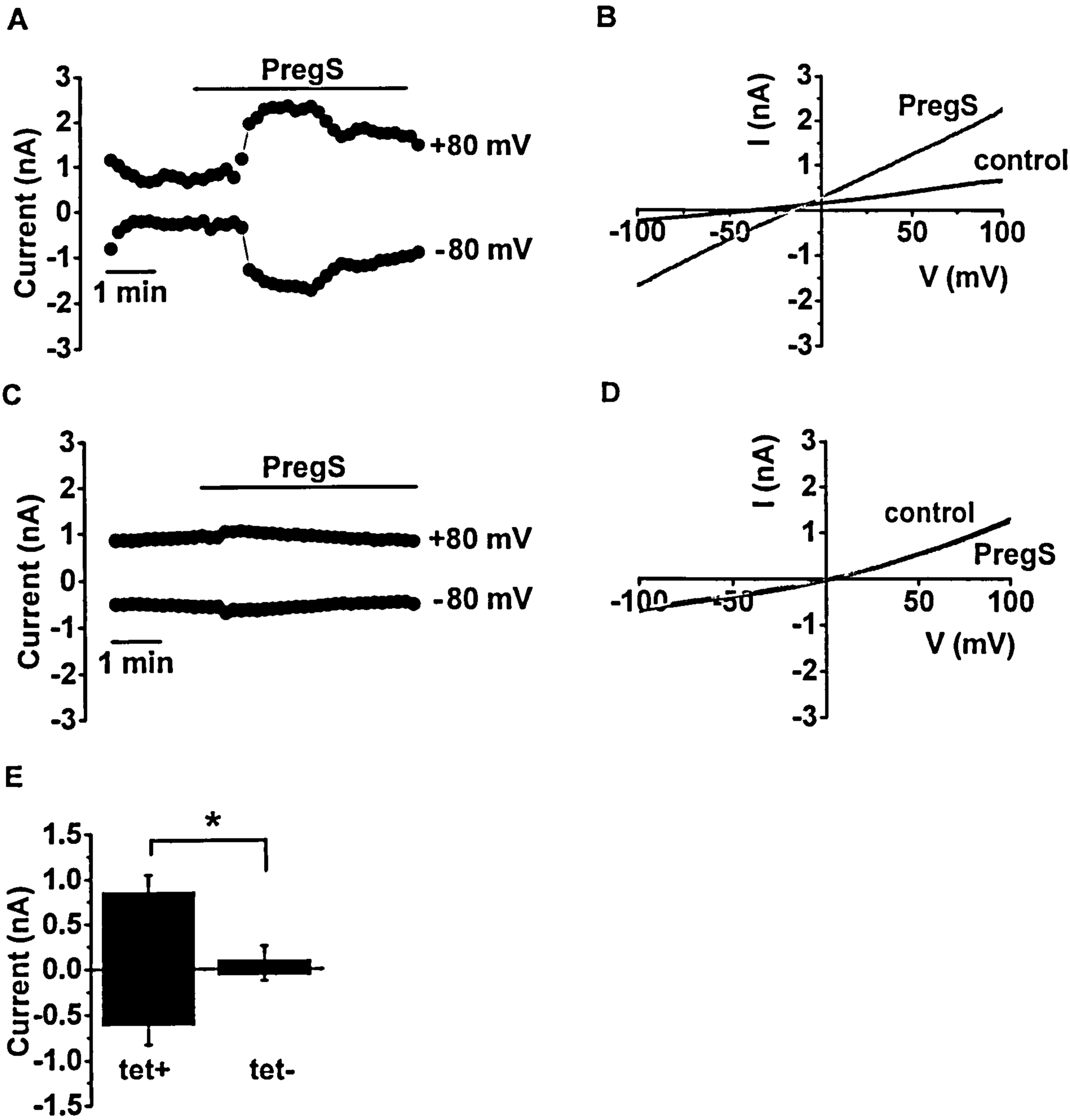

Figure 3.22. PregS activated TRPM3 currents Whole cell-voltage clamp performed using Port-a-Patch (A&B) or Patchliner (C-E). DMSO was present throughout experiments. **A.** Representative time-series data of whole cell currents at -80mV and +80 mV in a TRPM3-expressing (tet+) cell upon activation by PregS (25 μM). **B.** I-V relationship of a tet+ cell before and after PregS application. **C.** Representative time-series data of whole cell currents at -80mV and +80 mV in non-induced (tet-) cells upon application of PregS (25 μM). **D.** I-V relationship of a tet- cell before (black) and after (grey) PregS application. **E.** Mean data (±SEM) showing increase in current at +80mV and -80mV induced by PregS in tet+ (n=8) and tet- (n=3) cells. *Patchliner experiments performed by C. J. Milligan.*

TM3E3 inhibits PregS-induced currents

TM3E3 successfully inhibited Ca^{2+} responses in TRPM3-expressing cells. Further Patchliner experiments were performed to investigate the effect of TM3E3 on TRPM3 currents activated by PregS.

Application of dialysed TM3E3 at a 1:500 dilution inhibited PregS-induced currents within 5 min of application (Figure 3.23 A). TM3E3 inhibited both outward and inward current (Figure 3.23 B). When preadsorbed to its antigenic peptide, TM3E3 had no inhibitory effect (Figure 3.23 C and D). The mean data for whole cell currents at +80mV and -80mV show that TM3E3 caused a significant 37% block of PregS-induced inward current, and 24% of outward current, but had no effect if predsorbed to its antigenic peptide (Figure 3.23 E).

In summary, TM3E3 can significantly block PregS-induced current in TRPM3-expressing cells. The effect of the antibody does not appear to be voltage-dependent, as both the inward and outward current is inhibited.

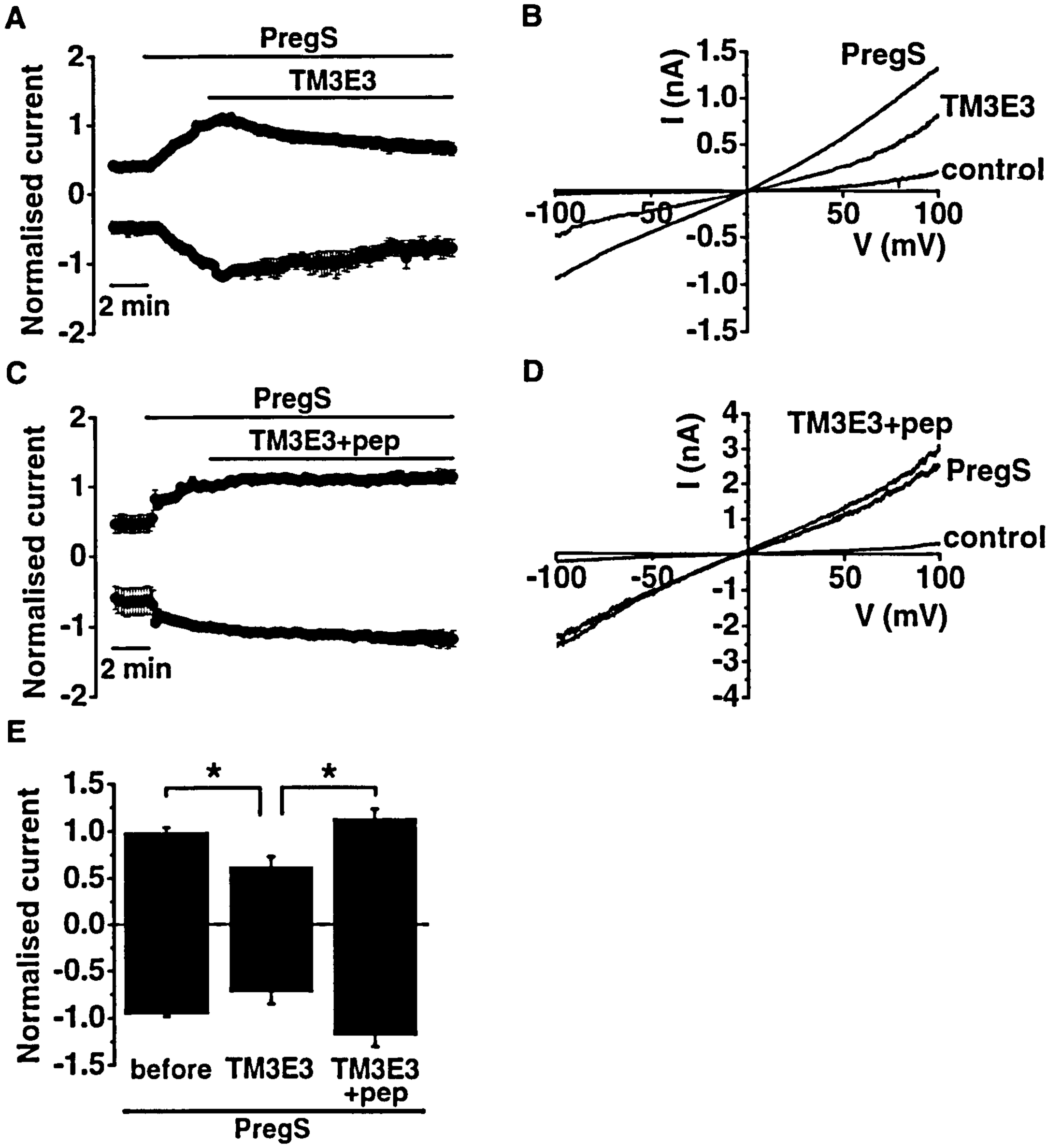

Figure 3.23. TM3E3 inhibited PregS-activated currents Whole cell-voltage clamp performed using Patchliner; DMSO was present throughout the experiment. All cells were tet+. **A.** Representative time-series data of whole cell currents at -80mV and +80 mV upon application of PregS (25 μM) and TM3E3 (1:500). **B.** I-V relationship before (black) and after (grey) PregS and (light grey) TM3E3 application. **C.** Representative time-series data of whole cell currents at -80mV and +80 mV upon application of PregS (25 μM) and TM3E3+pep (1:500). **D.** I-V relationship before (black) and after (grey) PregS and (light grey) TM3E3+pep application. **E.** Mean data (±SEM) for currents at +80mV and -80mV induced by PregS (n=12) and following TM3E3 (n=8) or TM3E3+pep (n=4) application. *Experiments performed by Dr C. J. Milligan.*

Discussion

The data presented in this chapter demonstrate that extracellular application of the polyclonal antibody TM3E3 gives a partial but significant inhibition of the TRPM3 cation channel, providing further evidence that peptide-specific antibody design can be used to create selective ion channel blockers, and demonstrating a new and important tool for the study of TRPM3.

PregS is a novel TRPM3 activator

The high percentage of TRPM3-expressing cells resulting from tetracycline-induction allowed for high throughput analysis of the TRPM3 Ca^{2+} response using a FlexStation fluorimeter. Published modulators of TRPM3, including sphingolipids and hypotonic solutions, produced small Ca^{2+} responses in TRPM3-expressing cells that, although significant, were not ideal for detailed studies. A novel, potent, and physiologically relevant TRPM3 activator was therefore necessary, and was found in PregS. PregS caused rapid, sustained Ca^{2+} responses and quickly activated currents in TRPM3-expressing cells (Figure 3.13). The concentration of PregS giving half maximal activation was determined as 1.83 μM, with the threshold for activation sitting at approximately the physiological levels in healthy individuals, which are the same for both sexes at ~0.1 μM (de Peretti *et al.*, 1983; Tagawa *et al.*, 2000). This would suggest that physiological concentrations of PregS may be sufficient to activate TRPM3. Contrary to the effect on TRPM3, PregS has been reported to inhibit capsaicin-induced TRPV1 currents in rat dorsal root ganglion neurons (Chen *et al.*, 2004). Although the physiological relevance of PregS modulation of TRP channels is unknown, it will serve as a useful TRPM3 activator and positive control for future experiments, and may be used to identify TRPM3 channels in their native cells and tissues.

PregS synthesis is believed to occur in the brain independently of other steroid generating organs, making it a neurosteroid and a precursor to many steroid hormones. Neurosteroid levels vary with age and during pregnancy or times of stress and depression, and PregS levels in particular have been shown to correlate with impaired memory function in rats (Vallee *et al.*, 1997). In addition PregS levels are reduced in the brains of Alzheimer's patients (Weill-Engerer *et al.*, 2002), and consequently PregS is

believed to have a neuroprotective role, and is commonly prescribed as a memory enhancing drug. The effect of PregS in the CNS as an allosteric modulator of ligand-gated ion channels is well characterised. It is established as an excitatory neurosteroid, acting as a negative modulator of the γ-aminobututyric acid type A ($GABA_A$) receptor, and a positive modulator the *N*-methyl-D-aspartate (NMDA) type of glutamate receptor. PregS acts as a non-competitive antagonist of the $GABA_A$ receptor, and the inhibition it causes is independent of GABA binding and receptor activation (Akk *et al.*, 2001). Pregnenolone (Preg), the non-sulphated precursor to PregS, is not active at the $GABA_A$ receptor, and a study of $GABA_A$ in *C. elegans* describes an extracellular arginine residue necessary for PregS inhibition of the receptor (Wardell *et al.*, 2006). This suggests the negative sulphate group of PregS is required for activity. Single channel recordings have shown that PregS acts directly on NMDA receptors as an allosteric modulator (Bowlby, 1993). Again Preg is ineffective, further evidence that the negative sulphate is essential. Interestingly Preg can also activate TRPM3, although it is less efficacious than PregS (J. Oberwinkler, personal communication). This suggests that unlike modulation of other ligand-gated ion channels, the sulphate group is not critical for TRPM3 activation, but may be beneficial.

The non-selective, cation inhibitors Gd^{3+} and 2-APB both reduced the PregS-induced Ca^{2+} response in TRPM3-expressing cells (Figure 3.15). Although the data are consistent with a direct effect of PregS on the TRPM3 channel, there is the possibility PregS works via a signalling pathway. The related steroids oestrogen and progesterone both have receptors in peripheral tissues, and there is evidence PregS binds to the oxytocin receptor (Grazzini *et al.*, 1998). However another candidate for PregS binding is the sigma (σ) receptor. Originally believed to be an opiate receptor, the σ receptor is now known to be distinct from other receptors, and exists in 2 isoforms, σ_1 and σ_2. The σ_1 isoform is a single 223 amino acid polypeptide that is able to bind steroids, including PregS (Maurice *et al.*, 1999). Although mainly expressed in the CNS, σ receptors are also present in the periphery, and are believed to be involved in signal transduction. There is evidence that neurosteroids can increase glutamate release through a G_i-coupled σ receptor, and despite possessing an N-terminal ER retention signal, activation of the σ_1 receptor causes its translocation to the plasma membrane where it stimulates PLC via a G_i protein (Morin-Surun *et al.*, 1999). Additionally there are reports that the σ_1 receptor can modulate channels at the plasma membrane, such as inhibition of Kv1.4 (Aydar *et al.*, 2002) and voltage-dependent Ca^{2+} channels in rat neurons (Zhang *et al.*,

2002). An argument against PregS modulating TRPM3 via a σ_1 receptor-related signalling pathway is that the Ca^{2+} response is fairly rapid. Furthermore, PregS can only activate TRPM3 from the extracellular side of the membrane (J. Oberwinkler, personal communication). Nevertheless it seems premature to rule out involvement of the ER bound σ_1 receptor. Perhaps PregS exerts its effect on the σ_1 receptor via changes in intracellular Ca^{2+} as a result of TRPM3 activation. The suggestion that PregS exerts its inhibitory effect on TRPV1 by inserting into the membrane and perturbing membrane lipids adjacent to the channel (Chen et al., 2004) presents an alternative mechanism of activation. Steroids are lipophilic, and insertion into the plasma membrane seems favourable, thus causing a non-direct effect on TRPM3 as a result of stretch of the membrane, or even managing to transverse the membrane completely to activate σ_1 receptors. Although they are less potent, the structurally related compounds Preg, DHEA and DHEAS can also activate TRPM3, perhaps by a common mechanism of membrane insertion (J. Oberwinkler, personal communication). Incorporation into the membrane resulting in stretch-activation of the TRPM3 channel may be similar to the mechanism of activation resulting from hypotonic shock-induced cell swelling.

Although a TRPM3 splice variant is reported to be a store-operated channel (Lee *et al.*, 2003a), the variant $TRPM3_{1325}$ is reported to be unaffected by thapsigargin (Tg) (Grimm et al., 2005). It is interesting that in this study, preincubation with Tg reduced the amplitude of the PregS-response (Figure 3.16 C). As the Ca^{2+} response was not completely inhibited, this suggests that the majority of the PregS-induced Ca^{2+} response in TRPM3-expressing cells results from Ca^{2+} influx across the plasma membrane through the TRPM3 channel. However the inhibition by Tg suggests store release cannot be completely disregarded as a contributor. PregS is known to activate nuclear σ-receptors, therefore is able to cross the plasma membrane, and in theory could act on TRPM3 channels expressed in the membrane of intracellular Ca^{2+} stores.

In addition to the inhibition of the PregS response, Tg also caused an increase in the baseline of resting cells, presumably as a result of the activation of endogenous store-operated channels (Figure 3.16 A). As the increase in baseline was of a similar magnitude in both non-induced and TRPM3-expressing cells (Figure 3.16 B), this is evidence that TRPM3 is not store operated. Therefore a possible explanation for the Tg effect is that the PregS response saturated, and due to the increased starting baseline the Ca^{2+} response to PregS in a Tg-treated cell was unable to increase by the same

magnitude as a control cell. If this was the case, Tg did not inhibit the PregS effect, and store release is not a factor in PregS activation of TRPM3. Repeating experiments in the absence of extracellular Ca^{2+} confirmed the PregS response was the result of Ca^{2+} influx, and does not involve Ca^{2+} stores (Figure 3.17). The inhibitory action of Tg may have been the result of changes in local intracellular Ca^{2+} concentration. Intracellular Ca^{2+} is a common regulator of TRP channels; TRPV6 is inhibited by intracellular Ca^{2+} (Bodding *et al.*, 2002) and the activation of TRPM4 and TRPM2 is dependent on intracellular Ca^{2+} (McHugh *et al.*, 2003). Therefore it is possible that TRPM3 is also a Ca^{2+} sensitive channel.

RT-PCR revealed TRPM3 mRNA is present in HEK 293 cells (Figure 3.9), which was confirmed by immunostaning with the TM3E3 antibody (Figure 3.12). Native expression of TRPM3 would explain why SPH and DHS caused a Ca^{2+} response in control, YFP-transfected cells (Figure 3.2 C & 3.3 C). However, PregS did not activate Ca^{2+} entry or current in control cells (Figure 3.10). Although several splice variants are reported for TRPM3, few are fully characterised. Even small splicing events can change the selectivity of the ion pore while retaining conserved TRPM3 characteristics (Oberwinkler *et al.*, 2005). Perhaps a novel splice variant, similar enough in sequence to be identified by the $TRPM3_{1325}$ primer pair, is responsible for a channel sensitive to SPH and DHS, but not PregS. Alternatively, endogenous TRPM3 PregS-responses may be inhibited in native cells.

E3-targeting to generate a specific TRPM3 channel blocker

A functional role for TRPM3 has yet to be determined. When over-expressed in HEK 293 cells, TRPM3 is activated by hypotonic stimulation, most likely as a result of cell swelling (Grimm *et al.*, 2003). Volume-regulation of TRP channels is common, and has been demonstrated for several family members, including TRPV4, TRPC1, TRPC6, TRPV2, TRPM2, TRPM4 and TRPP2 (Kraft *et al.*, 2005; Muraki *et al.*, 2003; Nilius *et al.*, 2004b). The physiological relevance of SPH activation of TRPM3 is also unknown. Serum levels of free SPH are reported to be between 64-273 nM (Abnet *et al.*, 2001), whereas the EC_{50} for SPH activation of TRPM3 is 12 μM (Grimm *et al.*, 2005), well above the physiological range. Sphingosine is believed to result almost exclusively from the metabolism of ceramide by ceramidase, as *de novo* synthesis does not occur

(Cuvillier, 2002). Ceramidase is present at the plasma membrane (Tani *et al.*, 2007), and is expressed at high levels in human kidney (El Bawab *et al.*, 2000). Additionally, human sphingosine-1-phosphate phosphatase, responsible for the dephosphorylation of sphingosine-1-phosphate to SPH, is also expressed in most tissues (Johnson *et al.*, 2003). Therefore SPH cannot be completely ruled out as a physiological modulator of TRPM3, as the concentration it reaches locally to the TRPM3 channel is unknown, and may well be sufficient for activation. A specific inhibitor for the TRPM3 channel would serve as a useful tool for functional investigations.

While existing, small molecule TRP channel antagonists are non-specific, many have still proven useful in the characterisation of the TRP family. Lanthanide ions are known to block Ca^{2+} permeable cation channels (Halaszovich *et al.*, 2000), 2-aminoethoxydiphenylborate (2-APB) can inhibit store-operated calcium channels and some TRP isoforms (Bootman *et al.*, 2002; Xu *et al.*, 2005a), SKF96365 inhibits receptor-mediated calcium entry, and ruthenium red is a non-selective inhibitor of all TRPV and some TRPM channels (Gunthorpe *et al.*, 2002). More recently, antibodies have emerged as selective channel blockers, designed to specifically recognise individual ion channel proteins by exploiting conserved or unique regions of sequence. It is the common properties of antibodies that make them ideal as tools to investigate ion channel function; they are highly specific, and in the case of externally targeted antibodies, do not require complicated intracellular delivery methods.

TRP channel structure is believed to resemble that of voltage-gated potassium channels. Although a crystal structure is not yet available for TRP, hydrophobicity analysis gives a good indication of the location and amino acid sequence of TM domains and connecting intra- and extracellular loops. The third extracellular loop seems an ideal target for antibody generation as it is not glycosylated and tends to be of sufficient length to allow for good antibody access, while other extracellular loops are smaller with post translational modifications that could hinder antibody access (Xu *et al.*, 2005b). The method of E3-targeting was applied to TRPM3 to create an anti-TRPM3 antibody capable of blocking both SPH and PregS activation of the channel.

It is important to determine whether a custom made antibody is specific for its designated target. In this study, this was demonstrated by immunostaining and western blotting with the stable TRPM3 cell line. For immunostaining, cells were not

permeabilised prior to staining with TM3E3, indicating that the signal observed in TRPM3-expressing cells was due to the antibody binding an extracellular epitope as predicted (Figure 3.12). Non-induced control cells also exhibited a small degree of staining, consistent with native expression of TRPM3. TM3E3 also successfully identified a protein in western blotting similar to the predicted molecular weight for TRPM3 of 157 kDa (Figure 3.11). Often, a western blot signal will not exactly match the predicted size of the protein due to post-translational modifications or the formation of heteromers that gives an apparent increase in size. Western blotting with TM3E3 revealed 2 bands at 150 and 100 kDa (Figure 3.11). As both bands were reduced in the peptide control lane, they are most likely not due to non-specific labelling. A possible explanation for the smaller molecular weight band is degradation of the protein sample by endogenous proteases to produce a truncated TRPM3 peptide that was still detected by the antibody. A useful, further control for antibody selectivity would be to compare staining or blotting in tissues known to express TRPM3 with those that don't, such as by using siRNA to transiently knockdown the TRPM3 mRNA, or by using tissues from a knockout animal. As yet, there is not a TRPM3 knockout available.

E3-targeted antibodies are particularly suitable for functional experiments as there is a much reduced chance of non-specific interactions when cells are intact, allowing only extracellular regions of membrane-bound proteins to be exposed to antibody, and not the whole proteome. Preincubation of live cells with TM3E3 inhibits calcium entry and current, indicating TM3E3 can binds its extracellular epitope and exert a functional effect. Additionally, immunostaining and western blotting suggest that the antibody remains bound to the channel following washing steps; therefore despite not being present in solutions throughout actual recordings, it can be assumed that the antibody remained bound to TRPM3.

In functional studies, TM3E3 appears specific for TRPM3, with the ability to inhibit Ca^{2+} responses to both the published TRPM3 modulator D-*erythro*-sphingosine (SPH), and the novel modulator pregnenolone sulphate (PregS) (Figures 3.8 & 3.18). It was necessary to confirm the antibody had a direct effect on the TRPM3 channel, rather than causing a non-specific effect on the cell as a whole. Preimmune serum is a good control as it contains exactly the same components as the antibody sera, except that it lacks the peptide-directed antibodies. Presumably any non-specific effects of sera would be apparent in preimmune sera as well. A further control was to preabsorb TM3E3 to its

peptide so that it was unable to bind its TRPM3 epitope, and this peptide-bound antibody had no inhibitory effect on PregS currents. The use of the antigenic peptide confirms the antibody does bind the correct epitope in TRPM3. In addition, TM3E3 only inhibited TRPM3-related cellular responses, and did not affect endogenous ATP responses in non-induced cells, nor did a second E3-targeted antibody, T1E3, have any effect on cell responses to TRPM3 activators (Figure 3.18). Also, the antibody had no effect on cells which do not present the antigen (Figure 3.20). It would appear from these experiments that the antibody only has an inhibitory effect when it is bound to the TRPM3 channel. Importantly TRPM3 and its close relative TRPM2 share 74% sequence homology in the 3rd extracellular loop, yet the antibody could successfully distinguish between the two, further demonstrating its specificity for TRPM3.

TM3E3 typically blocked channel activity by 30-50% after a 0.5-3 hour preincubation. Although inhibition of channel activity is partial, this is sufficient to study TRPM3 in native cells and tissues, and the selectivity of the antibody compensates for an incomplete block. The native structure of TRPM3 may give a different arrangement of the extracellular loops than is indicated by a linear peptide representative, perhaps hindering antibody access and preventing a complete block of the channel. Also, accessibility may be an issue, as cells in culture are adhered to a flat surface and therefore some channels will not be exposed to antibody. However, in Patchliner experiments cells were in solution, and presumably were well exposed to antibody, yet still there was not a complete inhibition, although this is presumably due to a shorter duration of exposure to the antibody. A partial effect could occur as a result of only partial occlusion of the channel pore or an incomplete conformation change, as will be examined later in this discussion. There is little information as to the suitability of antibodies targeted to other extracellular regions of TRP channels, although antibodies to intracellular regions of potassium channels have been successful blockers, while antibodies to sodium channels can be inhibitory or stimulatory (Dallas *et al.*, 2005). Future experiments may discover regions of the protein that serve as superior antibody targets that will provide a stronger or complete channel block.

The antibody concentration used in experiments is important as it must give maximum inhibition while minimising non-specific background suppression (Zhou *et al.*, 1998). For this reason, cells were preincubated with the antibody for a relatively short time prior to experiments to minimise changes to the native protein levels and cellular

localisation (Xu *et al.*, 2001). The short incubation time did not appear to have an effect on blocking activity, as direct application in patching experiments shows a significant block can be achieved within 10 minutes, therefore a longer preincubation may be unnecessary. The antibody has further advantage in that it can inhibit TRPM3 function reasonably quickly with minimal effects on the cell as a whole. This is a common disadvantage with siRNA knockdown or knockout animals, which can result in other proteins compensating for the effects of the gene removal, masking the exact effect of the knockdown.

Mechanism of antibody blockade

The underlying mechanism of E3-antibody blockade has yet to be determined. Polyclonal antibodies present in sera are a mixture of structurally different IgG immunoglobins, each of which will recognise a different epitope on the sequence of a specific antigen. This means the exact polyclonal within the anti-sera that acts as a blocker, plus its epitope, is unknown. The simplest explanation for channel inhibition is that when bound to the channel, the blocking antibody can obstruct the pore. Rabbit IgG consist of 2 heavy and 2 light chain polypeptides, making them typically ~160 kDa. Compared to the predicted size of TRPM3 of 157 kDa, this would certainly seem sufficient to obstruct the pore, but may be too large to actually fit into the pore.

It has also been suggested that one or more different polyclonal antibodies must bind in order to achieve channel inhibition. This would explain why rabbit monoclonal antibodies targeted to the 3rd extracellular loop of human TRPV1 did not cause inhibition, as a single species of IgG was insufficient to inhibit function (Klionsky *et al.*, 2006). In the same study, a polyclonal antibody generated against rat TRPV1 was effective at blocking both proton and chemical activation of the channel, activation mechanisms known to be independent of each other, suggesting the antibody locks the channel in a closed state. This also implies E3 antibodies do not interact with the agonist binding site. Although the exact binding site and mechanism of activation for TRPM3 are unknown, like TRPV1 it is unlikely the antibody would function as a competitive inhibitor agonist because it can inhibit activation by two structurally unrelated activators, SPH and PregS, which in all probability do not share a binding site. However if regulatory proteins are required for activation, and have binding sites

distinct to activator binding sites, perhaps the antibody masks their binding and thus prevents allosteric interactions required for normal channel function.

TM3E3 binding to the TRPM3 protein may result in a conformational change in the channel to lead to obstruction of the pore, to lock the channel in the closed state, or even to mark the TRPM3 protein for internalisation and degradation. Alternatively the antibody could prevent a conformational change necessary for channel opening. If the antibody causes internalisation of TRPM3 channels, the number of channels present at the plasma membrane would be reduced, thus reducing the overall cellular response. However the YFP-tagged TRPM3 protein used in this study did not appear to exhibit different activation or function than the non-YFP tagged inducible TRPM3. This indicates that a C terminal protein addition was not sufficient to cause TRPM3 internalisation, therefore perhaps neither would a bound antibody.

Alternative splicing allows the TRPM3 gene to encode several different proteins. There are currently 7 reported variants of human TRPM3, seemingly with different functions. TRPM3 variants a-f vary in the pore domain and N terminus, and TRPM3a is store-operated (Lee *et al.*, 2003a), while the variant $TRPM3_{1325}$ as used in this study has a shorter N terminus and longer C terminus, and is not store operated (Grimm *et al.*, 2005). Additionally, alternative splicing in the pore region of mouse TRPM3 changes the cation selectivity of the pore (Oberwinkler *et al.*, 2005). This indicates alternative splicing could be a mechanism used to produce channels not only with different selectivity, but also different mechanisms of activation and cellular function. The antibody should in theory inhibit all TRPM3 variants, as for all those reported so far the 3rd extracellular loop is conserved save for TRPM3c, which contains an extra 12 amino acids, although the antigenic peptide sequence is conserved fully and unaffected by splicing. It is acceptable to assume the antibody will not be able to distinguish between splice variants.

Antisera containing polyclonal antibodies generated against the channel of choice is a finite supply - the exact polyclonal antibody acting as a blocker and its precise epitope on the channel structure are unknown, so future use of the same technique may not produce the same effective blocker again. Monoclonal antibodies (mAbs) however can be produced in recombinant systems, creating large amounts of pure antibodies. The unlimited diversity and exquisite specificity has meant that currently mAbs are very

popular, with over 350 now undergoing clinical trials against a broad range of different diseases and conditions. Yet a mAb directed against TRPV1 was ineffective (Klionsky *et al.*, 2006). Despite identifying 26 different mAbs that could bind the channel, none caused inhibition, indicating they did not target the correct epitope required for channel blockade. However polyclonal antibody serum directed against the same region of TRPV1 was a successful inhibitor, perhaps because it bound the entire extracellular loop to which it was targeted, whereas the mAbs despite possessing higher affinity have smaller epitopes. A recent study has presented evidence to the contrary, developing the first monoclonal antibody to be a successful ion channel blocker (Gomez-Varela *et al.*, 2007). Their antibody specifically and potently reduces current through the hEag1 ion channel. Furthermore the antibody implicates hEag1 expression is linked to tumour cell growth, evidence for E3-targeted antibodies as tools to determine ion channel function.

Summary

In the near future, it is expected that custom-made antibodies will have further important therapeutic applications due to their specificity and unlimited diversity. Currently, an antibody that can specifically block a channel is a valuable tool for further study of the protein, particularly for those where the function remains elusive. TRPM3 is one such functionally mysterious channel, and TM3E3 will be undoubtedly useful for further characterisation of the channel.

Chapter 4

TRPM3 in human saphenous vein smooth muscle cells

The previous chapter introduced TM3E3 as a specific blocker for the TRPM3 ion channel. The antibody is potentially an important tool for determining the native expression and localisation of TRPM3, and its effectiveness gives it the potential to specifically inhibit channel function in living cells and tissues.

TRP channels are widely expressed in the vasculature and are activated by lipids and second messengers known to be present at increased concentrations in disease states such as atherosclerosis, a major contributing factor to heart disease. The longest vein in the human body is the great saphenous vein, and it is sections of this vessel that are commonly used as the graft tissue in coronary bypass surgery, a treatment for atherosclerotic occlusion of vessels. Like all blood vessels, human saphenous vein (HSV) consists of 3 layers; an outer layer of connective tissue termed the adventitia, a medial layer of smooth muscle, and an inner layer of endothelium, termed the intima.

Surgical processes including bypass surgery, and also angioplasty, regularly lead to extensive vascular remodelling, resulting from smooth muscle cell proliferation and migration to invade the intima and occlude the vessels. This neointimal hyperplasia is instigated by a phenotypic switch in the smooth muscle from a contractile to proliferative state, which is associated with down-regulation of L-type Ca^{2+} channels (Quignard *et al.*, 1997). The loss of L-type channels is compensated by different types of Ca^{2+} channel in the proliferating cells.

The *in vitro* culture of HSV has proved a useful model to demonstrate neointimal proliferation (Porter *et al.*, 1996). The isolation and culture of human saphenous vein smooth muscle cells (HSV SMC) is also a useful model, and together these techniques have been used to show that inhibition of Ca^{2+} entry through TRPC channels can significantly reduce neointimal formation in human vein, and inhibit cultured SMC proliferation (Kumar *et al.*, 2006). This suggests that TRP channels may play the role of the compensatory channel present in proliferating SMC.

The aim of this chapter was to investigate TRPM3 expression and function in vascular smooth muscle using immunocytochemistry, calcium measurement techniques and assays of HSV SMC secretion. Furthermore experiments would determine whether, in addition to over-expressed TRPM3 channels, TM3E3 could block endogenous channels in primary cell types, serving as a useful tool to elucidate native channel function.

Detection of TRPM3 in HSV SMC

The expression of TRPM3 mRNA in smooth muscle cells isolated from human saphenous vein (HSV) was investigated using solution PCR. Alternative splicing is common for members of the TRP superfamily (Li *et al.*, 2005), and TRPM3 is reported to exist in many splice variant forms (Lee *et al.*, 2003a; Oberwinkler *et al.*, 2005). The human splice variants TRPM3a-f vary in the pore domain and N terminal regions, while the variant $TRPM3_{1325}$ described in Chapter 3 of this study is unique in that it has a longer N terminus. Using the aligned gene sequences for all reported variants, small diffences in the amino acid sequences were exploited to design splice-specific primers to probe HSV SMC cDNA for alternatively spliced TRPM3 variants. A schematic depicting the alignment of TRPM3 splice variants, plus details of the primers used and the expected products are given in Chapter 2 (Figure 2.6 and Table 2.1).

Primers directed to the N terminus of the TRPM3 splice variant $TRPM3_{1325}$ amplified a single amplicon of the predicted size 335 bp (Figure 4.1 A). Control reactions without reverse transcriptase (-RT) were also performed.

HSV SMC cDNA was also probed for further splice variant mRNA (Figure 4.1 B). Product bands were excised from the gel, cleaned, subjected to further round of PCR to amplify DNA present, and sequenced. Primers specific for $TRPM3_{1325}$ were included as a positive control, and gave a single amplicon of 335 bp as previously described, confirmed by sequencing $TRPM3_{1325}$ (A). Primers spanning exon 4 of the TRPM3 gene, designed to identify the TRPM3f variant, produced a single product band of approximately 250 bp (B), which sequencing revealed was due to the $TRPM3_{1325}$ variant. Primers spanning exons 11-12 & 14-15 were predicted to give 4 products of similar sizes, relating to TRPM3b, TRPM3e, TRPM3d and all remaining variants. A single product of approximately 300 bp was visible on the gel (C). Although amplicons of such similar sizes are difficult to resolve by electrophoresis, sequencing revealed the single band was due to $TRPM3_{1325}$. Finally, primers spanning a 12 amino acid sequence that is only present in the TRPM3c variant gave a single product of ~200 bp (D), which again was revealed as $TRPM3_{1325}$ by sequencing. It was not possible to design primers specific for variant TRPM3a as there were no variations unique to this splice variant to exploit. Low molecular weight bands designated by * are most likely a consequence of the extension of self-annealed primers, (primer dimers).

Previously, immunostaining with an anti-TRPM3 antibody detected TRPM3 protein in the intimal and medial layers of human saphenous vein (B. Kumar thesis, 2004). The presence of TRPM3 protein was further confirmed in this study with immunocytochemistry, using the E3-targeted antibody TM3E3. HSV SMC were fixed with 2% PFA and exposed to TM3E3 at a 1:4000 dilution. TRPM3 protein was detected throughout cells (Figure 4.2). Preincubation of TM3E3 with its antigenic peptide (TM3E3 + pep) or omission of the primary antibody were used as negative controls, and showed no staining.

In summary, RT-PCR amplification identified TRPM3 mRNA is present in HSV SMC, and $TRPM3_{1325}$ is the predominant splice variant. In addition, TRPM3 protein is present in this primary cell type.

A

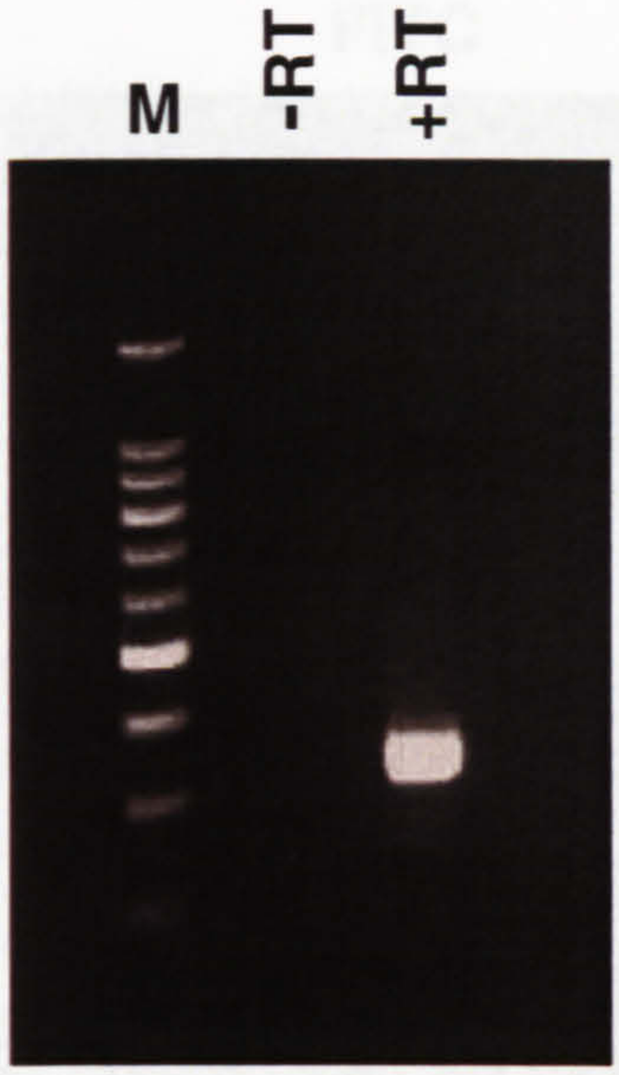

B

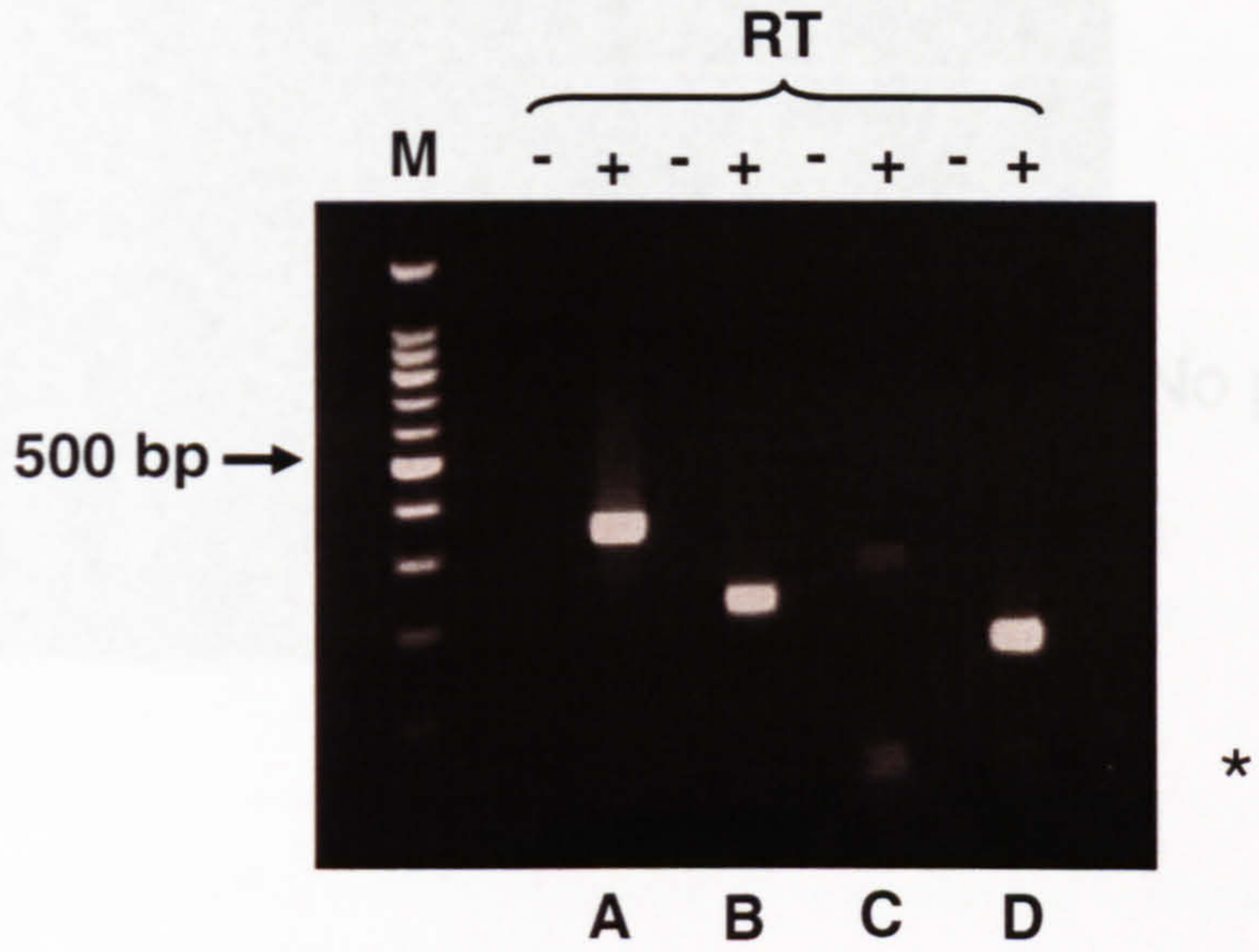

Figure 4.1. TRPM3 expression in HSV SMC DNA gel stained with ethidium bromide. M depicts 100 bp marker. PCR was performed using primers designed to amplify different splice variant cDNA from reverse transcribed HSV SMC mRNA. Non-reverse transcribed mRNA (-RT) was included as a control. **A.** Variant $TRPM3_{1325}$. **B.** Variants TRPM3f (B), TRPM3b,e,d (C) and TRPM3c (D). $TRPM3_{1325}$ was included as a positive control (A). Gel is representative of 4 separate experiments on cDNA samples from 4 different patients.

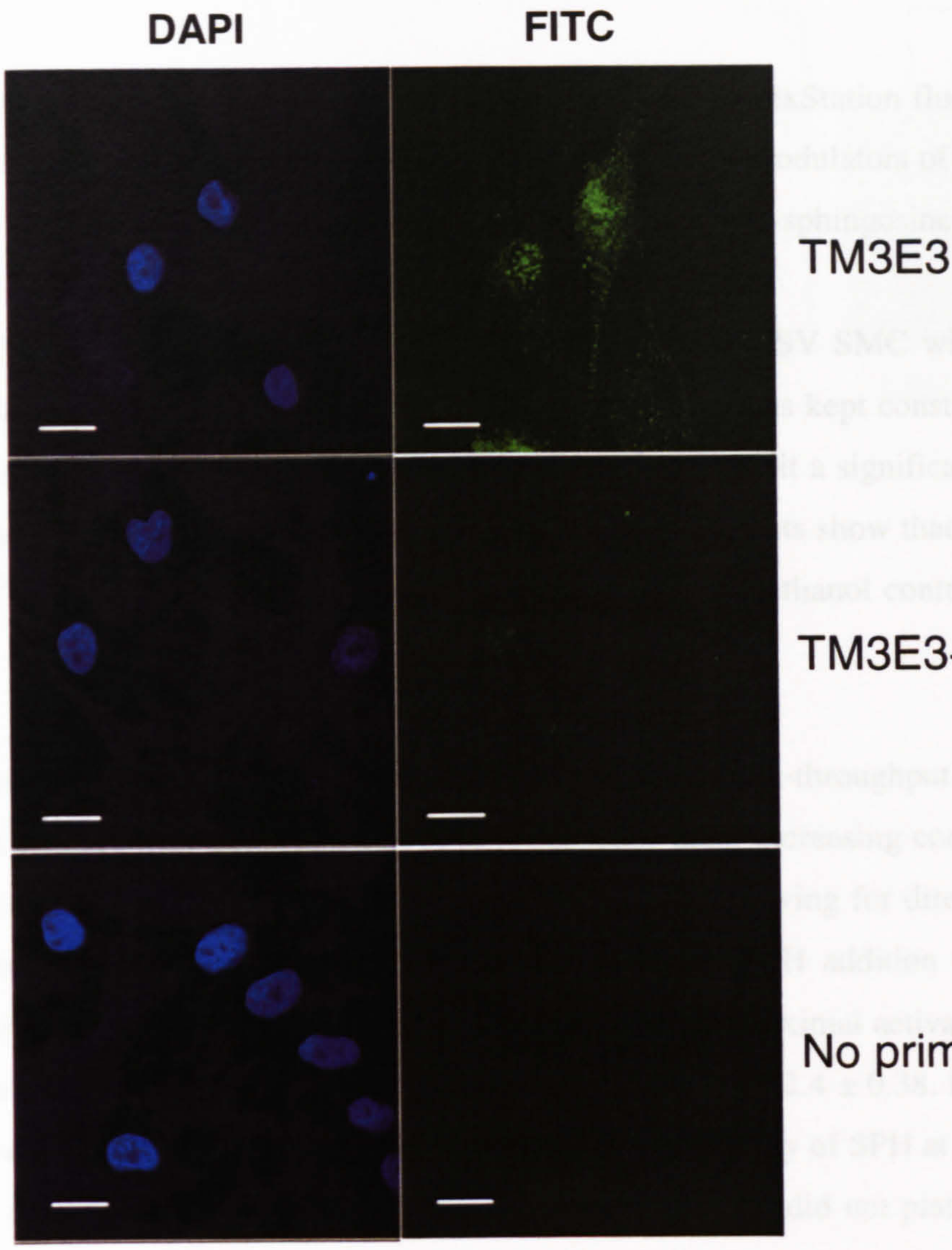

Figure 4.2. Immunofluorescence detection of TRPM3 Staining was performed on non-permeabilised HSV SMC fixed with 2% PFA using DAPI to label nuclei (left hand panel) and with TM3E3 antibody with FITC conjugated secondary antibody to label TRPM3 protein (right hand panel). For negative controls, TM3E3 was preadsorbed to its antigenic peptide (TM3E3 + pep) or primary antibody was omitted. Scale bars represent 20μm.

SPH increases intracellular Ca^{2+} in HSV SMC

Experiments using the ratiometric Ca^{2+} dye Fura-2 and a FlexStation fluorimeter were performed to investigate Ca^{2+} entry in HSV SMC. Known modulators of TRPM3 were used to search for functional TRPM3, starting with D-*erythro*-sphingosine (SPH).

SPH (20 μM) caused an increase in intracellular Ca^{2+} in HSV SMC within 1 min of application (Figure 4.3 A). Ethanol (the solvent for SPH) was kept constant at 0.1% in recording solutions throughout experiments and failed to elicit a significant Ca^{2+} signal in the absence of SPH. The mean data from 4 different patients show that after 2.5 min, the Ca^{2+} response to SPH was significantly larger than the ethanol control (Figure 4.3 B).

As demonstrated in the previous chapter, the FlexStation high-throughput system allows for fast and accurate determination of dose response data. Increasing concentrations of SPH were applied to HSV SMC within the same plate, allowing for direct comparison between wells. Dose response data taken 2.5 min after SPH addition were analysed using the Hill equation (Figure 4.3 C). The value for half maximal activation, the EC_{50}, was determined as 15.8 ±1.67 μM, with a Hill coefficient of 2.4 ± 0.38. Data points for the dose response curve were limited due to the poor solubility of SPH at concentrations higher than 50 μM, and as a result the dose response curve did not plateau. Therefore the EC_{50} given may be an under-estimate of the true value.

The data show that the TRPM3 activator SPH causes Ca^{2+} responses in HSV SMC, possibly as a result of TRPM3-activation.

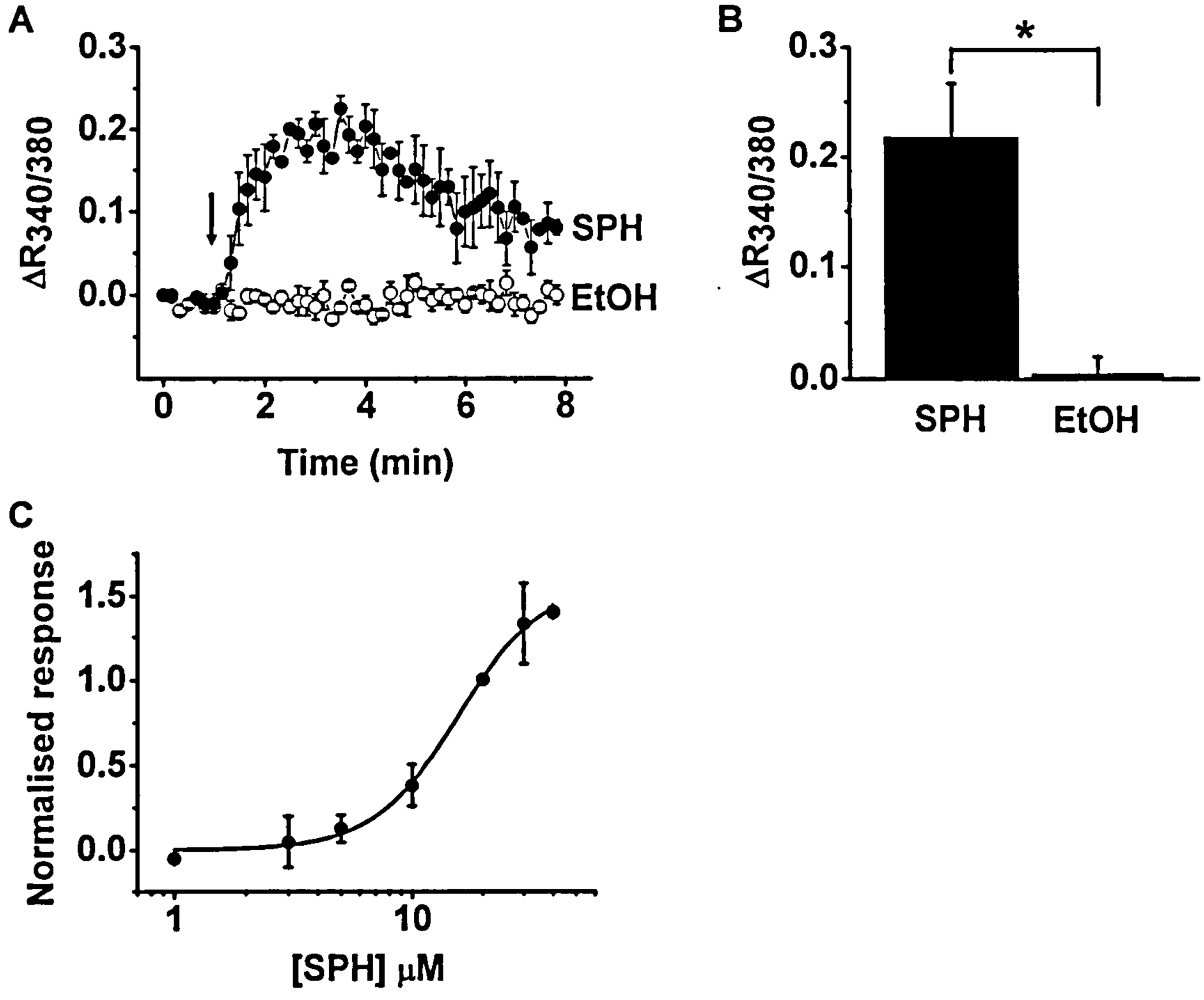

Figure 4.3. D-*erythro*-sphingosine (SPH) evokes Ca^{2+} responses in HSV SMC Ca^{2+} signals were measured as the 340/380 ratio of emission in fura-2 loaded HSV SMC using a FlexStation fluorimeter. Ethanol (vehicle) was present throughout recordings. **A.** Representative mean data (±SEM) from 5 wells within a single plate. SPH (20 μM) application (arrow) causes an increase in Ca^{2+} in HSV SMC compared to vehicle control (open circles). **B.** Mean data (±SEM) showing significant increase in Ca^{2+} 2.5 min after SPH application (SPH n/N=4/25, EtOH n/N=4/19). **C.** Mean dose response (±SEM) data taken 2.5 min after SPH application from 4 independent experiments, normalised to 20 μM response, and analysed using the Hill equation.

TRPM3 activators increase intracellular Ca^{2+} in HSV SMC

Further Ca^{2+} measurements were made using additional TRPM3 modulators D-*erythro*-dihydro-sphingosine (DHS) and D-*erythro*-N,N-dimethyl-sphingosine (DMS). Sphingosine-1-phosphate is an important intracellular second messenger for several plasma membrane proteins, and a TRP channel activator (Xu *et al.*, 2006b). DHS and DMS are both potent sphingosine kinase inhibitors. Therefore in addition to probing TRPM3 function, they also served to ensure the activation they caused was not a result of their metabolism to S1P by endogenous sphingosine kinase. Ethanol (vehicle) was kept constant at 0.1% throughout experiments which were performed at RT.

DHS (20 μM) caused a rapid and transient increase in intracellular Ca^{2+} in HSV SMC (Figure 4.4 A). In the absence of DHS, the vehicle control failed to elicit a significant increase in Ca^{2+}. The mean data from 5 different patients shows that after 2.5 min DHS caused a Ca^{2+} response that was significantly larger than the vehicle control (Figure 4.4 B). Dose response data for DHS activation, taken 2.5 min after DHS addition, were analysed using the Hill equation (Figure 4.4 C). The value for half maximal activation, the EC_{50}, was determined as 11.3 ± 0.52 μM, with a Hill coefficient of 4.3 ± 0.87.

DMS (20 μM) also caused an initial transient increase in intracellular Ca^{2+}, but this was followed by a sustained increase in Ca^{2+} (Figure 4.5 A). The mean data from 5 different patients shows that after 2.5 min, the Ca^{2+} response to DMS was not significantly larger than the vehicle control, however at 4 min after application the response was significant (Figure 4.5 B). For this reason dose response data for DMS activation were analysed using points taken 4 min after DMS addition (Figure 4.5 C). The value for half maximal activation, the EC_{50}, was determined as 19.9 ± 4.94 μM, with Hill coefficient of 1.9 ± 0.32. Again, the dose response curve did not saturate, giving an under-estimation of the true EC_{50}.

In summary, the TRPM3 activators DHS and DMS cause Ca^{2+} responses in HSV SMC, further evidence that the TRPM3 protein is functionally expressed in this cell type. In addition, the data indicate that Ca^{2+} responses to SPH do not result from its conversion to S1P, as structurally related, sphingosine kinase inhibitors also activate the channel.

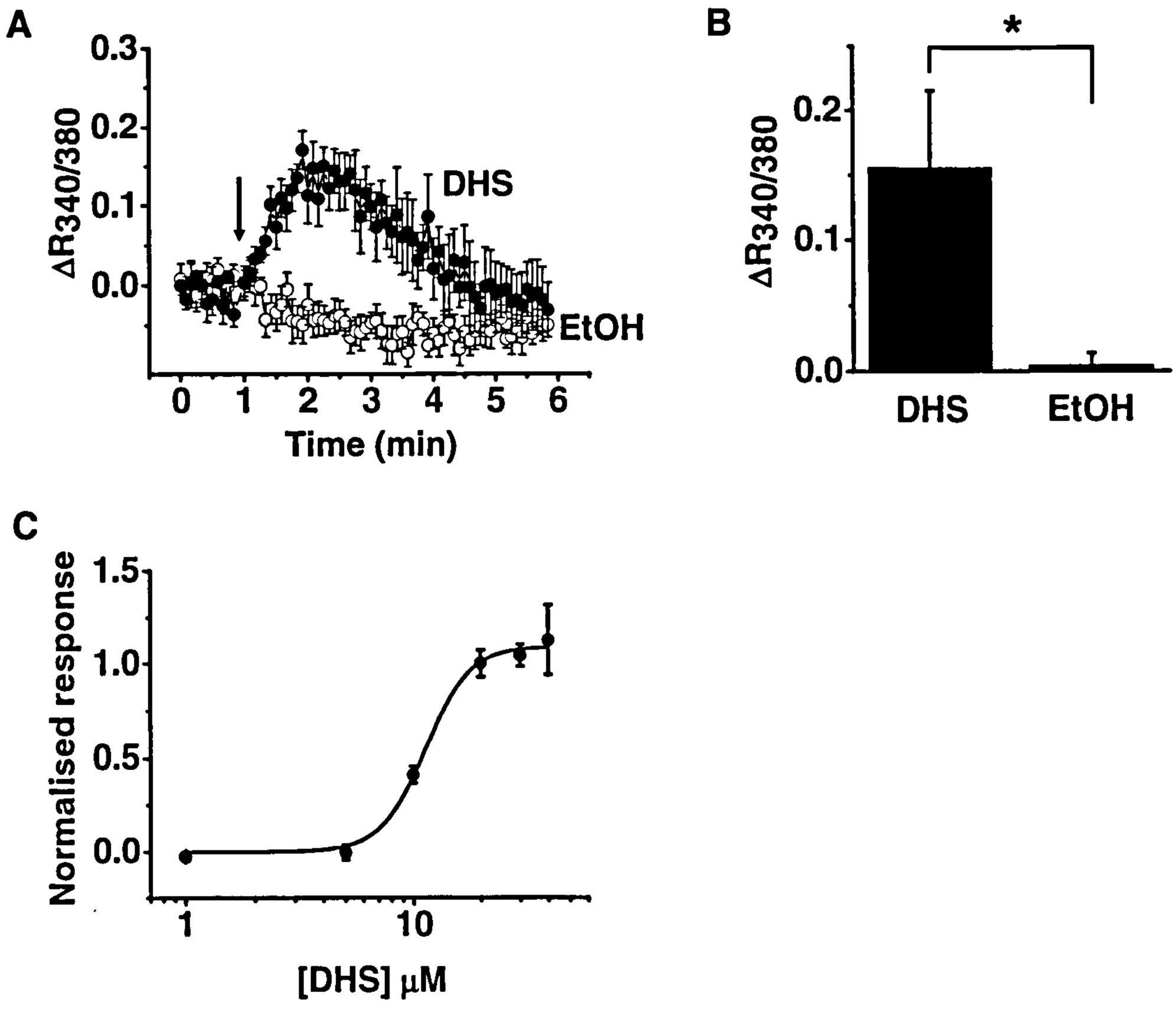

Figure 4.4. D-*erythro*-dihydro-sphingosine (DHS) evokes Ca^{2+} responses in HSV SMC Ca^{2+} signals were measured as the 340/380 ratio of emission. Ethanol (vehicle) was present throughout recordings. **A.** Representative mean data (±SEM) from 5 wells within a single plate. DHS (20 μM) application (arrow) causes an increase in Ca^{2+} in HSV SMC compared to vehicle control (open circles). **B.** Mean data (±SEM) showing significant increase in Ca^{2+} 2.5 min after DHS application (DHS n/N=4/14, EtOH n/N=4/17). **C.** Mean dose response data (±SEM) taken 2.5 min after DHS application from a single experiment, normalised to 20 μM response, and analysed using the Hill equation.

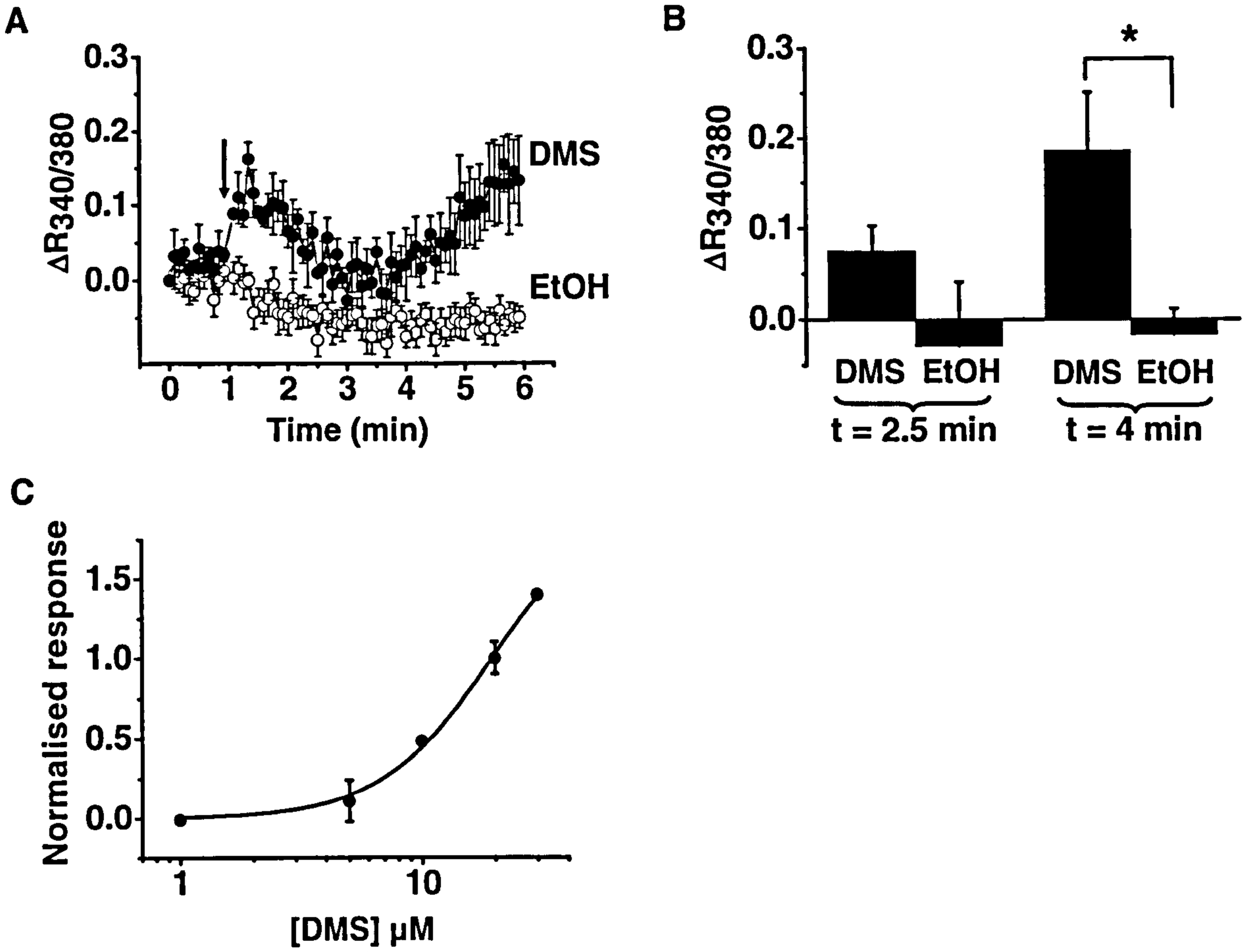

Figure 4.5. D-*erythro*-N,N-dimethyl sphingosine (DMS) evokes Ca^{2+} responses in HSV SMC Ca^{2+} signals were measured as the 340/380 ratio of emission. Ethanol (vehicle) was present throughout recordings. **A.** Representative mean data (±SEM) from 5 wells within a single plate. DMS (20 μM) application (arrow) causes an increase in Ca^{2+} in HSV SMC compared to vehicle control (open circles). **B.** Mean data (±SEM) showing Ca^{2+} responses 2.5 min or 4 min after DMS application (DMS n/N=5/15, EtOH n/N=5/18). **C.** Mean dose response data (±SEM) taken 4 min after DMS application from a single experiment, normalised to 20 μM response, and analysed using the Hill equation.

Characterisation of SPH-induced Ca^{2+} responses in HSV SMC

Thapsigargin (Tg), an inhibitor of sarco(endo)plasmic reticulum Ca^{2+}-ATPase (SERCA) and recognised TRP channel inhibitors were used to further characterise the SPH-induced Ca^{2+} response in HSV SMC. Fura-2 loaded cells were preincubated for 30 min with inhibitors before high-throughput fluorimetry was performed.

Tg (1 μM) partially inhibited the SPH-induced Ca^{2+} response, suggesting that Ca^{2+} or Ca^{2+} stores may be involved in TRPM3 activation in HSV SMC (Figure 4.6 A). The mean data indicate that 2.5 min after SPH application Tg blocked the SPH response by 52.6%, and was slightly more effective at 4 min after application, giving a 58.5% block of the response (Figure 4.6 D).

The non-specific TRP channel inhibitors gadolinium (Gd^{3+}, 100 μM) initially inhibited the SPH response, although the eventual size of the response was increased (Figure 4.6 B). The mean data show that at 2.5 min after application, Gd^{3+} blocked SPH-induced Ca^{2+} responses by an average 46.5%, however at 4 min after application the Ca^{2+} response was significantly potentiated (Figure 4.6 D).

2-aminoethoxydiphenylborate (2-APB, 75 μM) was also able to inhibit Ca^{2+}-responses evoked by SPH with varying success. In the example trace shown, 2-APB inhibition was very effective (Figure 4.6 C). However, the mean data reveal that 2-APB blocked Ca^{2+} responses by an average 47.7% at 2.5 min after application, and was less effective at 4 min, producing a 25.1% block at this time point (Figure 4.6 D).

In summary, the data provide evidence that the SPH-induced Ca^{2+}-responses in HSV SMC in response to application of SPH are in part due to Ca^{2+} influx across the plasma membrane, most likely through functional TRPM3 channels.

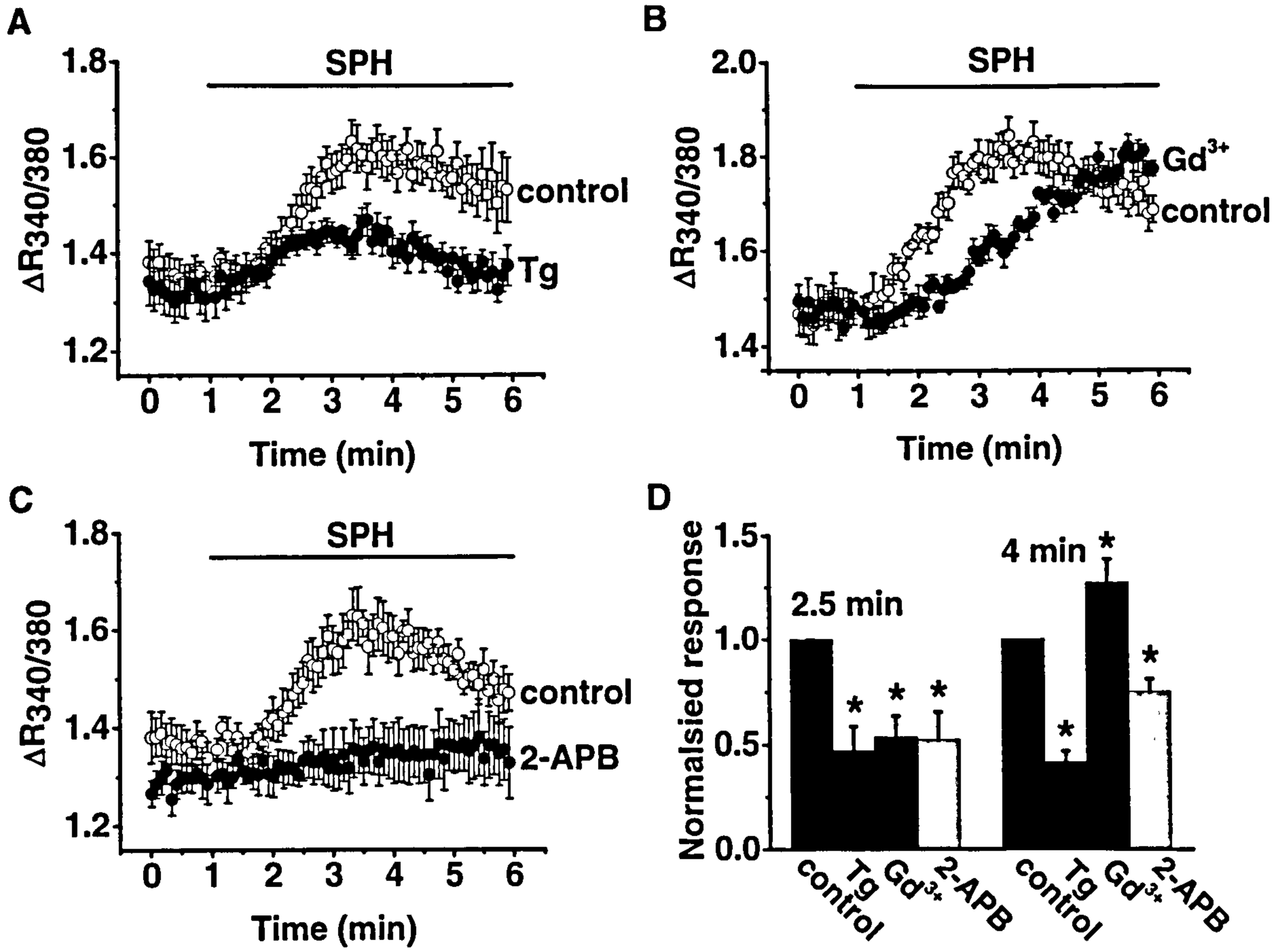

Figure 4.6. Characterisation of the SPH-induced Ca^{2+} response Ca^{2+} signals were measured as the 340/380 ratio of emission. Traces are representative mean data (±SEM) from 6 wells within a single plate. Ethanol (vehicle), Gd^{3+} and 2-APB were present for the duration of recordings, which were performed at RT. **A.** SPH (20 μM) application caused an increase in Ca^{2+} in HSV SMC that was inhibited by preincubation with Tg (1 μM). **B.** SPH-induced Ca^{2+} responses were inhibited by Gd^{3+} (100 μM). **C.** 2-APB (75 μM) also inhibited Ca^{2+} entry. **D.** Mean data (±SEM) showing significant effects on Ca^{2+} responses with all 3 compounds at both 2.5 and 4 min after SPH application (control n/N=3/18, Tg n/N=3/14, Gd^{3+} and 2-APB n/N=3/17).

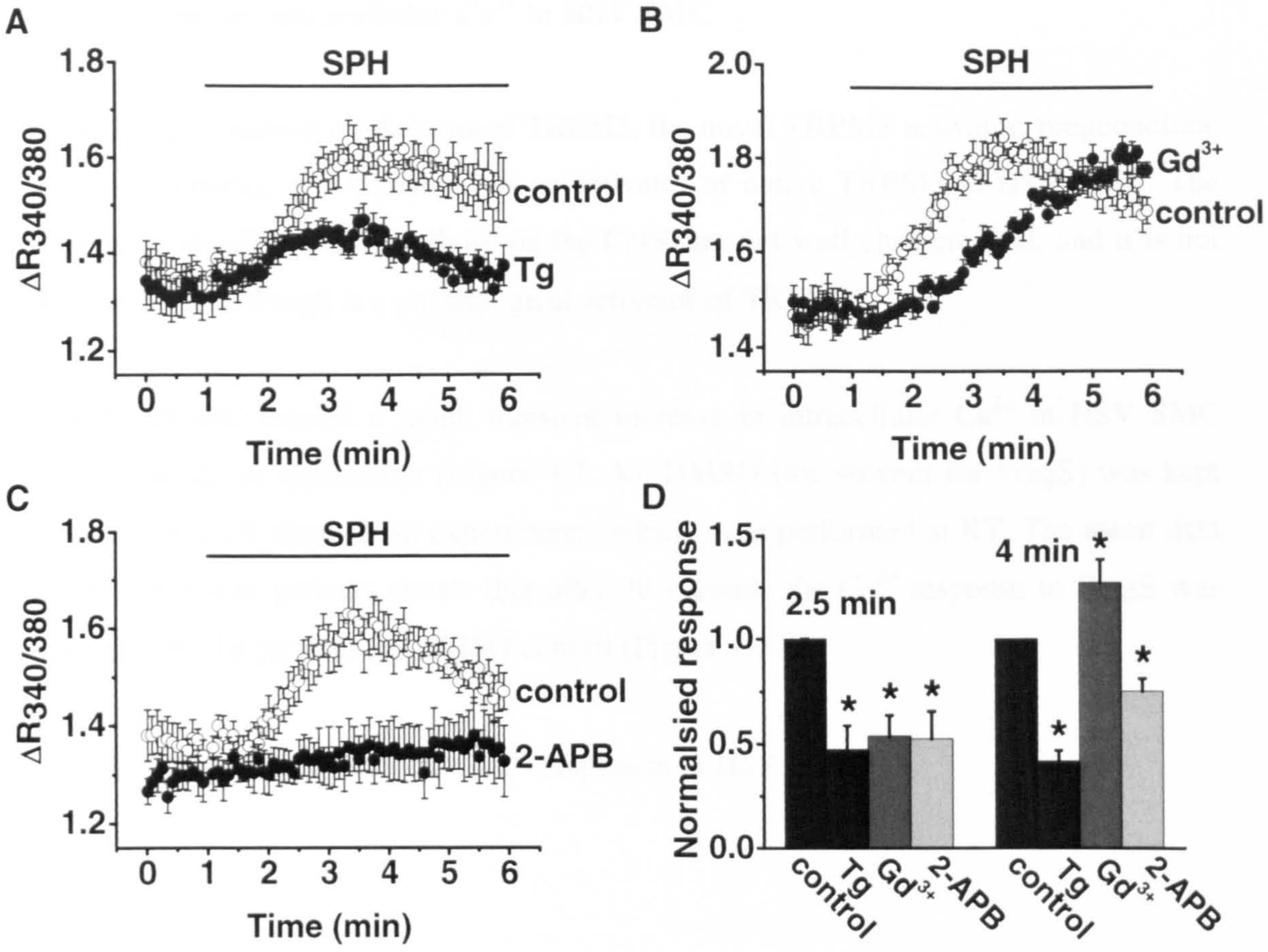

Figure 4.6. Characterisation of the SPH-induced Ca^{2+} response Ca^{2+} signals were measured as the 340/380 ratio of emission. Traces are representative mean data (±SEM) from 6 wells within a single plate. Ethanol (vehicle), Gd^{3+} and 2-APB were present for the duration of recordings, which were performed at RT. **A.** SPH (20 μM) application caused an increase in Ca^{2+} in HSV SMC that was inhibited by preincubation with Tg (1 μM). **B.** SPH-induced Ca^{2+} responses were inhibited by Gd^{3+} (100 μM). **C.** 2-APB (75 μM) also inhibited Ca^{2+} entry. **D.** Mean data (±SEM) showing significant effects on Ca^{2+} responses with all 3 compounds at both 2.5 and 4 min after SPH application (control n/N=3/18, Tg n/N=3/14, Gd^{3+} and 2-APB n/N=3/17).

PregS increases intracellular Ca^{2+} in HSV SMC

In addition to known modulators of TRPM3, the novel TRPM3 activator, pregnenolone sulphate (PregS), was examined as an activator of native TRPM3 in HSV SMC. The effects of PregS, aside from those on the CNS, are not well characterised, and it is not known whether PregS is a physiological activator of TRPM3.

PregS (25 μM) caused a rapid, transient increase in intracellular Ca^{2+} in HSV SMC within 30 sec of application (Figure 4.7. A). DMSO (the solvent for PregS) was kept constant at 0.1% throughout experiments, which were performed at RT. The mean data from 3 different patients shows that after 30 seconds the Ca^{2+} response to PregS was significantly larger than the DMSO control (Figure 4.7. B).

The data show PregS can evoke Ca^{2+} responses in HSV SMC.

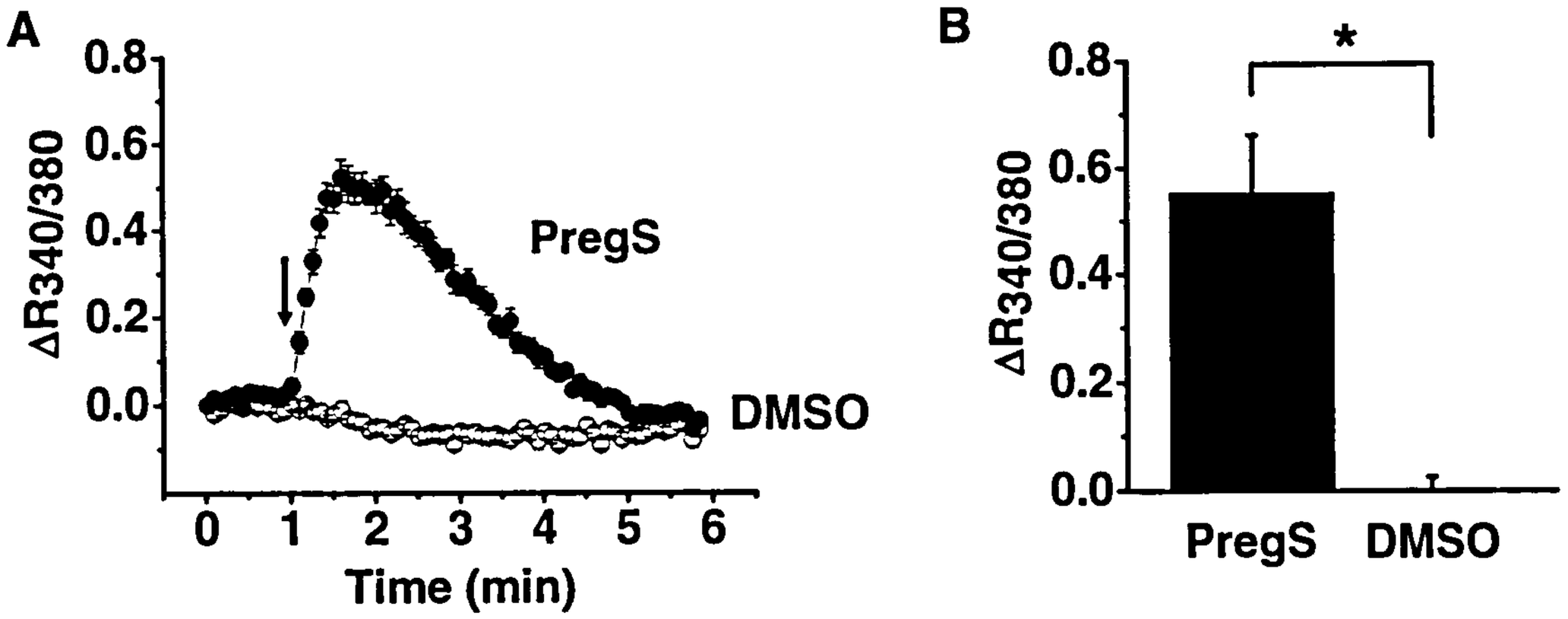

Figure 4.7. Pregnenolone sulphate (PregS) evokes Ca^{2+} responses in HSV SMC Ca^{2+} signals were measured as the 340/380 ratio of emission. DMSO (vehicle) was present throughout recordings. **A.** Representative mean data (±SEM) from 10 wells within a single plate. PregS (25 μM) application (arrow) causes an increase in Ca^{2+} in HSV SMC compared to vehicle control (open circles). **B.** Mean data (±SEM) showing significant increase in Ca^{2+} 1 min after PregS application (PregS n/N=3/31, DMSO n/N=3/27).

Characterisation of PregS-induced Ca^{2+} responses

As previously described for SPH-induced Ca^{2+} responses, the PregS response was further characterised using the SERCA-inhibitor Tg and known TRP channel modulators.

Preincubation with Tg (1 μM) partially inhibited the PregS-induced Ca^{2+} response, indicating not all of the Ca^{2+} response was due to Ca^{2+} influx (Figure 4.8 A). At 1 min after PregS application, Tg blocked 71.9% of the PregS-induced Ca^{2+} response. However, at 2 min, this was significantly less at only 28.8%, indicating that Tg is a better inhibitor of the initial PregS response (Figure 4.8 D). This would suggest that perhaps the PregS response occurs in 2 phases, an early phase dependent on Ca^{2+} stores, followed by a later phase due to Ca^{2+} entry across the plasma membrane.

Gd^{3+} (100 μM) almost completely inhibited the PregS-induced Ca^{2+}-response, and also reduced the starting baseline compared to control cells, suggesting inhibition of constitutive channel activity (Figure 4.8 B). The mean data show that this inhibition was consistent, with Gd^{3+} causing an 83.6% PregS-induced Ca^{2+} responses after 1 min, and a 57.3% inhibition after 2 min.

2-APB (75 μM) was also an effective inhibitor of PregS-induced Ca^{2+}-responses and reduced constitutive channel activity (Figure 4.8 C). The mean data reveal that 2-APB blocked Ca^{2+} responses by an average 57.1% 1 min after PregS application, and inhibition was reduced to 36.2% at 2 min. (Figure 4.8 D). 2-APB is recognized as a blocker of store-operated Ca^{2+} entry, which is reported to involve TRP channels, by blocking IP_3-receptors (Bootman *et al.*, 2002). If Ca^{2+} stores are involved with the PregS-response, this may explain why 2-APB appears to have had a stronger inhibitory effect at the earlier time point.

In summary, the data provide further evidence for the functional expression of TRPM3 in HSV SMC, and demonstrate that Ca^{2+} responses to PregS are in part due to Ca^{2+} influx, although the involvement of store operated Ca^{2+} release can not be ruled out and requires further investigation.

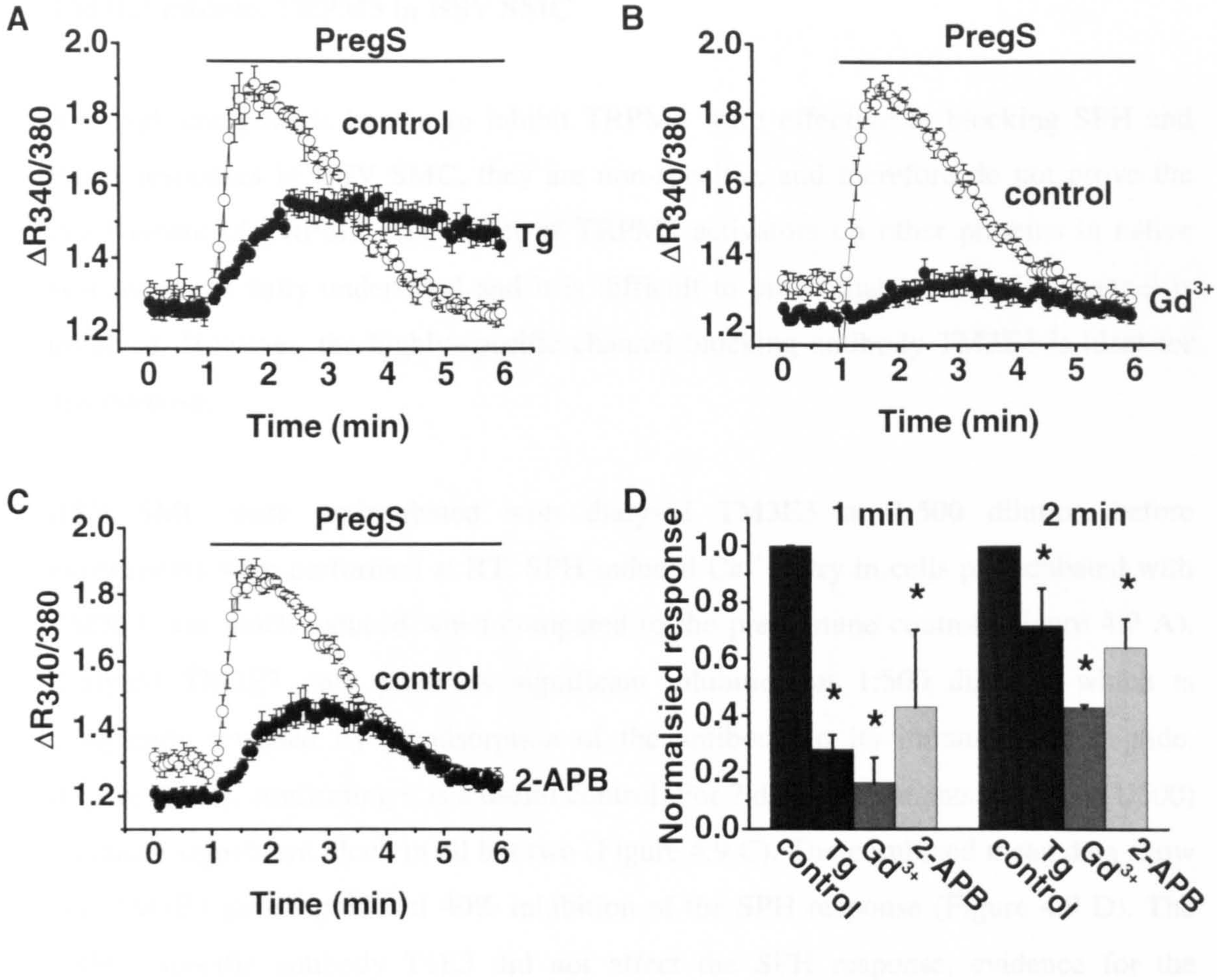

Figure 4.8. Characterisation of PregS-induced Ca^{2+} response Ca^{2+} signals were measured as the 340/380 ratio of emission. Traces are representative mean data (±SEM) from 6 wells within a single plate. DMSO (vehicle), Gd^{3+} and 2-APB were present for the duration of recordings, which were performed at RT. **A.** PregS (25 μM) application caused an increase in Ca^{2+} in HSV SMC that was inhibited by preincubation with Tg (1 μM). **B.** PregS-induced Ca^{2+} responses were inhibited by Gd^{3+} (100 μM) **C.** 2-APB (75 μM) also inhibited Ca^{2+} entry. **D.** Mean data (±SEM) showing significant inhibition of Ca^{2+} with all 3 compounds, both 1 and 2 min after PregS application (control n/N=4/15, Tg n/N=4/18, Gd^{3+} n/N= 3/11 and 2-APB n/N=3/16).

TM3E3 inhibits TRPM3 in HSV SMC

Although compounds known to inhibit TRPM3 were effective at blocking SPH and PregS responses in HSV SMC, they are non-specific, and therefore do not prove the involvement of TRPM3. The effect of TRPM3 activators on other proteins in native systems is not fully understood and it is difficult to prove that a particular channel is involved. However, the highly-specific channel blocking antibody TM3E3 is ideal for this purpose.

HSV SMC were preincubated with dialysed TM3E3 at 1:500 dilution before experiments were performed at RT. SPH-induced Ca^{2+}-entry in cells preincubated with TM3E3 was much reduced when compared to the preimmune control (Figure 4.9 A). Dialysed TM3E3 only produces significant inhibition at 1:500 dilution, which is completely reversed by preadsorption of the antibody to its immunogenic peptide. (Figure 4.9 B), confirming it is a useful control. For 7 different patients, TM3E3 (1:500) produced significant block in all but two (Figure 4.9 C). The combined mean data show that TM3E3 gave significant 40% inhibition of the SPH response (Figure 4.9 D). The TRPC1-specific antibody T1E3 did not affect the SPH response, evidence for the selectivity of E3-targetted antibodies and suggesting TRPC1 is not involved in the SPH response.

TM3E3 also inhibited PregS-induced Ca^{2+}-entry in HSV SMC compared to the preimmune control (Figure 4.10 A). For 6 different patients, TM3E3 produced significant block of the PregS-induced Ca^{2+} response in all but one (Figure 4.10 B). The mean data shows TM3E3 gave an average 45% inhibition (Figure 4.10 D). Interestingly the TRPC1-specific antibody T1E3 potentiates activation by PregS (Figure 4.10 C & D). This mechanism remains to be investigated. However as the SPH response was unaffected by T1E3, this would suggest T1E3 does not influence the PregS-response as a result of an effect on the TRPM3 channel.

The data suggest that TRPM3 is present and functional in HSV SMC, and its activation by SPH and PregS can be specifically and significantly inhibited by TM3E3.

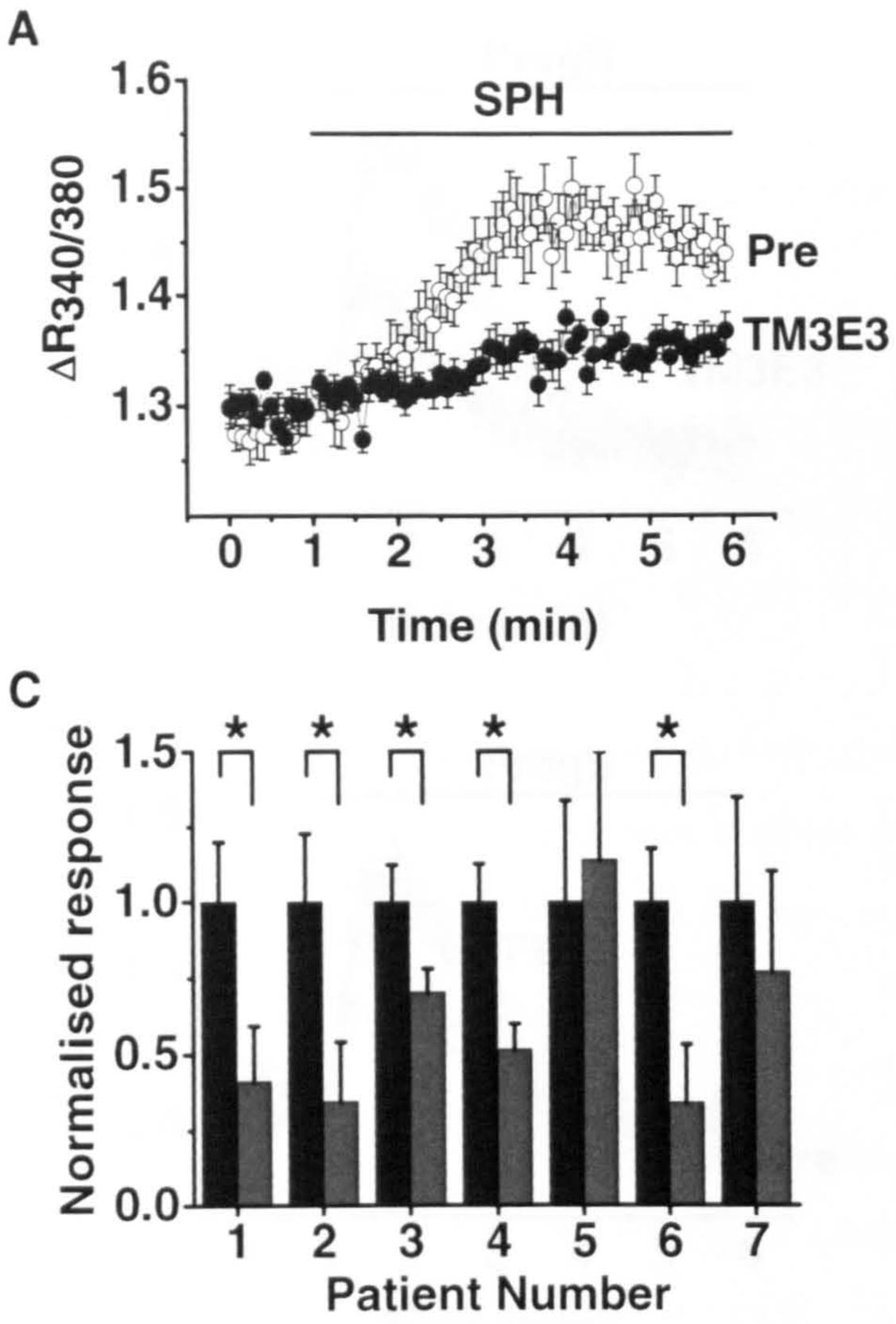

Figure 4.9. TM3E3 inhibits SPH-induced Ca^{2+} response in HSV SMC Ca^{2+} signals were measured as the 340/380 ratio of emission. Ethanol (vehicle) was present throughout recordings, which were performed at RT. **A.** Representative mean data (±SEM) from 9 wells within a single plate. SPH (20 μM) application caused an increase in Ca^{2+} in HSV SMC that was inhibited by preincubation with dialysed TM3E3 antiserum (closed circles) compared to preimmune serum (open circles). **B.** Antisera dilution data from 4 independent experiments for preimmune (black bars), TM3E3 (grey bars) and TM3E3 preadsorbed to antigenic peptide (dark grey bars). **C.** Normalised Ca^{2+} response for 7 independent experiments with preimmune (black bars) or TM3E3 (grey bars) at 1:500 dilution. **D.** Mean data (±SEM) showing significant inhibition of Ca^{2+} response by TM3E3, but not T1E3, 2.5 min after SPH application (TM3E3 n/N=7/76, T1E3 n/N=6/47).

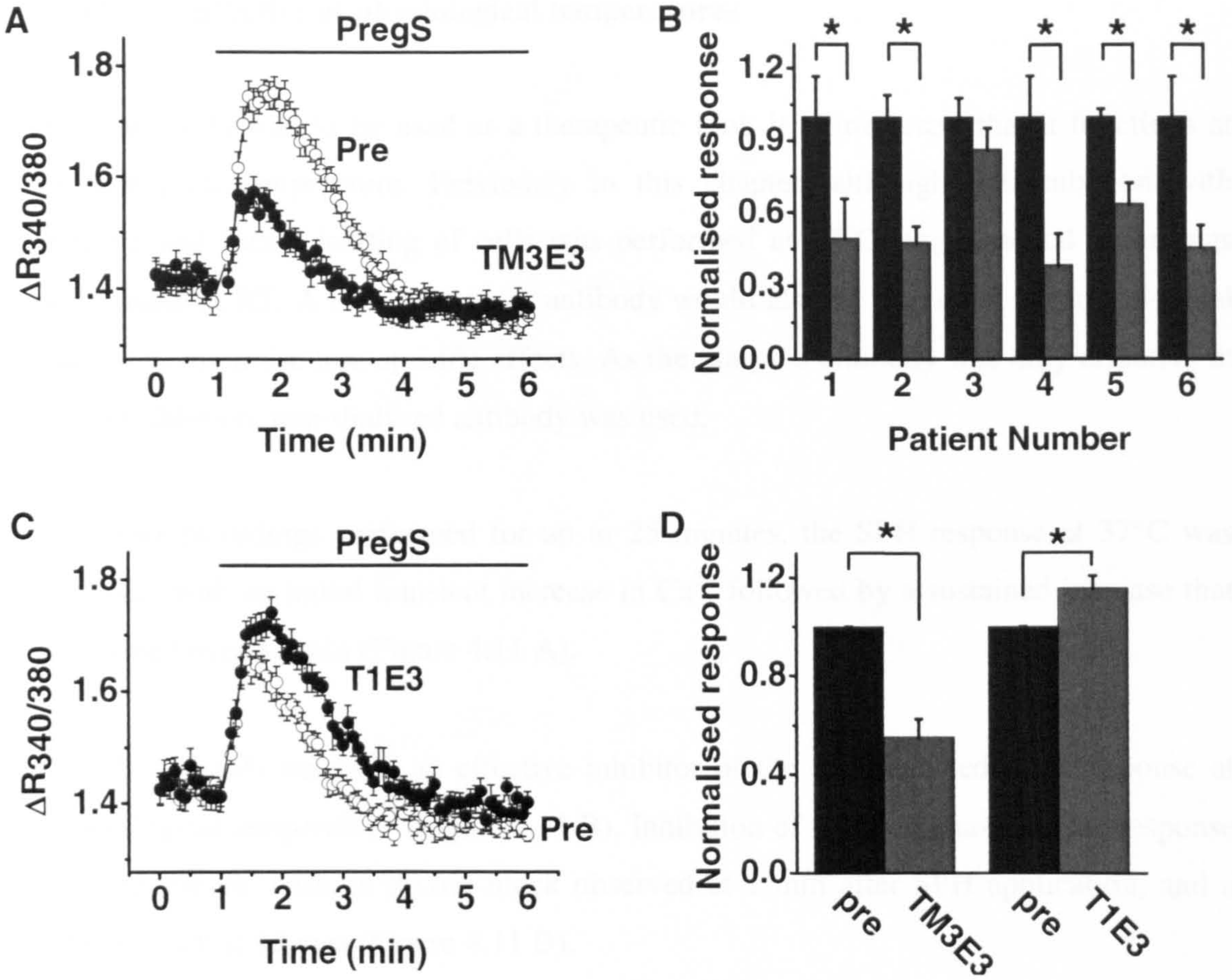

Figure 4.10. TM3E3 inhibits PregS-induced Ca^{2+} response in HSV SMC Ca^{2+} signals were measured as the 340/380 ratio of emission. DMSO (vehicle) was present throughout recordings, which were performed at RT. **A.** Representative mean data (±SEM) from 12 wells within a single plate. PregS (25 μM) application caused an increase in Ca^{2+} in HSV SMC that was inhibited by preincubation with dialysed TM3E3 antiserum (closed circles) compared to preimmune serum (open circles). **B.** Normalised Ca^{2+} response for 6 different patients with preimmune (black bar) or TM3E3 (grey bar) at 1:500 dilution. **C.** Representative mean data (±SEM) from 12 wells within a single plate shows that T1E3 (1:500 dilution) preincubation potentiates the PregS response (closed circles) compared to preimmune serum control (open circles). **D.** Mean data (±SEM) showing significant inhibition of Ca^{2+} response by TM3E3, and potentiation by T1E3, 1 min after PregS application (TM3E3 n/N=6/44, T1E3 n/N=6/46).

TM3E3 is effective at physiological temperatures

If an antibody was to be used as a therapeutic tool, it is important that it functions at physiological temperature. Previously in this chapter, although preincubation with antisera and fura-2 loading of cells was performed at 37°C, experimental recordings were made at RT. A low dilution of antibody would also be important in physiological studies to minimise non-specific effects. As the dialysed antibody was only effective at a 1:500 dilution, non-dialysed antibody was used.

In longer recordings performed for up to 25 minutes, the SPH response at 37°C was biphasic, with an initial transient increase in Ca^{2+} followed by a sustained increase that developed over 15 min (Figure 4.11 A).

2-APB (75 μM) was still an effective inhibitor of the SPH-induced Ca^{2+} response at physiological temperature (Figure 4.11 B). Inhibition of the both phases of the response was significant, with an 86.0% block observed at 1 min after SPH application, and a 73.6% block at 10 min (Figure 4.11 D).

Gd^{3+} (100 μM) also effectively inhibited the initial transient Ca^{2+} response, however was unable to block the sustained phase (Figure 4.11 C). The mean data show a significant 73.5% inhibition of the SPH-response at 1 min after application, while at 10 min the average block was 20.4%, and not significant (Figure 4.11 D).

Preincubation with non-dialysed antibody at 1:4000 dilution inhibited the SPH response (Figure 4.12 A). The mean data from 9 different patients shows TM3E3 gives a significant block of both phases, 20.7% after 1 min after SPH application and a slightly stronger block of 29.9% after 10 min (Figure 4.12 B).

In summary, non-specific TRP channel blockers and TM3E3 can significantly inhibit TRPM3 under physiological conditions.

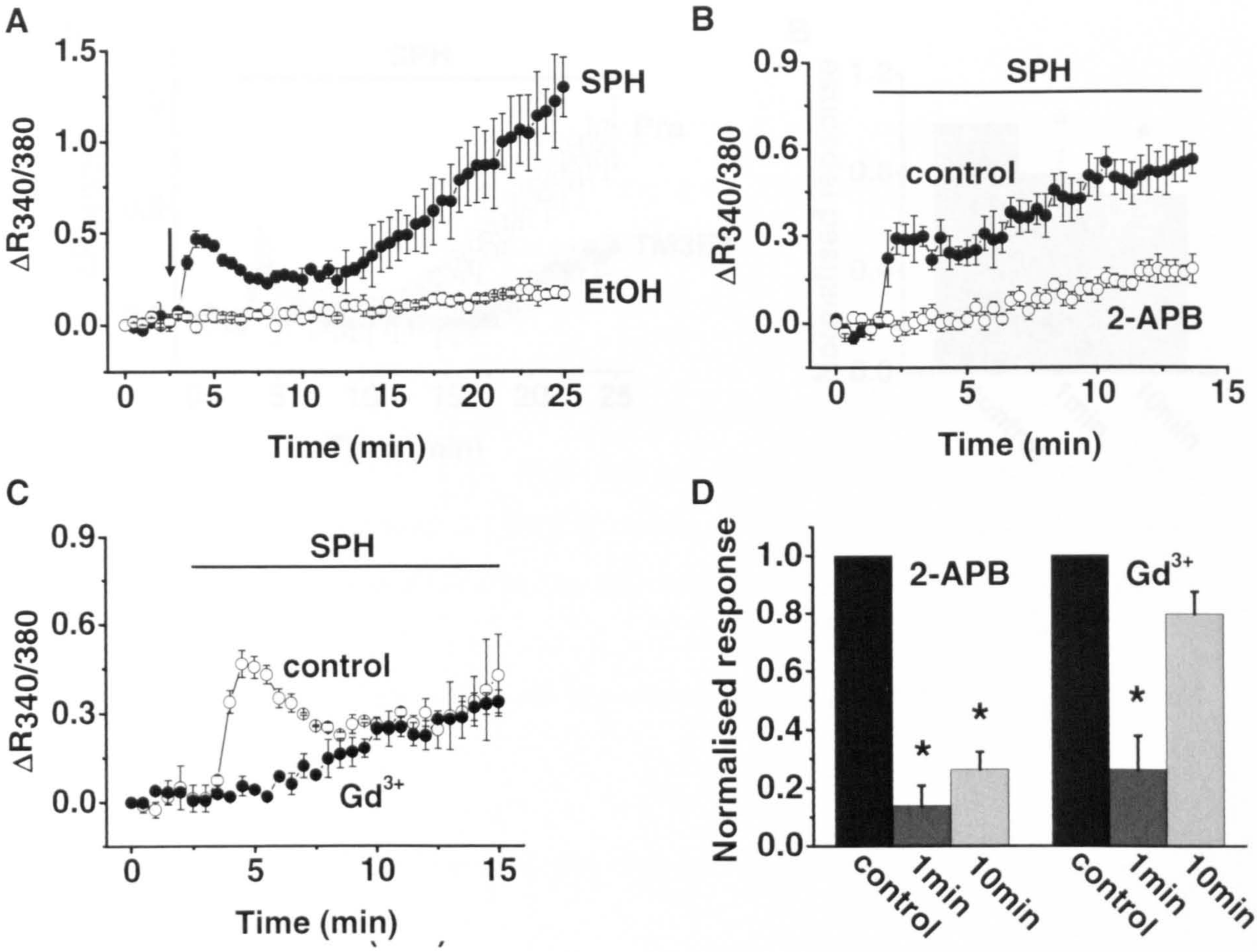

Figure 4.11. Inhibition of the SPH-induced Ca^{2+} response at physiological temperature Ca^{2+} signals were measured as the 340/380 ratio of emission. Traces are representative mean data (±SEM) from 6 wells within a single plate. Ethanol (vehicle) was present throughout recordings, which were performed at 37°C. **A.** SPH (20 μM) application (arrow) caused a biphasic Ca^{2+} response in HSV SMC compared to EtOH control. **B.** The SPH response was inhibited by preincubation with 2-APB (75 μM, closed circles) compared to vehicle control (open circles). **C.** The SPH response was also inhibited by preincubation with Gd^{3+} (100 μM, closed circles). **D.** Mean data (±SEM) showing significant inhibition of both phases of the Ca^{2+} response at 1 and 10 min after SPH application. Data are normalised to control response in absence of inhibitor (2-APB n/N=4/25, Gd^{3+} n/N=3/14).

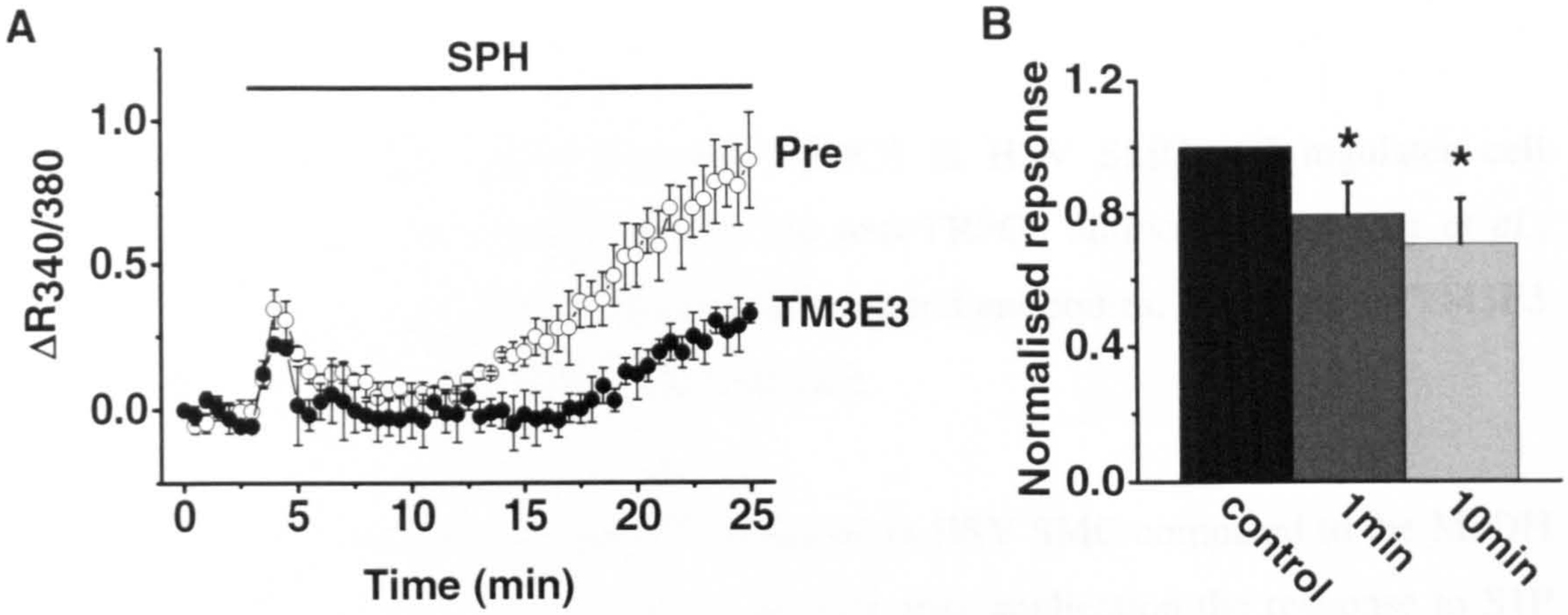

Figure 4.12. TM3E3 inhibits SPH-induced Ca^{2+} response at physiological temperature Ca^{2+} signals were measured as the 340/380 ratio of emission. EtOH (vehicle) was present throughout recordings, which were performed at 37°C. **A.** Representative mean data (±SEM) from 6 wells within a single plate. The SPH response was inhibited by preincubation with dialysed TM3E3 antiserum (open circles) compared to preimmune serum (closed circles). **B.** Mean data (±SEM) normalised to preimmune control showing significant inhibition of both phases of the Ca^{2+} response by TM3E3 at 1 or 10 min after SPH application (pre n/N=9/45, TM3E3 n/N=9/46).

Specificity of TM3E3

Sphingosine-1-phosphate (S1P) activates TRPC5 in HSV SMC and regulates cell motility, effects that can be inhibited by the anti-TRPC5 antibody T5E3 (Xu *et al.*, 2006b). To demonstrate the specificity of E3-targeted antibodies, the effect of TM3E3 on the S1P response in HSV SMC was examined.

In this study, S1P (10 μM) caused Ca^{2+} response in HSV SMC compared to the MeOH (vehicle) control (Figure 4.13 A). At 30 seconds after application the response to S1P was significantly larger than the MeOH control (Figure 4.13 B). Preincubation with dialysed TM3E3 at 1:500 dilution had no effect on this response (Figures 4.13 C & D).

In addition, TM3E3 does not block the endogenous ATP response in HSV SMC (Figures 4.13 E & F).

The data demonstrate TM3E3 specifically inhibits TRPM3 in HSV SMC.

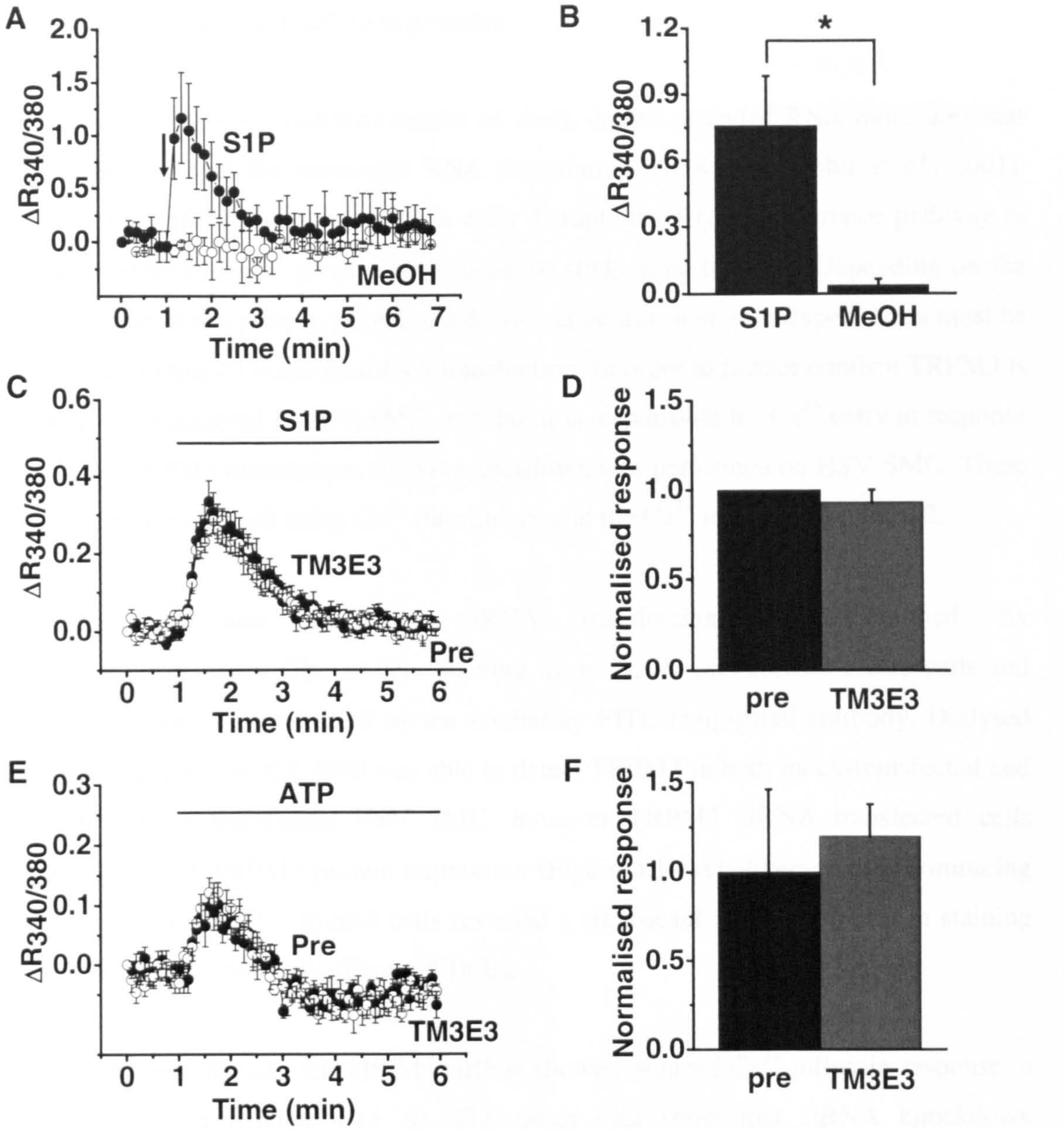

Figure 4.13. TM3E3 does not inhibit S1P- or ATP-induced Ca^{2+} responses Recordings were performed at RT. Traces are representative mean data (±SEM) from 4-6 wells within a single plate. **A.** S1P (10 μM) application (arrow) causes an increase in Ca^{2+} in HSV SMC compared to methanol (MeOH) control. **B.** Mean data (±SEM) showing significant Ca^{2+} increase 30 sec after S1P application (S1P n/N=5/21, MeOH n/N=5/18). **C.** The S1P response was not inhibited by preincubation with dialysed TM3E3 antiserum. **D.** Mean data (±SEM) normalised to preimmune control show no inhibition of the Ca^{2+} response by TM3E3 30 sec after S1P application (n/N=2/9 for each). **E.** ATP (100 μM) caused Ca^{2+} responses that were not inhibited by preincubation with dialysed TM3E3 antiserum. **F.** Mean data (±SEM) normalised to preimmune control show no inhibition of the Ca^{2+} response by TM3E3, 30 sec after ATP application (n/N=1/6 for each).

siRNA knockdown of TRPM3 expression

Small interfering RNA (siRNA) consist of short, double stranded RNA molecules that act as mediators of the messenger RNA degradation pathway (Elbashir *et al.*, 2001). Transfecting siRNAs into mammalian cells disrupts the RNA interference pathway to prevent expression of a given gene in order to study gene function. Depending on the turnover rate of the protein, gene knockdown can be transient, thus experiments must be performed within 48 hours of siRNA transfection. In order to further confirm TRPM3 is present and functional in HSV SMC, and that it is responsible for Ca^{2+} entry in response to known TRPM3 modulators, siRNA knockdown was performed on HSV SMC. These cells were then assayed using Ca^{2+} fluorimetry and the Ca^{2+} indicator dye Fura-2.

TRPM3 expression following siRNA transfection was examined by immunocytochemistry. The nuclear staining agent DAPI was used to locate cells and TM3E3 staining was indicated by the secondary FITC conjugated antibody. Dialysed TM3E3 at a dilution of 1:4000 was able to detect TRPM3 in both mock-transfected and TRPM3 siRNA-transfected HSV SMC, however TRPM3 siRNA transfected cells showed reduced TRPM3 protein expression (Figure 4.14 A). Average data comparing the percentage of FITC stained cells revealed a significant 38.2% decrease in staining for siRNA transfected cells (Figure 4.14 B).

HSV SMC transfected with TRPM3 siRNA showed reduced Ca^{2+} influx in response to SPH application (Figure 4.15 A). The mean data show that siRNA knockdown produced a 67.9% inhibition of the SPH response (Figure 4.15 B). TRPM3 siRNA also inhibited PregS-stimulation (Figure 4.15 C), producing an average 21.1% inhibition of the Ca^{2+}-response (Figure 4.15 D).

In summary, HSV SMC cells transfected with TRPM3 siRNA show a reduction in TM3E3 staining, indicating a reduction in TRPM3 protein expression as a result of successful knockdown of the TRPM3 gene in these cells. Furthermore siRNA knockdown strengthens the idea that TRPM3 is responsible for Ca^{2+}-entry in vascular smooth muscle.

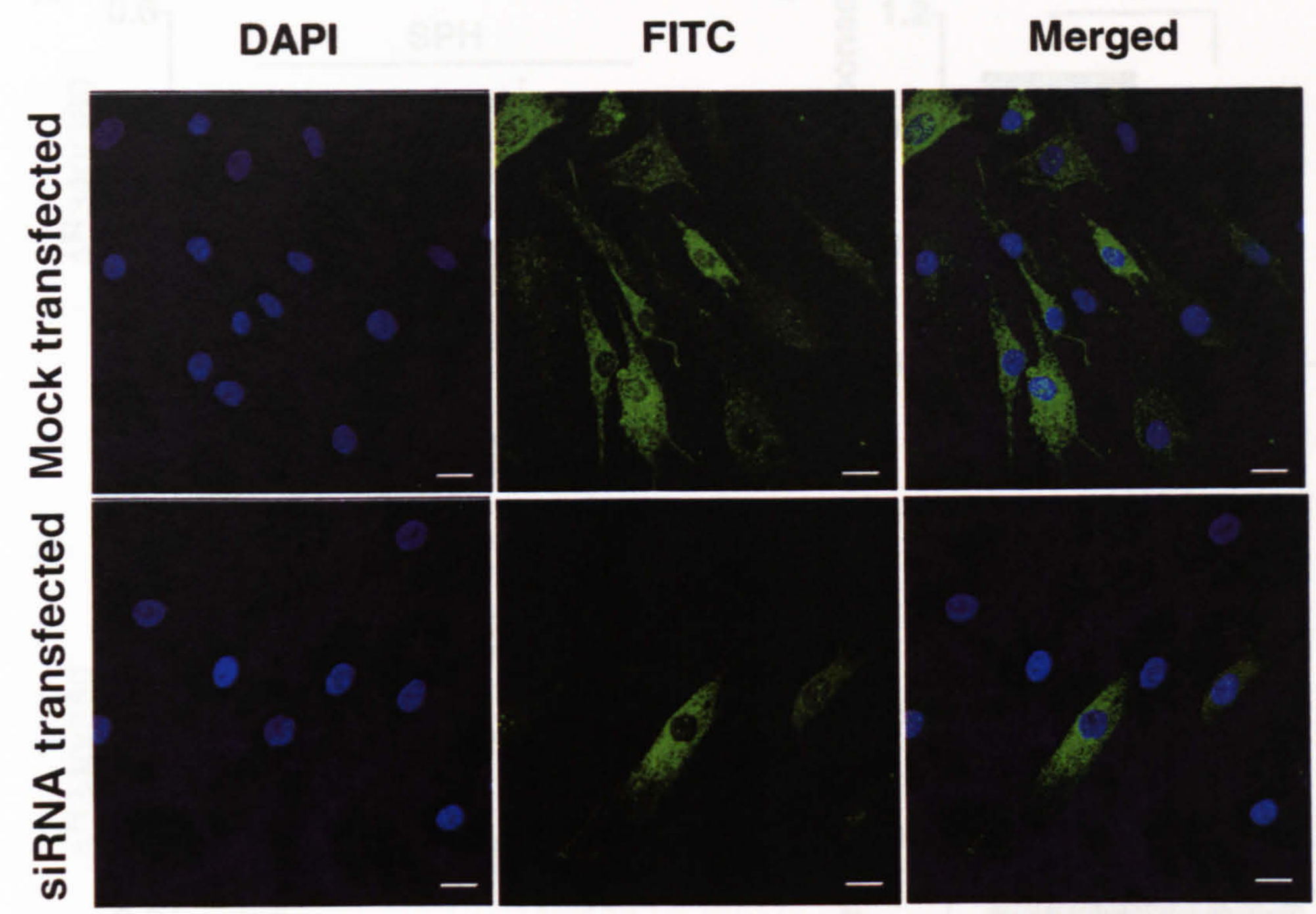

Figure 4.14. siRNA knockdown of TRPM3 A. Immunocytology performed on non-permeabilised HSV SMC fixed with 2% PFA. Cells were co-stained with DAPI and TM3E3 antibody plus a FITC conjugated secondary antibody. For negative controls, TM3E3 was preadsorbed to its antigenic peptide (TM3E3 + pep) or primary antibody was omitted. Images are representative of cells from 3 different patients. Scale bars represent 20μm. **B.** Mean data (±SEM) showing significant reduction in the number of TM3E3 stained cells for siRNA transfected cells (-siRNA n/N=4/81, +siRNA n/N=4/100). *TRPM3 siRNA transfections performed by Dr. J. Li.*

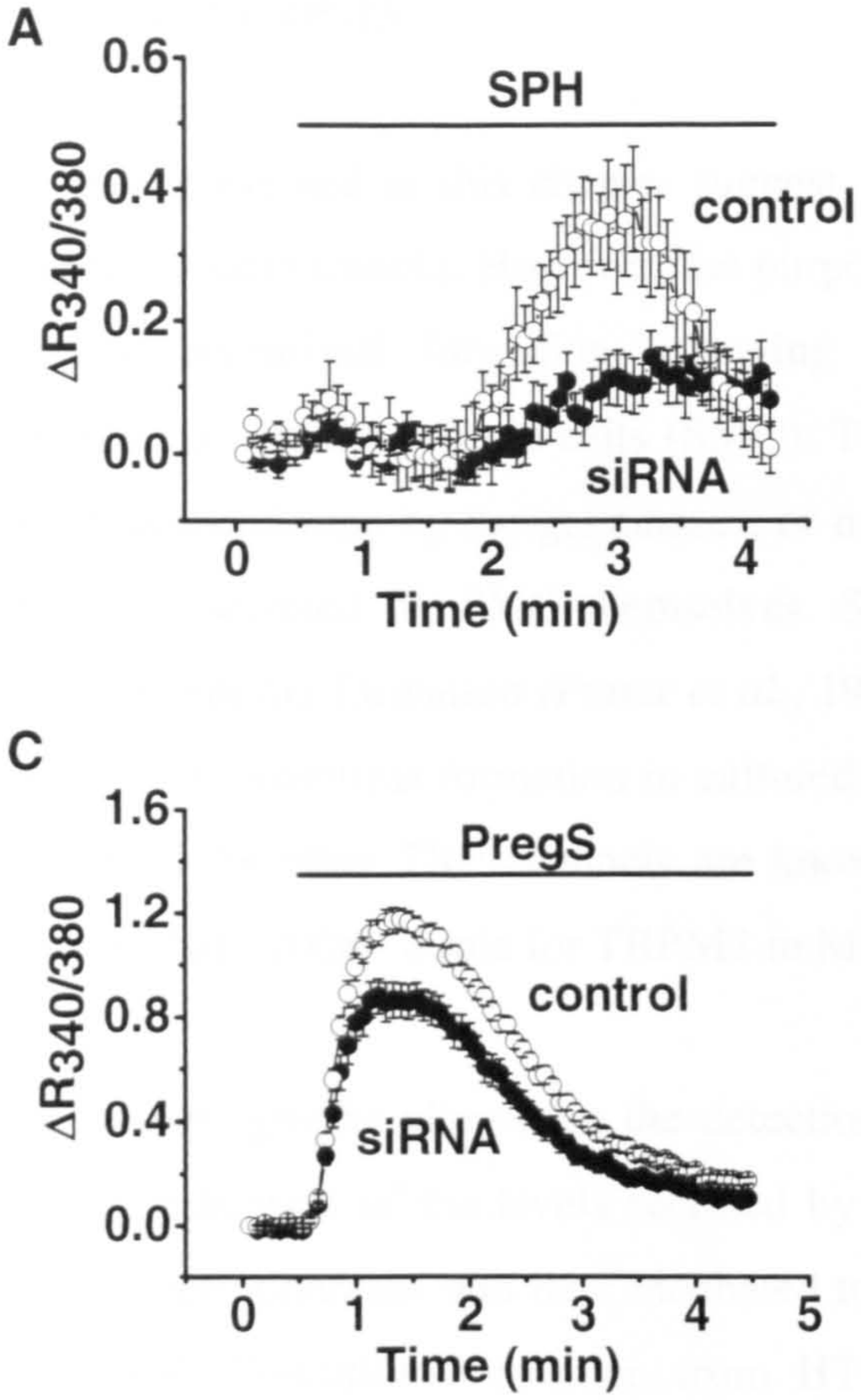

Figure 4.15. TRPM3 siRNA inhibits TRPM3-like Ca^{2+} responses Ca^{2+} signals were measured as the 340/380 ratio of emission. Traces are mean data (±SEM) representative of 6 wells within a single plate. Ethanol or DMSO (vehicle) were present throughout recordings, which were performed at RT. **A.** SPH (20 μM) application caused an increase in Ca^{2+} in HSV SMC that was reduced in cells transfected with siRNA (open circles) compared to mock transfected control (closed circles). **B.** Normalised mean SPH data (±SEM) for cells transfected with control (black bar) or TRPM3 siRNA (grey bar). n/N=3/18 for each. **C.** PregS (25 μM) application caused an increase in Ca^{2+} in HSV SMC that was reduced in cells transfected with siRNA (open circles) compared to mock transfected control (closed circles). **D.** Normalised mean PregS data (±SEM) for cells transfected with control (black bar) or TRPM3 siRNA (grey bar). n/N=3/18 for each.. *Experiments performed by Dr. J. Li.*

Function of TRPM3

The data presented in this chapter suggest that TRPM3 forms functional channels in vascular smooth muscle. However, the purpose of such a channel is unknown. An early stage in neointimal formation following bypass surgery is the proliferation and migration of smooth muscle cells (SMC). This is dependent on the degradation of the basement membrane by the gelatinases, or matrix metalloproteinases (MMP) -9 and -2, which are secreted by SMC themselves. Specifically, production of MMP-9 occurs during neointima formation (Porter *et al.*, 1998), and the inhibition of MMP-9 causes a reduction in neointima formation in cultured human saphenous vein segments (Porter *et al.*, 2002). As other TRP channels are known to be involved in neointimal formation (Kumar *et al.*, 2006), a role for TRPM3 in MMP secretion was thus examined.

Gelatin zymography allows for the detection of MMP-2 and MMP-9 in cell media to give an indication of the levels secreted by SMC. The proteins are resolved by SDS-PAGE electrophoresis, and then incubated to allow digestion of a gelatin infused SDS-PAGE gel. Conditioned medium from HT-1080 (HT) cells is used as a control to identify MMP-9 and MMP-2 bands.

MMP-2 secretion from HSV SMC is constitutive, whereas MMP-9 secretion can be induced by the phorbol ester, 12-*O*-tetradecanoylphorbol 13-acetate (TPA, 100nM) (Turner *et al.*, 2005). In this study, zymography analysis confirmed TPA treatment significantly increased MMP-9 secretion after a 48 hour period (Figure 4.16 A&B). As the secretion of MMP-2 was much greater than that of MMP-9, the MMP2 band saturated. For this reason, MMP-2 could not quantified by densitometry.

The effect of TRPM3 modulators on TPA-induced MMP-9 secretion was subsequently examined. SPH appeared to slightly reduce MMP-9 secretion compared to the vehicle control, but this was not significant, and inclusion of TM3E3 also had no effect (Figure 4.16 C). However, PregS treatment caused a significant reduction in MMP-9 secretion, while inclusion of TM3E3 had no significant effect, suggesting a reversal of the PregS effect (Figure 4.16 D).

In summary, the TRPM3 activator PregS causes a reduction in TPA-induced MMP-9 secretion by HSV SMC, an effect that does not occur in the presence of TM3E3.

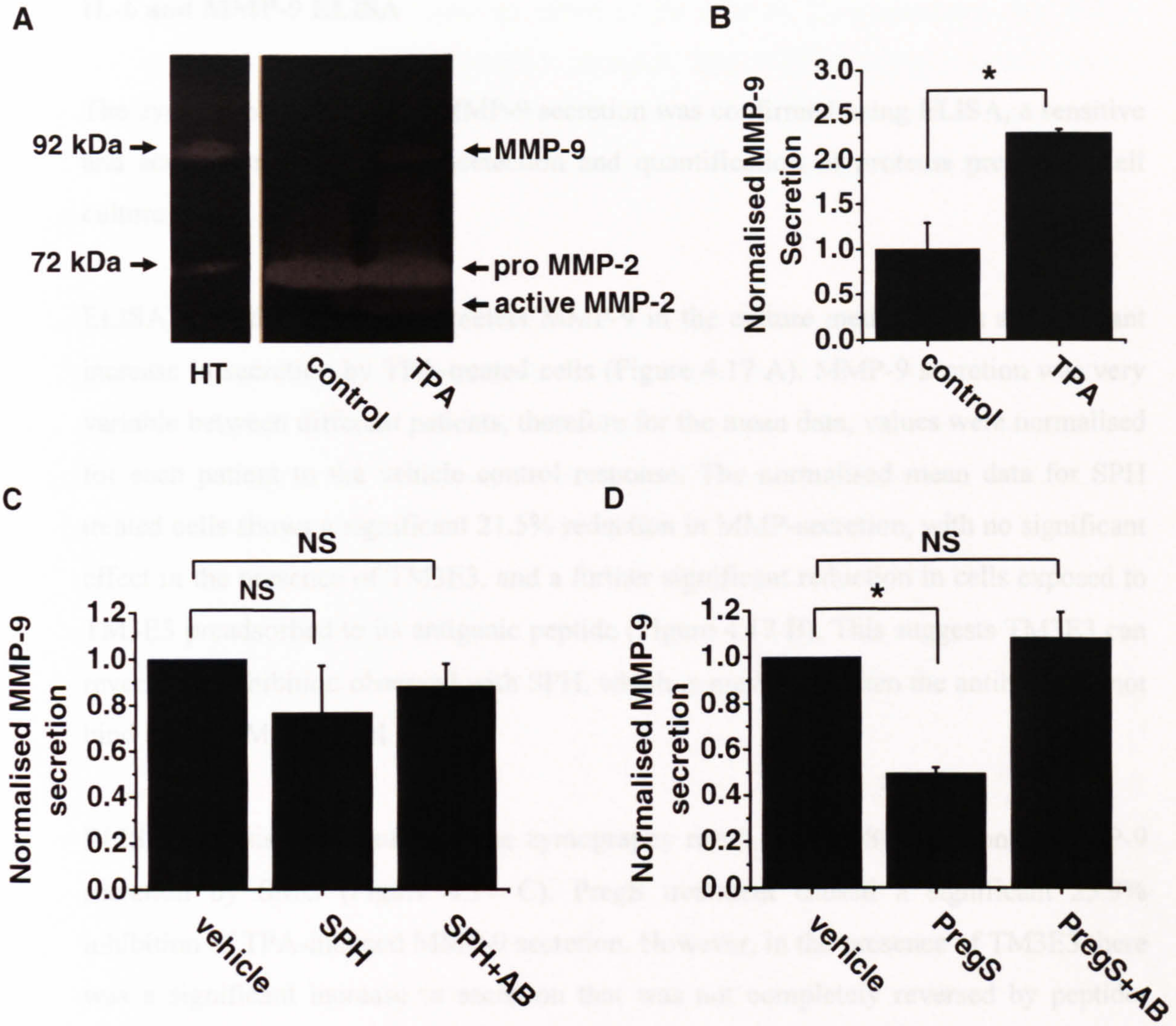

Figure 4.16. TPA increases MMP-9 secretion, which is inhibited by PregS Densitometric values for bands of lysis at 92 kDa (MMP-9) were determined using Image J software. Mean data (±SEM) are from 3 different patients, normalised to control (without TPA treatment) or vehicle response. **A.** Representative gelatin zymogram of HSV SMC culture medium. Bands of lysis were apparent at 92 kDa (MMP-9), 72 kDa (pro-MMP-2) and 66 kDa (MMP-2). Conditioned medium from HT-1080 cells was included as a positive control. **B.** Mean data (±SEM) show TPA causes a significant increase in MMP-9 secretion. **C.** Mean data (±SEM) shoe SPH alone and in the presence of TM3E3 (SPH+AB) has no significant effect on MMP-9 secretion. **D.** Mean data (±SEM) show PregS alone causes a significant reduction in MMP-9 secretion, which does not occur in the presence of TM3E3 (PregS+AB).

IL-6 and MMP-9 ELISA

The zymography analysis of MMP-9 secretion was confirmed using ELISA, a sensitive and accurate method for the detection and quantification of proteins present in cell culture media.

ELISA analysis performed to detect MMP-9 in the culture media shows a significant increase in secretion by TPA-treated cells (Figure 4.17 A). MMP-9 secretion was very variable between different patients, therefore for the mean data, values were normalised for each patient to the vehicle control response. The normalised mean data for SPH treated cells shows a significant 21.5% reduction in MMP-secretion, with no significant effect in the presence of TM3E3, and a further significant reduction in cells exposed to TM3E3 preadsorbed to its antigenic peptide (Figure 4.17 B). This suggests TM3E3 can reverse the inhibition observed with SPH, which is prevented when the antibody cannot bind the TRPM3 channel.

ELISA analysis also confirmed the zymography result for PregS inhibition of MMP-9 secretion by SMC (Figure 4.17 C). PregS treatment caused a significant 25.9% inhibition of TPA-induced MMP-9 secretion. However, in the presence of TM3E3 there was a significant increase in secretion that was not completely reversed by peptide-preadsorption. This suggests that TM3E3 may have a non-specific effect to cause secretion independently of PregS effect.

In addition to MMP-9, IL-6 is also an important regulatory factor secreted by VSMC. SMC secrete IL-6 in response to biomechanical stress, a mechanism that may contribute to the onset of atherosclerosis (Zampetaki *et al.*, 2005). For this reason, the effect of TRPM3 modulators on IL-6 secretion was also examined by ELISA. ELISA analysis shows a significant increase in IL-6 secretion by TPA-treated cells (Figure 4.18 A). The mean data for SPH treated cells shows no significant effect on IL-6 secretion with TM3E3 or peptide-bound antibody treatment (Figure 4.18 B). For PregS treatment, the ELISA indicated a 52.9% reduction in secretion, however there was no significant effect on secretion when TM3E3 was present, suggesting the antibody had prevented the PregS inhibitory effect (Figure 4.18 C). As for MMP-9, this data indicates TM3E3 can reverse the effect of PregS, although for IL-6 secretion the peptide bound-antibody control was not able to significantly reverse the antibody effect.

As the antibody appeared to have an effect of its own on IL-6 secretion, this was examined in the absence of a TRPM3 stimulus. The DMSO vehicle control was however still present throughout these experiments. TM3E3 caused a significant increase in IL-6 secretion, while when preadsorbed to its antigenic peptide had no significant effect. (Figure 4.18 D).

In summary, the data suggest that PregS and to some extent SPH have an effect on TPA-induced MMP-9 and IL-6 secretion in HSV SMC. The role of TRPM3 cannot be exclusively proved as the antibody also has an effect on secretion, potentially representing inhibition of constitutive TRPM3 activity, although non-specific effects can't be ruled out at this stage.

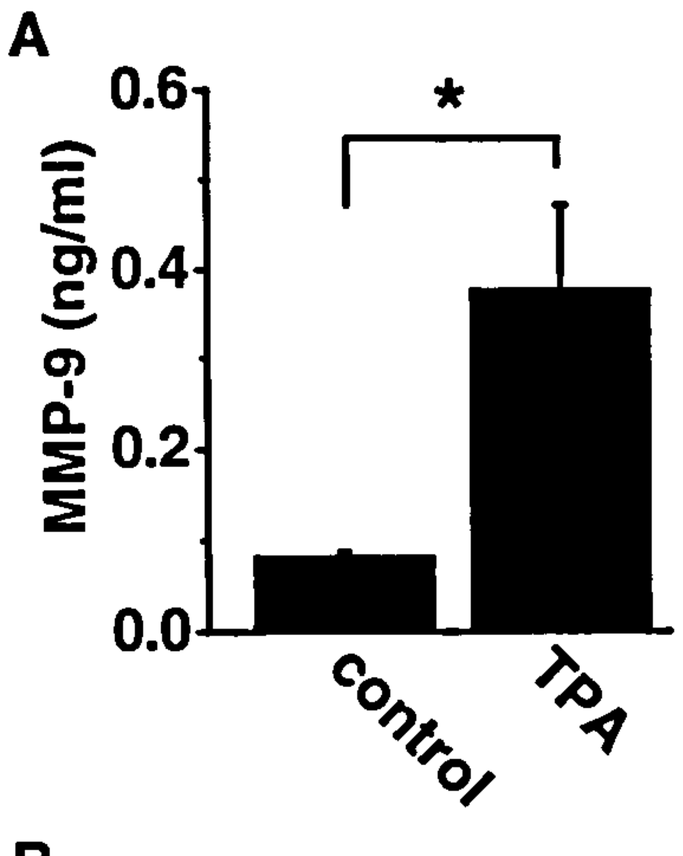

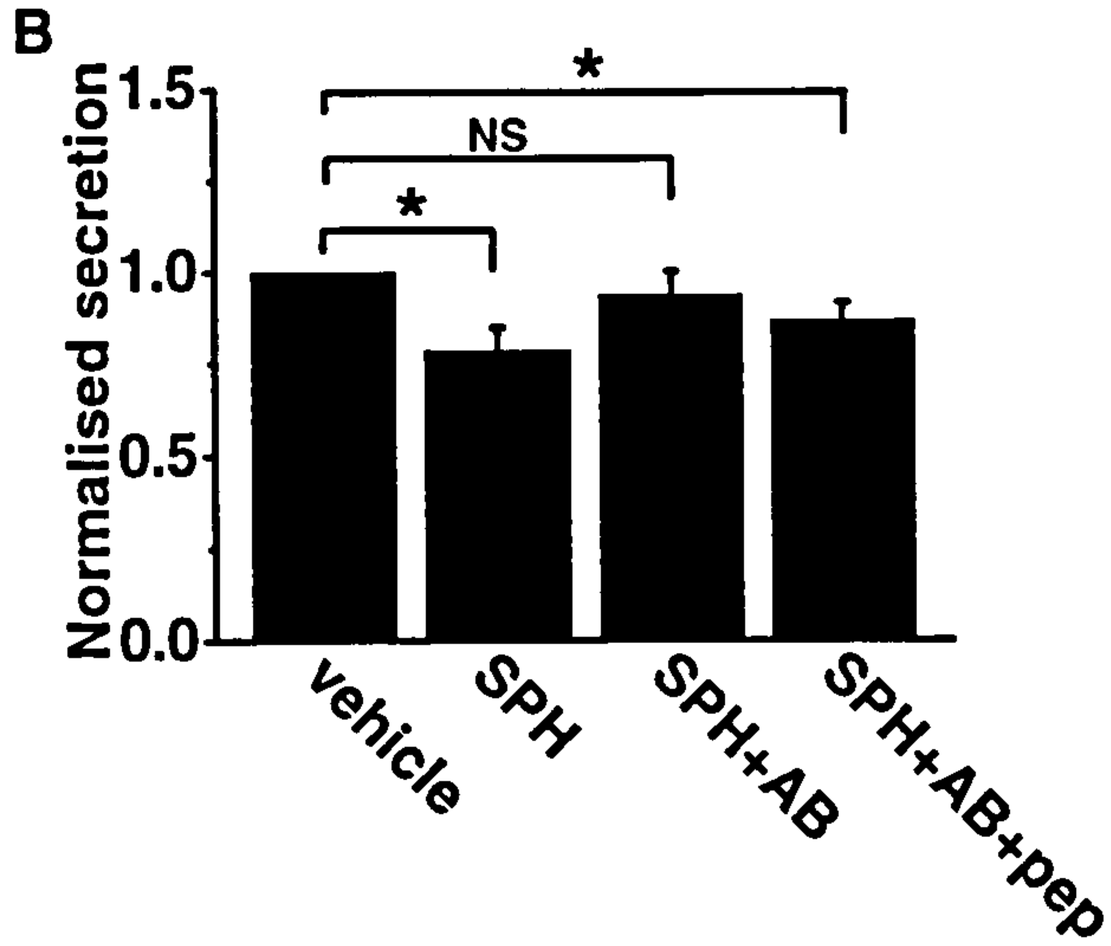

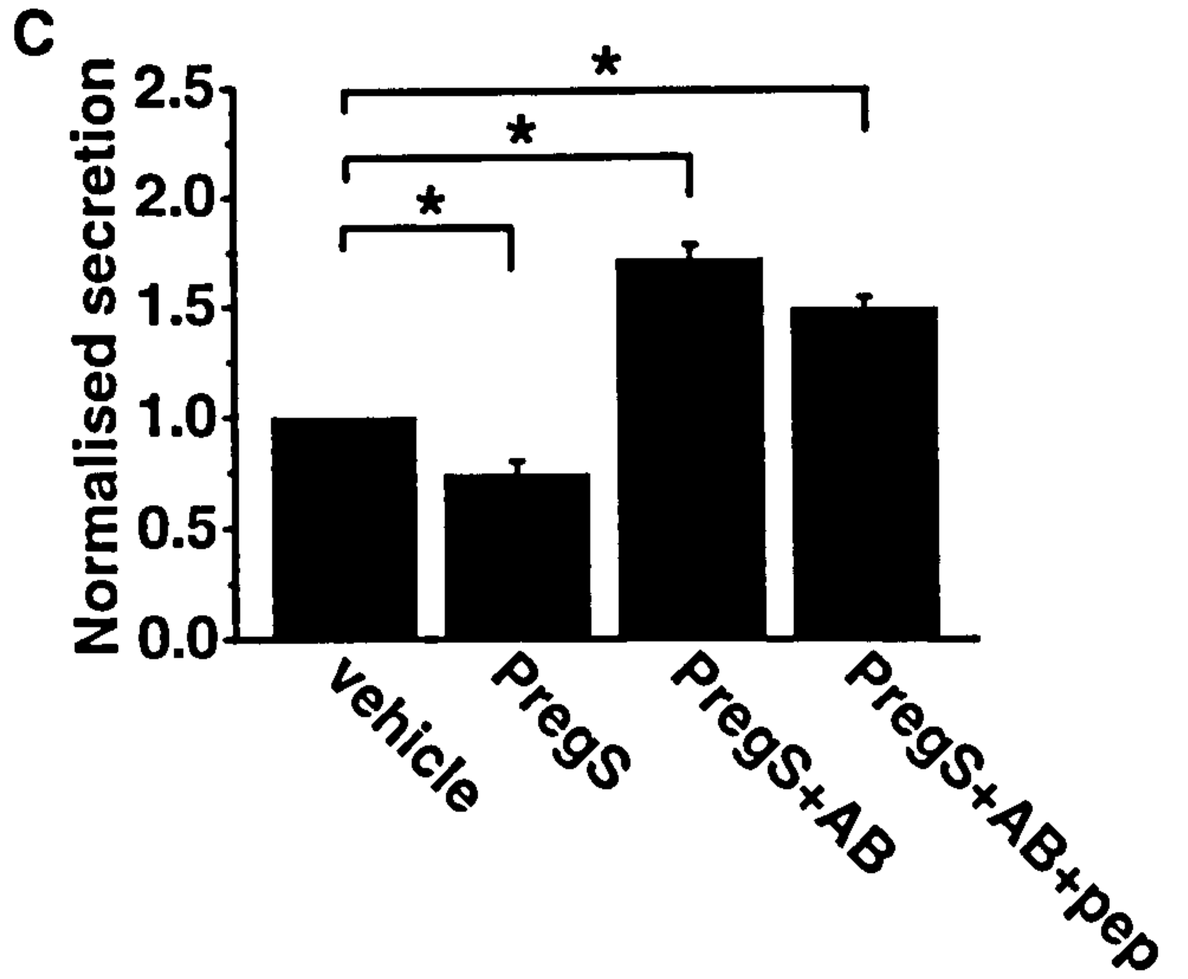

Figure 4.17. ELISA analysis of MMP-9 secretion Conditioned media were collected and MMP-9 concentration determined by ELISA. Mean data (±SEM) are from 6 different patients, normalised to vehicle response. **A.** TPA induces secretion of MMP-9. **B.** SPH causes a significant reduction in MMP-9 secretion, which does not occur in the presence of TM3E3 (AB). **C.** PregS alone causes a significant reduction in MMP-9 secretion, however in the presence of TM3E3 (AB) or peptide-bound TM3E3 (AB+pep), secretion is significantly increased.

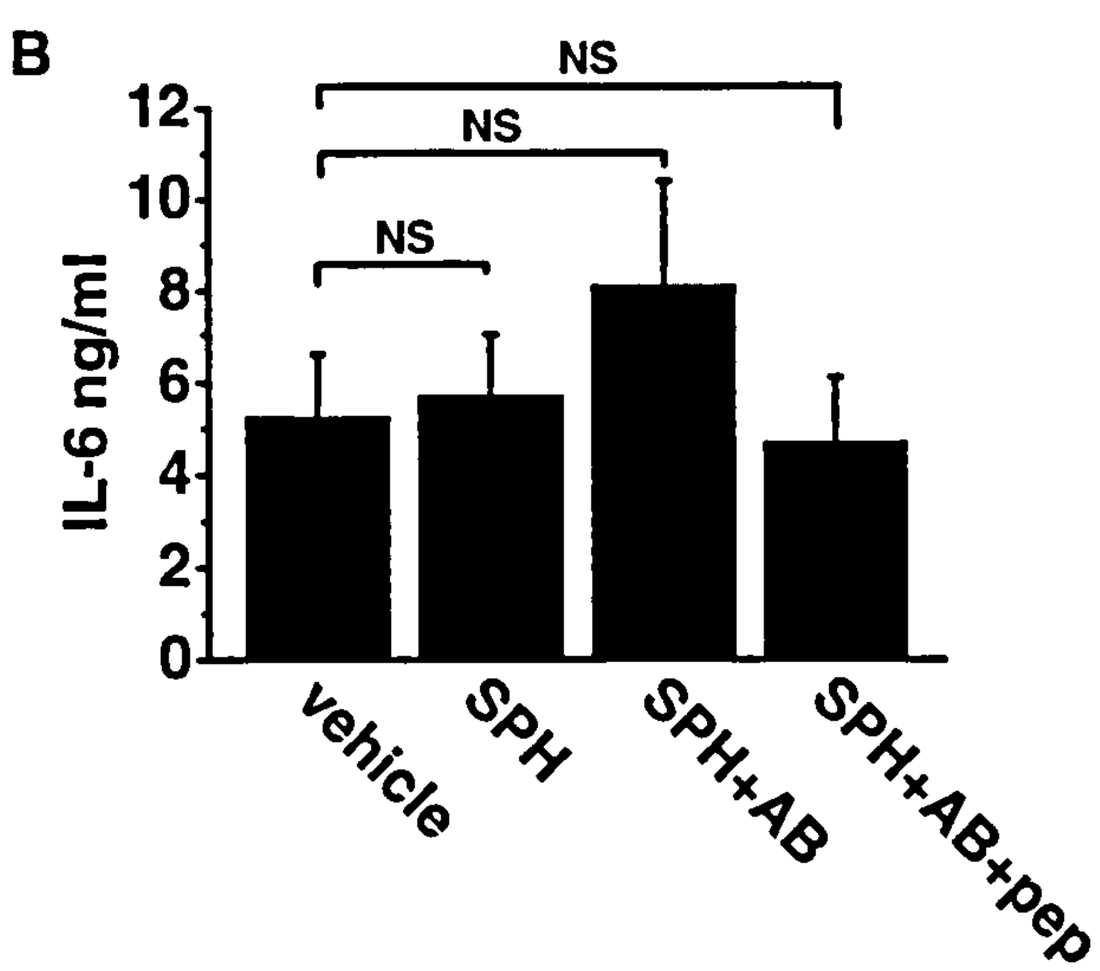

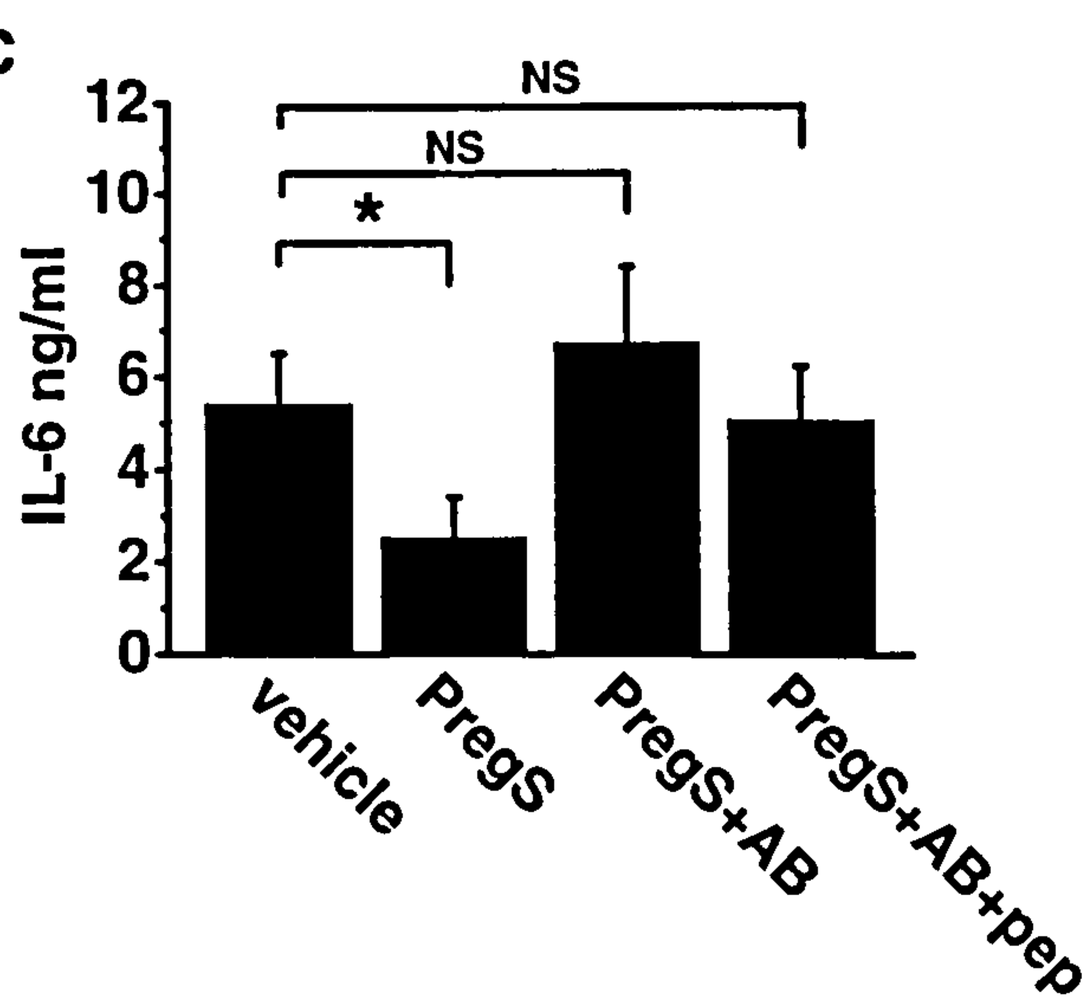

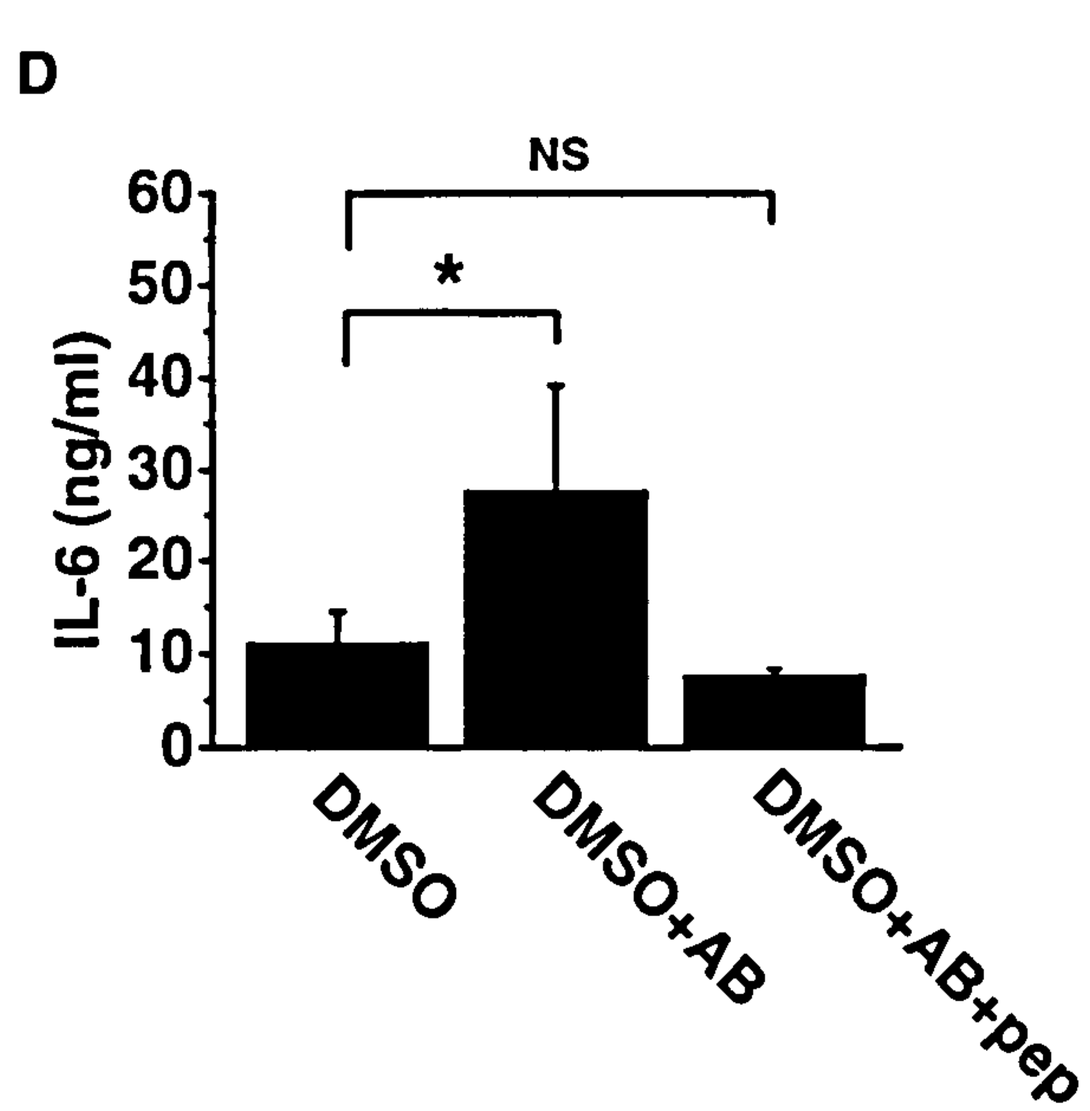

Figure 4.18. ELISA analysis of IL-6 secretion Conditioned media were collected and IL-6 concentration determined by ELISA. Mean data (±SEM) are from 6 different patients. **A.** TPA induces secretion of IL-6. **B.** SPH has no significant effect on IL-6 secretion. **C.** PregS causes a significant reduction in IL-6 secretion, which does not occur in the presence of TM3E3 (AB). **D.** TM3E3 affects IL-6 secretion independently of TRPM3-activation.

Discussion

The data presented in this chapter demonstrate that TM3E3 is valuable for the characterisation of expression and function of native TRPM3, and importantly that TRPM3 is a novel calcium channel of vascular smooth muscle.

TRPM3 activation in HSV SMC

The mechanism of TRPM3 activation in HSV SMC is not yet understood. Gd^{3+} and 2-APB both caused significant inhibition of SPH- and PregS-activation of TRPM3, suggesting that Ca^{2+}-responses in HSV SMC were at least partly due to influx through cation channels (Figures 4.6 & 4.8). TM3E3 inhibition suggests this cation channel is TRPM3 (Figures 4.9 & 4.10). However, the inhibition of TRPM3 responses by Tg-induced store depletion suggests that not all of the SPH- or PregS-induced Ca^{2+} response is due to influx across membrane, and there may be some contribution of store depletion to the activation of TRPM3. This could be investigated further by performing experiments in the absence of extracellular Ca^{2+}. Alternatively, Tg, 2-APB and Gd^{3+} may alter local Ca^{2+} concentrations within the cell, a mechanism which can modulate several Ca^{2+} sensitive TRP channels.

Interestingly, following pre-treatment with Tg the starting baseline in HSV SMC was not altered, unlike the baseline in the stable TRPM3 cell line which was significantly increased (Figure 3.16). Although the evidence appears to suggest there are no endogenous SOC in HSV SMC, this is not the case, as previous reports have confirmed the presence of SOC in VSM (Xu *et al.*, 2001). A more plausible explanation is that there are SOC present, but they have had time to desensitise, or that they are Ca^{2+}-inactivated channels, thus the baseline Ca^{2+} levels have returned to resting levels before recording. A further discrepancy between the native and over-expressed systems is that stores did not contribute to the PregS repsonse in the stable cell line, whereas there is clear inhibition of the PregS response in HSV SMC (Figure 4.8 C). Although further experiments in the absence of extracellular Ca^{2+} are needed to explore this effect, a possible explanation is that in native cells, PregS can activate a channel other than TRPM3, in particular one that is sensitive to Tg. This would also explain why TM3E3

and siRNA inhibit the PregS response to a lesser extent than they do the SPH response (Figure 4.16), suggesting another channel contributes to the response.

Established as an endogenous inhibitor of PKC (Hakomori *et al.*, 1998), SPH is also reported to be an endogenous vasoactive agent, having a vasoconstrictive role in the vasculature. Micromolar concentrations cause concentration dependent contraction of rat mesenteric vessels (Bischoff *et al.*, 2000), and cause contraction of porcine coronary arteries (Murohara *et al.*, 1996). Upregulation of lipids in disease states is common, and in particular the phosphorylated metabolite of SPH, S1P, is known to play a role in the inflammatory response to vascular injury (Siess, 2002). As sphingolipid metabolism is closely regulated, a role for SPH in vascular disease either directly, or related to S1P, cannot be ruled out.

The role of a neurosteroid such as PregS in the vasculature is not well understood, and the case may be that PregS is not a physiologically relevant activator for TRPM3 in HSV SMC, and instead may be relevant in other cell types and tissue that express TRPM3. However, steroids are known to affect vasoconstriction, thus the hormonal regulation of blood pressure by PregS can not be excluded, and further experiments such as contraction studies are required.

Antibodies as tools to determine native ion channel function

E3-targeted antibodies are useful for studies involving live cells as they target an extracellular epitope. Therefore, permeabilisation of cells or a complex intracellular delivery method is not required for inhibitory activity. This proved useful for Ca^{2+} imaging and especially for secretion assays, where native activity of TRPM3 could be examined over a period of several days with no apparent adverse affect on the cells involved.

Members of the TRP family are believed to exist as tetramers. TRPM6 and TRPM7 are known to form heteromers (Chubanov *et al.*, 2004), and the coiled coil domain of TRPM2 is required for the assembly of functional channels, suggesting a common structural motif for TRPM channel assembly (Mei *et al.*, 2006). The sequence similarity with other TRPM family members and the conserved C-terminal coiled coil domain

suggests that TRPM3 could form multiple different channels with different combinations of splice variants or other TRPs, creating more than one type of functional channel. Although the heteromeric structure of TRPM3 may affect its native pharmacology, this chapter demonstrates that TM3E3 can block native TRPM3 channels, regardless of how it exists in native tissues. The same is also true for the E3-targeted anti-TRPC5 antibody, which can inhibit TRPC1-TRPC5 heteromers (Xu *et al.*, 2006b).

Function of TRPM3

Neointimal hyperplasia is initiated in blood vessels as a result of tissue damage caused during bypass grafting, and is dependent on SMC proliferation and migration (Angelini et al., 1989). The movement of SMC is dependent on degradation of basement membranes by matrix metalloproteinase MMP-9 and MMP-2, which are secreted by the SMC themselves in response to vascular damage. The MMP-9 knockout mouse shows decreased SMC migration to the intima, suggesting MMP-9 is necessary for formation of neointima (Cho et al., 2002), and MMP-9 activity is increased during neointima formation in cultured HSV (Porter et al., 1998). Recently statins have been suggested to delay the progression of vein graft failure by decreasing MMP-9 mRNA levels, thus inhibiting MMP-9 secretion (Turner et al., 2005). My own study has suggested a possible role for TRPM3 in MMP-9 secretion, demonstrating that channel activation can reduce MMP-9 secretion (Figures 4.16 & 4.17).

TRPM3 also appears to play a role in IL-6 secretion (Figures 4.19). IL-6 is a proinflammatory cytokine implicated in the development of vascular diseases and present in the arterial atherosclerotic wall (Rus et al., 1996). IL-6 is also upregulated in the neointima following vascular injury (Takaoka et al., 2006). Atherosclerosis is chronic inflammatory process, known to be mediated by the production of inflammatory cytokines such as IL-6, and parallels can be drawn between the SMC pathogenesis of neointimal hyperplasia, suggesting that an agent that delays graft failure may also help in the treatment of atherosclerosis. Neointimal hyperplasia results from both proliferation and migration of the smooth muscle cells, and if TRPM3 regulation of SMC secretion could be directly linked to both of these processes, therapeutic

treatments could be developed. TM3E3 appears to increase secretion independently of TRPM3 activation, perhaps as a result of inhibiting constitutive TRPM3 activity. However, TM3E3 does not increase IL-6 secretion in the presence of SPH (Figure 4.17). This would suggest SPH has a dual effect on TRPM3-regulated secretion. SPH can activate TRPM3 and therefore decrease IL-6 secretion, however it can also prevent the effect of TM3E3, suggesting that a longer exposure to SPH downregulates constitutively active channels. Alternatively, the antibody may have a non-specific effect on secretion. Perhaps the antiserum or the TM3E3 antibody itself can increase IL-6 secretion independently of the TRPM3 channel.

Summary

E3-targeted antibodies will prove useful for further characterisation of endogenous TRPM3 in other cell types and tissues. For the time being, TM3E3 has successfully shown that TRPM3 is a functional Ca^{2+} channel of vascular smooth muscle with a role in regulating secretion. The exact mechanism by which TRPM3 regulates MMP-9 and IL-6 remains to be seen, and may be a result of TRPM3 modulation of signalling pathways by changes in intracellular Ca^{2+}. While the stimulatory effect TM3E3 has on secretion rules out the antibody itself as a therapeutic tool for the treatment of vascular damage, the antibody will serve as a useful tool for further study. Understanding mechanisms of SMC proliferation and migration will enable a therapeutic approach to prevent HSV graft stenosis and perhaps even the development of atherosclerosis.

Chapter 5
Pharmacology of TRPM3

To further realize the importance of the TRPM3 channel and its physiological function, it is necessary to understand fully its pharmacology. As discussed throughout this thesis, existing TRP channel modulators are non-specific and, although they have been used to investigate TRP-mediated function, rarely selective.

The application of high-throughput screening (HTS) has been used by the pharmaceutical industry for drug discovery for 20 years (Pereira *et al.*, 2007). HTS allows for the *in vitro* investigation of large numbers of compounds to identify novel modulators of a biological target or pathway. This may involve screening chemical libraries for activators or inhibitors of a particular receptor or ion channel. Usually fully automated, HTS can generate a large amount of experimental data very quickly. A HTS assay should be considered as a screen of potentially active compounds, and it is vital any positive compounds are followed up with further experimentation and appropriate controls. This will usually involve generation of concentration response data to determine EC_{50} or IC_{50} values, testing compounds under physiological conditions, and demonstrating selectivity for a particular target by cross-testing 'hits' against related targets.

In drug discovery, active compounds identified by a HTS that share structural or chemical features can be studied by chemists and used to generate drugs with increased activity at the designated target, and to enhance the pharmacological activity of said compound as a drug. At this stage pharmokinetics are important, and the adsorption, distribution, metabolism and excretion (ADME) of the drug must be considered.

For the purpose of the study of TRPM3 function, the identification of a complete set of pharmacological tools such as agonists, allosteric modulators, inhibitors and so on would be useful for the further characterisation of the channel. The aim of this chapter was to perform HTS for the TRPM3 ion channel to identify interesting targets for further study. Due to the expression of TRPM3 in HSV SMC, we were particularly interested to find TRPM3 modulators with potential vascular relevance.

Known TRP channel modulators as regulators of TRPM3

Mechanisms of TRP channel activation are diverse. Often, structurally related compounds will have similar effects on a particular ion channel, and may even also modulate related channels. For this reason, known TRP modulators were examined for an effect on TRPM3.

Sphingosine (SPH) is known to activate TRPM3 (Grimm *et al.*, 2005). SPH-related compounds including ceramide, glucosylsphingosine (psychosine), sphingosine-1-phosphate (S1P) and the upstream metabolite palmitoyl Coenzyme A, plus a naturally occurring mixture of varying chain length SPH (bovine SPH), were screened for TRPM3 modulation using FlexStation fluorimetry. In addition, the known TRP modulators 4αPDD, L-α-lysophosphatidylcholine (LPC), L-α-lysophosphatidylinositol (LPI), gadolinium (Gd^{3+}), carbachol (CCh) and hydrogen peroxide (H_2O_2) were also tested. A 2 addition protocol was adopted, which comprised a 1st addition of the test compound, followed by a 2nd addition of PregS (10 μM) as a positive control and to search for channel inhibitors.

There was no significant difference between Ca^{2+} responses in tet- and tet+ TRPM3 cells, suggesting none of the compounds can activate TRPM3 (Figure 5.1 A). However, several of the compounds inhibited or potentiated the Ca^{2+} response to PregS (Figure 5.1 B).

In summary, TRPM3 is not activated by SPH-related compounds, despite structural similarities, although S1P can inhibit the PregS-response. In addition, TRPM3 is inhibited by 4αPDD and H_2O_2, compounds which are known to activate TRP family members TRPV4 and TRPM2 respectively (Hara *et al.*, 2002; Watanabe *et al.*, 2002). PregS responses were potentiated by the known TRPC5 activators LPC and LPI (Flemming *et al.*, 2006). TRPM3 was also inhibited by the recognised TRP blocker Gd^{3+}, consistent with previous reports (Grimm *et al.*, 2003; Lee *et al.*, 2003a). The data demonstrate that TRPM3 can be affected by existing physiological TRP modulators.

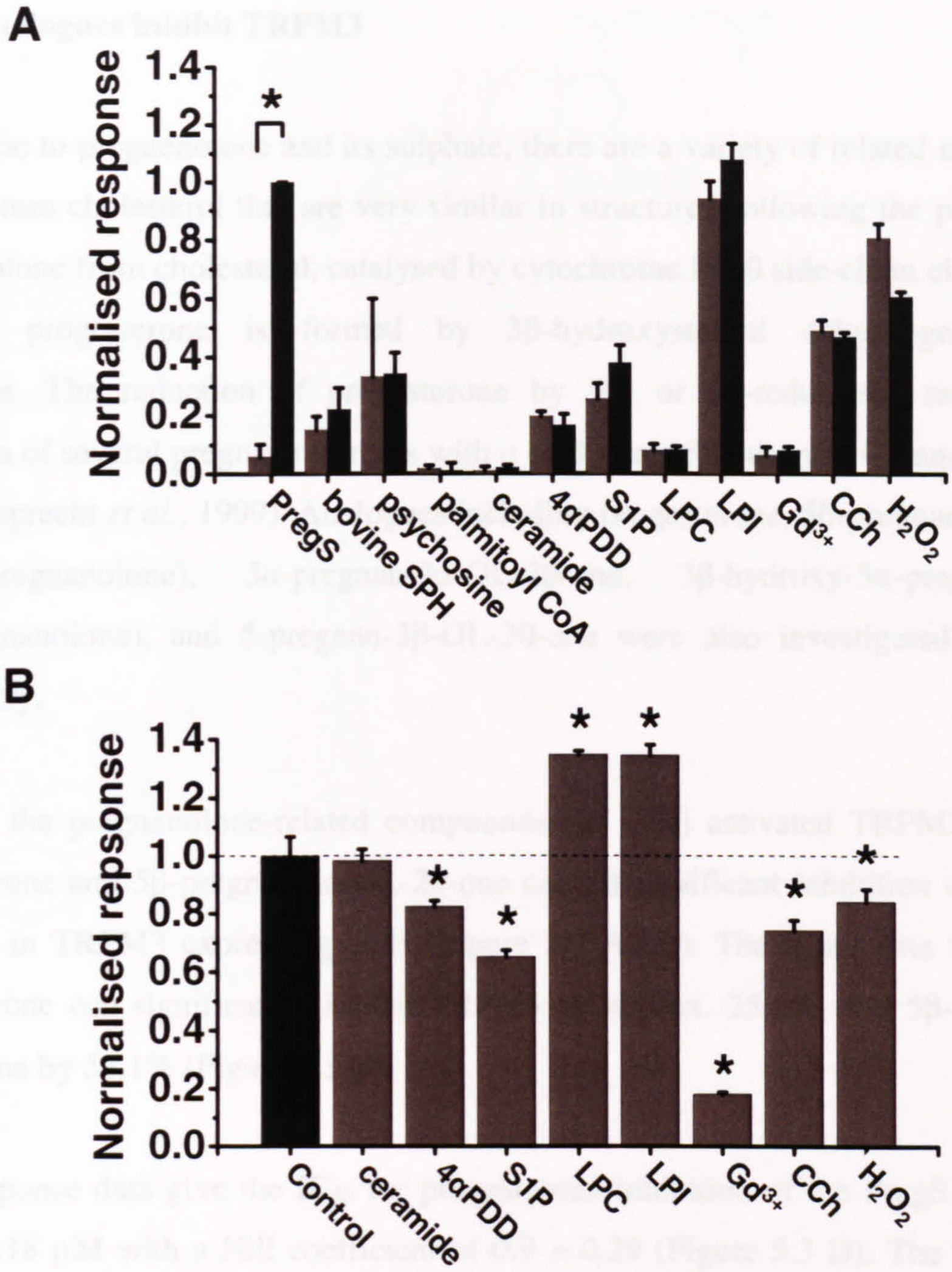

Figure 5.1. Effect of TRP channel modulators on TRPM3 FlexStation screen performed at RT. Cells were induced by incubation with tetracycline (tet+), non-induced cells (tet-) were included as a control. **A.** Mean data (±SEM) from 3 independent experiments shows activation in tet+ (black) compared to tet- (grey) cells (n/N=3/9). **B.** Inhibition of PregS response 1 min after PregS application (n/N=3/9). Control refers to 1st application of vehicle (DMSO), followed by PregS addition. Data are normalised to control PregS response. Significance from control determined using Student's t test, *$p<0.05$.

PregS analogues inhibit TRPM3

In addition to pregnenolone and its sulphate, there are a variety of related neurosteroids formed from cholesterol that are very similar in structure. Following the production of pregnenolone from cholesterol, catalysed by cytochrome P450 side-chain cleavage (scc) enzyme, progesterone is formed by 3β-hydroxysteroid dehydrogenase/Δ5-Δ4-isomerase. The reduction of progesterone by 5α- or 5β-reductases results in the formation of several pregnane steroids with α or β stereochemistry at C3 and C5 (Figure 5.2) (Rupprecht *et al.*, 1999). Analogues including progesterone, 5β-pregnan-3α-OL-20-one (pregnanolone), 5α-pregnan-3α-OL-20-one, 3β-hydroxy-5α-pregnan-20-one (allopregnanolone), and 5-pregnan-3β-OL-20-one were also investigated using Ca^{2+} fluorimetry.

None of the pregnenolone-related compounds (25 μM) activated TRPM3. However, progesterone and 5β-pregnan-3α-OL-20-one caused significant inhibition of the PregS response in TRPM3 expressing cells (Figure 5.3 A&B). The mean data indicate that progesterone can significantly inhibit TRPM3 by approx. 25.6%, and 5β-pregnan-3α-OL-20-one by 54.1% (Figure 5.3 C).

Dose response data give the IC_{50} for progesterone inhibition of the PregS response as 35.5 ± 9.18 μM with a Hill coefficient of 0.9 ± 0.29 (Figure 5.3 D). The IC_{50} for 5β-pregnan-3α-OL-20-one inhibition of the PregS response was 11.9 ± 3.28 μM with a Hill coefficient of 0.9 ± 0.18 (Figure 5.3 E).

The data indicate that converse to the effect of PregS, some pregnenolone-related neurosteroids have an inhibitory effect on the TRPM3 channel.

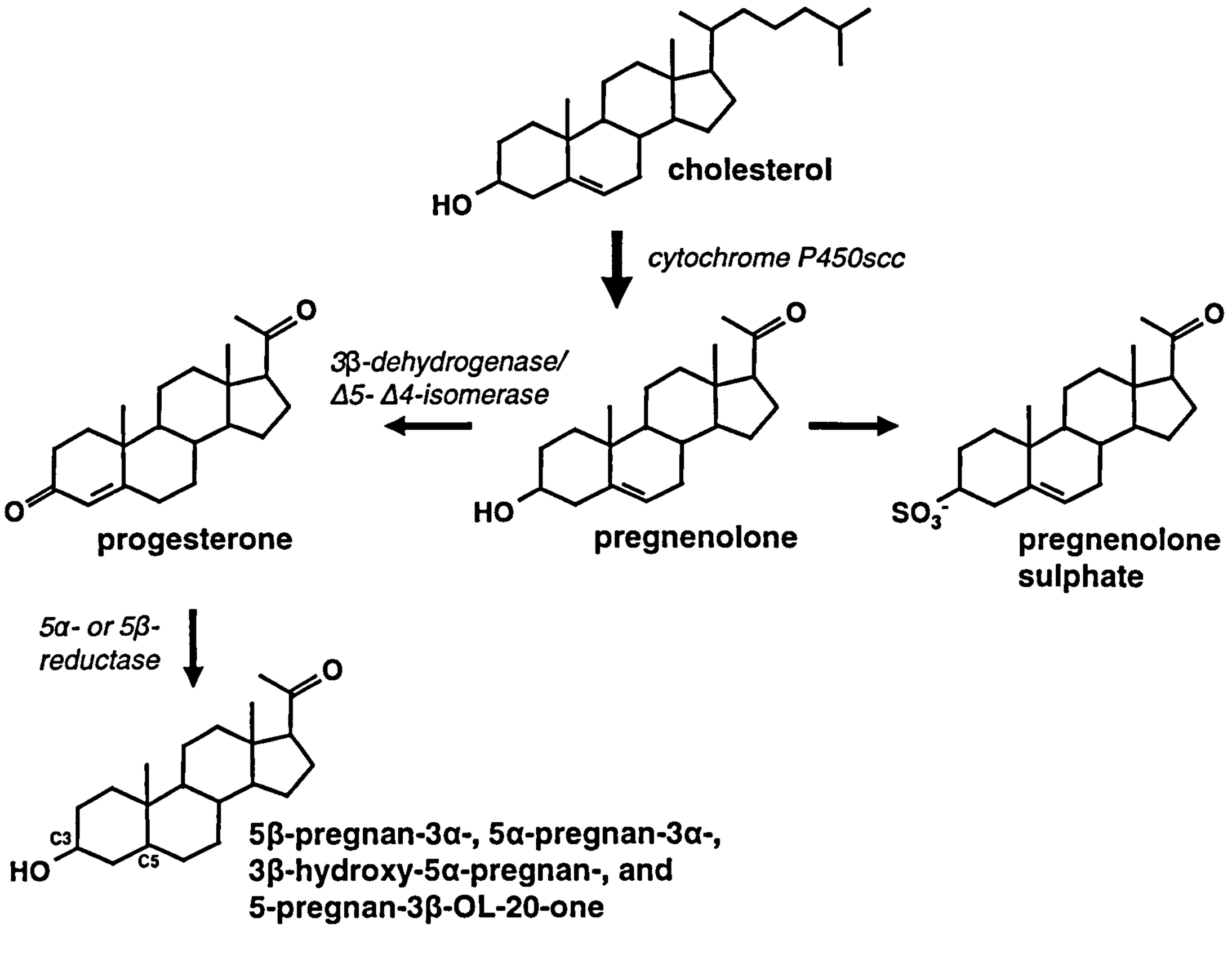

Figure 5.2. Biosynthesis of neuroactive steroids Shown are the chemical structures of cholesterol and common neurosteroids, plus the enzymes that catalyse their formation. Pregnane steroids produced by 5α- or 5β-reductases are diverse due to α or β stereochemistry at positions C3 and C5.

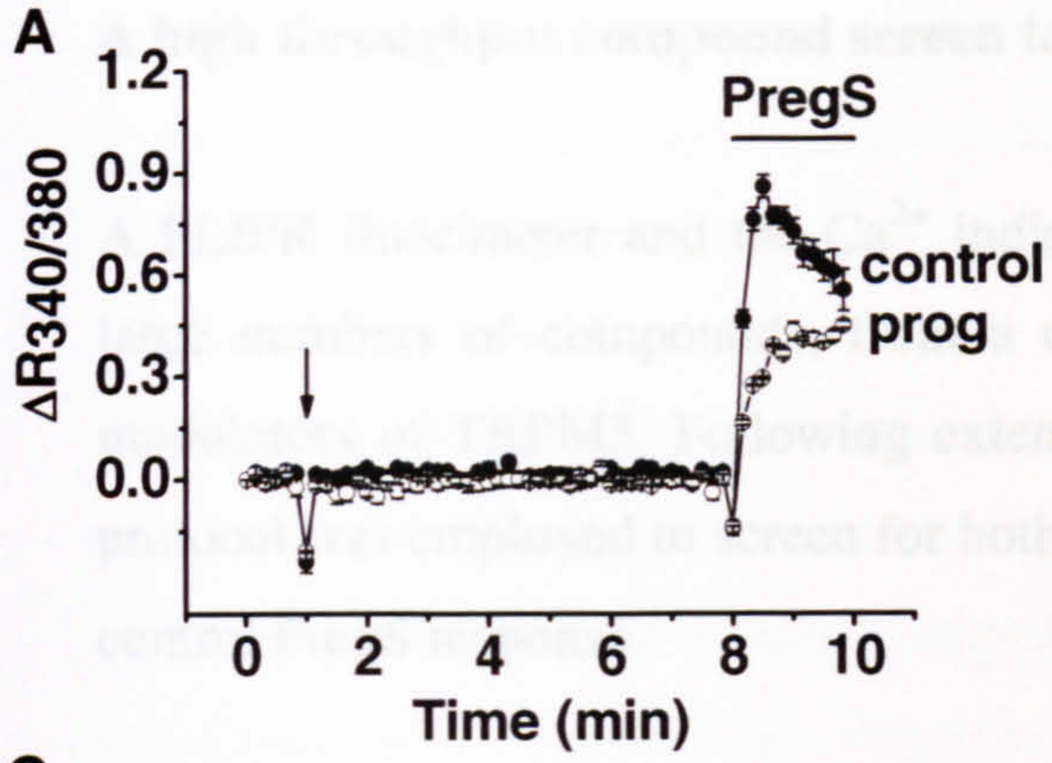

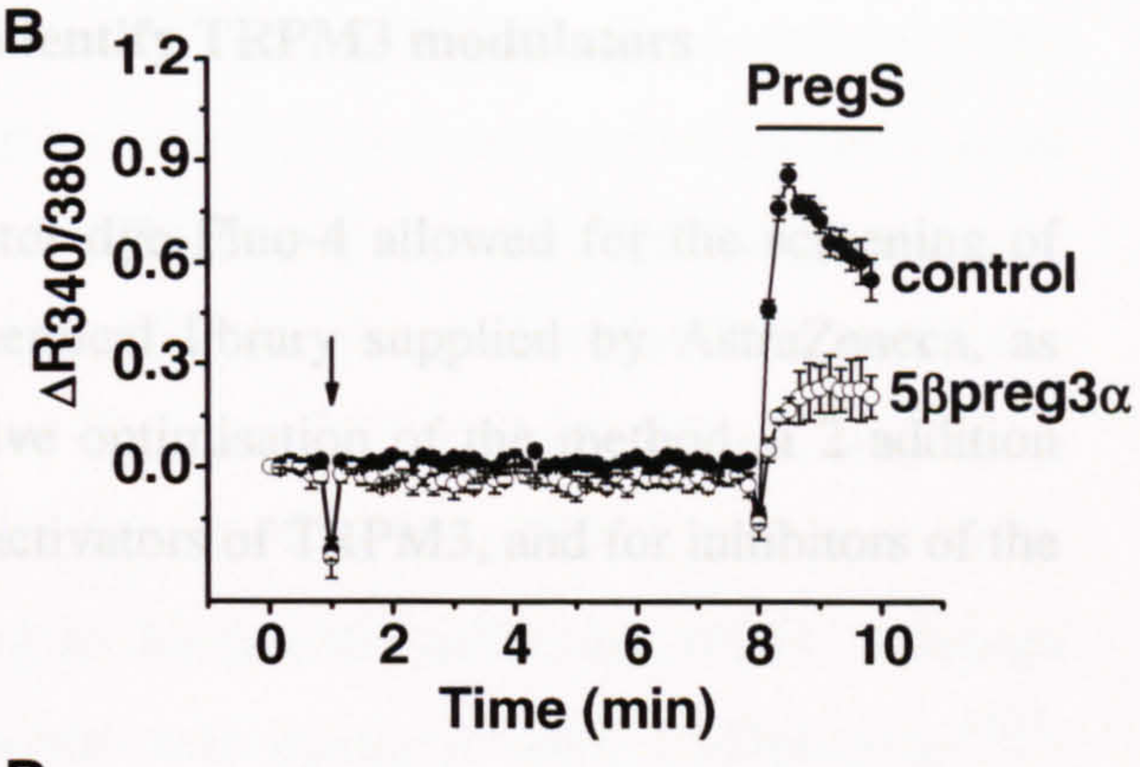

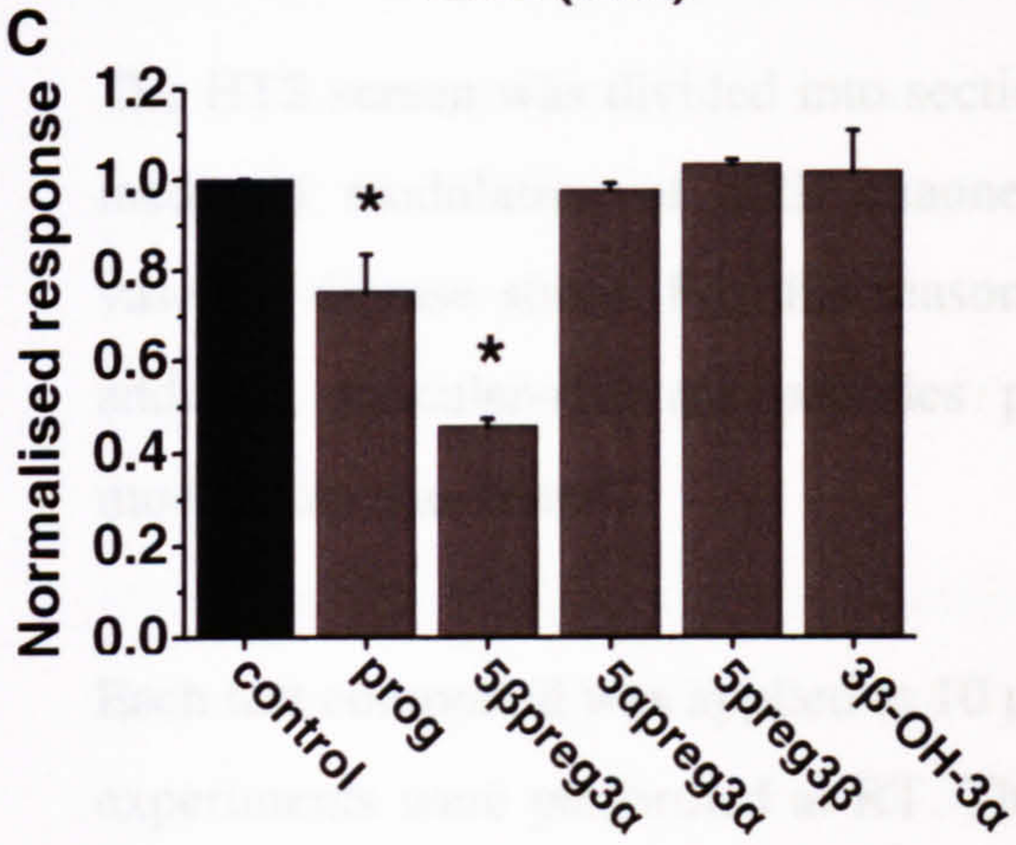

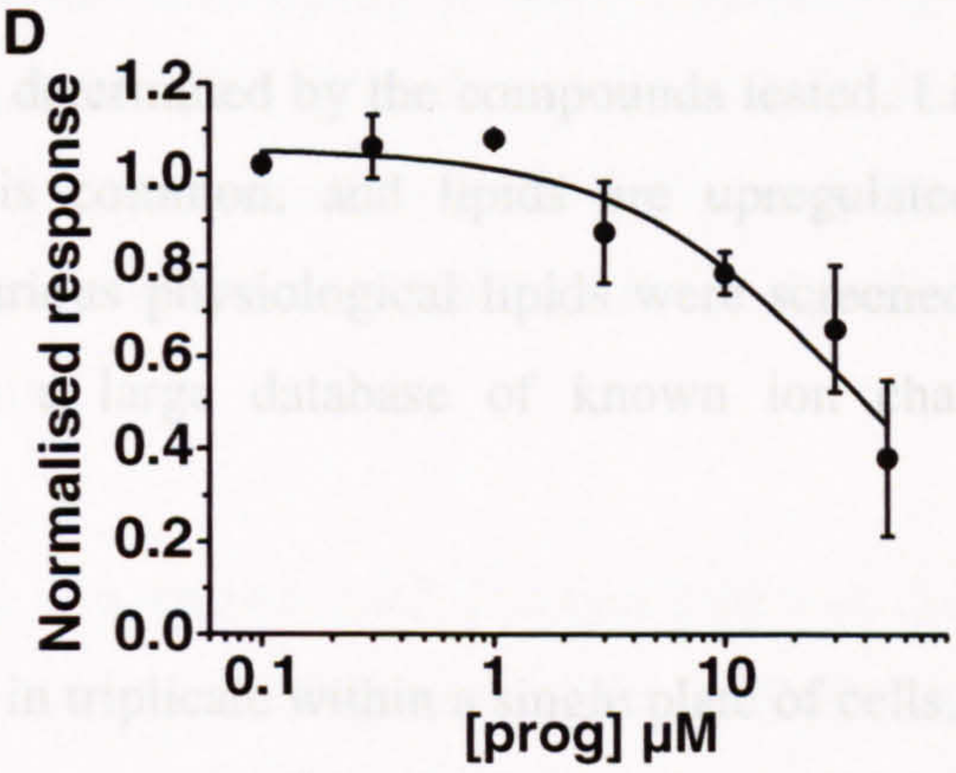

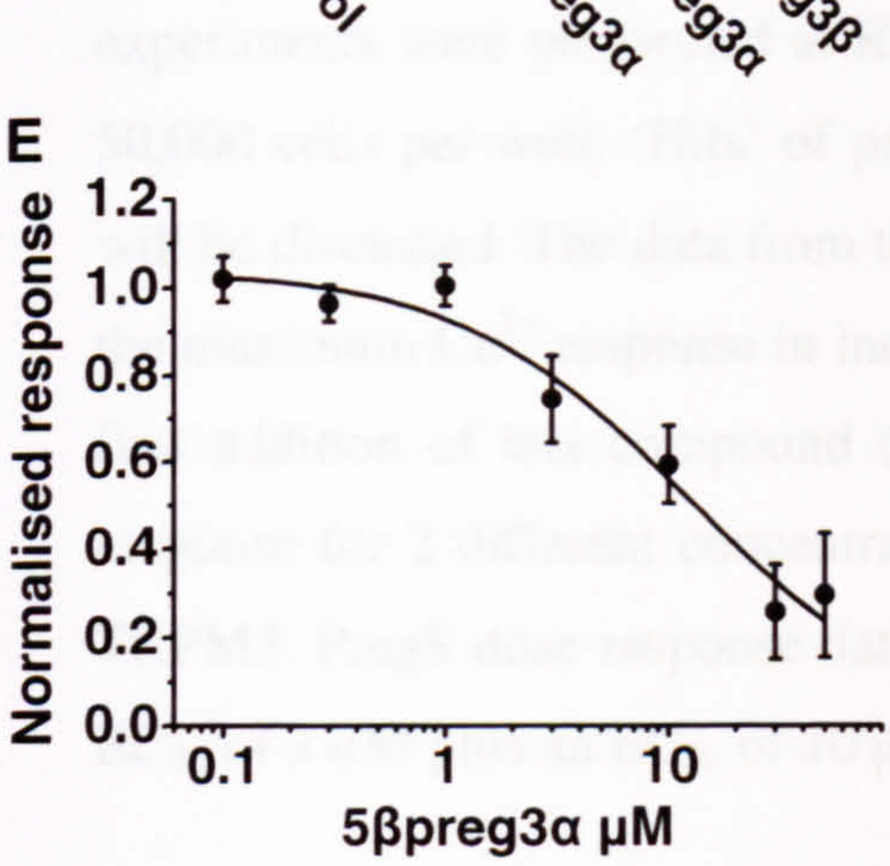

Figure 5.3. Effect of PregS-analogues on TRPM3-expressing cells Ca^{2+} signals were measured as the 340/380 ratio of emission in fura-2 loaded cells. DMSO (vehicle) was present throughout recordings, which were performed at RT. 1st addition of test compound or control at 1 min (arrow), followed by 2nd addition of PregS at 8 min. Traces are mean data (±SEM) from 3 wells within a single plate, and show inhibition of the PregS response by **A.** progesterone (prog) and **B.** 5β-pregnan-3α-OL-20-one (5βpreg3α). **C.** Mean data (±SEM) showing inhibition 1 min after PregS application (control n/N=3/18, test n/N=3/9). Data are normalised to control (1st application of vehicle (DMSO), followed by PregS addition). **D.** Mean dose response data (±SEM) normalised to control PregS response, show inhibition of the PregS response by prog (n/N=3/9), and **E.** 5βpreg3α (n/N=3/9).

A high throughput compound screen to identify TRPM3 modulators

A FLIPR fluorimeter and the Ca^{2+} indicator dye Fluo-4 allowed for the screening of large numbers of compounds, from a chemical library supplied by AstraZeneca, as modulators of TRPM3. Following extensive optimisation of the method, a 2 addition protocol was employed to screen for both activators of TRPM3, and for inhibitors of the control PregS response.

The HTS screen was divided into sections determined by the compounds tested. Lipid-mediated modulation of TRP channels is common, and lipids are upregulated in vascular disease states. For this reason various physiological lipids were screened. In addition, vascular-relevant peptides plus a large database of known ion channel modulators was tested.

Each test compound was applied at 10 μM in triplicate within a single plate of cells, and experiments were performed at RT. The number of cells per well was kept constant at 50,000 cells per well. 'Hits' of particular interest were subjected to further analysis as will be discussed. The data from the compound screen are presented as a comparison of the maximum Ca^{2+} response in induced (tet+) and non-induced cells (tet-) following the first addition of test compound (10 μM), or as inhibition of the control PregS Ca^{2+} response for 2 different concentrations, the EC_{20} and the EC_{80} for PregS activation of TRPM3. PregS dose response data were determined prior to experiments, and gave an EC_{20} of 3 μM plus an EC_{80} of 10 μM.

The peptide screen failed to identify any compounds with a convincing effect on TRPM3, although there was a significant but small inhibitory effect of Arg-vasopressin, bombesin and neurotensin on the PregS-response (Figure 5.4). Several of the screened lipids gave small but significant activation of TRPM3, including SPH-related compounds DHS and safingol, plus the alky lysophospholid ET-18-OCH_3, methanandamide (mAEA), α-lipoic acid, palmitic acid, thromboxane B2 (TX B2), the thromboxane A2 antagonist U-46619, the prostaglandin E2 antagonist AH6809 and several dihydroxyeicosatetraenoic acids (DiHETEs) (Figure 5.6, 5.8 & 5.10). Convincing lipid activators of TRPM3 causing an increase in the fluorescence signal that was greater than 500 ΔRFU included hepoxillin A3 and β-cyclodextrin (Figure 9).

Lipids appeared much more effective at inhibiting the PregS response. The phospholipid phosphatidylinositol-4,5-bisphosphate (PIP_2), known to modulate several TRP channels and reported to activate the TRPM family member TRPM8 (Liu *et al.*, 2005), caused significant inhibition of the PregS response at both the EC_{20} and EC_{80} (Figure 5.5). Other lipids that also inhibited both the EC_{20} and EC_{80} PregS responses included SPH, ET-18-OCH3 and carbocyclic thromboxane A2 (CTX A2) (Figure 5.6 & 5.8). Prostaglandins as a whole appeared to have little inhibitory effect, although significant inhibition of the PregS response was apparent with 15-Deoxy-Δ-^{12,14}-prostaglandin J_2 (15d-PG J2) and prostaglandin K1 (PG K1) (Figure 5.8). Platelet activating factor (PAF)-16 plus related the compounds lyso PAF-16 and PAF-16 antagonist all inhibited TRPM3, while PAF-18 and lyso PAF-18 significantly potentiated the PregS response (Figure 5.10).

In the screen for ion channel modulators, the known TRP channel inhibitor 2-APB served as a useful positive control to demonstrate inhibition of the TRPM3 PregS-response (Figure 5.11). A further TRP channel inhibitor SKF 96365, reported to be ineffective at inhibiting TRPM3 (Grimm *et al.*, 2003), caused a significant inhibition of the PregS-response (Figure 5.17). Ruthenium red (RR), an established blocker of TRPV and TRPM channels, showed potent inhibition of the PregS response (Figure 5.14), while clotrimazole, a potent TRPM2 inhibitor, potentiated the PregS response (Figure 5.12). The TRPV1 activators anandamide (AEA) and capsaicin significantly inhibited TRPM3 (Figure 5.11 & 5.14), however arachadonic acid (AA) had no effect (Figure 5.10). Menthol, an activator of TRPM8, had no effect on TRPM3 (Figure 5.14).

Of all the known ion channel modulators screened, only nifedipine significantly activated TRPM3 (Figure 5.15 A). Related dihydropyridine L-type voltage-gated calcium channel blockers including nitrendipine, nicardipine, nimodipine, and the T-type blocker mibefradil did not activate, and instead inhibited TRPM3 (Figure 5.15). Conversely nifedipine appeared to potentiate the PregS response, as did felodipine (Figure 5.13). Established calcium channel blockers including the benzothiazepine diltiazem, and the phenylalkylamines verapamil and gallopamil had no effect on TRPM3 (Figure 5.13, 5.14 & 5.17).

The typical antipsychotics chlorpromazine (CPZ) and thioridazine, both of which are phenothiazines, plus haloperidol (a butyrophenone) and fluspirilene (a

diphenylbutylpiperidine), all inhibited the PregS response. The atypical benzamide antipsychotic sulpiride had no effect (Figure 5.20). Diphenhydramine hydrochloride (DPHA), commonly recognized by its trade name Benadryl, which can be used to treat side effects experienced with typical antipsychotics, also inhibited TRPM3 (Figure 5.16).

Antidepressants also inhibited the PregS response, regardless of their type. The selective serotonin reuptake inhibitors (SSRI) citalopram and fluoxetine, plus the tricyclic antidepressants (TCA) imipramine, nortriptyline, doxepin and amitriptyline, all inhibited TRPM3 (Figure 5.11-5.15). However, the SSRI fluoxamine, and venalfaxine, a serotonin-norepinephrine reuptake inhibitor (SNRI), did not inhibit TRPM3 activity (Figure 5.13 & 5.17).

Amino-amide type local anaesthetics mepivacaine, lidocaine and bupivacaine and benzocaine potentiate the PregS response, but quaternary derivatives of lidocaine, the membrane impermeant QX314 and QX222, had no effect. (Figure 5.11, 5.14 & 5.16).

Disodium 4,4'-diisothiocyanatostilbene-2,2'-disulfonate (DIDS) is a cross-linking reagent with isothiocyanate groups known to block TRPC4β (Walker *et al.*, 2002), inhibited the PregS response (Figure 5.12). Loperamide, a derivative of piperadine and an opoid receptor agonist, inhibited the PregS response (Figure 5.14), and the anti-anginal agents bepridil hydrochloride and perhexiline maleate significantly inhibited both EC_{20} and EC_{80} PregS response (Figure 5.11 & 5.16), as did the alkoid papaverine hydrochloride (Figure 5.16). The anti-arrhythmic agents mexiletene and amidarone, plus the PKC inhibitor Bisindolylmaleimide I (BIM I) and the K^+ channel blocker CP 339818, were also effective inhibitors (Figure 5.11, 5.12 & 5.15). N-acetylprocainamide (NAPA), also an anti-arrhythmic drug, had a dual effect on the channel and potentiated the EC_{20} but inhibited the EC_{80} PregS response; however its parent compound procainamide had no effect (Figure 5.15 & 5.16). The CaM antagonists calmidazolium chloride (CMZ) and N-(6-Aminohexyl)-5-chloro-1-naphthalenesulfonamide (W-7) inhibited the TRPM3 PregS response (Figure 5.12 & 5.15).

In summary, HTS is a useful method for identifying ion channel modulators of potential interest for further study.

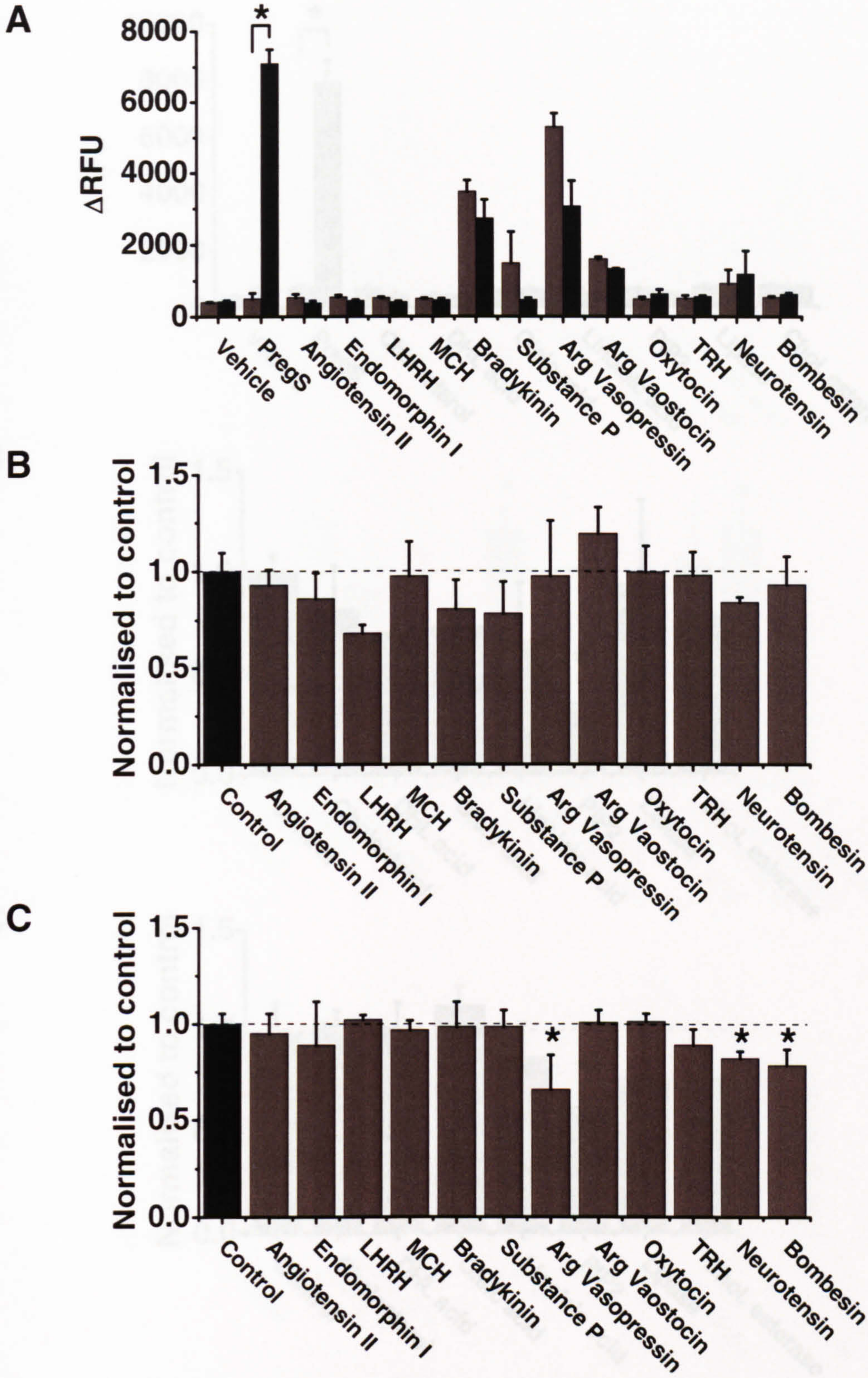

Figure 5.4. Peptide screen Figure 5.6. Lipid screen FLIPR compound screen performed at RT. Changes in Ca^{2+} were measured as relative fluorescence units (RFU) in fluo-4 loaded tet+ cells. DMSO (vehicle) was present throughout recordings. Mean data (±SEM) from 3 wells within a single plate, normalised to control PregS response, show: **A.** Activation in tet+ (black) compared to tet- (grey) cells, **B.** Inhibition of PregS response at EC_{20}, and **C.** Inhibition of PregS response at EC_{80}.

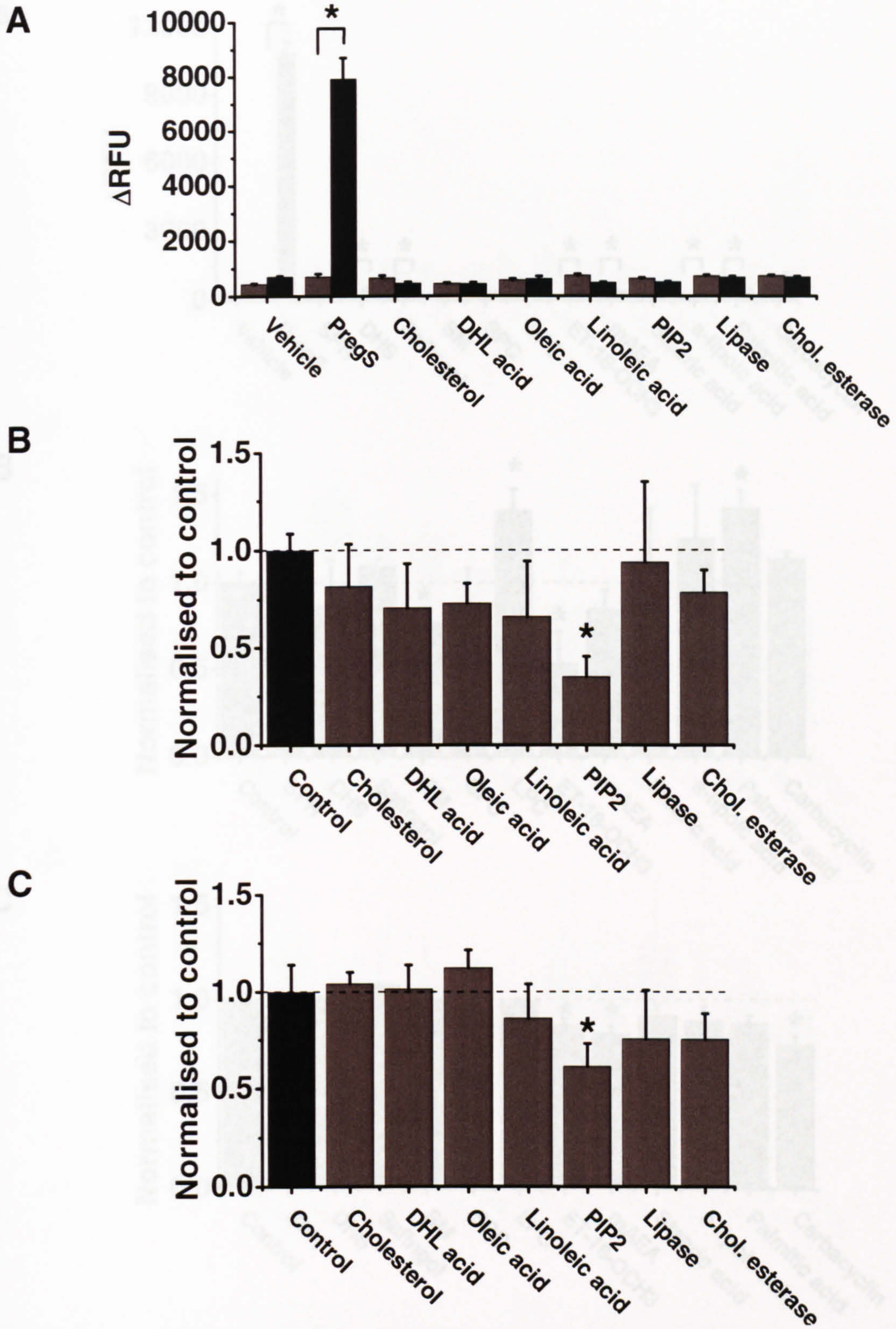

Figure 5.5. Lipid screen Figure 5.6. Lipid screen FLIPR compound screen performed at RT. Changes in Ca^{2+} were measured as relative fluorescence units (RFU) in fluo-4 loaded tet+ cells. DMSO (vehicle) was present throughout recordings. Mean data (±SEM) from 3 wells within a single plate, normalised to control PregS response, show: **A.** Activation in tet+ (black) compared to tet- (grey) cells, **B.** Inhibition of PregS response at EC_{20}, and **C.** Inhibition of PregS response at EC_{80}.

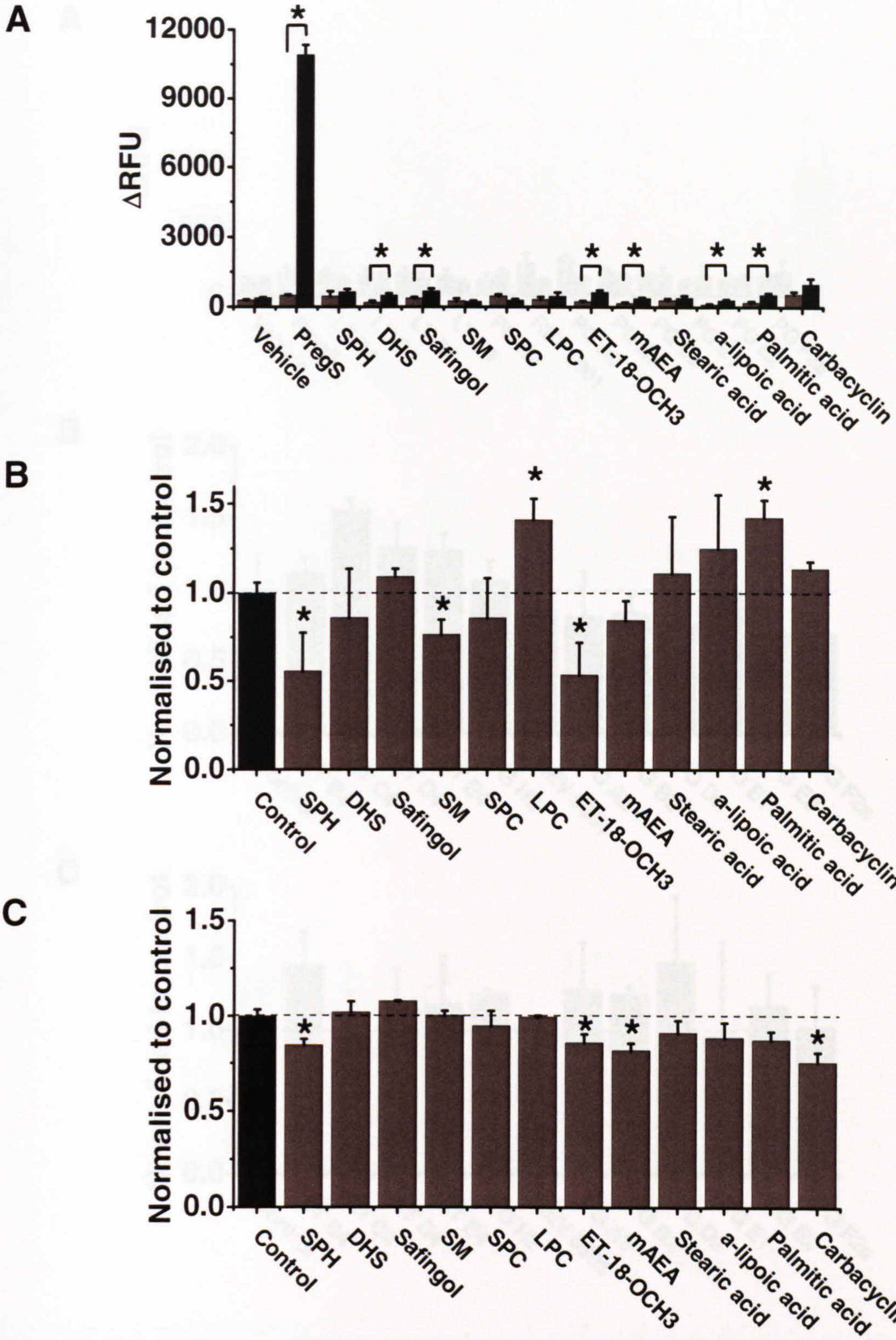

Figure 5.6. Lipid screen FLIPR compound screen performed at RT. Changes in Ca^{2+} were measured as relative fluorescence units (RFU) in fluo-4 loaded tet+ cells. Ethanol (vehicle) was present throughout recordings. Mean data (±SEM) from 3 wells within a single plate, normalised to control PregS response, show: **A.** Activation in tet+ (black) compared to tet- (grey) cells, **B.** Inhibition of PregS response at EC_{20}, and **C.** Inhibition of PregS response at EC_{80}.

Figure 5.7. Lipid screen FLIPR compound screen performed at RT. Changes in Ca^{2+} were measured as relative fluorescence units (RFU) in fluo-4 loaded tet+ cells. Ethanol (vehicle) was present throughout recordings. Mean data (±SEM) from 3 wells within a single plate, normalised to control PregS response, show: **A.** Activation in tet+ (black) compared to tet- (grey) cells, **B.** Inhibition of PregS response at EC_{20}, and **C.** Inhibition of PregS response at EC_{80}.

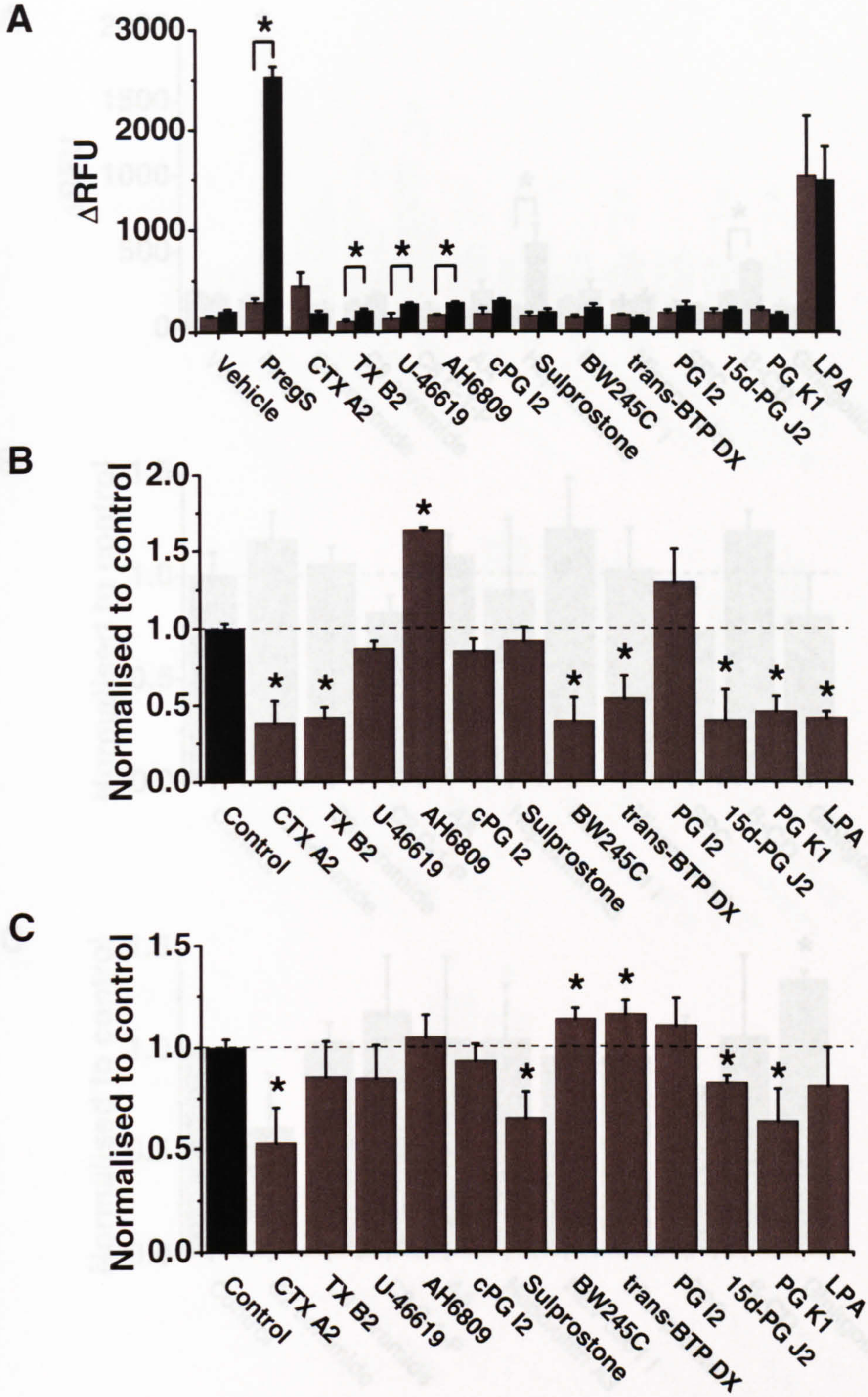

Figure 5.8. Lipid screen FLIPR compound screen performed at RT. Changes in Ca^{2+} were measured as relative fluorescence units (RFU) in fluo-4 loaded tet+ cells. Ethanol (vehicle) was present throughout recordings. Mean data (±SEM) from 3 wells within a single plate, normalised to control PregS response, show: **A.** Activation in tet+ (black) compared to tet- (grey) cells, **B.** Inhibition of PregS response at EC_{20}, and **C.** Inhibition of PregS response at EC_{80}.

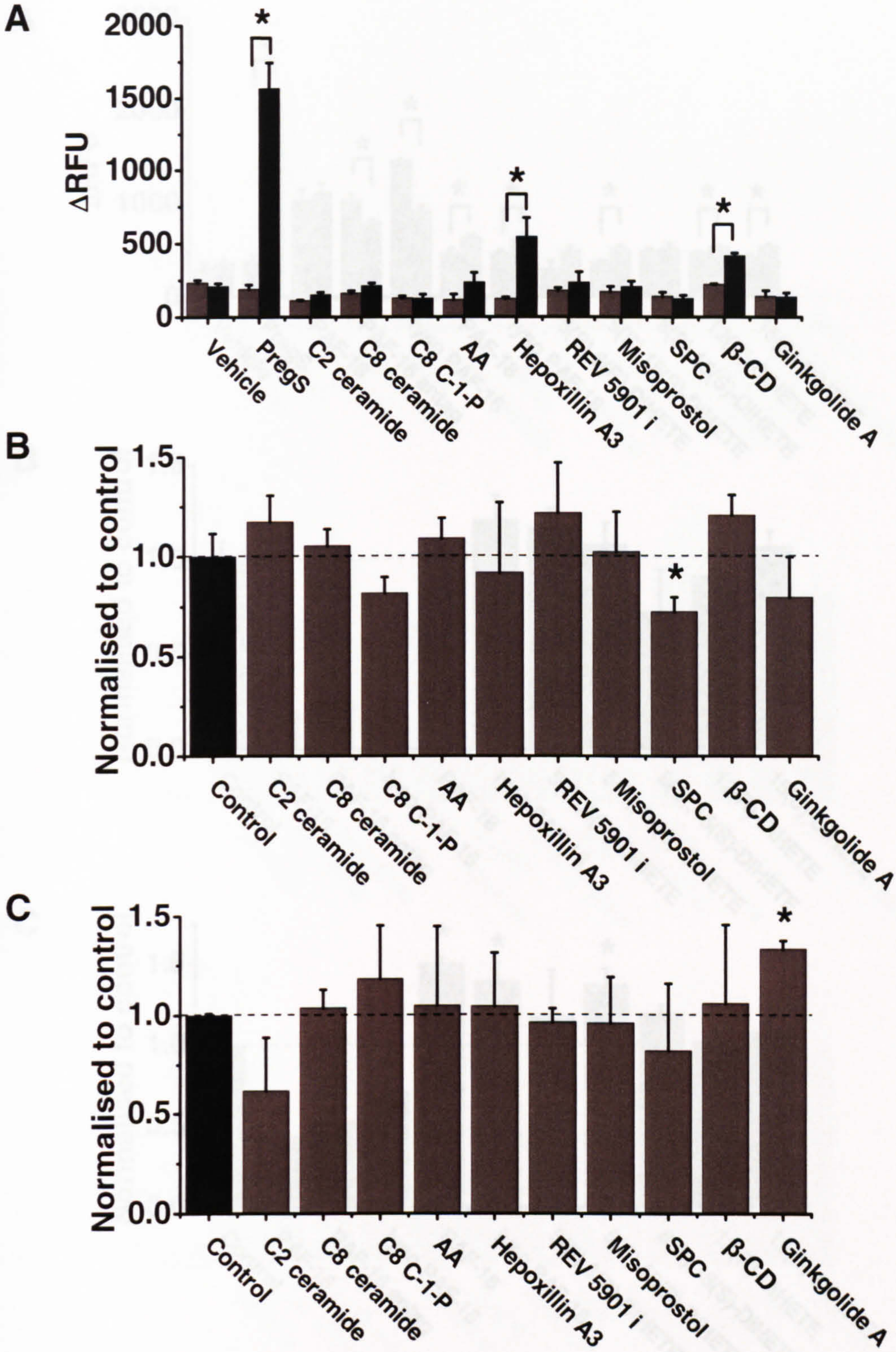

Figure 5.9. Lipid screen FLIPR compound screen performed at RT. Changes in Ca^{2+} were measured as relative fluorescence units (RFU) in fluo-4 loaded tet+ cells. Ethanol (vehicle) was present throughout recordings. Mean data (±SEM) from 3 wells within a single plate, normalised to control PregS response, show: **A.** Activation in tet+ (black) compared to tet- (grey) cells, **B.** Inhibition of PregS response at EC_{20}, and **C.** Inhibition of PregS response at EC_{80}.

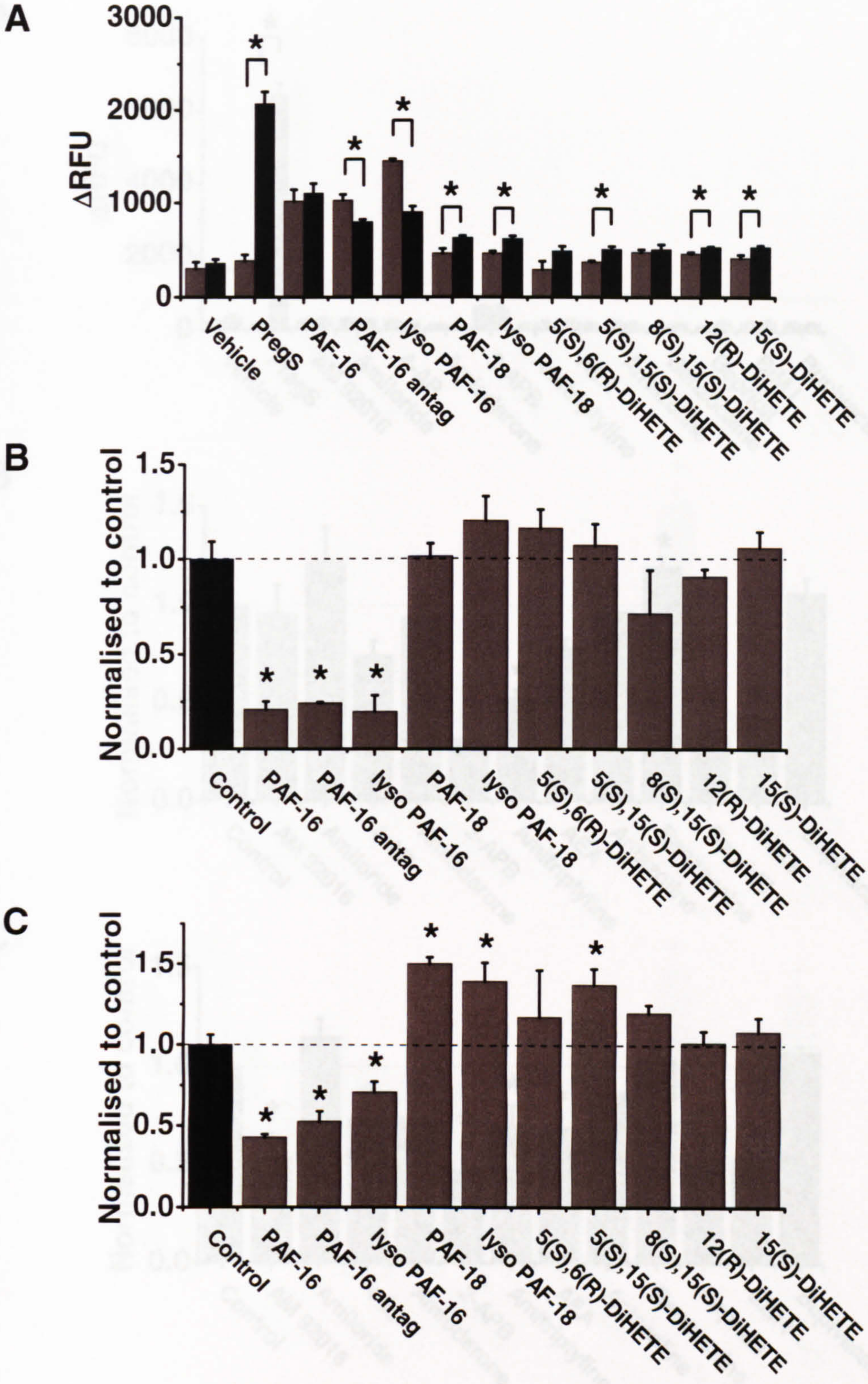

Figure 5.10. Lipid screen FLIPR compound screen performed at RT. Changes in Ca^{2+} were measured as relative fluorescence units (RFU) in fluo-4 loaded tet+ cells. Ethanol (vehicle) was present throughout recordings. Mean data (±SEM) from 3 wells within a single plate, normalised to control PregS response, show: **A.** Activation in tet+ (black) compared to tet- (grey) cells, **B.** Inhibition of PregS response at EC_{20}, and **C.** Inhibition of PregS response at EC_{80}.

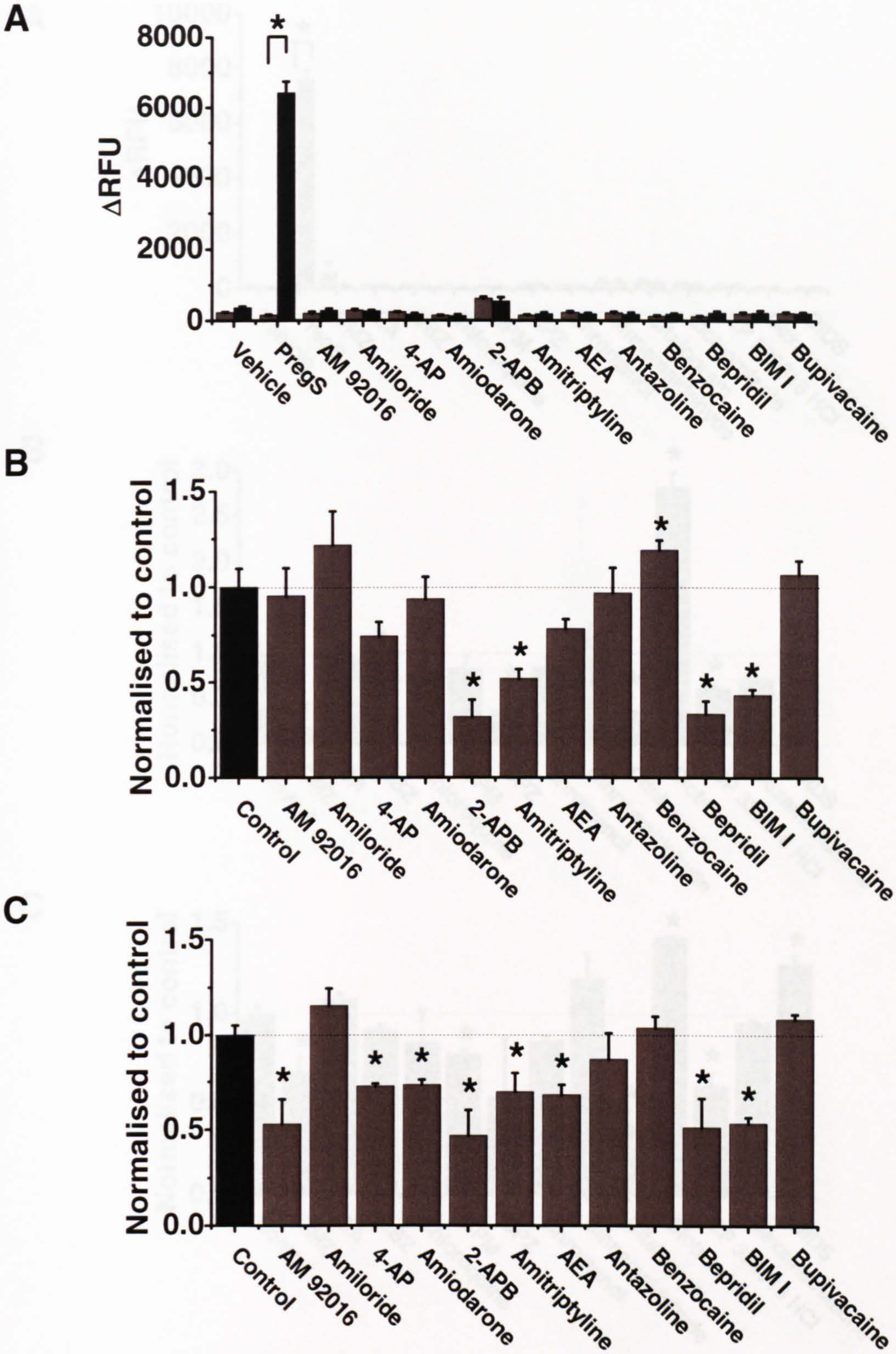

Figure 5.11. Ion channel modulators FLIPR compound screen performed at RT. Changes in Ca^{2+} were measured as relative fluorescence units (RFU) in fluo-4 loaded tet+ cells. DMSO (vehicle) was present throughout recordings. Mean data (±SEM) from 3 wells within a single plate, normalised to control PregS response, show: **A.** Activation in tet+ (black) compared to tet- (grey) cells, **B.** Inhibition of PregS response at EC_{20}, and **C.** Inhibition of PregS response at EC_{80}.

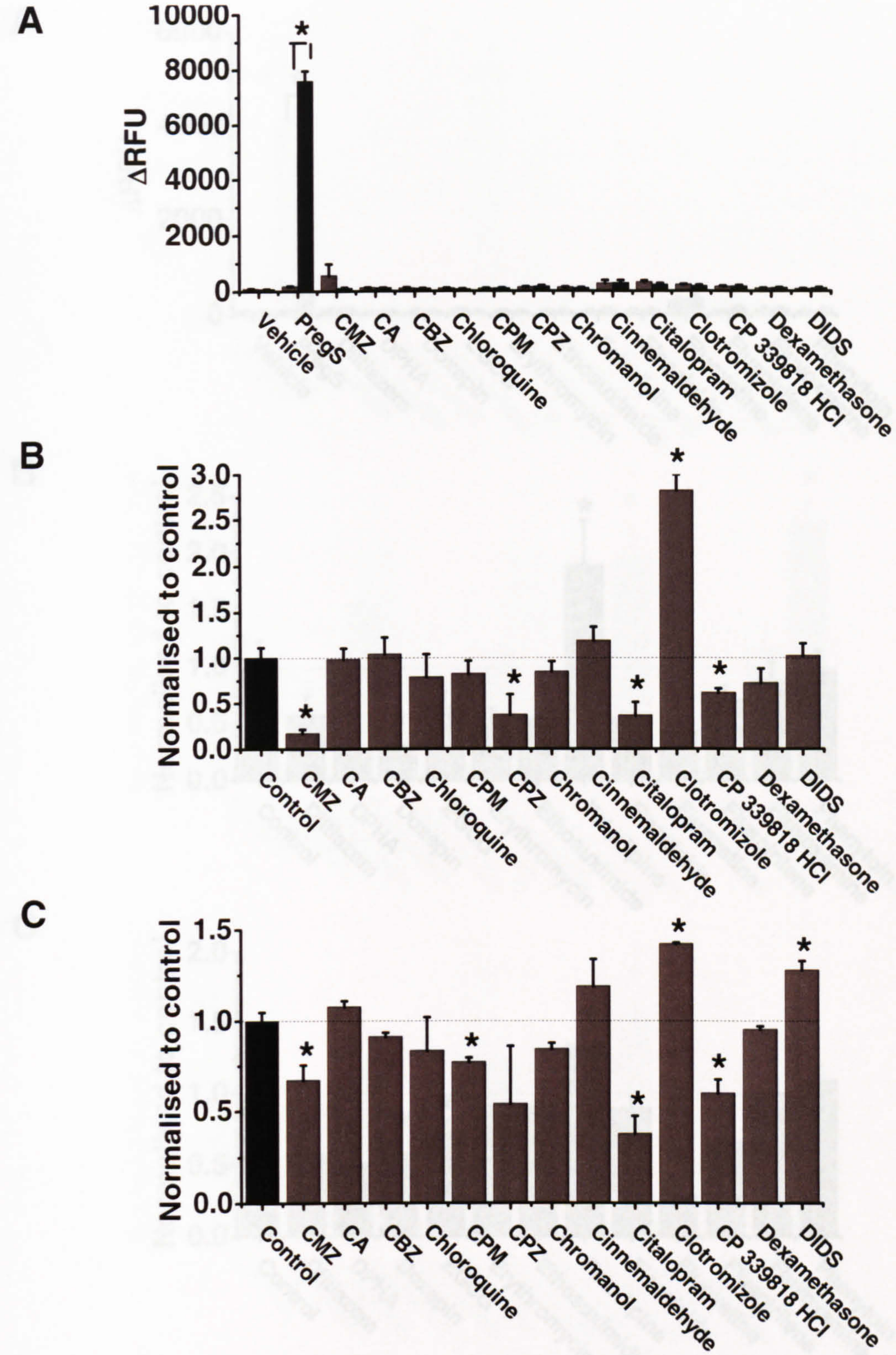

Figure 5.12. Ion channel modulators FLIPR compound screen performed at RT. Changes in Ca^{2+} were measured as relative fluorescence units (RFU) in fluo-4 loaded tet+ cells. DMSO (vehicle) was present throughout recordings. Mean data (±SEM) from 3 wells within a single plate, normalised to control PregS response, show: **A.** Activation in tet+ (black) compared to tet- (grey) cells, **B.** Inhibition of PregS response at EC_{20}, and **C.** Inhibition of PregS response at EC_{80}.

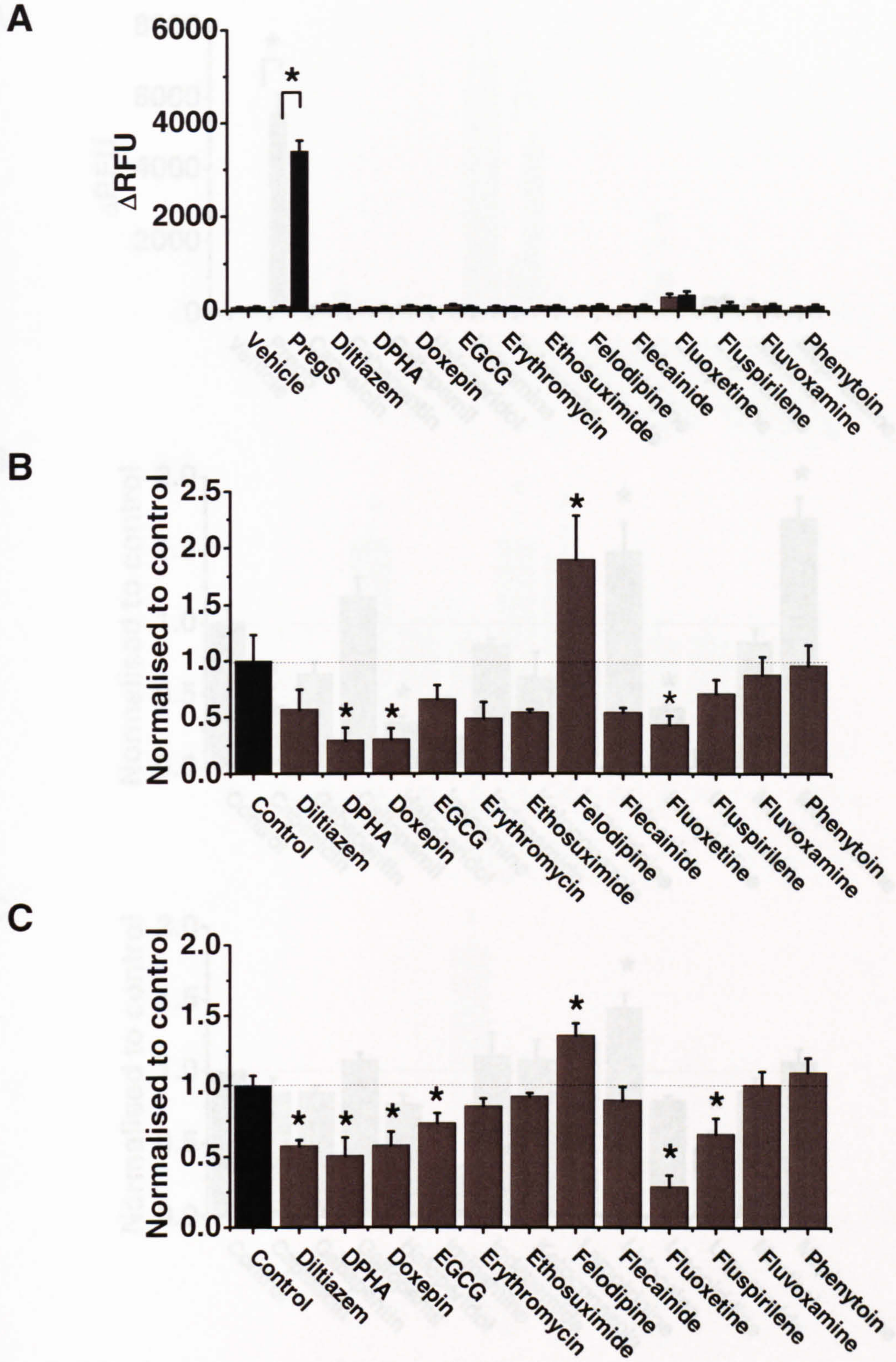

Figure 5.13. Ion channel modulators FLIPR compound screen performed at RT. Changes in Ca^{2+} were measured as relative fluorescence units (RFU) in fluo-4 loaded tet+ cells. DMSO (vehicle) was present throughout recordings. Mean data (±SEM) from 3 wells within a single plate, normalised to control PregS response, show: **A.** Activation in tet+ (black) compared to tet- (grey) cells, **B.** Inhibition of PregS response at EC_{20}, and **C.** Inhibition of PregS response at EC_{80}.

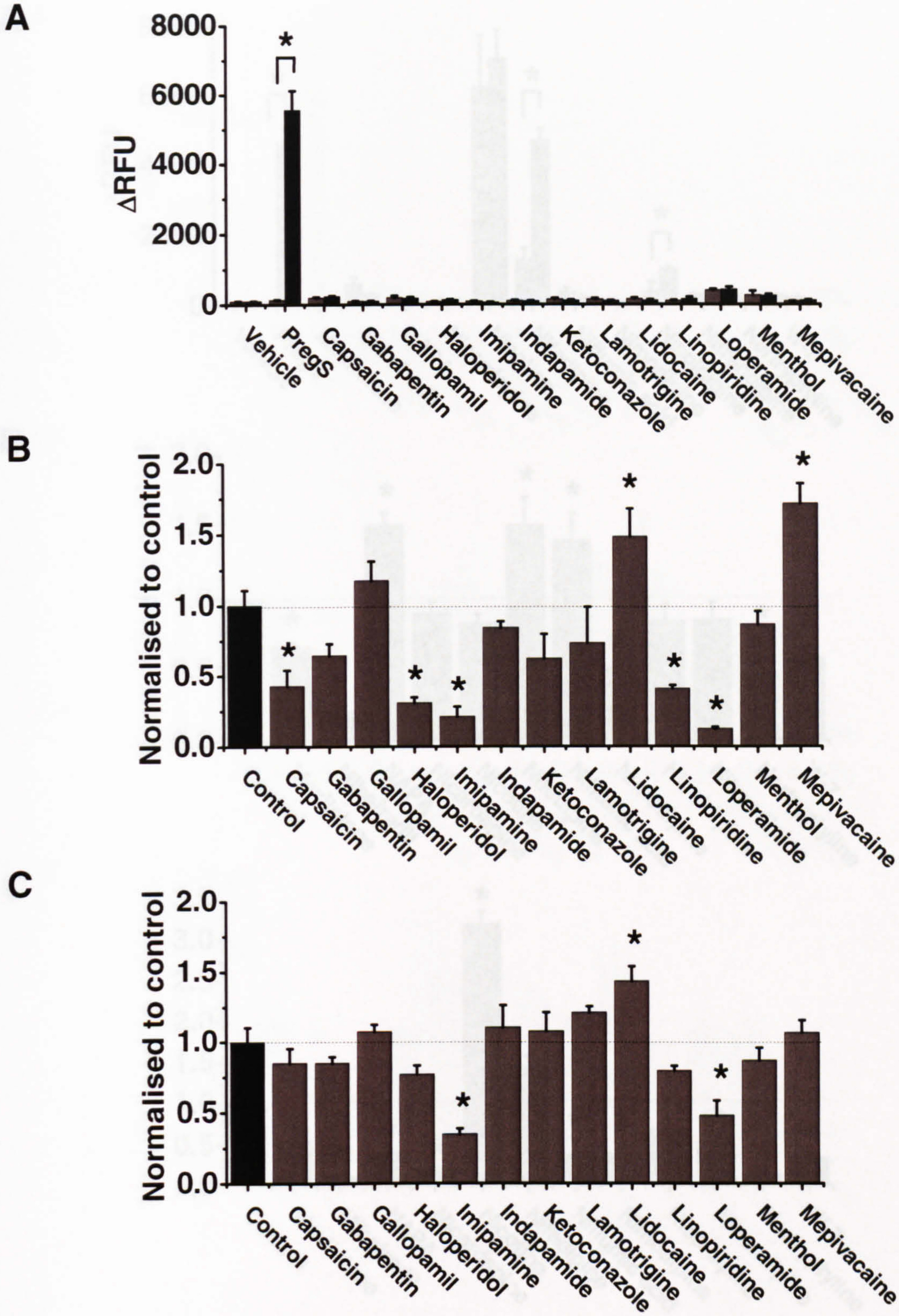

Figure 5.14. Ion channel modulators FLIPR compound screen performed at RT. Changes in Ca^{2+} were measured as relative fluorescence units (RFU) in fluo-4 loaded tet+ cells. DMSO (vehicle) was present throughout recordings. Mean data (±SEM) from 3 wells within a single plate, normalised to control PregS response, show: **A.** Activation in tet+ (black) compared to tet- (grey) cells, **B.** Inhibition of PregS response at EC_{20}, and **C.** Inhibition of PregS response at EC_{80}.

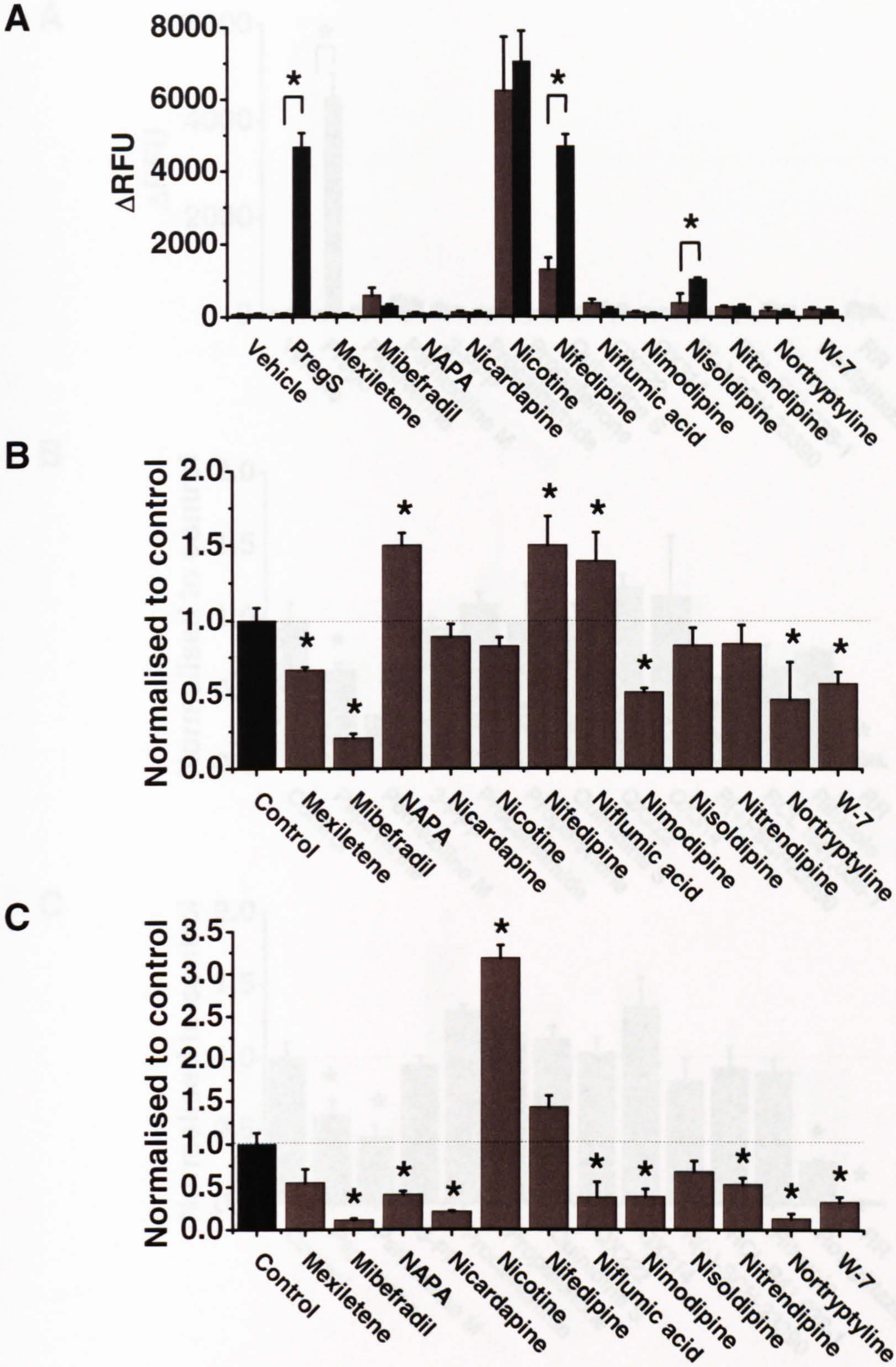

Figure 5.15. Ion channel modulators FLIPR compound screen performed at RT. Changes in Ca^{2+} were measured as relative fluorescence units (RFU) in fluo-4 loaded tet+ cells. DMSO (vehicle) was present throughout recordings. Mean data (±SEM) from 3 wells within a single plate, normalised to control PregS response, show: **A.** Activation in tet+ (black) compared to tet- (grey) cells, **B.** Inhibition of PregS response at EC_{20}, and **C.** Inhibition of PregS response at EC_{80}.

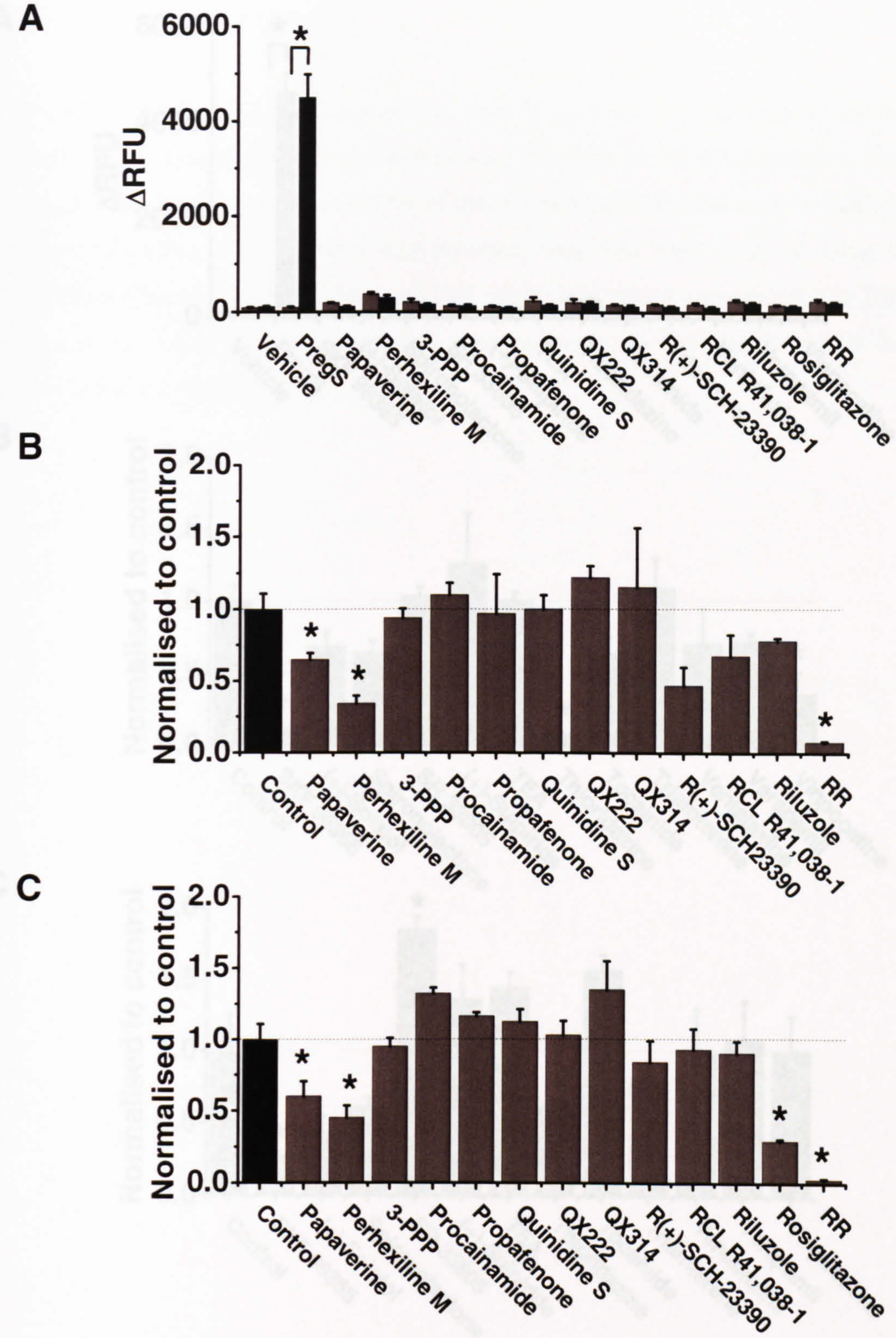

Figure 5.16. Ion channel modulators FLIPR compound screen performed at RT. Changes in Ca^{2+} were measured as relative fluorescence units (RFU) in fluo-4 loaded tet+ cells. DMSO (vehicle) was present throughout recordings. Mean data (±SEM) from 3 wells within a single plate, normalised to control PregS response, show: **A.** Activation in tet+ (black) compared to tet- (grey) cells, **B.** Inhibition of PregS response at EC_{20}, and **C.** Inhibition of PregS response at EC_{80}.

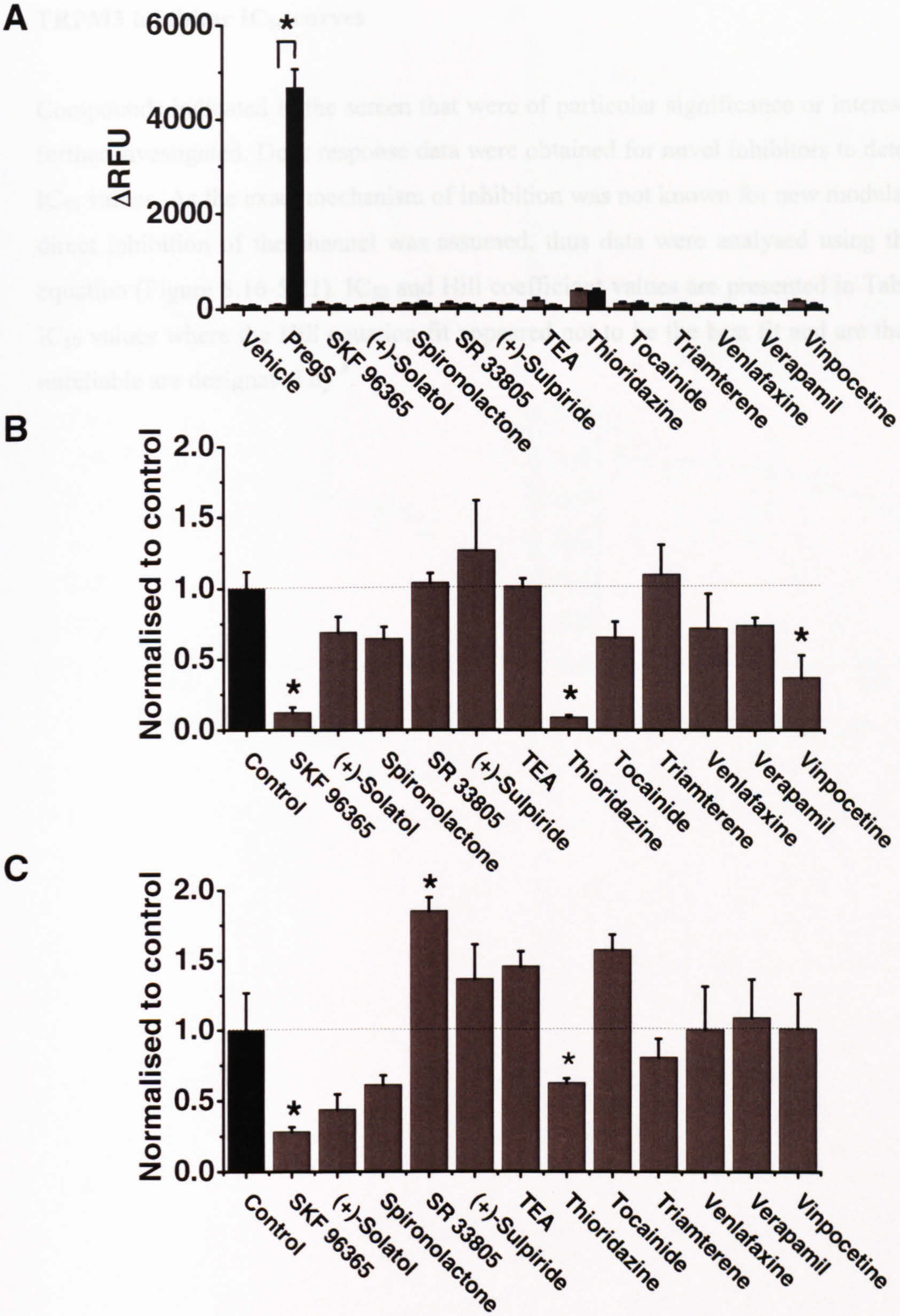

Figure 5.17. Ion channel modulators FLIPR compound screen performed at RT. Changes in Ca^{2+} were measured as relative fluorescence units (RFU) in fluo-4 loaded tet+ cells. DMSO (vehicle) was present throughout recordings. Mean data (±SEM) from 3 wells within a single plate, normalised to control PregS response, show: **A.** Activation in tet+ (black) compared to tet- (grey) cells, **B.** Inhibition of PregS response at EC_{20}, and **C.** Inhibition of PregS response at EC_{80}.

TRPM3 inhibitor IC_{50} curves

Compounds indicated in the screen that were of particular significance or interest were further investigated. Dose response data were obtained for novel inhibitors to determine IC_{50} values. As the exact mechanism of inhibition was not known for new modulators, a direct inhibition of the channel was assumed, thus data were analysed using the Hill equation (Figure 5.16-5.21). IC_{50} and Hill coefficient values are presented in Table 5.1. IC_{50} values where the Hill equation fit appeared not to be the best fit and are therefore unreliable are designated by $^{\#}$.

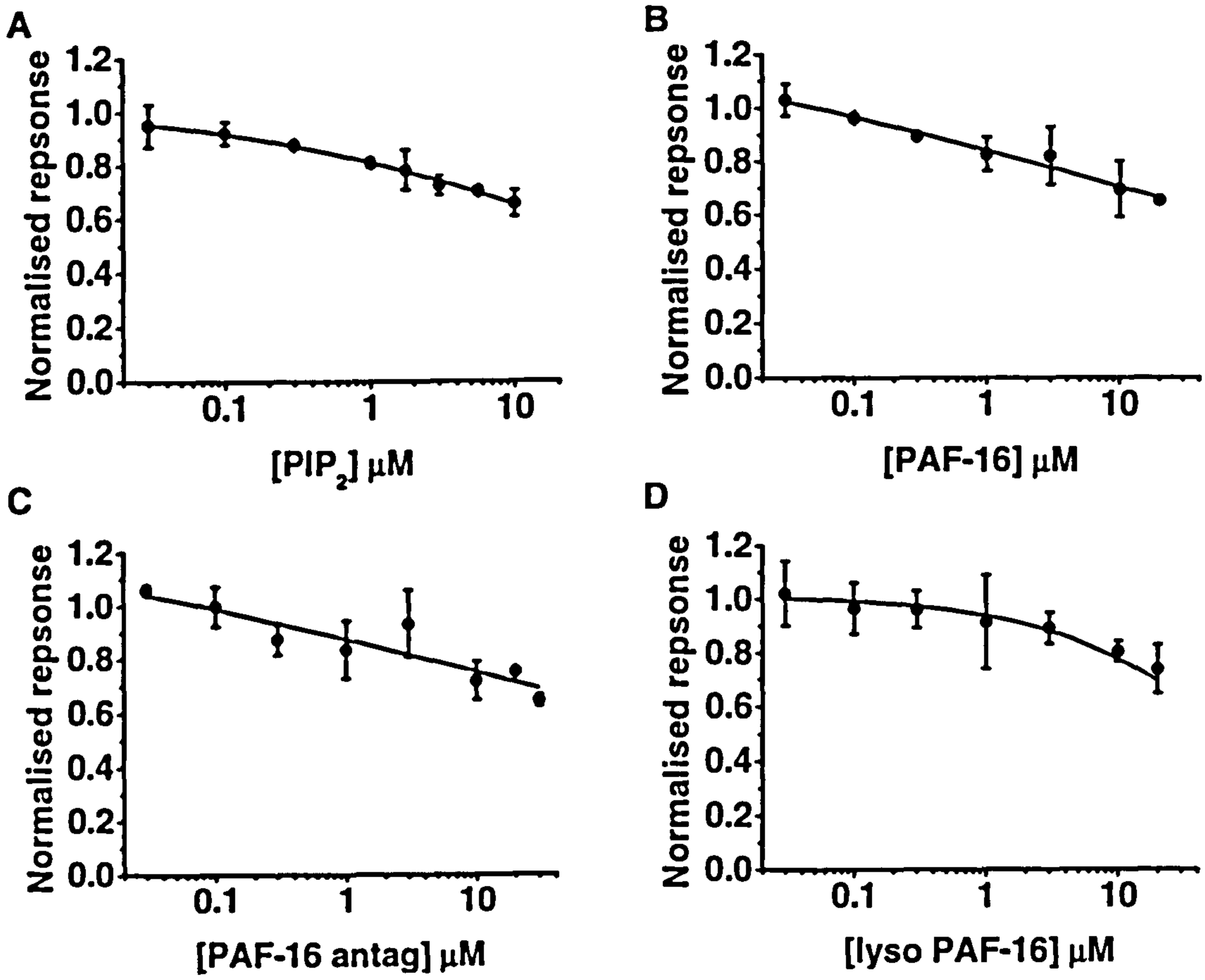

Figure 5.18. Lipid modulators IC_{50} Mean dose response data (±SEM) show inhibition of the PregS response by **A.** PIP_2, **B.** PAF-16, **C.** lyso PAF-16 and **D.** PAF-16 antagonist. Data are normalised to control PregS response, n/N=3/9 for each.

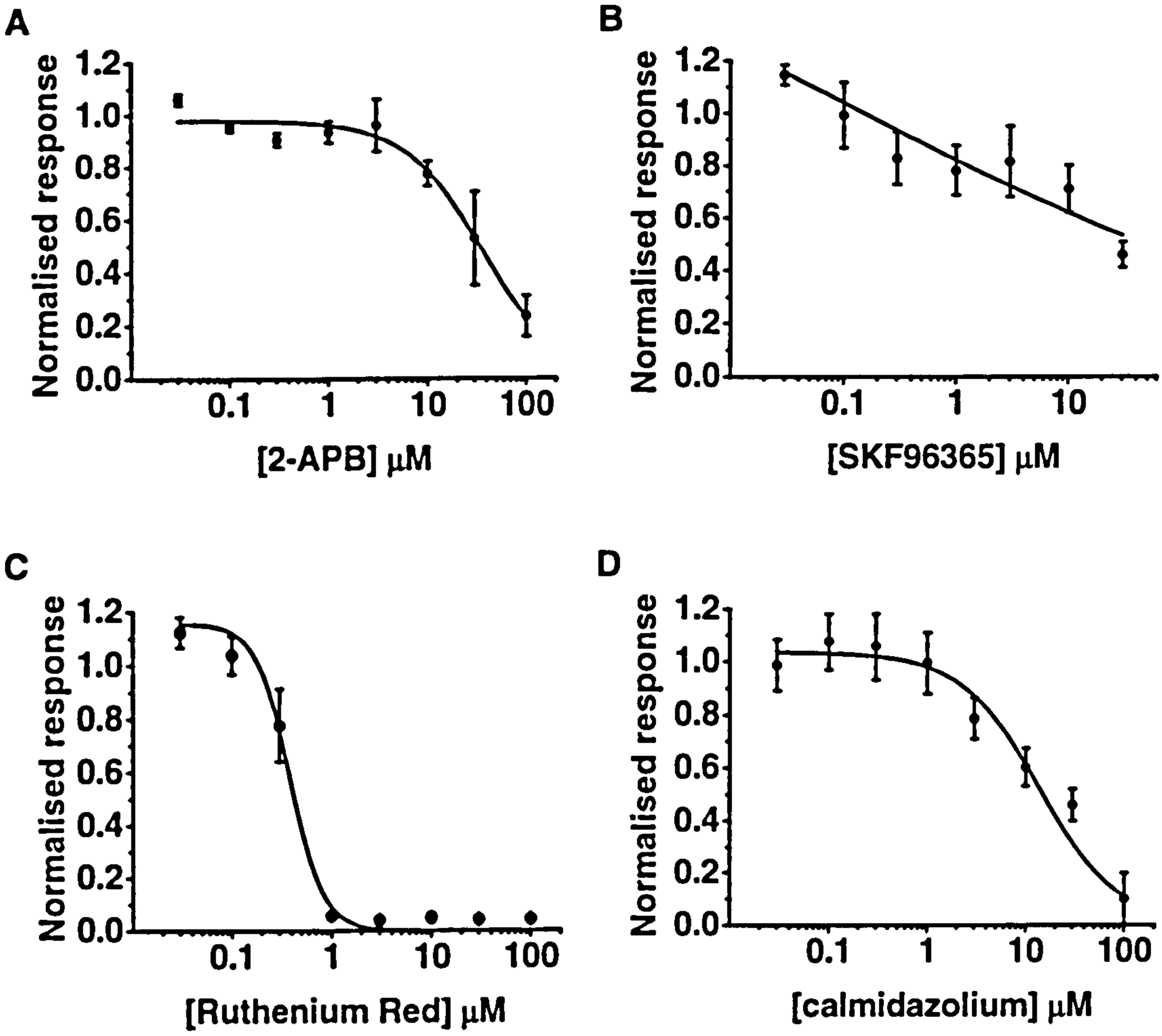

Figure 5.19. Ion channel modulators IC_{50} Mean dose response data (±SEM) show inhibition of the PregS response by **A.** 2-APB, **B.** SKF 96365, **C.** ruthenium red and **D.** calmidazolium chloride. Data are normalised to control PregS response, n/N=3/9 for each.

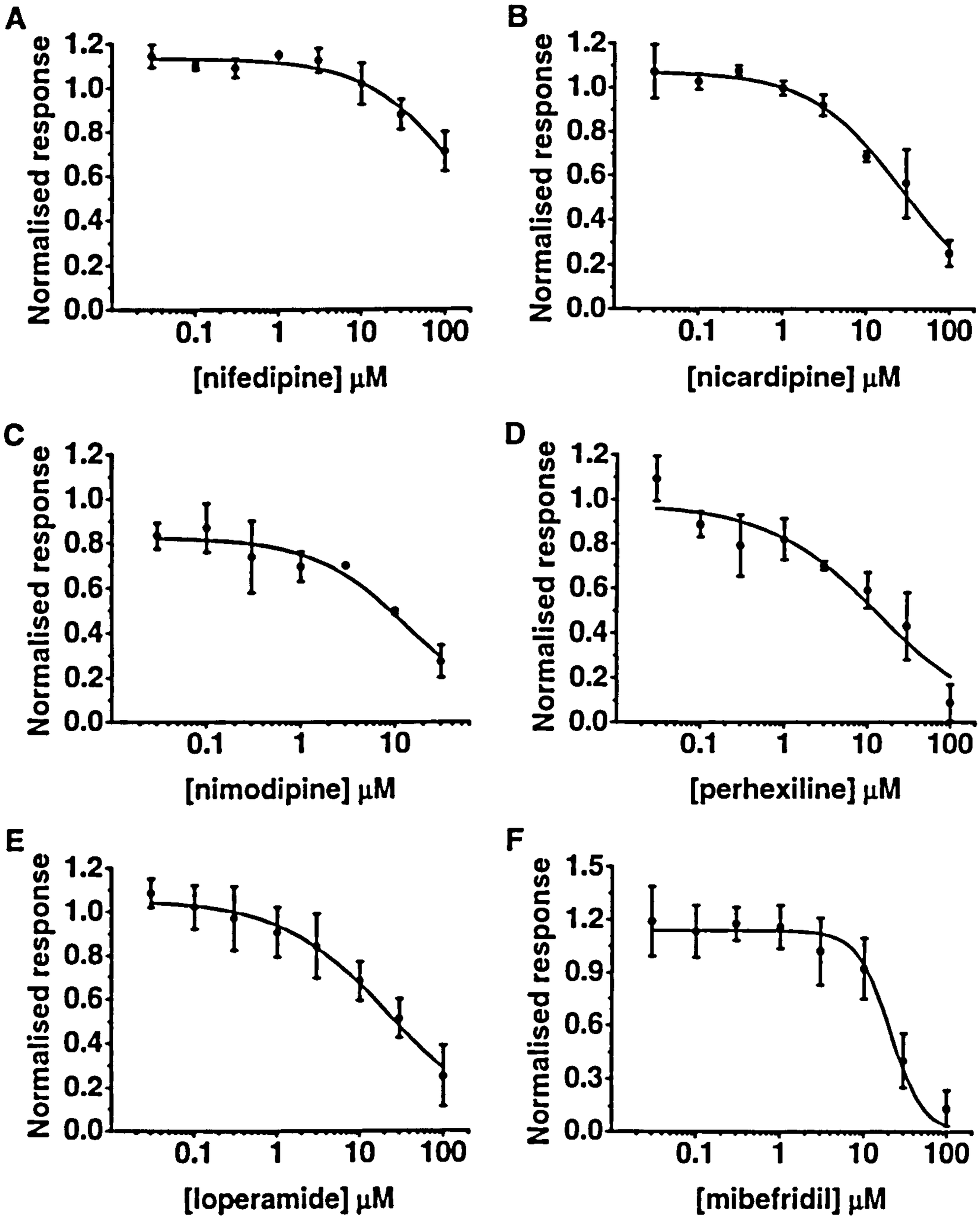

Figure 5.20. Ion channel modulators IC_{50} Mean dose response data (±SEM) show inhibition of the PregS response by **A.** nifedipine, **B.** nicardipine, **C.** nimodipine, **D.** perhexiline maleate, **E.** loperamide and **F.** mibefradil. Data are normalised to control PregS response, n/N=3/9 for each.

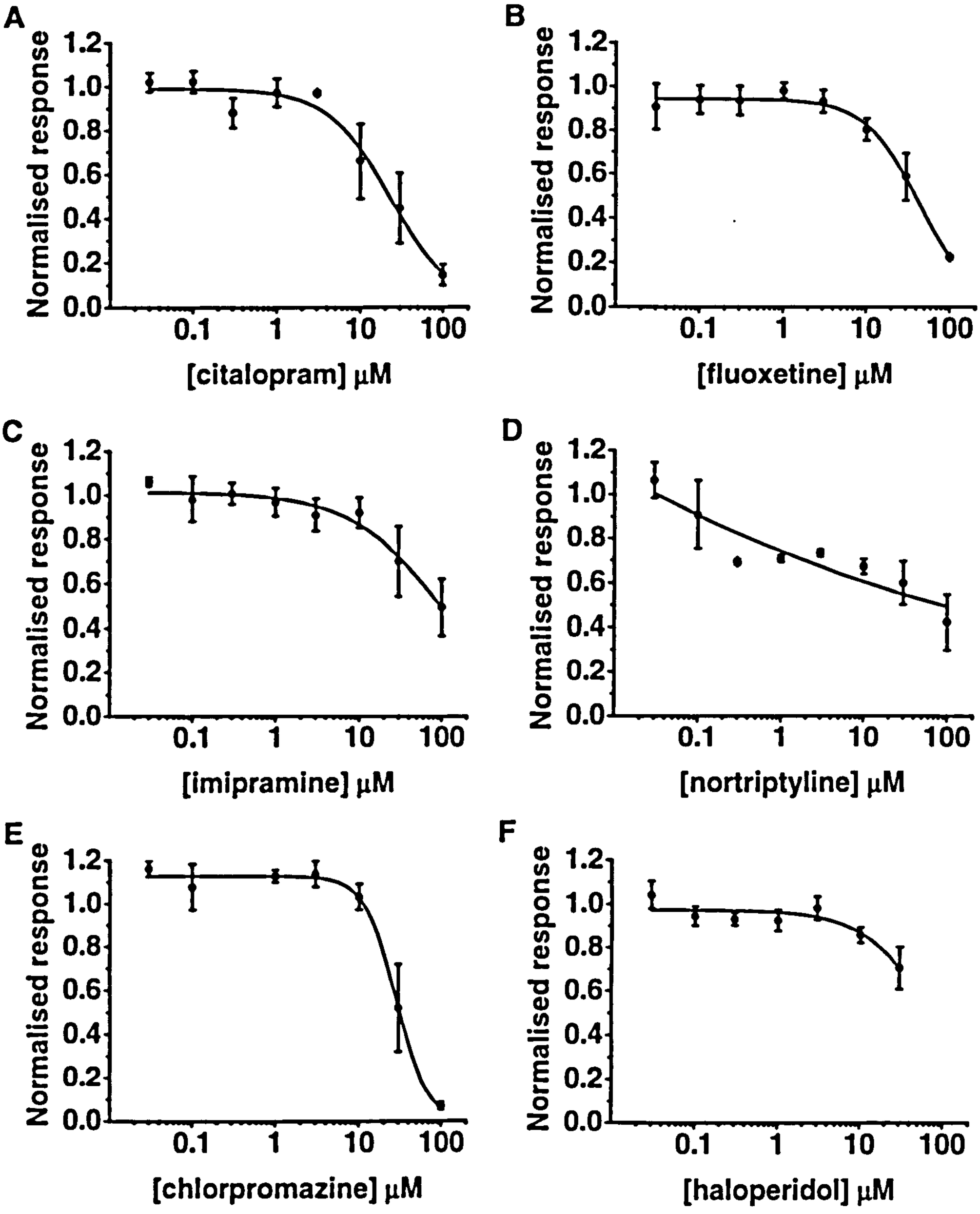

Figure 5.21. Ion channel modulators IC_{50} Mean dose response data (±SEM) show inhibition of the PregS response by **A.** citalopram, **B.** fluoxetine, **C.** imipramine, **D.** nortriptyline, **E.** chlorpromazine, and **F.** haloperidol. Data are normalised to control PregS response, n/N=3/9 for each.

Compound name	IC_{50}	Hill coefficient
[#] PIP_2	49.0 ± 6.29 μM	0.3 ± 0.04
[#] PAF-16	14.3 ± 44.78 μM	0.2 ± 0.09
Lyso PAF-16	75.3 ± 31.02 μM	0.6 ± 0.17
[#] PAF-16 antagonist	25.9 ± 52.71 μM	0.2 ± 0.22
2-APB	34.8 ± 5.46 μM	1.1 ± 0.19
[#] SKF 96365	0.1 ± 1.92 μM	0.2 ± 0.21
Ruthenium red	0.4 ± 0.04 μM	2.6 ± 0.66
Calmidazolium chloride	14.1 ± 4.90 μM	1.1 ± 0.37
Nifedipine	184.6 ± 42.33 μM	0.8 ± 0.15
Nicardipine	26.6 ± 3.81 μM	0.8 ± 0.10
Nimodipine	14.8 ± 3.65 μM	0.9 ± 0.22
Perhexiline maleate	13.2 ± 7.06 μM	0.7 ± 0.23
Loperamide	23.1 ± 3.55 μM	0.7 ± 0.08
Mibefradil	20.8 ± 3.39 μM	2.2 ± 0.63
Citalopram	22.7 ± 4.18 μM	1.2 ± 0.23
Fluoxetine	42.3 ± 3.20 μM	1.3 ± 0.13
Imipramine	92.0 ± 17.10 μM	0.8 ± 0.15
[#] Nortriptyline	1.4 ± 7.17 μM	0.1 ± 0.16
Haloperidol	75.5 ± 41.83 μM	1.1 ± 0.52
Chlorpromazine	28.1 ± 1.42 μM	2.2 ± 0.28

Table 5.1. IC_{50} and Hill coefficients for novel TRPM3 inhibitors Compounds where the Hill equation did not produce a good fit are designated by [#].

Cross screening of TRPM3 modulators against native ATP responses and TRPM2

Novel TRPM3 inhibitors identified by the HT screen were further investigated as modulators of endogenous ATP responses in TRPM3-expresing cells, and by cross screening against TRPM2 cells, to determine their selectivity for TRPM3. Furthermore IC_{50} values were calculated for TRPM2 inhibition and are presented in Table 5.2. IC_{50} values obtained when application of the Hill equation did not appear to give the best fit, suggesting they are unreliable, are designated by $^{\#}$.

In addition to inhibiting the TRPM3 PregS-response, 2-APB, lyso PAF-16, PAF-16, mibefradil and calmidazolium chloride also inhibited the endogenous ATP response, whereas fluoxetine significantly potentiated this response (Figure 5.22).

For TRPM2-expressing cells, clotrimazole served as a useful positive control for the dose-dependant inhibition of TRPM2 (Figure 5.23 A & 5.25 C). 2-APB is reported to be ineffective at blocking ADP-ribose activated TRPM2 current at concentrations up to 75 μM (Xu *et al.*, 2005a), yet this study demonstrates 54% inhibition of the H_2O_2 response by 2-APB (Figure 5.23 A). However, the inhibition observed with 2-APB was not reproduced in the dose response data at concentrations lower than 100 μM (Figure 5.25 A). Although the TRP inhibitor SKF 96365 also appeared to cause inhibition of TRPM2 (Figure 5.23 A), again there was a discrepancy with the dose response data and the block seems unreliable (Figure 5.25 B).

PIP_2, significantly inhibited the TRPM2 H_2O_2 response, while PAF-16 and lyso PAF-16 only displayed an inhibitory effect at high concentrations (Figure 5.23 & 5.24), as did the ion channel modulators calmidazolium chloride, perhexiline maleate, mibefradil, nortriptyline, chlorpromazine and loperamide (Figure 5.23, 5.25 & 5.26), suggesting that these compounds are not selective inhibitors of the TRPM3 channel. Converse to TRPM3, nifedipine did not activate TRPM2, and instead significantly inhibited the H_2O_2 response (Figure 5.23 & 5.26 A).

The data indicate that many recognised ion channel inhibitors are non-selective, and block both endogenous cellular responses and those of other TRP channels. In addition, discrepancies between the HTS and dose response data demonstrate the importance that leads identified by a compound screen are followed up with further investigation including repeat experiments and different experimental techniques.

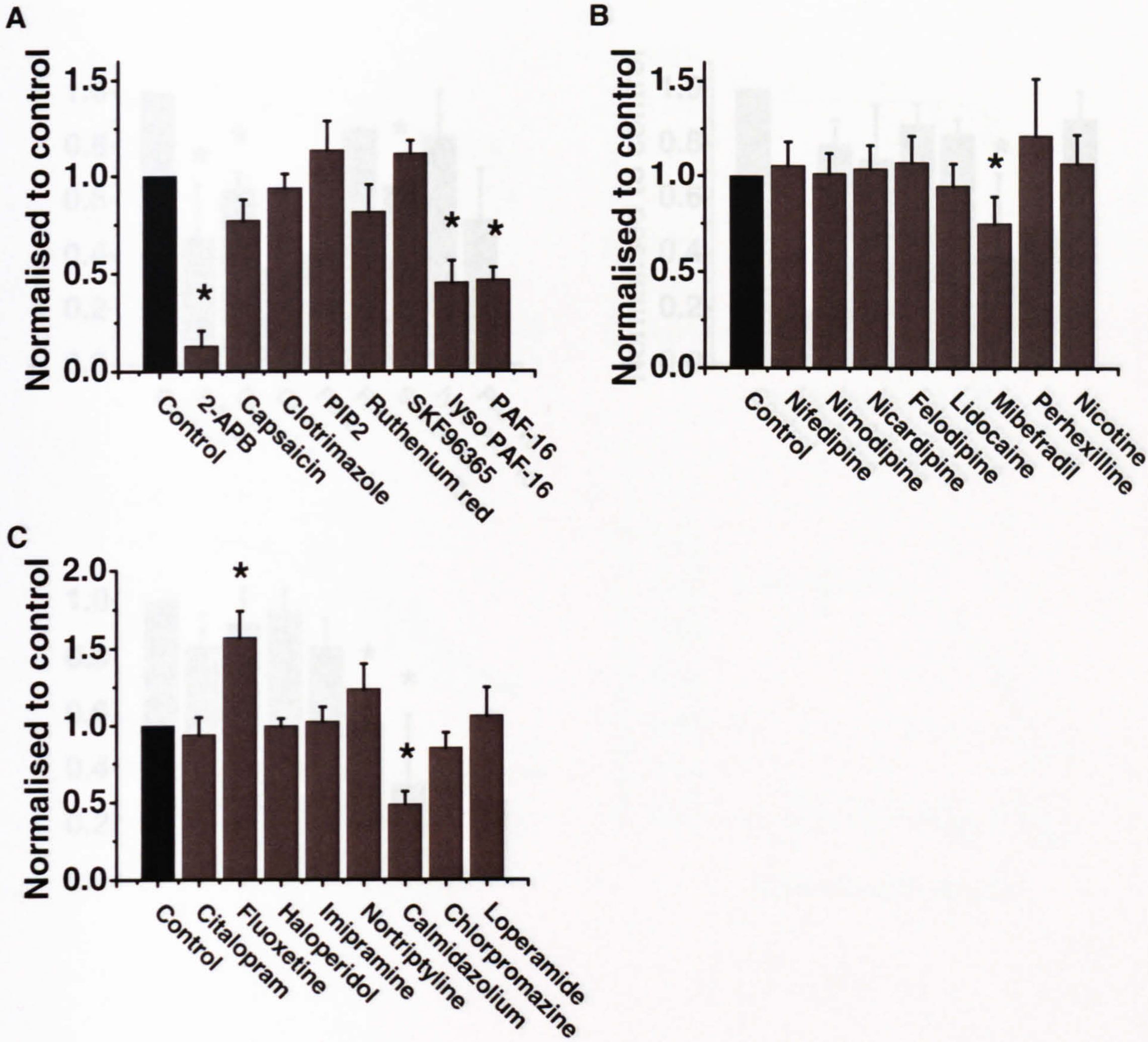

Figure 5.22. Ion channel modulators ATP FLIPR compound screen performed at RT. Changes in Ca^{2+} were measured as relative fluorescence units (RFU) in fluo-4 loaded tet+ cells. Mean data (±SEM) normalised to control ATP response, show: **A.** Inhibition of ATP response by TRP modulators. **B.** Inhibition of ATP response by Ca^{2+} channel blockers. **C.** Inhibition of ATP response by antidepressants and antipsychotics. n/N=3/9 for each.

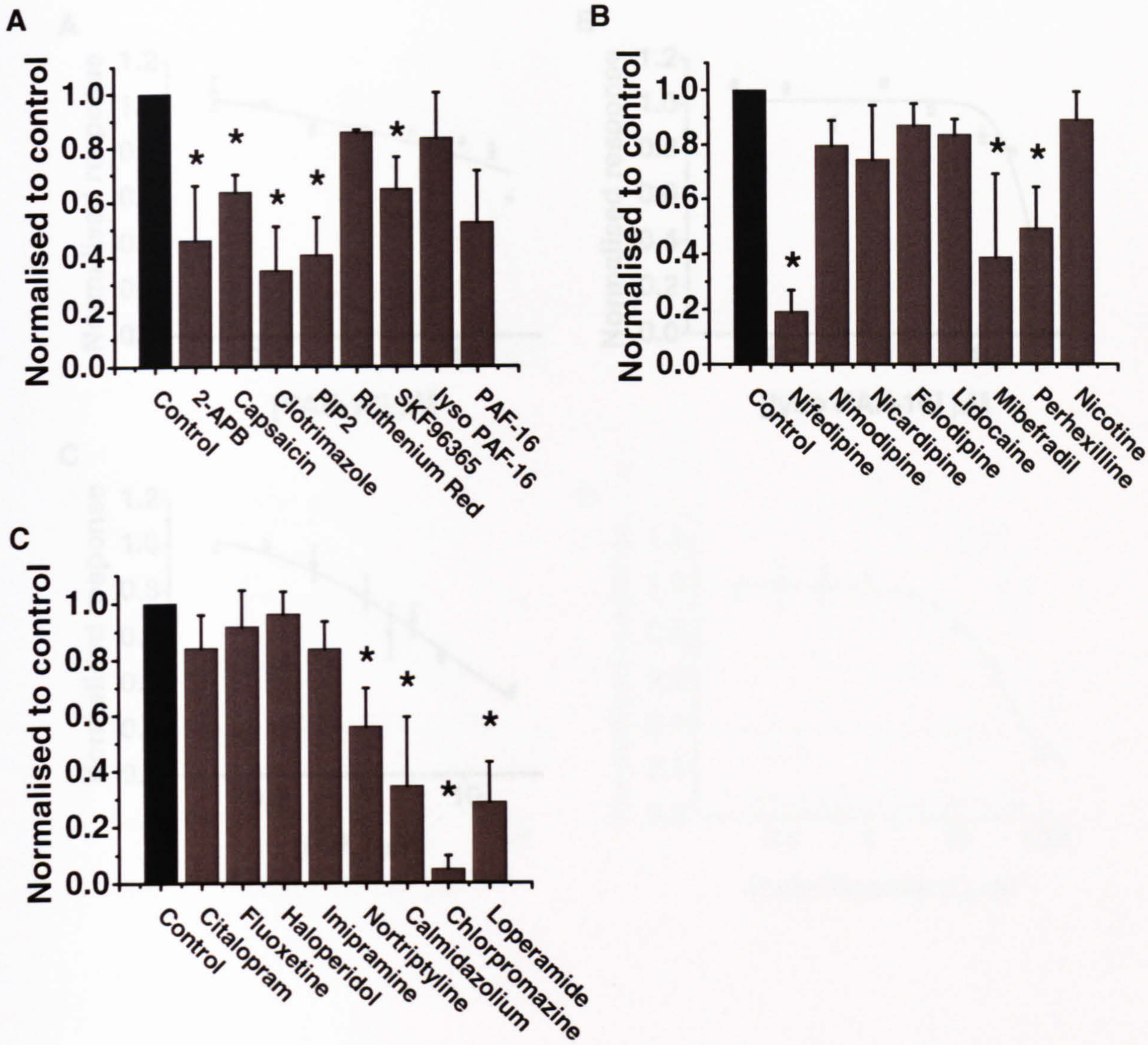

Figure 5.23. Ion channel modulators TRPM2 FLIPR compound screen performed at RT. Changes in Ca^{2+} were measured as relative fluorescence units (RFU) in fluo-4 loaded tet+ cells. Mean data (±SEM) normalised to control H_2O_2 response, show: **A.** Inhibition of H_2O_2 response by TRP modulators. **B.** Inhibition of H_2O_2 response by Ca^{2+} channel blockers. **C.** Inhibition of H_2O_2 response by antidepressants and antipsychotics. n/N=3/9 for each.

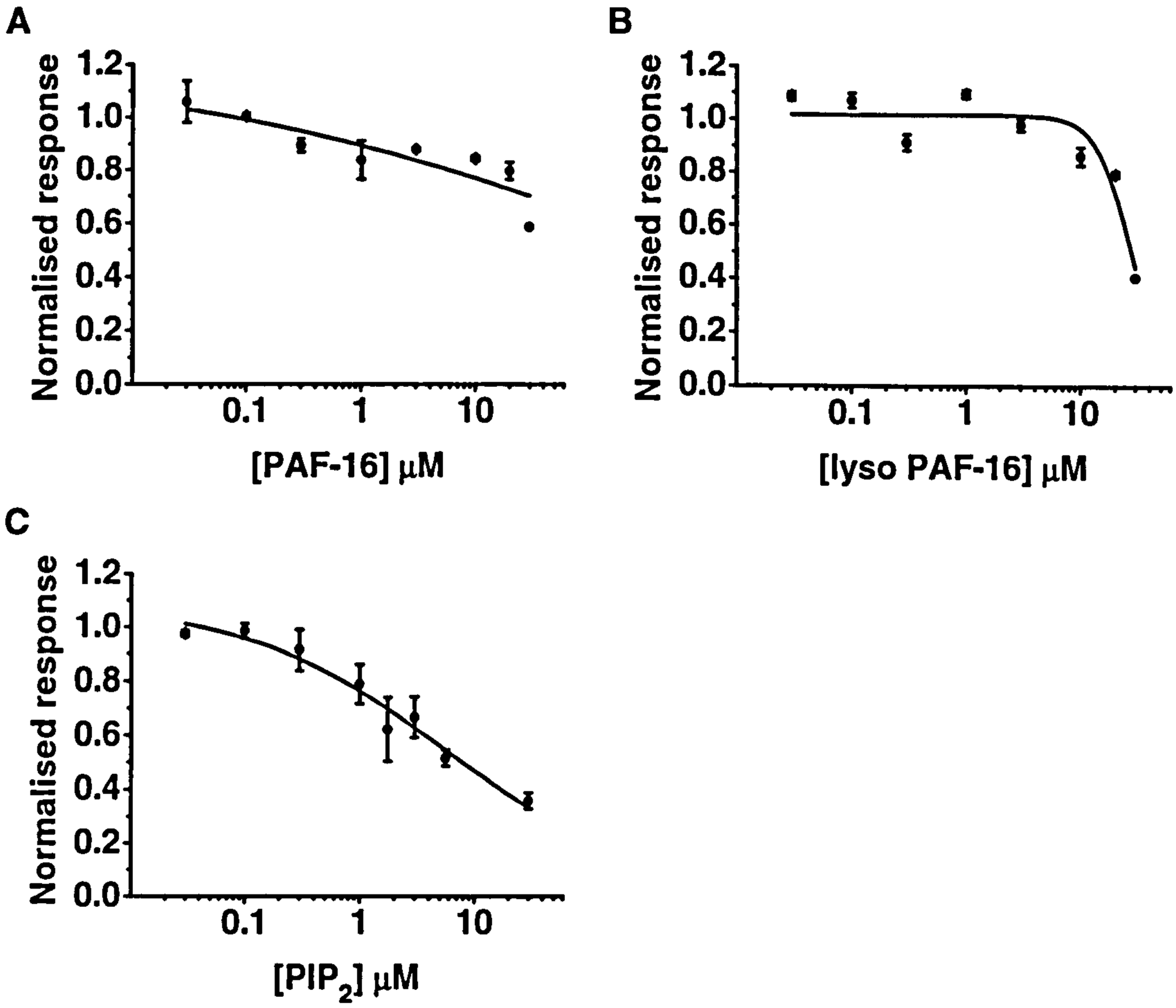

Figure 5.24. Ion channel modulators IC_{50} TRPM2 Mean dose response data (±SEM) show inhibition of the H_2O_2 response by **A.** PAF-16, **B.** lyso PAF-16 and **C.** PIP_2. Data are normalised to control H_2O_2 response, n/N=3/9 for each.

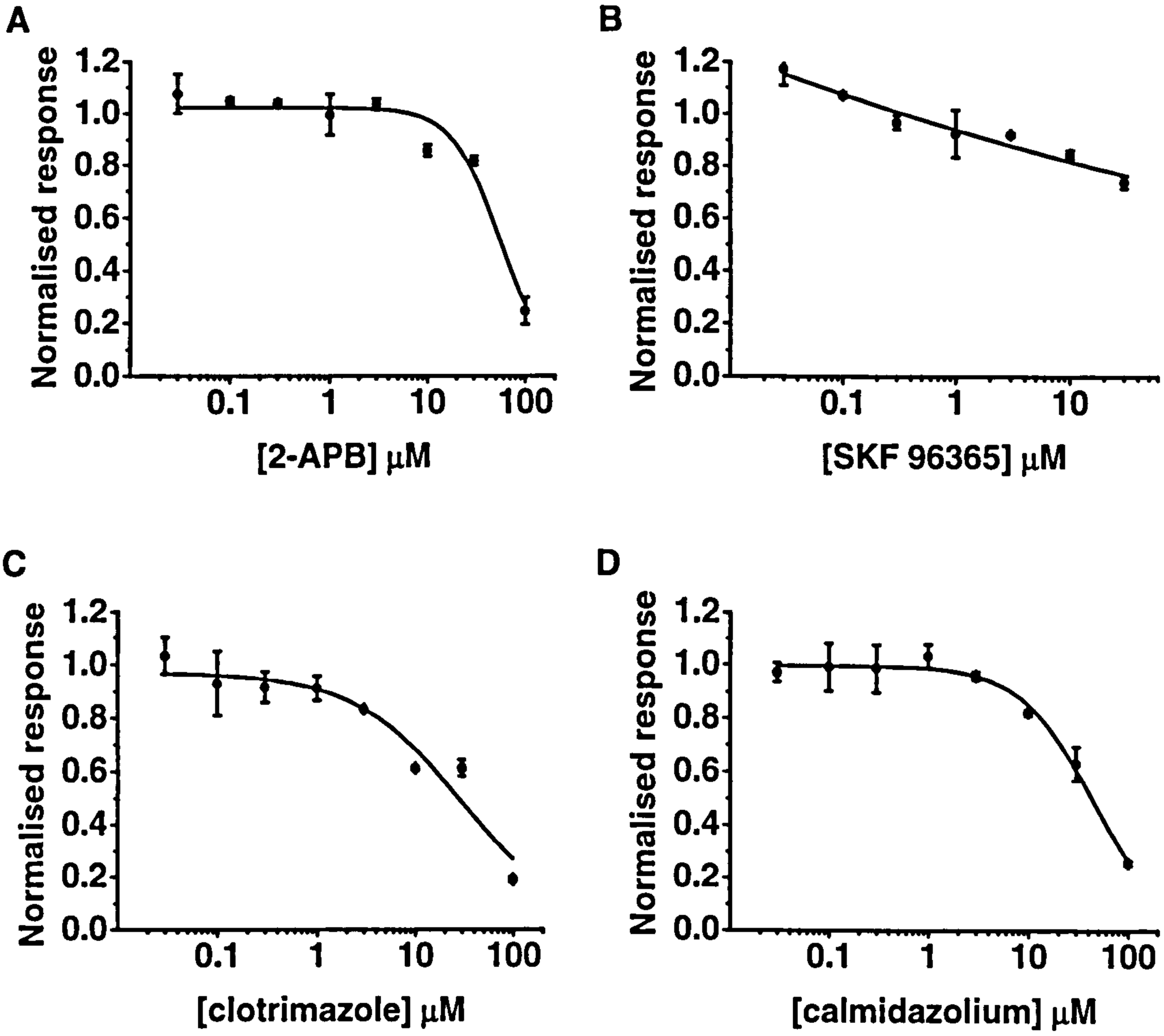

Figure 5.25. Ion channel modulators IC_{50} TRPM2 Mean dose response data (±SEM) show inhibition of the H_2O_2 response by **A.** 2-APB, **B.** SKF 96365, **C.** clotrimazole and **D.** calmidazolium chloride. Data are normalised to control H_2O_2 response, n/N=3/9 for each.

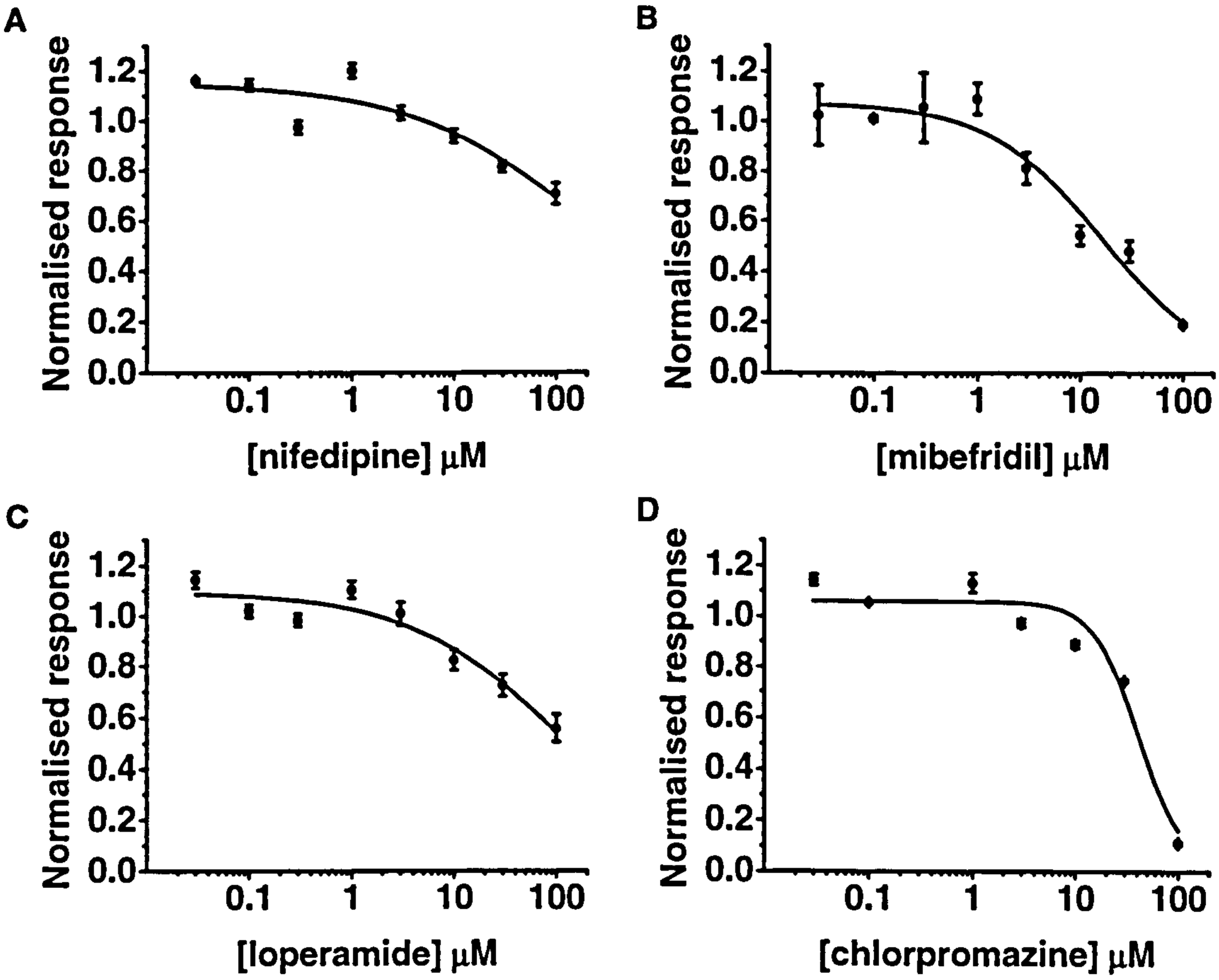

Figure 5.26. Ion channel modulators IC_{50} TRPM2 Mean dose response data (±SEM) show inhibition of the H_2O_2 response by **A.** nifedipine, **B.** mibefradil, **C.** loperamide and **D.** chlorpromazine. Data are normalised to control H_2O_2 response, n/N=3/9 for each.

Compound name	IC_{50}	Hill coefficient
PIP_2	5.7 ± 2.22 μM	0.5 ± 0.11
[#] PAF-16	162.0 ± 61.42 μM	0.2 ± 0.28
[#] Lyso PAF-16	27.3 ± 2.92 μM	2.9 ± 1.23
2-APB	55.6 ± 7.95 μM	1.8 ± 0.38
[#] SKF 96365	0.1 ± 2.40 μM	0.1 ± 0.11
Clotrimazole	29.8 ± 9.65 μM	0.8 ± 0.22
Calmidazolium chloride	43.7 ± 3.54 μM	1.2 ± 0.12
Nifedipine	225.0 ± 26.85 μM	0.4 ± 0.03
Mibefridil	16.1 ± 4.88 μM	0.8 ± 0.19
Loperamide	97.7 ± 35.00 μM	0.6 ± 0.18
Chlorpromazine	41.3 ± 7.65 μM	2.0 ± 0.61

Table 5.2. IC_{50} and Hill coefficients for TRPM2 inhibitors Compounds where the Hill equation did not produce a good fit are designated by [#].

Nifedipine activates TRPM3

The high throughput screen demonstrated significant activation of TRPM3 with the calcium channel inhibitor nifedipine, plus potentiation of the PregS response at low concentrations. In addition, nifedipine has been suggested as an activator of mouse variant TRPM3α2 (J. Oberwinkler, personal communication). FLIPR fluorimetry of fluo-4 loaded cells was used to further investigate the effect of nifedipine on TRPM3.

Nifedipine (10 μM) activated a rapid and sustained Ca^{2+} response in cells expressing TRPM3 (tet+) but not in non-induced cells (tet-) (Figure 5.27 A). The mean data show that after 3 min, nifedipine-induced responses in tet+ cells were significantly larger than tet- cells (Figure 5.27 B).

Increasing concentrations of nifedipine were applied to wells of test and control cells within the same plate, allowing for direct comparison. Responses increased in magnitude with higher concentrations, demonstrating concentration-dependant activation. Fitting of the Hill equation indicated the concentration for half maximal activation, the EC_{50}, was 26.0 ± 4.27 μM, with a Hill coefficient of 1.3 ± 0.16 (Figure 5.27 C), however this EC_{50} value is unreliable and may be an underestimate of the true value as a maximum response was not achieved.

The data confirm that nifedipine can activate human TRPM3 in a concentration dependant manner.

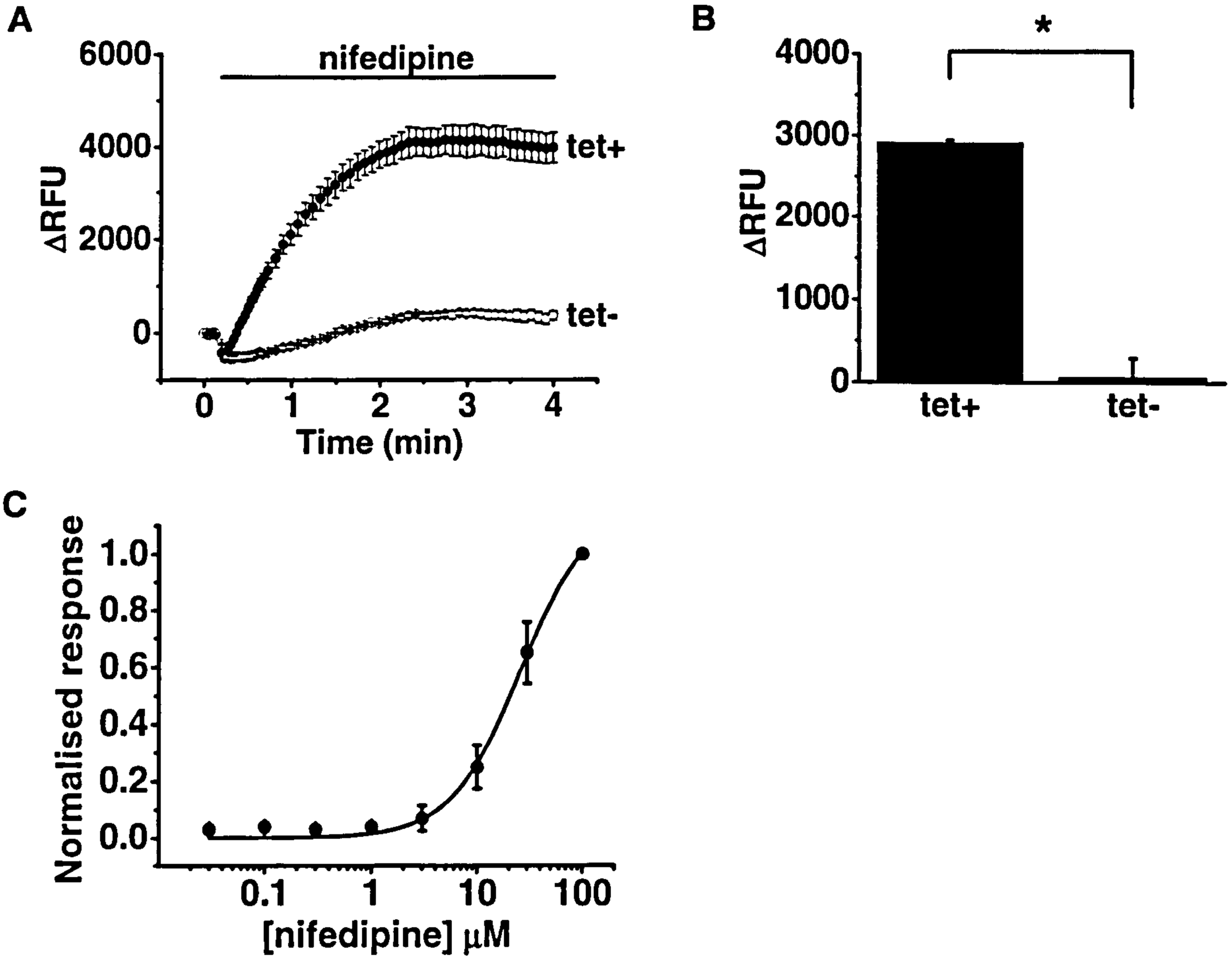

Figure 5.27. Nifedipine increases Ca^{2+} signals in tet+ TRPM3 cells Changes in Ca^{2+} were measured as relative fluorescence units (RFU) in fluo-4 loaded cells. Cells were induced by incubation with tetracycline (tet+). Cells not treated with tetracycline were included as a control (tet-). DMSO (vehicle) was present throughout recordings. **A.** Representative mean data (±SEM) from 3 wells within a single plate show nifedipine (10 μM) causes an increase in Ca^{2+} in tet+ TRPM3 compared to tet- (open circles). **B.** Mean data (±SEM) showing significant increase in Ca^{2+} 3 min after nifedipine application (n/N=3/9). **C.** Mean dose response data (±SEM) analysed using the Hill equation (n/N=3/9).

Cholesterol inhibits TRPM3

Cholesterol has important physiological functions. Most importantly, it maintains the structure of the cell membrane by regulating fluidity of the lipid bilayer (Spector *et al.*, 1985). Cholesterol also regulates the activity of membrane-bound proteins such as TRP channels (Bergdahl *et al.*, 2003). Cholesterol is a highly hydrophobic molecule, but can be made soluble in aqueous solutions through the formation of complexes with cyclodextrins. These cyclic oligosaccharides possess a hydrophilic exterior that makes them soluble, and a less hydrophilic interior that provides a favorable environment for hydrophobic molecules. Preincubation with an excess of the 7-sugar unit β-cyclodextrin (βCD) extracts cholesterol from the plasma membrane in live cells.

The high throughput lipid screen demonstrated small but significant activation of TRPM3 following direct application of βCD (Figure 5.9). FLIPR fluorimetry of fluo-4 loaded cells was used to further investigate this effect, and demonstrated that βCD (10 μM) activated a slowly developing small Ca^{2+}-response in both tet- and tet+ cells (Figure 5.28 A). The mean data show that after 4 min, βCD-induced responses in tet+ cells were significantly larger than tet- cells (Figure 5.28 B). Note that direct application of cholesterol (10 μM) had no significant effect on TRPM3 (Figure 5.5). This is most likely because the cholesterol was insoluble in the bath solution. Alternatively, TRPM3 may be tonically inhibited by cholesterol that is already present in the plasma membrane.

The effect of membrane cholesterol on the TRPM3 channel was further investigated by providing cholesterol complexed to methyl β-cyclodextrin (mβCD). This methylated derivative of βCD is more efficient than its parent compound at forming complexes with hydrophobic molecules such as cholesterol, thus enhances their solubility in aqueous solutions, and delivers them to cell membranes (Rodal *et al.*, 1999). Preincubation of cells with the soluble cholesterol complex at physiological temperature for 2 hours was sufficient to allow cholesterol molecules to insert into the favourable conditions of the plasma membrane (Hinzpeter *et al.*, 2007). Cholesterol enrichment of the cell membrane inhibited PregS-induced activation of TRPM3 (Figure 5.29 A). The mean data indicate that preincubation with the soluble cholesterol complex (1 mM) caused a 70.2% inhibition of the Ca^{2+} response, with no effect on non-induced (tet-) cells (Figure

5.29 B). Dose response data give the IC_{50} for this cholesterol inhibition as 0.5 ± 0.06 mM; with a Hill coefficient of 2.5 ± 0.58 (Figure 5.29 C).

To determine the specificity of cholesterol inhibition of TRPM3, the effect of cholesterol enrichment on other TRP family members was examined. Cholesterol decreased the starting baseline in tet+ and tet- TRPM2 cells, and potentiated the H_2O_2 response (Figure 5.30 A). In TRPC5-expressing cells, cholesterol completely inhibited the Gd^{3+}-response (Figure 5.30 B), but had no effect on the 4αPDD response in TRPV4-expressing cells (Figure 5.30 C).

The data demonstrate that TRPM3 activity is regulated by cholesterol, and that cholesterol enrichment of the cell membrane has varied effects on different TRP family members.

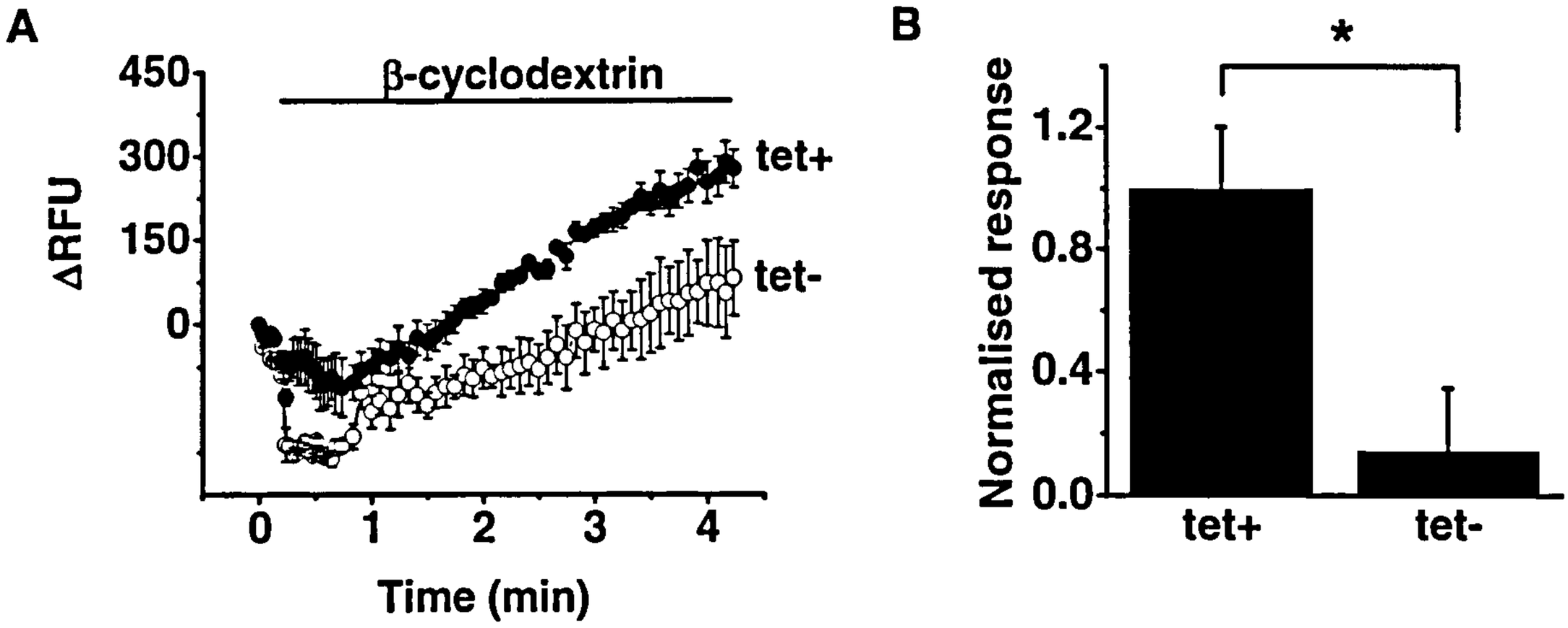

Figure 5.28. β-cyclodextrin increases Ca^{2+} signals in tet+ TRPM3 cells Changes in Ca^{2+} were measured as relative fluorescence units (RFU) in fluo-4 loaded cells. Cells were induced by incubation with tetracycline (tet+). Cells not treated with tetracycline were included as a control (tet-). **A.** Representatiive mean data (±SEM) from 3 wells within a single plate show β-cyclodextrin (10 μM) causes a greater Ca^{2+} increase in tet+ cells compared to tet- (open circles). **B.** Mean data (±SEM) showing significant increase in Ca^{2+} 3 min after β-cyclodextrin application (n/N=3/9).

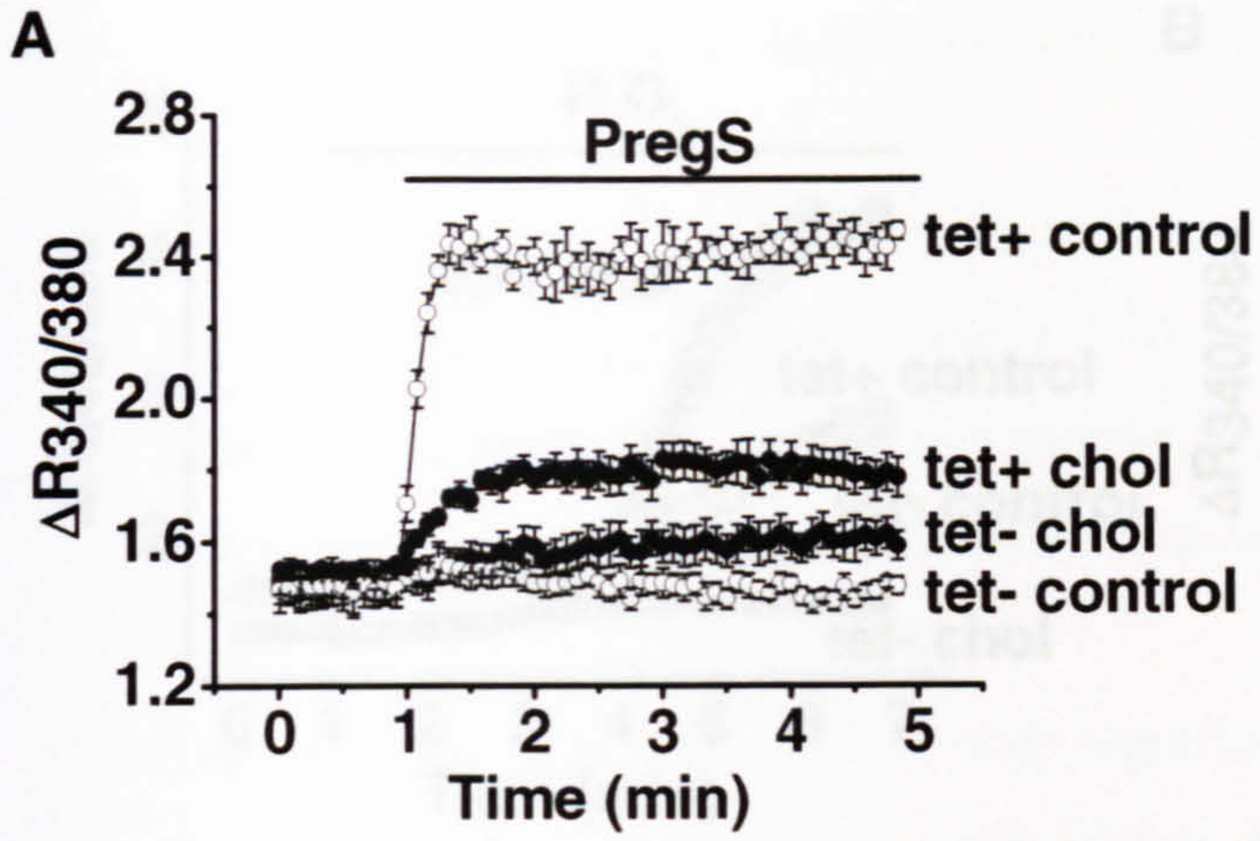

Figure 5.29. Cholesterol enrichment inhibits PregS induced Ca^{2+} response in tet+ TRPM3 cells Ca^{2+} signals were measured as the 340/380 nm ratio of emission in fura-2 loaded cells. Cells were induced by incubation with tetracycline (tet+). Cells not treated with tetracycline were included as a control (tet-). **A.** Repesentative mean data (±SEM) from 6 wells within a single plate show inhibition of the tet+ PregS response by cholesterol (chol, 1 mM). **B**. Mean data (±SEM) showing significant chol inhibition of Ca^{2+} responses 1 min after PregS application (n/N=3/18). **C.** Mean dose response data (±SEM) analysed using the Hill equation (n/N=3/9).

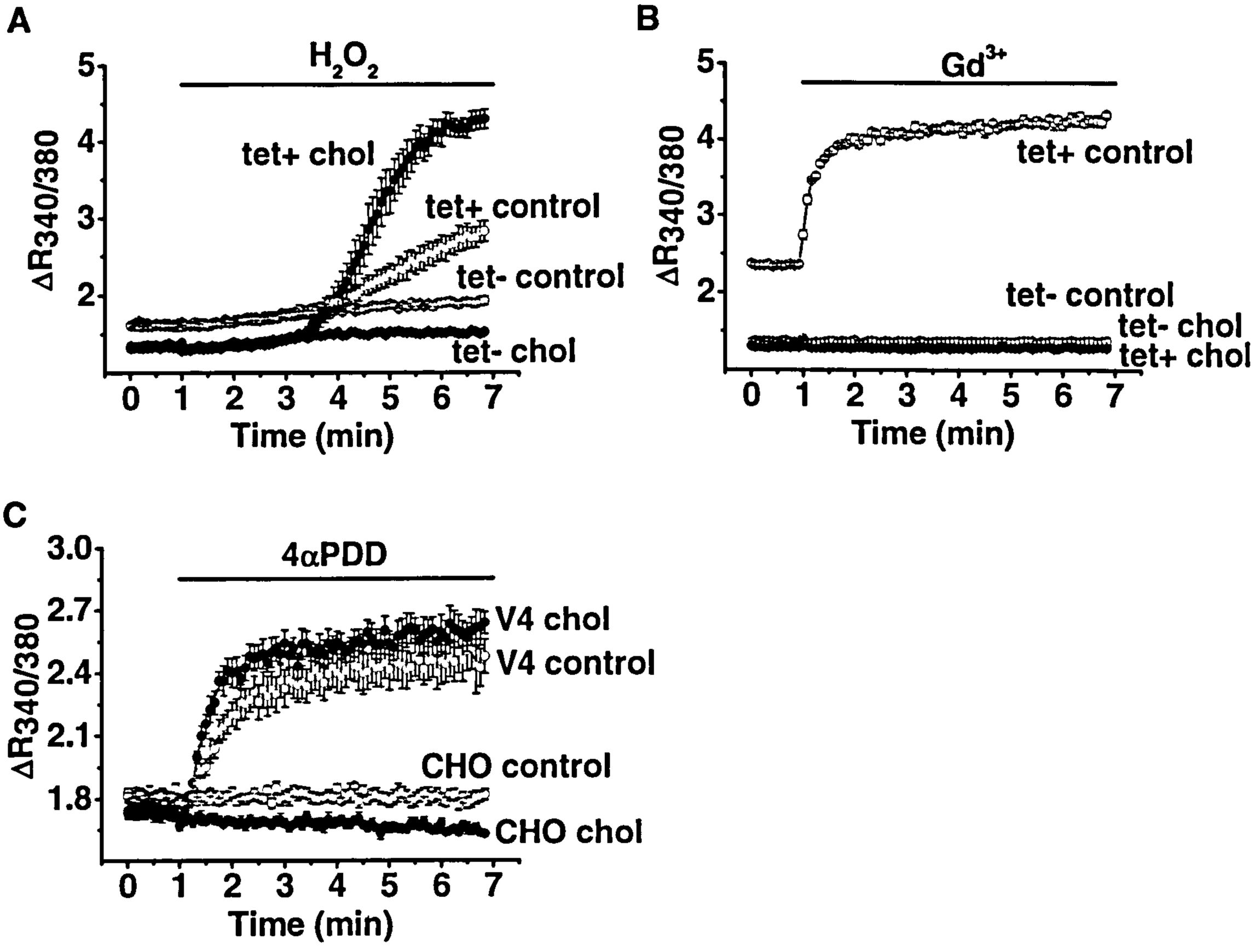

Figure 5.30. Cholesterol enrichment effect on other TRP channels Ca^{2+} signals were measured as the 340/380 nm ratio of emission in fura-2 loaded cells. TRPM2 and TRPC5 cells were induced by incubation with tetracycline (tet+). Cells not treated with tetracycline were included as a control (tet-). For TRPV4 cells, CHO parent cells were included as a control. Representative mean data (±SEM) shown are from 6 wells within a single plate for each cell type. **A.** Chol (1 mM) enrichment potentiates H_2O_2 activation of TRPM2. **B.** Chol inhibits Gd^{3+} (100 μM) activation of TRPC5. **C.** Chol does not affect TRPV4 activation by 4αPDD (10 μM).

Removal of membrane cholesterol activates TRPM3

Previous experiments demonstrating βCD activation of TRPM3 involved a direct, short application of βCD. A longer preincubation using mβCD, reported to be both more soluble and more effective at cholesterol removal (Rodal *et al.*, 1999), was used to investigate the effect of cholesterol depletion on TRPM3.

Preincubation with mβCD (10 mM) significantly increased the starting baseline for recording in both tet+ and tet- cells (Figure 5.31 A & B). This would suggest mβCD preincubation had already activated calcium entry into cells prior to PregS addition. The mean data show that there was a reduction in the magnitude of the PregS response in mβCD treated cells (Figure 5.31 C). This could be because the PregS response saturated, and could not increase by a similar magniturde in cells with a high starting baseline. Following mβCD preincubation, PregS was also able to elicit a significant Ca^{2+} response in tet- cells (Figure 5.31 C).

Further experiments were performed using stable cells expressing additional TRP channels. Preincubation with mβCD (10 mM) also increased the starting baseline in tet+ and tet- TRPM2 cells, and completely inhibited the H_2O_2 response (Figure 5.32 A). In TRPC5-expressing cells, again the baseline was increased following mβCD preincubation, and Gd^{3+}-induced Ca^{2+} entry reached a much higher maximum fluorescence, suggesting potentiation of the Gd^{3+} response (Figure 5.32 B). Interestingly, mβCD had no effect on the baseline or Ca^{2+} responses in TRPV4 expressing CHO cells (Figure 5.32 C).

The data show that in addition to cholesterol enrichment of cell membranes, the removal of cholesterol can also modulate TRPM3 and other TRP family members. Cholesterol depletion removes tonic inhibition of TRPM3, increasing the starting baseline for recordings. The same is true for TRPC5, and in addition the Gd^{3+} response is potentiated in the absence of cholesterol. However, cholesterol depletion inhibits the TRPM2 H_2O_2 response, and has no effect on TRPV4-expressing cells. The data provides evidence that cholesterol can differentially regulate TRP channels in the plasma membrane.

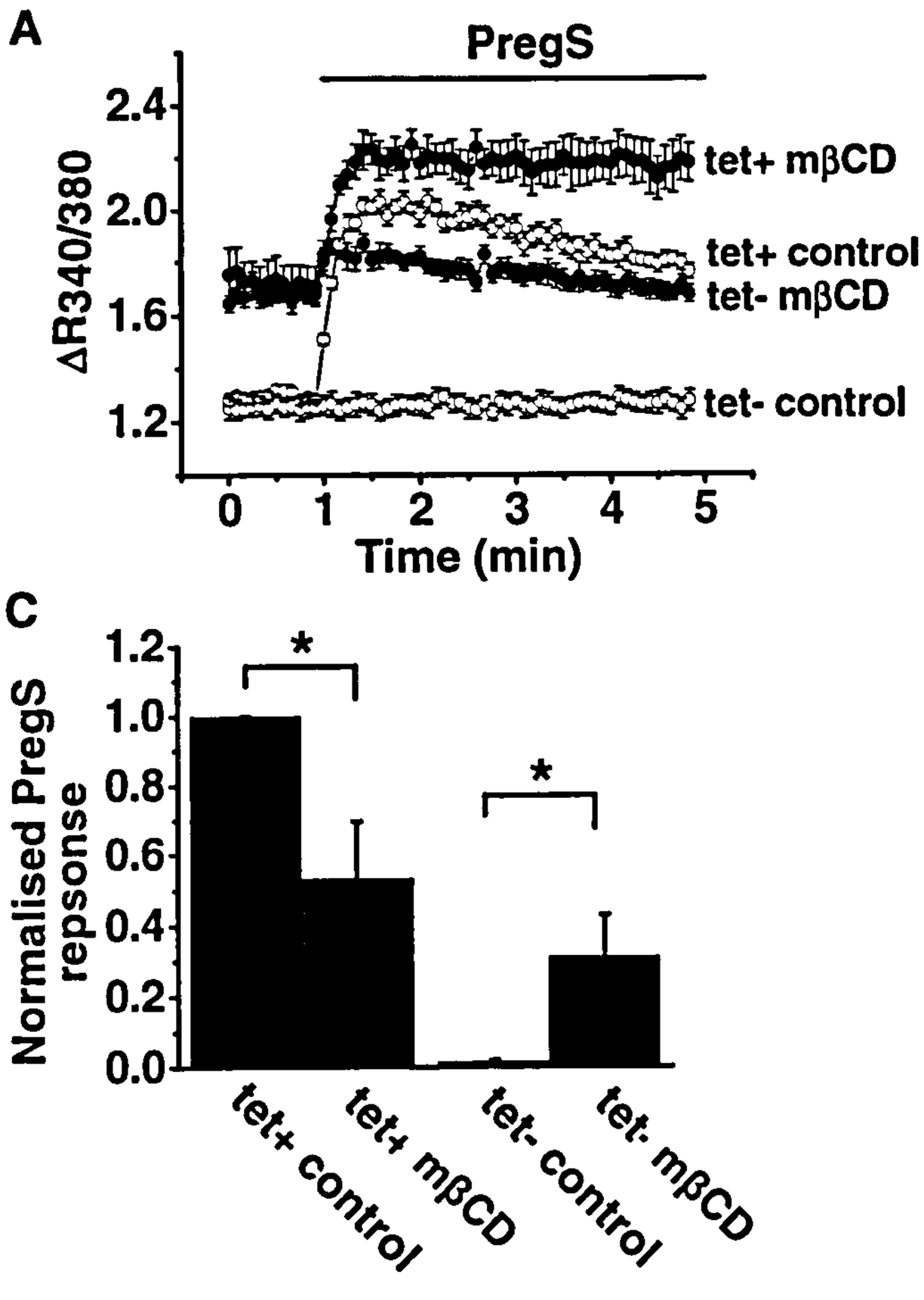

Figure 5.31. Methyl β-cyclodextrin preincubation modulates TRPM3 Ca^{2+} signals were measured as the 340/380 nm ratio of emission in fura-2 loaded cells. Cells were induced by incubation with tetracycline (tet+). Cells not treated with tetracycline were included as a control (tet-). **A.** Mean data (±SEM) from 6 wells within a single plate show that methyl β-cyclodextrin (mβCD) preincubation (10 mM) causes an increase in starting baseline for recordings. **B.** Mean data (±SEM) showing significant increase in baseline (n/N=3/18). **C.** Baseline subtracted mean data (±SEM) taken 1 min after PregS application. The tet+ PregS Ca^{2+} response is reduced in mβCD treated cells, whereas Ca^{2+} responses in tet- cells are increased in mβCD treated cells (n/N=3/18).

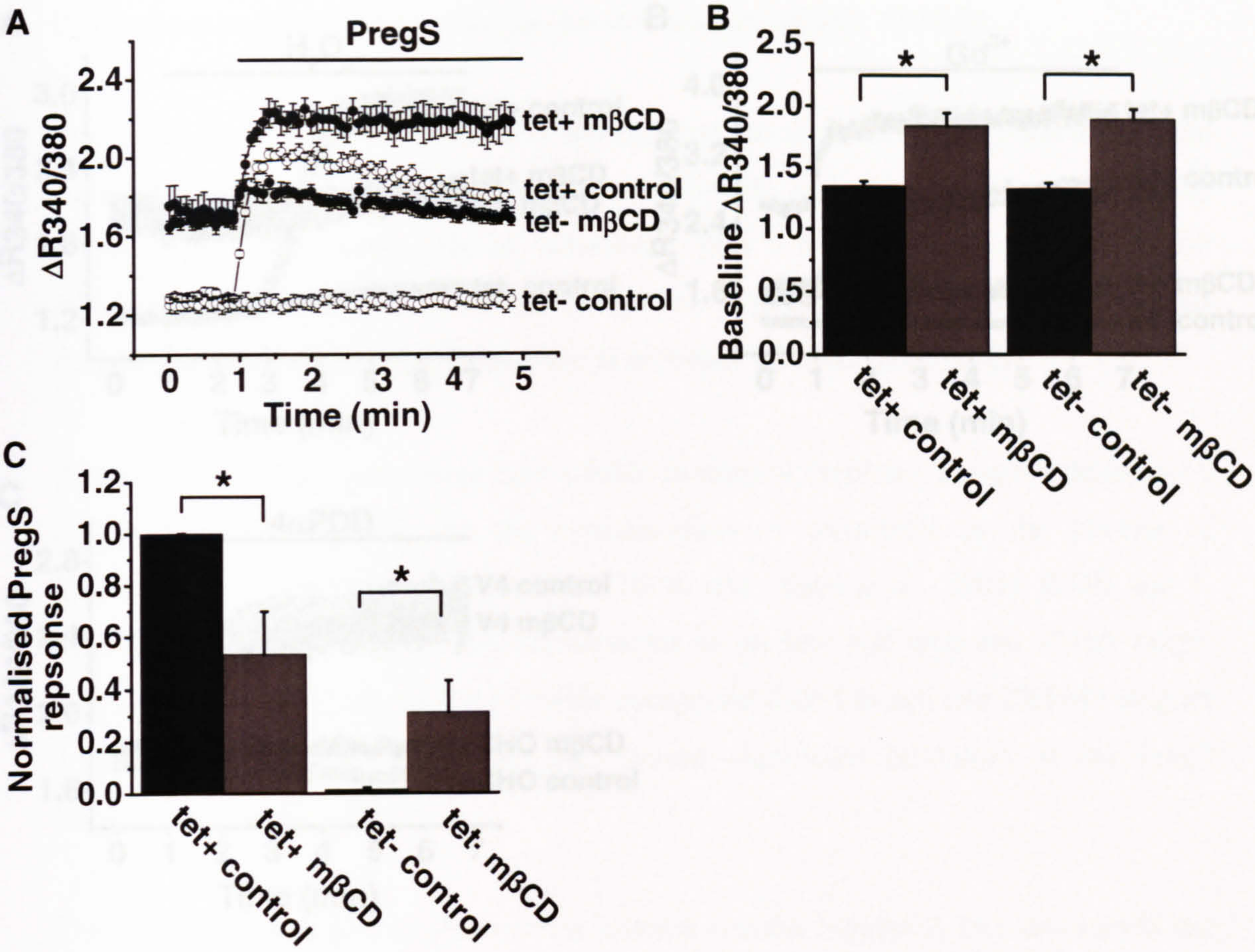

Figure 5.31. Methyl β-cyclodextrin preincubation modulates TRPM3 Ca^{2+} signals were measured as the 340/380 nm ratio of emission in fura-2 loaded cells. Cells were induced by incubation with tetracycline (tet+). Cells not treated with tetracycline were included as a control (tet-). **A.** Mean data (±SEM) from 6 wells within a single plate show that methyl β-cyclodextrin (mβCD) preincubation (10 mM) causes an increase in starting baseline for recordings. **B**. Mean data (±SEM) showing significant increase in baseline (n/N=3/18). **C.** Baseline subtracted mean data (±SEM) taken 1 min after PregS application. The tet+ PregS Ca^{2+} response is reduced in mβCD treated cells, whereas Ca^{2+} responses in tet- cells are increased in mβCD treated cells (n/N=3/18).

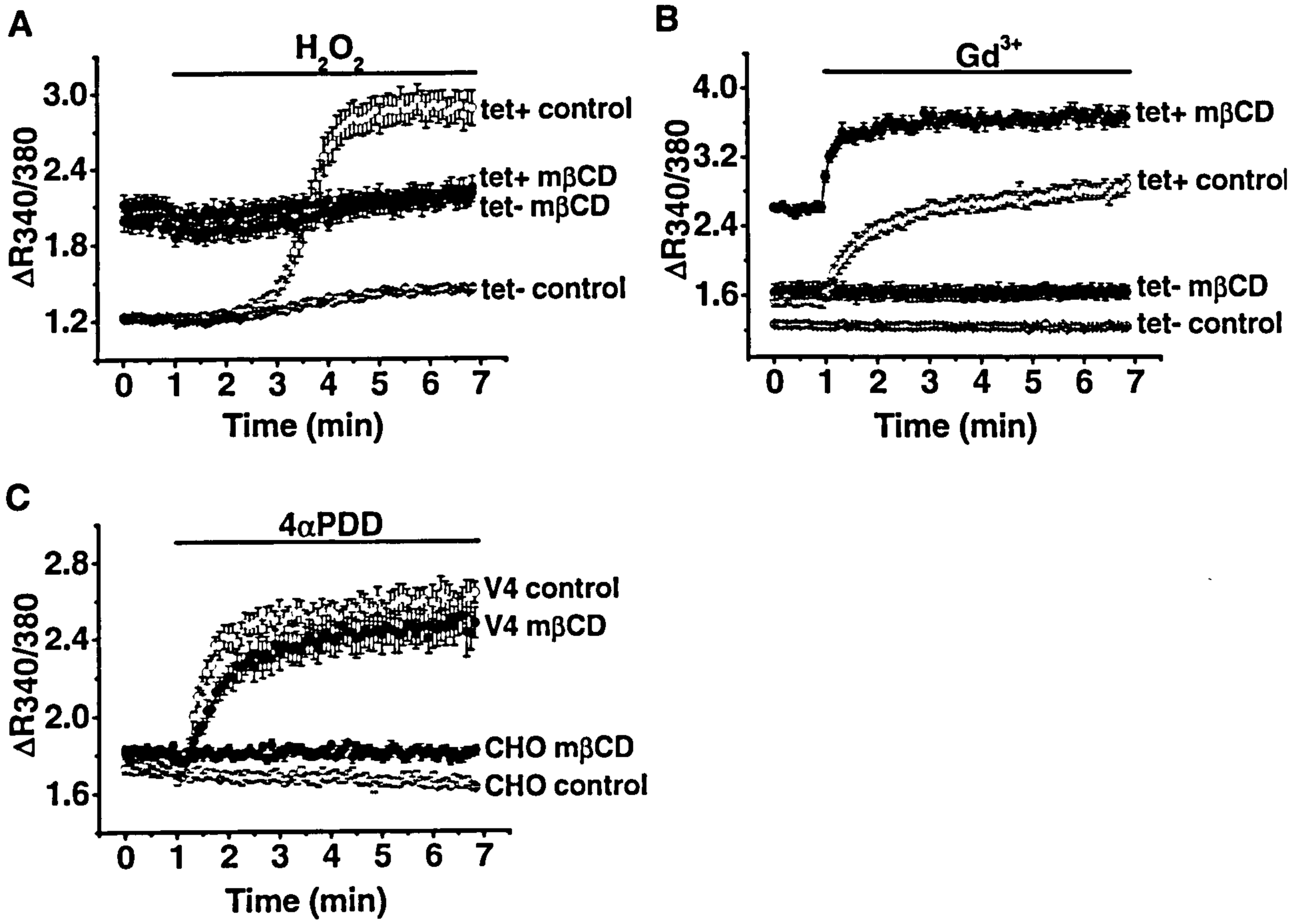

Figure 5.32. Cholesterol enrichment effect on other TRP channels Ca^{2+} signals were measured as the 340/380 nm ratio of emission in fura-2 loaded cells. TRPM2 and TRPC5 cells were induced by incubation with tetracycline (tet+). Cells not treated with tetracycline were included as a control (tet-). For TRPV4 cells, CHO parent cells were included as a control. Representative mean data (±SEM) shown are from 6 wells within a single plate for each cell type. **A.** mβCD (10 mM) preincubation inhibits H_2O_2 activation of TRPM2. **B.** mβCD potentiates Gd^{3+} (100 μM) activation of TRPC5. **C.** mβCD does not affect TRPV4 activation by 4αPDD (10 μM).

Cholesterol analogues important in the vasculature inhibit TRPM3

The metabolism of dietary cholesterol involves oxidation of the double bond to produce oxysterols including 7-β-hydroxycholesterol (β-OH) and 7-ketocholesterol (7-keto) (Figure 5.33). These oxysterols are believed to play a role in the development of the atherosclerotic plaque (Brown *et al.*, 1999). The importance of oxysterols in vascular disease makes them of particular interest as potential TRPM3 modulators.

The oxysterols investigated were both soluble in ethanol (vehicle); therefore delivery by mβCD was not required. As the concentration of oxysterols in the plasma of hypercholesterolemic patients is between 20-30 μM (Biasi *et al.*, 2004), β-OH and 7-keto were applied at 2 different concentrations at the low and high end of this range. The application of 10 or 50 μM of either compound failed to activate TRPM3 (Figure 5.34 A&B). However, β-OH (50 μM) caused significant inhibition of the PregS response (Figure 5.34 C).

The data indicate that in addition to cholesterol, certain oxysterols can also inhibit the TRPM3 PregS response.

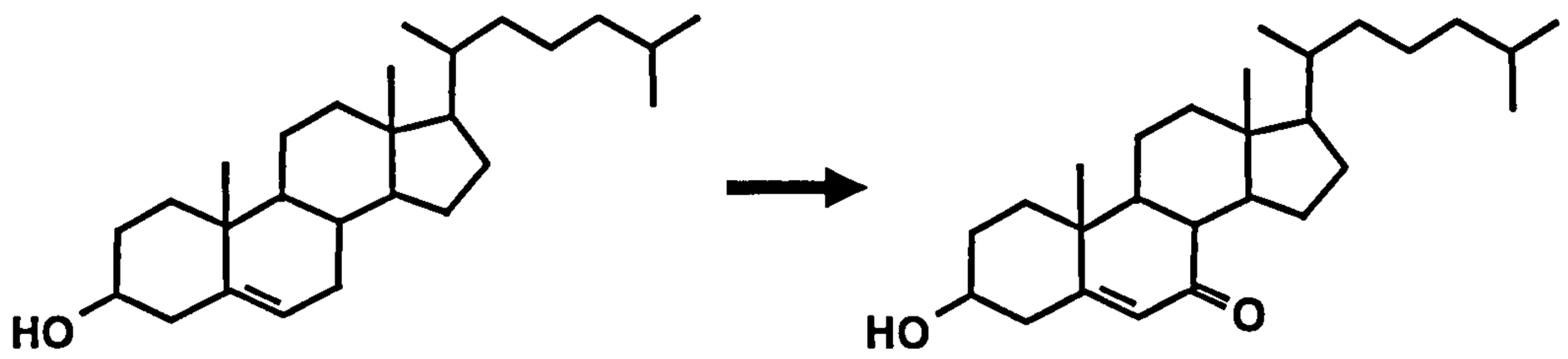

cholesterol

7-ketocholesterol

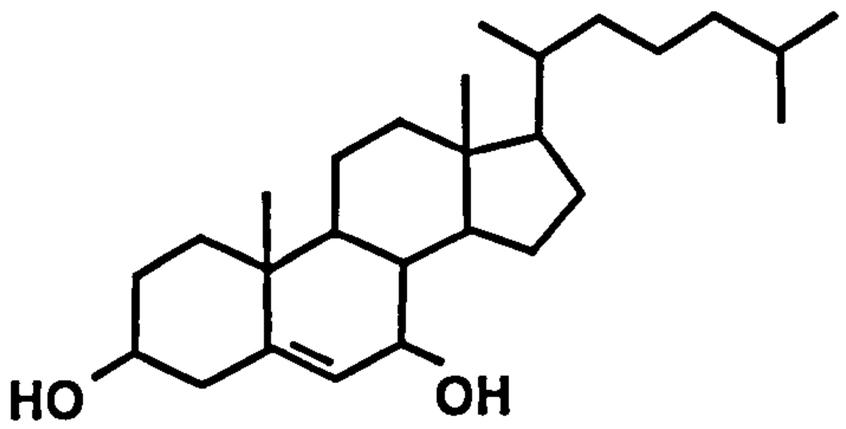

7-β-hydroxycholesterol

Figure 5.33. Biosynthesis of cholesterol analogues Chemical structures of cholesterol and the common oxysterols 7-ketocholesterol and 7-β-hydroxycholesterol.

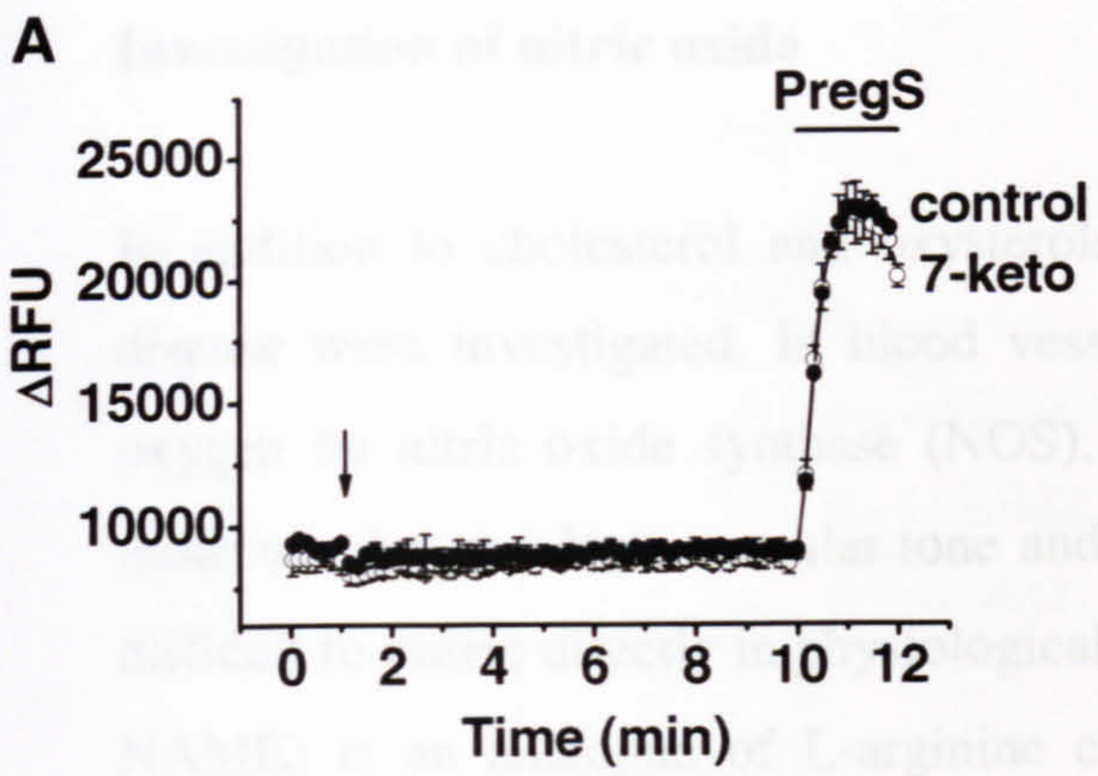

Figure 5.34 Effect of cholesterol analogues on the PregS response Changes in Ca^{2+} were measured as relative fluorescence units (RFU) in fluo-4 loaded tet+ cells. Ethanol (vehicle) was present throughout recordings. 1st addition of test compound or control at 1 min indicated by arrow, followed by 2nd addition of PregS control at 10 min. Traces are mean data (±SEM) from 3 wells within a single plate and show effect on the PregS response by **A.** 7-Ketocholesterol (7-keto, 50 μM) and **B.** 7-β-hydroxycholesterol (β-OH, 50 μM). **C.** Mean data (±SEM) show effect on Ca^{2+} responses 1 min after PregS application (n/N=3/9). Control refers to 1st application of vehicle (DMSO), followed by PregS addition, to which data are normalised.

Investigation of nitric oxide

In addition to cholesterol and oxysterols, further compounds implicated in vascular disease were investigated. In blood vessels, NO is synthesised from L-arginine and oxygen by nitric oxide synthase (NOS), and is an important inter-cellular signalling molecule that regulates vascular tone and blood pressure. NO is gaseous and therefore difficult to utilise directly in physiological studies. N^G-Nitro-L-arginine methyl ester (L-NAME) is an analogue of L-arginine characterised as an inhibitor of NOS, and is therefore useful for decreasing NO levels in cells and tissues. Alternatively, (±)-*S*-nitroso-*N*-acetylpenicillamine (SNAP), a derivative of nitrosothiol, can be used to release NO.

Preincubation of TRPM3-expressing cells with L-NAME (100 μM) slightly inhibited PregS (10 μM)-induced Ca^{2+}-responses in TRPM3-expressing cells (Figure 5.35 A). The mean data indicate that L-NAME can significantly inhibit TRPM3 by ~23% (Figure 5.35 C). It therefore seemed that an NO donor might potentiate the PregS response. However preincubation with SNAP (100 μM) did not affect the PregS response (Figure 5.35 B). In addition, direct application of SNAP (300 μM) did not activate TRPM3 when compared to the control PregS application (Figure 5.35 D).

In summary, the inhibition of PregS responses following L-NAME preincubation suggests that endogenous product of NOS may slightly potentiate TRPM3 activity, however the direct application of NO via SNAP failed to activate the channel.

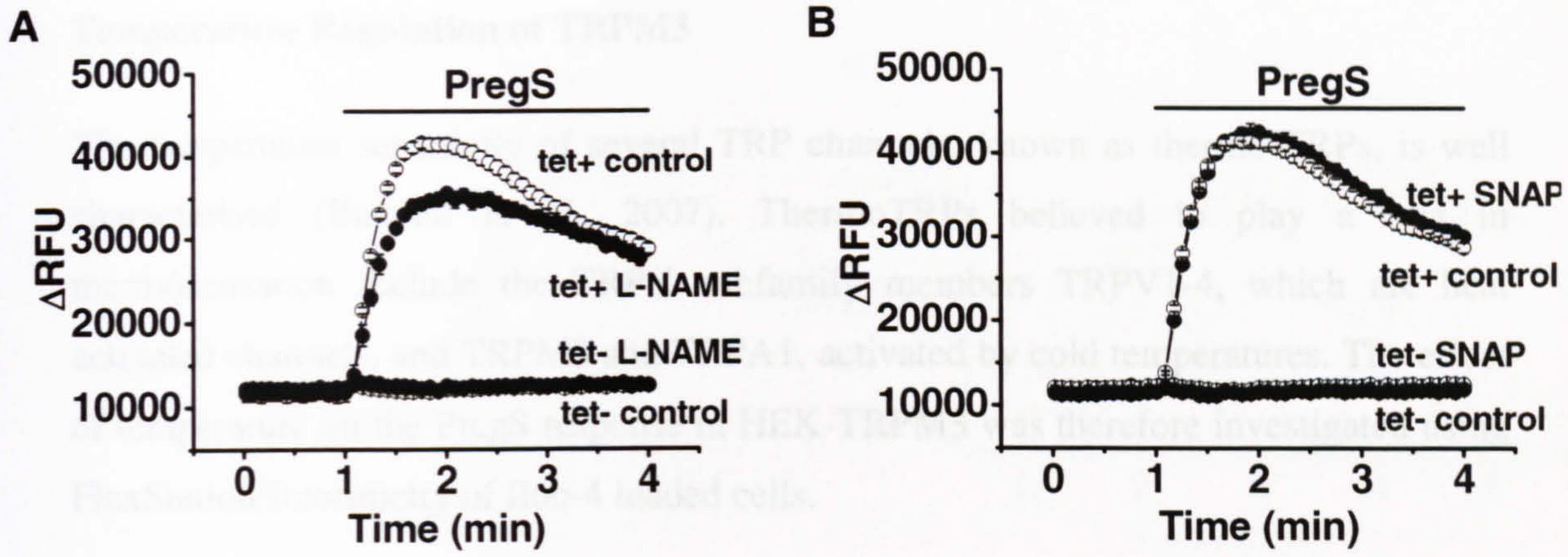

Figure 5.35. Nitric oxide effect on PregS induced Ca^{2+} response in tet+ TRPM3 cells Changes in Ca^{2+} were measured as relative fluorescence units (RFU) in fluo-4 loaded cells. DMSO (vehicle) was present throughout recordings, which were performed at RT. **A.** Representative mean data (±SEM) from 6 wells within a single plate show inhibition of PregS-response following preincubation with L-NAME (100μM). **B.** SNAP (100μM) preincubation did not affect the PregS-response. **C.** Mean data (±SEM) for PregS response inhibition taken 1 min after PregS application (10 μM), normalised to control response (control n/N=7/27, L-NAME n/N=6/21, SNAP=7/25). **D.** Mean data (±SEM) showing activation in tet+ (black) compared to tet- (grey) cells.

Temperature Regulation of TRPM3

The temperature sensitivity of several TRP channels, known as thermo-TRPs, is well characterised (Bandell *et al.*, 2007). ThermoTRPs believed to play a role in thermosensation include the TRPV subfamily members TRPV1-4, which are heat activated channels, and TRPM8 and TRPA1, activated by cold temperatures. The effect of temperature on the PregS response in HEK-TRPM3 was therefore investigated using FlexStation fluorimetry of fluo-4 loaded cells.

To demonstrate temperature dependence in TRP channels, experiments were first performed with TRPM2- and TRPV4-expressing cells. TRPM2 is activated by warm temperatures, and β-NAD^+- or ADP-ribose activation is potentiated (Togashi *et al.*, 2006). In agreement with this study, physiological temperature (37°C) potentiated the H_2O_2 response in TRPM2-expressing cells compared to RT resulting in a more rapid response, and also increased the starting baseline, indicating TRPM2 was already activated prior to H_2O_2 addition (Figure 5.36 A). Physiological temperatures are also reported to activate TRPV4 (Nilius *et al.*, 2004b). As for TRPM2, at 37°C the starting baseline was increased, consistent with temperature activation of TRPV4. However there was no effect on the maximum 4αPDD response, suggesting temperature and 4αPDD are independent activators of TRPV4 (Figure 5.36 B).

In TRPM3-expressing cells, PregS activated a rapid and sustained Ca^{2+} response at RT, whereas at 37°C the response was transient and had a much higher baseline (Figure 5.36 C). At 37°C the starting baseline was significantly higher for both TRPM3-expressing (tet+) and non-induced (tet-) cells. However as the baseline at 37°C for tet+ cells was significantly higher than for tet- cells, this indicates temperature activation of TRPM3 (Figure 5.36 D).

Background-subtracted data show that the magnitude and concentration dependence of PregS responses was not affected by temperature (Figure 5.37 A&B). Fitting of the Hill equation to mean data taken from the peak of the PregS response gave the EC_{50} at RT as 1.3 ± 0.16 μM, with a hill coefficient of 1.3 ± 0.18, while at 37°C this was slightly shifted right to 1.8 ± 0.24 μM, with a hill coefficient of 1.2 ± 0.15 (Figure 5.37 C).

It is evident that temperature is an important regulatory mechanism of TRP channel activity, and physiological temperature can significantly affect TRPM3 Ca^{2+} responses.

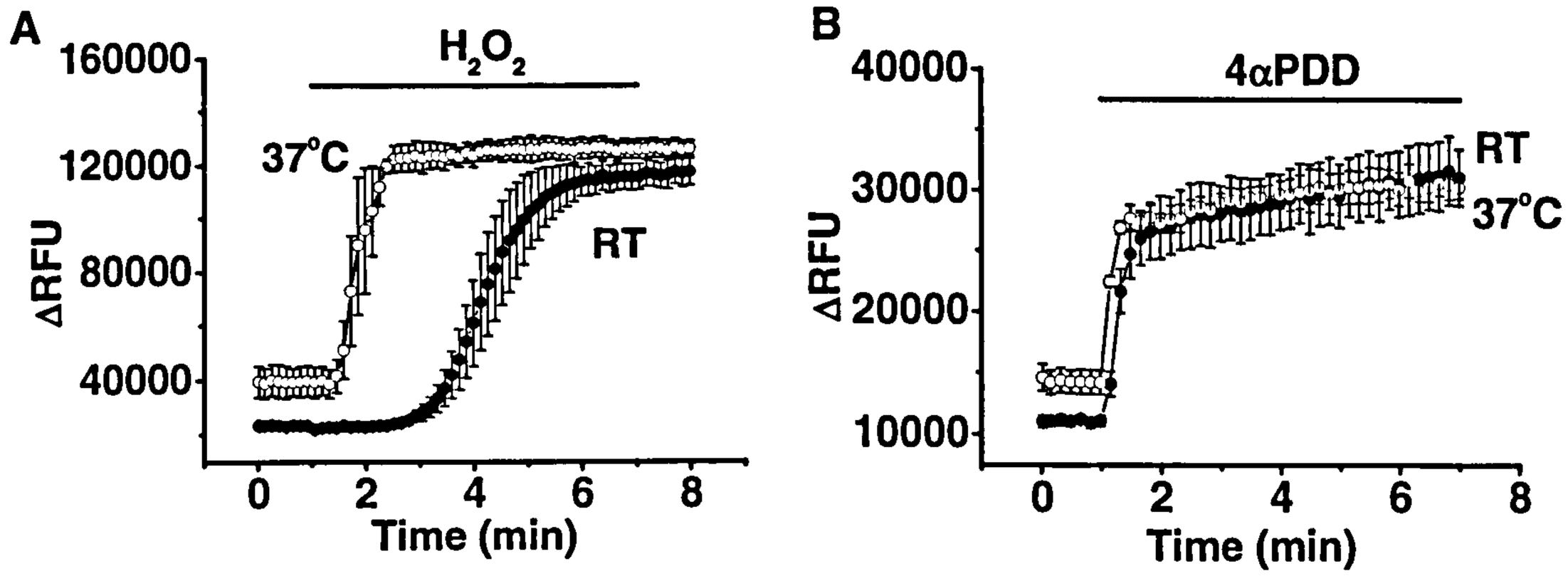

Figure 5.36. Temperature regulation of TRP channels Changes in Ca^{2+} were measured as relative fluorescence units (RFU) in fluo-4 loaded cells. TRPM2 and TRPM3 cells were induced by incubation with tetracycline (tet+). Traces are mean data (±SEM) from 6 wells within a single plate. Appropriate vehicle was present throughout recordings. **A.** Physiological temperature potentiates the TRPM2 H_2O_2 (1 mM) response. **B.** Physiological temperature does not affect the maximum TRPV4 4αPDD (10 μM) response. **C.** Physiological temperature increases the starting baseline for recording, and results in a more transient PregS response. **D.** Mean data (±SEM) showing effect of temperature on the starting baseline for TRPM3 recordings (n/N=3/18).

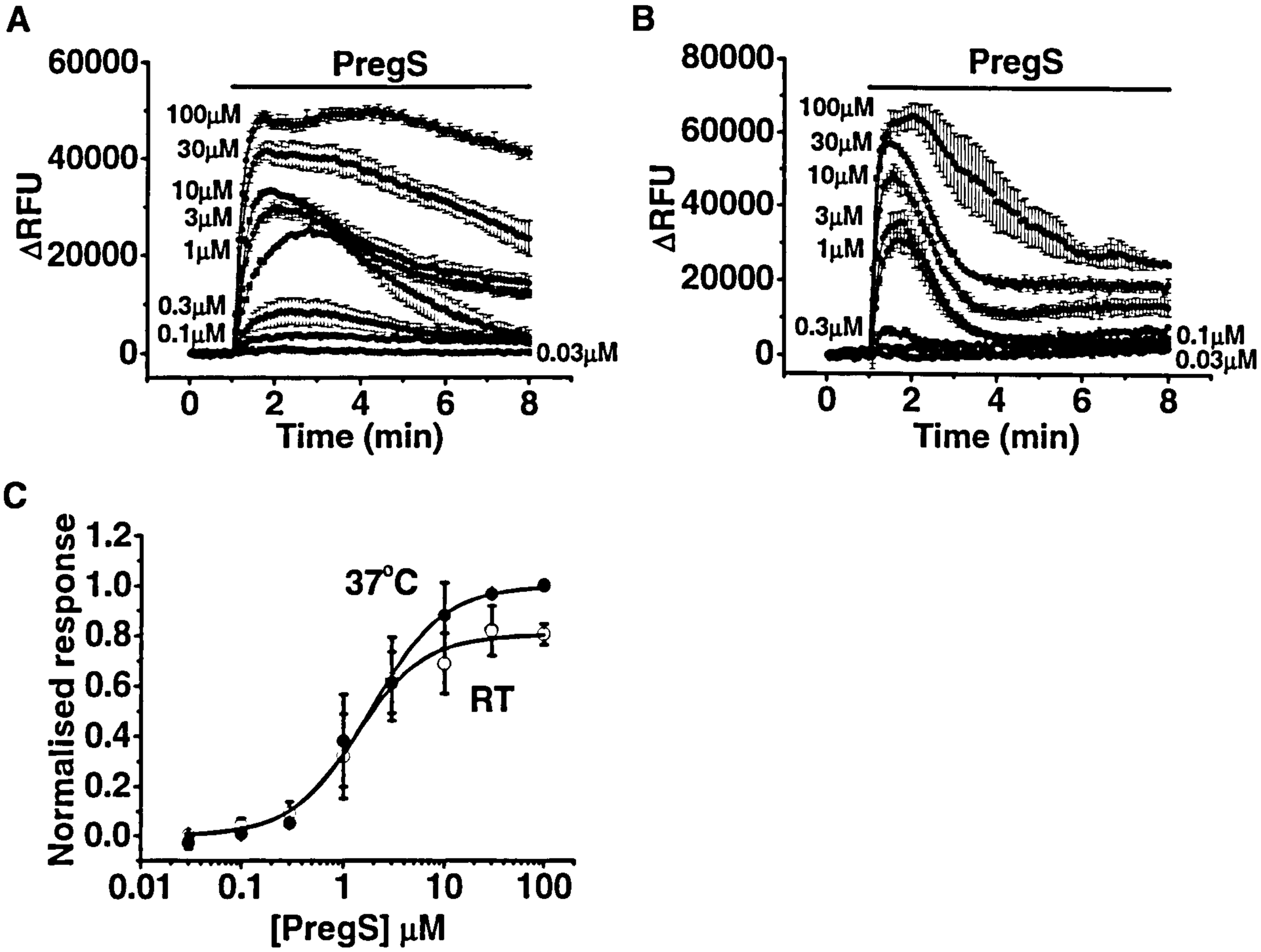

Figure 5.37. Temperature effect on PregS induced Ca^{2+} response in tet+ TRPM3 cells Cells were induced by incubation with tetracycline (tet+). DMSO (vehicle) was present throughout recordings. Representative nean data (±SEM) from 3 wells within a single plate show dose-dependent activation of TRPM3 expressing cells in response to PregS (0.03-100 μM) at **A.** RT and **B.** 37°C. **C.** Mean dose response data (±SEM) taken 1 min after PregS application and analysed using the Hill equation (n/N=3/9).

Discussion

The data presented in this chapter demonstrate that TRPM3 can be regulated by several different compounds and mechanisms, and that HTS is a useful method for identifying leads to search for ion channel modulators. Novel and seemingly selective small molecule inhibitors of TRPM3 include antipsychotics and antidepressants, CaM antagonists and ruthenium red, while nifedipine and local anaesthetics activate or potentiate the activation of the channel respectively. Apparent physiologically relevant modulators include PIP_2, cholesterol and temperature. TRP channels are commonly activated by several different signals within a single cell. TRPC5 exhibits both store-operated and receptor activation, and can also be activated by lanthanides and intracellular Ca^{2+} (Zeng *et al.*, 2004). Similarly, TRPV4 is gated by several factors, including hypotonicity, heat, 4αPDD, arachadonic acid (AA), endocannabinoids and epoxyeicosatrienoic acids (Nilius *et al.*, 2004b).

Pregnenolone analogues have opposite effects on TRPM3 activity

Data presented in previous chapters of this study revealed PregS is a novel activator of TRPM3. Interestingly, pregnenolone analogues do not activate TRPM3, and instead progesterone and 5β-pregnan-3α-OL-20-one cause dose-dependent inhibition (Figure 5.3). The differential activities of pregnenolone analogues and isomers are well characterised for ligand-gated ion channels including $GABA_A$ and NMDA receptors. Non-sulphated neurosteroids such as pregnanolone and allopregnanolone potentiate $GABA_A$ receptor function, while sulphated steroids like PregS are inhibitory, presumably as a result of the negatively charged sulphate group in the C-3 position (Park-Chung *et al.*, 1999). However this sulphate group is not essential for inhibition, as DHEA also inhibits $GABA_A$ receptors, albeit less potently than DHEAS. Sulphated and non-sulphated steroid do not share the same binding site, and as a further level of complexity the non-sulphated steroids require 3α stereochemistry for activity. The PregS inhibition of the receptor is independent of GABA binding, channel activation state, or membrane potential. In other words PregS is a non-competitive antagonist that acts allosterically, rather than occluding the ion pore (Gibbs *et al.*, 2006).

PregS also potentiates NMDA receptors. However analogues that differ only in the absence of the C-5 C-6 double bond such as pregnanolone sulphate and epipregnanolone sulphate, bind to distinct modulatory sites and inhibit NMDA activity (Park-Chung *et al.*, 1997). Pregnenolone and pregnanolone are inactive at NMDA receptors, suggesting the C-3 sulphate is again important for activity. Further study is needed to determine the mechanism of TRPM3 activation by PregS, but stereochemistry may prove to be major factor in TRPM3 modulation.

Established TRP regulatory mechanisms also modulate TRPM3

A common mechanism of TRP channel regulation is by PIP_2. PIP_2 activates the TRPM family members TRPM5, TRPM7 and TRPM8, plus the TRPV members TRPV5 and TRPV6, and has both an inhibitory and activating effect on TRPV1 (Lukacs *et al.*, 2007; Rohacs *et al.*, 2005). In contrast to other TRPM family members, this study demonstrates extracellular PIP_2 inhibition of TRPM3 and TRPM2 (Figure 5.5 & 5.23). The mechanism of TRPM inhibition by PIP_2 is not clear. Diacylglycerol (DAG) is produced as a result of PLC-mediated PIP_2 hydrolysis, and has an inhibitory action on TRPC1, 4 and 5 that is mediated by PKC (Venkatachalam *et al.*, 2003). The effect of PKC activation as an inhibitory mechanism of TRPM3 activity has not been examined, however the PKC inhibitor bisindolylmaleimide I (BIM I) strongly inhibited TRPM3 activity, suggesting PKC inhibition can also regulate the channel (Figure 5.11). This would suggest that perhaps PIP_2 has a direct effect on the TRPM3 channel. The C terminus of TRPV1 binds PIP_2 directly (Prescott *et al.*, 2003). Three positively charged residues within the conserved TRP domain motif are fully conserved in all TRPM family members, including TRPM3, and are responsible for PIP_2 sensitivity in TRPM8 required for PIP_2 binding in TRPM8 and TRPV5 (Rohacs *et al.*, 2005). This motif is also conserved in TRPM3, so it is perhaps not surprising that the channel appears to be regulated by PIP_2.

The majority of members of the TRP superfamily contain N- and C-terminal binding motifs that can interact the Ca^{2+}-sensing protein, calmodulin (CaM) and the binding of CaM is a common regulatory mechanism (Zhu, 2005). Although specific CaM binding sites have yet to be identified for TRPM3, this chapter demonstrates that the CaM inhibitors W-7, calmidazolium chloride (CMZ), chlorpromazine (CPZ) all inhibit

PregS-activation of TRPM3 (Figure 5.12 & 5.15). The same CaM inhibitors can also inhibit the activation of TRPC5 by disrupting signalling protein complexes (Kim *et al.*, 2006; Shimizu *et al.*, 2006). Conversely, CMZ activates TRPC4β, suggesting Ca^{2+}/calmodulin binding to TRPC4 channels causes inhibition of the channel (Walker *et al.*, 2002). The inhibition of the PregS response by CaM antagonists suggests CaM-binding may be an important regulatory feature of TRPM3, and further study to demonstrate the exact mechanism and the possible association with signalling protein complexes is required.

TRPM3 is activated by hypotonic shock (Grimm *et al.*, 2003), which is a common mechanism of activation for several TRP channels, including TRPC1, TRPC6, TRPV2, TRPM2, TRPM4 and TRPP2 (Kraft *et al.*, 2005). It has been suggested that the activation of TRPV4 by hypotonic shock is due to the cell swelling that results from PLA_2-mediated release of arachadonic acid (AA) and its metabolites (Stutzin *et al.*, 2006). Downstream products of PLA_2 do not activate TRPM3; for example, AA and LPC have no effect (Grimm *et al.*, 2005), nor do the majority of intermediates in AA metabolism, such as prostaglandins, leukotrienes and hydroxyeicosatetraenoic acids (HETEs) (Figure 5.7-5.10). However the endogenous lipid mediator hepoxillin A3, which activates the release of AA and DAG, did cause a small but significant activation of TRPM3 (Figure 5.9). Therefore AA metabolism cannot be completely ruled out as a mechanism for TRPM3 activation. Stretch-activated channels can be inhibited by chlorpromazine (CPZ), which interacts with membrane phospholipids to produce a concave curvature of the plasma membrane, an effect which is opposite to causing membrane stretch (Maingret *et al.*, 1999). CPZ inhibited PregS-activation of TRPM3 (Figure 5.12 & 5.21). This would suggest that PregS may need to insert into the plasma membrane to exert its effect in order access its TRPM3 binding site, thus causing a change in the curvature or fluidity of the surrounding membrane which regulates the channel.

TRPM3 baseline activity and PregS-induced Ca^{2+}-responses were potentiated by increased temperature (Figure 5.36). Temperature is a common modulator for several TRP channels involved in peripheral thermosensation (Huang *et al.*, 2006). The ability of TRPM8 and TRPV1 to sense temperature change has been linked to the intrinsic voltage dependent gating of the channels, and channel activation results from a shift in the voltage dependence of activation (Voets *et al.*, 2004a). Domain swapping studies

using TRPV1 and TRPM8 have demonstrated that residues necessary for thermosensation exist in the C terminus (Brauchi *et al.*, 2006).

Novel modulators with vascular importance

Cholesterol enrichment of the plasma membrane regulates TRPM3 (Figure 5.29). Cholesterol is an essential component of cell membranes and an important constituent of lipid rafts. These specialised regulatory membrane domains are enriched in cholesterol and protein components required for cell signalling. Cholesterol is also known to regulate ion channels, including TRP channels. Vascular store-operated calcium (SOC) activity is reduced following cholesterol depletion by cyclodextrin, presumably as a result of disruption of lipid rafts and the redistribution of TRPC1 channels (Bergdahl *et al.*, 2003). Furthermore, direct application of cholesterol-saturated mβCD activates TRPC3 and the induced cholesterol enrichment promotes TRPC3 expression at the plasma membrane (Graziani *et al.*, 2006). As previously discussed, ankyrin repeats have not been identified in TRPM3 channels. Therefore there is as yet no data to suggest TRPM3 can anchor itself to the cytoskeleton and associate with lipid rafts. Further study will demonstrate whether TRPM3 activity is dependent on changes in raft structure as a mechanism for regulating the channel in different cell types or in disease states where cholesterol levels are increased.

The direct application of mβCD caused significantly greater basal Ca^{2+} entry in TRPM3-expressing cells (Figure 5.31 A & B). This would suggest that membrane bound cholesterol is tonically inhibiting the constitutive activity of TRPM3, and its depletion by mβCD allows Ca^{2+} entry through the channel. It is interesting that cholesterol and the potent TRPM3 activator PregS are very similar in structure, and it is possible that they share a binding site on the channel. If this were true, PregS may exert its activatory effect by displacing cholesterol and releasing the tonic inhibition of the channel. Following preincubation with mβCD, tet- cells also displayed an increased basal Ca^{2+} entry, and responded to PregS (Figure 5.31 C). The data in Chapter 3 of this thesis demonstrated that SPH caused a small Ca^{2+}-response in tet- cells that was sensitive to block by TM3E3, suggesting it was the result of native TRPM3. RT-PCR confirmed TRPM3 expression; however PregS did not cause activation in the tet- cells. The data in this chapter (Figure 5.31) would suggest that mβCD has removed the tonic

inhibition of native TRPM3 in tet- cells, allowing for the activation of channels by PregS in tet-. SPH activation of the channel must occur via a distinct, cholesterol-independent mechanism.

Platelet-activating factor (PAF) is a pro-inflammatory lipid mediator that, unlike other phospholipid-derived mediators, functions as an intact phospholipid and binds a specific G-protein-coupled receptor to mediate intracellular effects. The carbon-16 compounds PAF-16 and lyso PAF-16 inhibited TRPM3, but the carbon-18 compounds PAF-18 and lyso PAF-18 did not (Figure 5.10). PAF-16 could also inhibit endogenous ATP responses in TRPM3-expressing cells (Figure 5.22), but did not inhibit H_2O_2-responses in TRPM2-expressing cells (Figure 5.23). This suggests that while PAF-16 may selectively inhibit TRPM3, it perhaps does not directly affect the TRPM3 channel. In relation to the underlying theme of this study, the progression of atherosclerosis, the PAF receptor (PAF-R) is expressed in human carotid arterial SMC of contractile phenotype, suggesting it is relevant to their proliferation and migration to invade the initima to form atherosclerotic plaques (Brocheriou *et al.*, 2000). As the previous chapter demonstrated TRPM3 is also expressed in the vasculature, the activity of PAF-R and TRPM3 channel may be directly related. TRPM3 inhibition was not related to products downstream of PAF-R activation, such as PLC induced DAG production, or PLA_2 induced AA, prostaglandin or leukotrienes (Grimm *et al.*, 2005). Furthermore the inactive lyso PAF-16 and PAF-16 antagonist both also inhibited PregS- and ATP-responses, further evidence that PAF-16 modulation of TRPM3 is independent of PAF-R activation.

L-NAME preincubation slightly inhibited subsequent activation of TRPM3 by PregS (Figure 5.35). However, it is unclear whether L-NAME exerts its effect on the TRPM3 channel indirectly by inhibiting the NO pathway (through competitive antagonism of NOS), or directly by interacting with the channel to prevent subsequent activation. L-NAME can bind to and inhibit the nicotinic acetylcholine receptor (nAChR) (Scheller *et al.*, 1998), so a direct effect on the TRPM3 channel that does not involve NO production cannot be ruled out. This may also explain why direct application of NO using SNAP did not activate the channel. The ineffectiveness of SNAP could also be explained if it is not NO, but some other intermediate, which inhibits TRPM3. The NO produced by L-NAME can rapidly react with superoxide to form the potent oxidant perxoynitrite (Murphy *et al.*, 1998). Peroxynitrite is a highly reactive species that can

induce lipid peroxidation, and is implicated in the development of atherosclerosis (Uppu *et al.*, 2007). Further investigation will elucidate whether the damaging effects of free radicals and their byproducts result from interactions with the TRPM3 channel.

Antipsychotics and antidepressants inhibit the PregS response

Antidepressants and antipsychotics display dose-dependant inhibition of TRPM3, regardless of their type (Figure 5.21). These drugs exert their effects by inhibiting the re-uptake of neurotransmitters, thereby increasing levels in the synapse in order to enhance mood. Other than direct effects in the central nervous system, the effect of these drugs elsewhere is poorly understood. Tricyclic antidepressants (TCA) in particular have been shown to inhibit ligand gated ion channels (LGIC) including nACh, GABA, NMDA and serotonin receptors (Ueta *et al.*, 2004). In addition, the two-pore domain K^+ channels TREK-1 and TREK-2, responsible for background or 'leak' K^+ current, are inhibited by both typical and atypical antipsychotic drugs with IC_{50} values in the micromolar range, similar to those obtained in this study for TRPM3 inhibition (Thummler *et al.*, 2007). Also, haloperidol binds to HERG K^+ channels and increases rate of their inactivation (Suessbrich *et al.*, 1997). The evidence suggests in addition to their major therapeutic effects, antipsychotics and antidepressants may also target ion channels expressed in the brain, including TRPM3, to mediate their effect or elucidate their side effects.

Summary

HTS has allowed for the development of a pharmacological profile for TRPM3, which will undoubtedly assist the understanding of biological function. The different modulatory properties of TRPM3 may be physiologically regulated by varying expression levels in different cell types, the differential expression of splice variants, or association with different signalling protein complexes. The expression of the TRPM3 channel in both in brain tissue and throughout the vasculature, plus regulation by known antipsychotic and anti-atherogenic modulators suggests a functional role in psychosis or the development of atherosclerosis. Ultimately the increased understanding of TRPM3 pharmacology and function may provide a basis to chemically improve existing modulators to produce more selective, improved agonists, or even drugs.

Chapter 6

Conclusions and further experiments

General summary

The aim of my thesis was to investigate the expression, modulation and biological function of the transient receptor potential channel TRPM3. These investigations were assisted by the development of a set of pharmacological tools specific for TRPM3. E3 targeting (Xu *et al.*, 2005b) was used to design and develop TM3E3, an antibody that served as a selective inhibitor of the TRPM3 ion channel. The antibody could specifically bind the channel in live cells, producing an inhibitory effect against known activators of TRPM3. Furthermore the development of a stable TRPM3 cell line allowed for the use of medium throughput technologies to search for TRPM3 modulators, and led to the identification of a novel TRPM3 inhibitor, cholesterol.

In combination these tools were used to explore the expression of TRPM3 in vascular smooth muscle. TM3E3 blocked endogenous TRPM3 channels, and proved a useful tool in the elucidation of native channel function. My findings suggest that TRPM3 is a functional Ca^{2+} channel of vascular smooth muscle cells, with a protective role as an inhibitor of MMP-9 and IL-6 secretion. Although the mechanism by which TRPM3 regulates secretion has yet to be determined, both MMP-9 and IL-6 play important roles in vascular remodelling, which contributes to vascular diseases such as atherosclerosis.

Screening a chemical library allowed me to find further TRPM3 modulators with potential vascular relevance. In particular cholesterol and an oxysterol inhibited TRPM3, and these effects may contribute to the damaging effects of these agents in coronary artery disease. It was originally hoped that TM3E3 may have therapeutic potential, although my data suggest that for neointimal hyperplasia and atherosclerosis it is a TRPM3 activator that would have therapeutic value. However, it remains to be seen whether the antibody could benefit situations where VSM profliferation and migration are necessary, such as providing new blood supply to skin grafts.

Ultimately, a better understanding of TRPM3 is required, aided by the selective TM3E3 tool, which may identify novel TRPM3 modulators that are suitable as therapeutic agents. While the findings of this study help the understanding of TRPM3

pharmacology and function, and provide a basis to develop novel therapeutic approaches to the treatment of cardiovascular disease, further investigation is still required.

Further experiments to investigate TRPM3 activation

The first chapter of the study identified PregS as a novel activator of TRPM3. PregS activated TRPM3 independently of store depletion, but its exact mechanism of action is not clear. Further experiments are required to determine whether PregS can directly bind to the TRPM3 channel, or whether it acts indirectly via signalling pathways, perhaps involving intracellular sigma (σ) or steroid receptors. Although expressed in a number of tissues including liver, spleen, testis, ovary, placenta and adrenal gland, σ receptor expression has not been demonstrated in vascular smooth muscle (Ola *et al.*, 2001). A combination of RT-PCR and immunostaining might demonstrate σ receptor expression, and perhaps show colocalisation with TRPM3. The dependence of TRPM3 activation on σ receptors could be investigated further using siRNA knockdown of the σ receptor gene, which might inhibit the PregS response. Furthermore, inhibitors specific for downstream intermediates in σ receptor signalling cascades could be used to investigate their involvement in the activation of the TRPM3 channel. If these experiments suggest direct PregS binding to TRPM3 this could be confirmed by excised patch data and lipid bilayer experiments to explore if PregS activates single channels in isolation. Mutagenesis could be employed to identify the PregS binding site, and may help determine the importance of stereochemistry, to develop new and more potent related activators.

Preincubation with thapsigargin (Tg) reduced the amplitude of the PregS-response. However, the Ca^{2+} response was completely inhibited in the absence of extracellular Ca^{2+}, suggesting that the PregS-induced Ca^{2+} response in TRPM3-expressing cells results entirely from Ca^{2+} influx across the plasma membrane. The inhibition observed with Tg is perhaps due to an initial increase in the baseline of resting cells, as a result of endogenous SOC activation, and then a saturation of the PregS response. This could be confirmed by repeating experiments with a less saturating concentration of PregS. In HSV SMC, Tg significantly inhibited TRPM3 responses, but did not affect the baseline. Further investigation is required to confirm this effect was a result of the involvement of

stores, such as repeating experiments in the absence of extracellular Ca^{2+} to demonstrate the responses result from Ca^{2+} influx. Alternatively the inhibitory action of Tg may prove to be as a result of changes in the local intracellular Ca^{2+} concentration, a known modulator of many TRP channels.

TRPM3 is a constitutively active channel (Grimm *et al.*, 2003). Chapter 5 of this study demonstrated that the constitutive TRPM3 activity was significantly increased at elevated temperatures. It would be interesting to repeat the chemical screening at physiological temperature in an effort to reveal previously ineffective activators, inhibitors and potentiators of the TRPM3 response. Constitutive activity could be further explored using whole cell patch clamping to investigate the direct application of TRP channel inhibitor Gd^{3+} and 2-APB, and even the TM3E3 antibody, on basal TRPM3 activity.

TRPM3 can also be activated by hypotonic shock, suggesting it may function as a stretch activated channel (Grimm *et al.*, 2003). My own data show that chlorpromazine, a compound that causes a concave curvature of the plasma membrane, inhibits TRPM3. Further experiments could involve the use of cell-attached voltage clamping to determine pressure sensitivity of TRPM3, or the application of the mechanosensitive channel activator 2, 4, 6-trinitrophenol to mimic membrane stretch and induce activation. Preincubation with TM3E3, or including the antibody in the patch pipette, should inhibit stretch activation, proving the effect is TRPM3-related.

Several agents known to modulate TRP channels were identified by the chemical screen as significant activators or inhibitors of the TRPM3 channel. Further experiments using PKC activators, or inhibitors of phosphoinositide 3-kinases such as wortmanin, could be used to investigate the mechanism of PIP_2 inhibition, which is suggested to directly bind other TRP channels (Rohacs *et al.*, 2005). The covalent modification of cysteine residues by agents including iodoacetamide and (2-aminoethyl)methanethiosulphonate activates TRPA1 (Macpherson *et al.*, 2007). In addition, free cysteine residues in TRPA1 are predicted to react with dihydropyridines, resulting in channel activation (C. Jones, personal communication). The dihydropyridine nifedipine caused significant TRPM3 activation. Cysteine modifying agents could be employed to discover a putative activation mechanism for TRPM3, providing further evidence for the polymodal nature of TRPM3.

Further experiments to characterise the TM3E3 antibody

The means by which E3-targeted antibodies cause channel inhibition has yet to be elucidated. All E3-targeted antibodies block by ~30-40% within 10 min of application, suggesting a shared mechanism of inhibition. Protein trafficking studies using fluorescent labels and immunostaining techniques may be useful to investigate the possibility that antibody-bound TRPM3 channels are internalised. If the data indicate a direct occlusion of the channel pore, it may be possible to target antibodies to different regions and even other extracellular loops in an effort to produce more effective inhibitors. The production of a monoclonal TRPM3 antibody is also possible. Although monoclonal E3-targeted antibodies have proven less effective channel blockers (Klionsky *et al.*, 2006), they are useful in that large amounts of identical antibodies can be produced, unlike polyclonal antibodies for which there is a finite supply.

Improvement of the antibody by affinity purification will further improve the use of the TM3E3 as a pharmacological tool. The removal of non-specific effects of the antiserum would allow for further experiments to search for TRPM3 expression in native tissue, particularly in techniques such as western blotting where non-specific bands are a problem. A useful, further, control for antibody selectivity would be to compare staining or blotting in tissues known to express TRPM3 with those that do not, such as by using siRNA to transiently knockdown the TRPM3 mRNA, or by using tissues from a knockout animal. As yet, there is not a TRPM3 knockout available.

Further experiments to determine TRPM3 function

Cholesterol enrichment of the plasma membrane inhibited TRPM3 activity. It would be interesting to examine if cholesterol can affect TRPM3 Ca^{2+}-responses in HSV SMC, and in particular whether cholesterol can regulate MMP-9 and IL-6 secretion. As TRPM3 activation decreases secretion, it would be expected that inhibition by cholesterol would have the opposite effect, and increase secretion.

The secretion data presented in Chapter 4 of this study still requires further work. There was often a large amount of variation between patient samples, resulting in large SEM. This will be markedly improved by increasing the n number of these experiments.

Further experiments are required to determine the concentration dependence of the PregS and SPH effect on MMP-9 and IL-6 secretion, in order to identify and use physiologically relevant concentrations. It would also be useful to perform siRNA knockdown of the TRPM3 gene to confirm TRPM3 role in secretion experiments; this should parallel the antibody effect and prevent decrease in secretion following TRPM3 activation.

Interestingly TM3E3 did not increase secretion in the presence of SPH (Figure 4.17). This suggests that SPH has a dual effect on TRPM3-regulated secretion, causing both activation of TRPM3 (thus inhibition of TRPM3-related secretion) but also inhibition of the TM3E3 effect. This effect must be further investigated, and may be aided by the use of an affinity purified antibody to rule out non-specific effects of the anti sera. It would also be useful to determine whether pre-treatment with SPH can inhibit the PregS inhibitory effect on secretion.

Further to effects on secretion, an obvious experiment would be to investigate a role for TRPM3 in SMC proliferation and migration. The anti-TRPC5 antibody, T5E3, has been shown to inhibit S1P-induced SMC migration (Xu *et al.*, 2006b), and furthermore the anti-TRPC1 antibody, T1E3, implicated TRPC1 in progression of neointimal hyperplasia (Kumar *et al.*, 2006). Similar experiments could be used to demonstrate an involvement for TRPM3 activators in proliferation and migration, the effects of which should be blocked by TM3E3. TRP channels are also described as regulators of myogenic tone (Earley *et al.*, 2004). A role for TRPM3 in the regulation of blood pressure could be assessed using contraction studies. Sphingosine causes contraction of both rat mesenteric vessels and porcine coronary arteries (Murohara *et al.*, 1996, Bischoff *et al.*, 2000), and it would be interesting to investigate whether this effect can be inhibited using TM3E3. Sphingosine is also well characterised as an apoptotic agent (Taha *et al.*, 2006), and cell viability experiments would be useful to determine whether the effect of SPH on secretion is the result of cell death. Knock-out mice have also proven useful for demonstrating a role for TRP channels in the vasculature (Kim *et al.*, 2000), and may be useful for TRPM3.

Final conclusion

This investigation has revealed several novel pharmacological tools that have proven useful for the characterisation of TRPM3. The expression of the TRPM3 channel both in brain tissue and throughout the vasculature, plus regulation by known antipsychotic and anti-atherogenic modulators suggests a functional role in psychosis or the development of atherosclerosis. TM3E3 has served as a valuable selective tool for the description of the TRPM3 channel in both over-expressed and native systems, and in particular has allowed for the identification of TRPM3 as a functional channel in VSM. TRPM3 is involved in both IL-6 and MMP-9 secretion, and may play a protective role in VSM, perhaps mediating the negative effects of well-characterised vascular damaging agents. Although the exact mechanisms of the role of TRPM3 in the vasculature remain to be investigated, this study has demonstrated the effectiveness of medium throughput screening in identifying both TRPM3 ion channel modulators and areas that show promise as potential therapeutic targets.

Although custom-made antibodies can have important therapeutic applications due to their specificity and unlimited diversity, it would appear TM3E3 inhibition of TRPM3 may have a negative physiological effect, upregulating the secretion of atherogenic factors. However, the antibody will prove useful for the further characterisation of endogenous TRPM3 in a multitude of cell types and tissues.

References

ABNET, C.C., BORKOWF, C.B., QIAO, Y.L., ALBERT, P.S., WANG, E., MERRILL, A.H., JR., MARK, S.D., DONG, Z.W., TAYLOR, P.R. & DAWSEY, S.M. (2001). A cross-sectional study of human serum sphingolipids, diet and physiologic parameters. *J Nutr*, **131,** 2748-52.

AKK, G., BRACAMONTES, J. & STEINBACH, J.H. (2001). Pregnenolone sulfate block of GABA(A) receptors: mechanism and involvement of a residue in the M2 region of the alpha subunit. *J Physiol*, **532,** 673-84.

ANGELINI, G.D. & NEWBY, A.C. (1989). The future of saphenous vein as a coronary artery bypass conduit. *Eur Heart J*, **10,** 273-80.

AUGE, N., ANDRIEU, N., NEGRE-SALVAYRE, A., THIERS, J.C., LEVADE, T. & SALVAYRE, R. (1996). The sphingomyelin-ceramide signaling pathway is involved in oxidized low density lipoprotein-induced cell proliferation. *J Biol Chem*, **271,** 19251-5.

AYDAR, E., PALMER, C.P., KLYACHKO, V.A. & JACKSON, M.B. (2002). The sigma receptor as a ligand-regulated auxiliary potassium channel subunit. *Neuron*, **34,** 399-410.

BANDELL, M., MACPHERSON, L.J. & PATAPOUTIAN, A. (2007). From chills to chilis: mechanisms for thermosensation and chemesthesis via thermoTRPs. *Curr Opin Neurobiol*, **17,** 490-7.

BANKS, F.C.L., KNIGHT, G.E., CALVERT, R.C., TURMAINE, M., THOMPSON, C.S., MIKHAILIDIS, D.P., MORGAN, R.J. & BURNSTOCK, G. (2006). Smooth Muscle and Purinergic Contraction of the Human, Rabbit, Rat, and Mouse Testicular Capsule. *Biol Reprod*, **74,** 473-480.

BEECH, D.J. (2005). Emerging functions of 10 types of TRP cationic channel in vascular smooth muscle. *Clin Exp Pharmacol Physiol*, **32,** 597-603.

BEECH, D.J., MURAKI, K. & FLEMMING, R. (2004). Non-selective cationic channels of smooth muscle and the mammalian homologues of Drosophila TRP. *J Physiol*, **559,** 685-706.

BEHRENDT, H.J., GERMANN, T., GILLEN, C., HATT, H. & JOSTOCK, R. (2004). Characterization of the mouse cold-menthol receptor TRPM8 and vanilloid receptor type-1 VR1 using a fluorometric imaging plate reader (FLIPR) assay. *Br J Pharmacol*, **141,** 737-45.

BERGDAHL, A., GOMEZ, M.F., DREJA, K., XU, S.Z., ADNER, M., BEECH, D.J., BROMAN, J., HELLSTRAND, P. & SWARD, K. (2003). Cholesterol depletion impairs vascular reactivity to endothelin-1 by reducing store-operated Ca^{2+} entry dependent on TRPC1. *Circ Res*, **93**, 839-47.

BERRIDGE, M.J. (1995). Capacitative calcium entry. *Biochem J*, **312 (Pt 1)**, 1-11.

BERRIDGE, M.J., LIPP, P. & BOOTMAN, M.D. (2000). The versatility and universality of calcium signalling. *Nat Rev Mol Cell Biol*, **1**, 11-21.

BEVAN, S. & SZOLCSANYI, J. (1990). Sensory neuron-specific actions of capsaicin: mechanisms and applications. *Trends Pharmacol Sci*, **11**, 330-3.

BIASI, F., LEONARDUZZI, G., VIZIO, B., ZANETTI, D., SEVANIAN, A., SOTTERO, B., VERDE, V., ZINGARO, B., CHIARPOTTO, E. & POLI, G. (2004). Oxysterol mixtures prevent proapoptotic effects of 7-ketocholesterol in macrophages: implications for proatherogenic gene modulation. *Faseb J*, **18**, 693-5.

BIRNBAUMER, L., ZHU, X., JIANG, M., BOULAY, G., PEYTON, M., VANNIER, B., BROWN, D., PLATANO, D., SADEGHI, H., STEFANI, E. & BIRNBAUMER, M. (1996). On the molecular basis and regulation of cellular capacitative calcium entry: roles for Trp proteins. *Proc Natl Acad Sci U S A*, **93**, 15195-202.

BISCHOFF, A., CZYBORRA, P., FETSCHER, C., MEYER ZU HERINGDORF, D., JAKOBS, K.H. & MICHEL, M.C. (2000). Sphingosine-1-phosphate and sphingosylphosphorylcholine constrict renal and mesenteric microvessels in vitro. *Br J Pharmacol*, **130**, 1871-7.

BODDING, M., WISSENBACH, U. & FLOCKERZI, V. (2002). The recombinant human TRPV6 channel functions as Ca^{2+} sensor in human embryonic kidney and rat basophilic leukemia cells. *J Biol Chem*, **277**, 36656-64.

BOLTON, T.B. (1979). Mechanisms of action of transmitters and other substances on smooth muscle. *Physiol Rev*, **59**, 606-718.

BOOTMAN, M.D., COLLINS, T.J., MACKENZIE, L., RODERICK, H.L., BERRIDGE, M.J. & PEPPIATT, C.M. (2002). 2-aminoethoxydiphenyl borate (2-APB) is a reliable blocker of store-operated Ca^{2+} entry but an inconsistent inhibitor of $InsP_3$-induced Ca^{2+} release. *Faseb J*, **16**, 1145-50.

BOWLBY, M.R. (1993). Pregnenolone sulfate potentiation of N-methyl-D-aspartate receptor channels in hippocampal neurons. *Mol Pharmacol*, **43**, 813-9.

BRADLEY, J., REISERT, J. & FRINGS, S. (2005). Regulation of cyclic nucleotide-gated channels. *Curr Opin Neurobiol*, **15**, 343-9.

BRAUCHI, S., ORTA, G., SALAZAR, M., ROSENMANN, E. & LATORRE, R. (2006). A hot-sensing cold receptor: C-terminal domain determines thermosensation in transient receptor potential channels. *J Neurosci*, **26,** 4835-40.

BREKKE, O.H. & SANDLIE, I. (2003). Therapeutic antibodies for human diseases at the dawn of the twenty-first century. *Nat Rev Drug Discov*, **2,** 52-62.

BROCHERIOU, I., STENGEL, D., MATTSSON-HULTEN, L., STANKOVA, J., ROLA-PLESZCZYNSKI, M., KOSKAS, F., WIKLUND, O., LE CHARPENTIER, Y. & NINIO, E. (2000). Expression of platelet-activating factor receptor in human carotid atherosclerotic plaques: relevance to progression of atherosclerosis. *Circulation*, **102,** 2569-75.

BROWN, A.J. & JESSUP, W. (1999). Oxysterols and atherosclerosis. *Atherosclerosis*, **142,** 1-28.

BRUEGGEMANN, A., GEORGE, M., KLAU, M., BECKLER, M., STEINDL, J., BEHRENDS, J.C. & FERTIG, N. (2004). Ion channel drug discovery and research: the automated Nano-Patch-Clamp technology. *Curr Drug Discov Technol*, **1,** 91-6.

BRUGGEMANN, A., STOELZLE, S., GEORGE, M., BEHRENDS, J.C. & FERTIG, N. (2006). Microchip technology for automated and parallel patch-clamp recording. *Small*, **2,** 840-6.

CHEN, S.C. & WU, F.S. (2004). Mechanism underlying inhibition of the capsaicin receptor-mediated current by pregnenolone sulfate in rat dorsal root ganglion neurons. *Brain Res*, **1027,** 196-200.

CHENG, K.T., CHAN, F.L., HUANG, Y., CHAN, W.Y. & YAO, X. (2003). Expression of olfactory-type cyclic nucleotide-gated channel (CNGA2) in vascular tissues. *Histochem Cell Biol*, **120,** 475-81.

CHEONG, A., BINGHAM, A.J., LI, J., KUMAR, B., SUKUMAR, P., MUNSCH, C., BUCKLEY, N.J., NEYLON, C.B., PORTER, K.E., BEECH, D.J. & WOOD, I.C. (2005). Downregulated REST transcription factor is a switch enabling critical potassium channel expression and cell proliferation. *Mol Cell*, **20,** 45-52.

CHO, A. & REIDY, M.A. (2002). Matrix metalloproteinase-9 is necessary for the regulation of smooth muscle cell replication and migration after arterial injury. *Circ Res*, **91,** 845-51.

CHUBANOV, V., WALDEGGER, S., MEDEROS Y SCHNITZLER, M., VITZTHUM, H., SASSEN, M.C., SEYBERTH, H.W., KONRAD, M. & GUDERMANN, T. (2004). Disruption of TRPM6/TRPM7 complex formation by a mutation in the TRPM6 gene causes

hypomagnesemia with secondary hypocalcemia. *Proc Natl Acad Sci U S A*, **101,** 2894-9.

CHUNG, M.K., LEE, H., MIZUNO, A., SUZUKI, M. & CATERINA, M.J. (2004). 2-aminoethoxydiphenyl borate activates and sensitizes the heat-gated ion channel TRPV3. *J Neurosci*, **24,** 5177-82.

CLAPHAM, D.E. (2003). TRP channels as cellular sensors. *Nature*, **426,** 517-24.

CLAPHAM, D.E., RUNNELS, L.W. & STRUBING, C. (2001). The TRP ion channel family. *Nat Rev Neurosci*, **2,** 387-96.

COREY, D.P., GARCIA-ANOVEROS, J., HOLT, J.R., KWAN, K.Y., LIN, S.Y., VOLLRATH, M.A., AMALFITANO, A., CHEUNG, E.L., DERFLER, B.H., DUGGAN, A., GELEOC, G.S., GRAY, P.A., HOFFMAN, M.P., REHM, H.L., TAMASAUSKAS, D. & ZHANG, D.S. (2004). TRPA1 is a candidate for the mechanosensitive transduction channel of vertebrate hair cells. *Nature*, **432,** 723-30.

CRIBBS, L.L. (2006). T-type Ca^{2+} channels in vascular smooth muscle: multiple functions. *Cell Calcium*, **40,** 221-30.

CUVILLIER, O. (2002). Sphingosine in apoptosis signaling. *Biochim Biophys Acta*, **1585,** 153-62.

DALLAS, M., DEUCHARS, S.A. & DEUCHARS, J. (2005). Immunopharmacology--antibodies for specific modulation of proteins involved in neuronal function. *J Neurosci Methods*, **146,** 133-48.

DE PERETTI, E. & MAPPUS, E. (1983). Pattern of plasma pregnenolone sulfate levels in humans from birth to adulthood. *J Clin Endocrinol Metab*, **57,** 550-6.

DI VIRGILIO, F., STEINBERG, T.H. & SILVERSTEIN, S.C. (1990). Inhibition of Fura-2 sequestration and secretion with organic anion transport blockers. *Cell Calcium*, **11,** 57-62.

DIETRICH, A., CHUBANOV, V., KALWA, H., ROST, B.R. & GUDERMANN, T. (2006). Cation channels of the transient receptor potential superfamily: their role in physiological and pathophysiological processes of smooth muscle cells. *Pharmacol Ther*, **112,** 744-60.

DOLPHIN, A.C. (2006). A short history of voltage-gated calcium channels. *Br J Pharmacol*, **147 Suppl 1,** S56-62.

DRAY, A., FORBES, C.A. & BURGESS, G.M. (1990). Ruthenium red blocks the capsaicin-induced increase in intracellular calcium and activation of membrane currents in sensory neurones as well as the activation of peripheral nociceptors in vitro. *Neurosci Lett*, **110,** 52-9.

DUNCAN, L.M., DEEDS, J., CRONIN, F.E., DONOVAN, M., SOBER, A.J., KAUFFMAN, M. & MCCARTHY, J.J. (2001). Melastatin expression and prognosis in cutaneous malignant melanoma. *J Clin Oncol*, **19**, 568-76.

EARLEY, S., HEPPNER, T.J., NELSON, M.T. & BRAYDEN, J.E. (2005). TRPV4 forms a novel Ca^{2+} signaling complex with ryanodine receptors and BK_{Ca} channels. *Circ Res*, **97**, 1270-9.

EARLEY, S., WALDRON, B.J. & BRAYDEN, J.E. (2004). Critical role for transient receptor potential channel TRPM4 in myogenic constriction of cerebral arteries. *Circ Res*, **95**, 922-9.

ECHEVARRIA, W., LEITE, M.F., GUERRA, M.T., ZIPFEL, W.R. & NATHANSON, M.H. (2003). Regulation of calcium signals in the nucleus by a nucleoplasmic reticulum. *Nat Cell Biol*, **5**, 440-6.

EKEMA, G.M., ZHENG, W., WANG, L. & LU, L. (2001). Modulation of recombinant GABA receptor/channel subunits by domain-specific antibodies in Xenopus oocytes. *J Membr Biol*, **183**, 205-13.

EL BAWAB, S., RODDY, P., QIAN, T., BIELAWSKA, A., LEMASTERS, J.J. & HANNUN, Y.A. (2000). Molecular cloning and characterization of a human mitochondrial ceramidase. *J Biol Chem*, **275**, 21508-13.

ELBASHIR, S.M., HARBORTH, J., LENDECKEL, W., YALCIN, A., WEBER, K. & TUSCHL, T. (2001). Duplexes of 21-nucleotide RNAs mediate RNA interference in cultured mammalian cells. *Nature*, **411**, 494-8.

FLEMMING, P.K., DEDMAN, A.M., XU, S.Z., LI, J., ZENG, F., NAYLOR, J., BENHAM, C.D., BATESON, A.N., MURAKI, K. & BEECH, D.J. (2006). Sensing of lysophospholipids by TRPC5 calcium channel. *J Biol Chem*, **281**, 4977-82.

GARCIA-MARTINEZ, C., MORENILLA-PALAO, C., PLANELLS-CASES, R., MERINO, J.M. & FERRER-MONTIEL, A. (2000). Identification of an aspartic residue in the P-loop of the vanilloid receptor that modulates pore properties. *J Biol Chem*, **275**, 32552-8.

GIBBS, T.T., RUSSEK, S.J. & FARB, D.H. (2006). Sulfated steroids as endogenous neuromodulators. *Pharmacol Biochem Behav*, **84**, 555-67.

GOMEZ-VARELA, D., ZWICK-WALLASCH, E., KNOTGEN, H., SANCHEZ, A., HETTMANN, T., OSSIPOV, D., WESELOH, R., CONTRERAS-JURADO, C., ROTHE, M., STUHMER, W. & PARDO, L.A. (2007). Monoclonal antibody blockade of the human Eag1 potassium channel function exerts antitumor activity. *Cancer Res*, **67**, 7343-9.

GRAZIANI, A., ROSKER, C., KOHLWEIN, S.D., ZHU, M.X., ROMANIN, C., SATTLER, W., GROSCHNER, K. & POTESER, M. (2006). Cellular cholesterol controls TRPC3 function: evidence from a novel dominant-negative knockdown strategy. *Biochem J*, **396**, 147-55.

GRAZZINI, E., GUILLON, G., MOUILLAC, B. & ZINGG, H.H. (1998). Inhibition of oxytocin receptor function by direct binding of progesterone. *Nature*, **392**, 509-12.

GRIMM, C., KRAFT, R., SAUERBRUCH, S., SCHULTZ, G. & HARTENECK, C. (2003). Molecular and functional characterization of the melastatin-related cation channel TRPM3. *J Biol Chem*, **278**, 21493-501.

GRIMM, C., KRAFT, R., SCHULTZ, G. & HARTENECK, C. (2005). Activation of the melastatin-related cation channel TRPM3 [corrected] by D-erythro-sphingosine. *Mol Pharmacol*, **67**, 798-805.

GUERINI, D. (1998). The significance of the isoforms of plasma membrane calcium ATPase. *Cell Tissue Res*, **292**, 191-7.

GUNTHORPE, M.J., BENHAM, C.D., RANDALL, A. & DAVIS, J.B. (2002). The diversity in the vanilloid (TRPV) receptor family of ion channels. *Trends Pharmacol Sci*, **23**, 183-91.

HAKOMORI, S., YAMAMURA, S. & HANDA, A.K. (1998). Signal transduction through glyco(sphingo)lipids. Introduction and recent studies on glyco(sphingo)lipid-enriched microdomains. *Ann N Y Acad Sci*, **845**, 1-10.

HALASZOVICH, C.R., ZITT, C., JUNGLING, E. & LUCKHOFF, A. (2000). Inhibition of TRP3 channels by lanthanides. Block from the cytosolic side of the plasma membrane. *J Biol Chem*, **275**, 37423-8.

HAMERS-CASTERMAN, C., ATARHOUCH, T., MUYLDERMANS, S., ROBINSON, G., HAMERS, C., SONGA, E.B., BENDAHMAN, N. & HAMERS, R. (1993). Naturally occurring antibodies devoid of light chains. *Nature*, **363**, 446-8.

HAMILL, O.P. & MCBRIDE, D.W., JR. (1996). The pharmacology of mechanogated membrane ion channels. *Pharmacol Rev*, **48**, 231-52.

HARA, Y., WAKAMORI, M., ISHII, M., MAENO, E., NISHIDA, M., YOSHIDA, T., YAMADA, H., SHIMIZU, S., MORI, E., KUDOH, J., SHIMIZU, N., KUROSE, H., OKADA, Y., IMOTO, K. & MORI, Y. (2002). LTRPC2 Ca^{2+}-permeable channel activated by changes in redox status confers susceptibility to cell death. *Mol Cell*, **9**, 163-73.

HE, Y., YAO, G., SAVOIA, C. & TOUYZ, R.M. (2005). Transient receptor potential melastatin 7 ion channels regulate magnesium homeostasis in vascular smooth muscle cells: role of angiotensin II. *Circ Res*, **96,** 207-15.

HERMOSURA, M.C., NAYAKANTI, H., DOROVKOV, M.V., CALDERON, F.R., RYAZANOV, A.G., HAYMER, D.S. & GARRUTO, R.M. (2005). A TRPM7 variant shows altered sensitivity to magnesium that may contribute to the pathogenesis of two Guamanian neurodegenerative disorders. *Proc Natl Acad Sci U S A*, **102,** 11510-5.

HEWAVITHARANA, T., DENG, X., SOBOLOFF, J. & GILL, D.L. (2007). Role of STIM and Orai proteins in the store-operated calcium signaling pathway. *Cell Calcium*, **42,** 173-82.

HILL, K., BENHAM, C.D., MCNULTY, S. & RANDALL, A.D. (2004a). Flufenamic acid is a pH-dependent antagonist of TRPM2 channels. *Neuropharmacology*, **47,** 450-60.

HILL, K., MCNULTY, S. & RANDALL, A.D. (2004b). Inhibition of TRPM2 channels by the antifungal agents clotrimazole and econazole. *Naunyn Schmiedebergs Arch Pharmacol*, **370,** 227-37.

HINZPETER, A., FRITSCH, J., BOROT, F., TRUDEL, S., VIEU, D.L., BROUILLARD, F., BAUDOUIN-LEGROS, M., CLAIN, J., EDELMAN, A. & OLLERO, M. (2007). Membrane cholesterol content modulates ClC-2 gating and sensitivity to oxidative stress. *J Biol Chem*, **282,** 2423-32.

HOENDEROP, J.G., VOETS, T., HOEFS, S., WEIDEMA, F., PRENEN, J., NILIUS, B. & BINDELS, R.J. (2003). Homo- and heterotetrameric architecture of the epithelial Ca^{2+} channels TRPV5 and TRPV6. *Embo J*, **22,** 776-85.

HOFMANN, T., SCHAEFER, M., SCHULTZ, G. & GUDERMANN, T. (2002). Subunit composition of mammalian transient receptor potential channels in living cells. *Proceedings of the National Academy of Sciences*, **99,** 7461-7466.

HU, H.Z., XIAO, R., WANG, C., GAO, N., COLTON, C.K., WOOD, J.D. & ZHU, M.X. (2006). Potentiation of TRPV3 channel function by unsaturated fatty acids. *J Cell Physiol*, **208,** 201-12.

HUANG, J., ZHANG, X. & MCNAUGHTON, P.A. (2006). Modulation of temperature-sensitive TRP channels. *Semin Cell Dev Biol*, **17,** 638-45.

HUBER, T.B., KWOH, C., WU, H., ASANUMA, K., GODEL, M., HARTLEBEN, B., BLUMER, K.J., MINER, J.H., MUNDEL, P. & SHAW, A.S. (2006). Bigenic mouse models of focal segmental glomerulosclerosis involving pairwise interaction of CD2AP, Fyn, and synaptopodin. *J Clin Invest*, **116,** 1337-45.

INOUE, R., JENSEN, L.J., SHI, J., MORITA, H., NISHIDA, M., HONDA, A. & ITO, Y. (2006). Transient receptor potential channels in cardiovascular function and disease. *Circ Res*, **99**, 119-31.

INOUE, R., OKADA, T., ONOUE, H., HARA, Y., SHIMIZU, S., NAITOH, S., ITO, Y. & MORI, Y. (2001). The Transient Receptor Potential Protein Homologue TRP6 Is the Essential Component of Vascular {{alpha}}1-Adrenoceptor-Activated Ca^{2+}-Permeable Cation Channel. *Circ Res*, **88**, 325-332.

ISHIMARU, Y., INADA, H., KUBOTA, M., ZHUANG, H., TOMINAGA, M. & MATSUNAMI, H. (2006). Transient receptor potential family members PKD1L3 and PKD2L1 form a candidate sour taste receptor. *Proc Natl Acad Sci U S A*, **103**, 12569-74.

JOHNSON, K.R., JOHNSON, K.Y., BECKER, K.P., BIELAWSKI, J., MAO, C. & OBEID, L.M. (2003). Role of human sphingosine-1-phosphate phosphatase 1 in the regulation of intra- and extracellular sphingosine-1-phosphate levels and cell viability. *J Biol Chem*, **278**, 34541-7.

JORDT, S.E. & JULIUS, D. (2002). Molecular basis for species-specific sensitivity to "hot" chili peppers. *Cell*, **108**, 421-30.

JUNG, S., MUHLE, A., SCHAEFER, M., STROTMANN, R., SCHULTZ, G. & PLANT, T.D. (2003). Lanthanides potentiate TRPC5 currents by an action at extracellular sites close to the pore mouth. *J Biol Chem*, **278**, 3562-71.

KALAPESI, F.B., TAN, J.C. & CORONEO, M.T. (2005). Stretch-activated channels: a mini-review. Are stretch-activated channels an ocular barometer? *Clin Experiment Ophthalmol*, **33**, 210-7.

KERSCHBAUM, H.H., KOZAK, J.A. & CAHALAN, M.D. (2003). Polyvalent cations as permeant probes of MIC and TRPM7 pores. *Biophys J*, **84**, 2293-305.

KIM, K., DRUMMOND, I., IBRAGHIMOV-BESKROVNAYA, O., KLINGER, K. & ARNAOUT, M.A. (2000). Polycystin 1 is required for the structural integrity of blood vessels. *Proc Natl Acad Sci U S A*, **97**, 1731-6.

KIM, M., SPELTA, V., SIM, J., NORTH, R.A. & SURPRENANT, A. (2001). Differential assembly of rat purinergic $P2X_7$ receptor in immune cells of the brain and periphery. *J Biol Chem*, **276**, 23262-7.

KIM, M.T., KIM, B.J., LEE, J.H., KWON, S.C., YEON, D.S., YANG, D.K., SO, I. & KIM, K.W. (2006). Involvement of calmodulin and myosin light chain kinase in activation of mTRPC5 expressed in HEK cells. *Am J Physiol Cell Physiol*, **290**, C1031-40.

KLIONSKY, L., TAMIR, R., HOLZINGER, B., BI, X., TALVENHEIMO, J., KIM, H., MARTIN, F., LOUIS, J.C., TREANOR, J.J. & GAVVA, N.R. (2006). A polyclonal antibody to the pre-pore loop of TRPV1 blocks channel activation. *J Pharmacol Exp Ther,* **319,**192-8.

KOHLER, G. & MILSTEIN, C. (1975). Continuous cultures of fused cells secreting antibody of predefined specificity. *Nature*, **256,** 495-7.

KOTTGEN, M. (2007). TRPP2 and autosomal dominant polycystic kidney disease. *Biochim Biophys Acta*, **1772,** 836-50.

KRAFT, R. (2007). The Na^+/Ca^{2+} exchange inhibitor KB-R7943 potently blocks TRPC channels. *Biochem Biophys Res Commun*, **361,** 230-6.

KRAFT, R., GRIMM, C., FRENZEL, H. & HARTENECK, C. (2006). Inhibition of TRPM2 cation channels by N-(p-amylcinnamoyl)anthranilic acid. *Br J Pharmacol*, **148,** 264-73.

KRAFT, R. & HARTENECK, C. (2005). The mammalian melastatin-related transient receptor potential cation channels: an overview. *Pflugers Arch*, **451,** 204-11.

KUMAR, B., DREJA, K., SHAH, S.S., CHEONG, A., XU, S.Z., SUKUMAR, P., NAYLOR, J., FORTE, A., CIPOLLARO, M., MCHUGH, D., KINGSTON, P.A., HEAGERTY, A.M., MUNSCH, C.M., BERGDAHL, A., HULTGARDH-NILSSON, A., GOMEZ, M.F., PORTER, K.E., HELLSTRAND, P. & BEECH, D.J. (2006). Upregulated TRPC1 channel in vascular injury in vivo and its role in human neointimal hyperplasia. *Circ Res*, **98,** 557-63.

KYTE, J. & DOOLITTLE, R.F. (1982). A simple method for displaying the hydropathic character of a protein. *J Mol Biol*, **157,** 105-32.

LAUNAY, P., FLEIG, A., PERRAUD, A.L., SCHARENBERG, A.M., PENNER, R. & KINET, J.P. (2002). TRPM4 is a Ca^{2+}-activated nonselective cation channel mediating cell membrane depolarization. *Cell*, **109,** 397-407.

LEE, N., CHEN, J., SUN, L., WU, S., GRAY, K.R., RICH, A., HUANG, M., LIN, J.H., FEDER, J.N., JANOVITZ, E.B., LEVESQUE, P.C. & BLANAR, M.A. (2003a). Expression and characterization of human transient receptor potential melastatin 3 (hTRPM3). *J Biol Chem*, **278,** 20890-7.

LEE, Y.M., KIM, B.J., KIM, H.J., YANG, D.K., ZHU, M.H., LEE, K.P., SO, I. & KIM, K.W. (2003b). TRPC5 as a candidate for the nonselective cation channel activated by muscarinic stimulation in murine stomach. *Am J Physiol Gastrointest Liver Physiol*, **284,** G604-616.

LEWIS, C.J. & EVANS, R.J. (2001). P2X receptor immunoreactivity in different arteries from the femoral, pulmonary, cerebral, coronary and renal circulations. *J Vasc Res*, **38**, 332-40.

LI, S., GOSLING, M. & POLL, C. (2005). Determining the functional role of TRPC channels in primary cells. *Pflugers Arch*, **451**, 43-52.

LIU, B. & QIN, F. (2005). Functional control of cold- and menthol-sensitive TRPM8 ion channels by phosphatidylinositol 4,5-bisphosphate. *J Neurosci*, **25**, 1674-81.

LIYANAGE, Y., HOCH, W., BEESON, D. & VINCENT, A. (2002). The agrin/muscle-specific kinase pathway: new targets for autoimmune and genetic disorders at the neuromuscular junction. *Muscle Nerve*, **25**, 4-16.

LOBATO, M.N. & RABBITTS, T.H. (2003). Intracellular antibodies and challenges facing their use as therapeutic agents. *Trends Mol Med*, **9**, 390-6.

LUKACS, V., THYAGARAJAN, B., VARNAI, P., BALLA, A., BALLA, T. & ROHACS, T. (2007). Dual Regulation of TRPV1 by Phosphoinositides. *J. Neurosci.*, **27**, 7070-7080.

MACDONALD, J.F. & NOWAK, L.M. (1990). Mechanisms of blockade of excitatory amino acid receptor channels. *Trends Pharmacol Sci*, **11**, 167-72.

MACPHERSON, L.J., DUBIN, A.E., EVANS, M.J., MARR, F., SCHULTZ, P.G., CRAVATT, B.F. & PATAPOUTIAN, A. (2007). Noxious compounds activate TRPA1 ion channels through covalent modification of cysteines. *Nature*, **445**, 541-5.

MACPHERSON, L.J., HWANG, S.W., MIYAMOTO, T., DUBIN, A.E., PATAPOUTIAN, A. & STORY, G.M. (2006). More than cool: promiscuous relationships of menthol and other sensory compounds. *Mol Cell Neurosci*, **32**, 335-43.

MAINGRET, F., PATEL, A.J., LESAGE, F., LAZDUNSKI, M. & HONORE, E. (2000). Lysophospholipids open the two-pore domain mechano-gated K(+) channels TREK-1 and TRAAK. *J Biol Chem*, **275**, 10128-33.

MAINGRET, F., PATEL, A.J., LESAGE, F., LAZDUNSKI, M. & HONORE, E. (1999). Mechano- or acid stimulation, two interactive modes of activation of the TREK-1 potassium channel. *J Biol Chem*, **274**, 26691-6.

MALECOT, C.O., BITO, V. & ARGIBAY, J.A. (1998). Ruthenium red as an effective blocker of calcium and sodium currents in guinea-pig isolated ventricular heart cells. *Br J Pharmacol*, **124**, 465-72.

MARUYAMA, I., HASEGAWA, T., YAMAMOTO, T. & MOMOSE, K. (1989). Effects of pluronic F-127 on loading of fura 2/AM into single smooth muscle cells isolated from guinea pig taenia coli. *J Toxicol Sci*, **14**, 153-63.

MARUYAMA, Y., NAKANISHI, Y., WALSH, E.J., WILSON, D.P., WELSH, D.G. & COLE, W.C. (2006). Heteromultimeric TRPC6-TRPC7 channels contribute to arginine vasopressin-induced cation current of A7r5 vascular smooth muscle cells. *Circ Res*, **98**, 1520-7.

MAURICE, T., PHAN, V.L., URANI, A., KAMEI, H., NODA, Y. & NABESHIMA, T. (1999). Neuroactive neurosteroids as endogenous effectors for the sigma1 (sigma1) receptor: pharmacological evidence and therapeutic opportunities. *Jpn J Pharmacol*, **81**, 125-55.

MCHUGH, D., FLEMMING, R., XU, S.Z., PERRAUD, A.L. & BEECH, D.J. (2003). Critical intracellular Ca^{2+} dependence of transient receptor potential melastatin 2 (TRPM2) cation channel activation. *J Biol Chem*, **278**, 11002-6.

MEI, Z.Z., XIA, R., BEECH, D.J. & JIANG, L.H. (2006). Intracellular coiled-coil domain engaged in subunit interaction and assembly of melastatin-related transient receptor potential channel 2. *J Biol Chem*, **281**, 38748-56.

MICHELANGELI, F., MEZNA, M., TOVEY, S. & SAYERS, L.G. (1995). Pharmacological modulators of the inositol 1,4,5-trisphosphate receptor. *Neuropharmacology*, **34**, 1111-22.

MIGNEN, O., THOMPSON, J.L. & SHUTTLEWORTH, T.J. (2007). STIM1 regulates Ca^{2+} entry via arachidonate-regulated Ca^{2+}-selective (ARC) channels without store depletion or translocation to the plasma membrane. *J Physiol*, **579**, 703-715.

MONTELL, C. & RUBIN, G.M. (1989). Molecular characterization of the Drosophila trp locus: a putative integral membrane protein required for phototransduction. *Neuron*, **2**, 1313-23.

MORIN-SURUN, M.P., COLLIN, T., DENAVIT-SAUBIE, M., BAULIEU, E.E. & MONNET, F.P. (1999). Intracellular sigma1 receptor modulates phospholipase C and protein kinase C activities in the brainstem. *Proc Natl Acad Sci U S A*, **96**, 8196-9.

MURAKI, K., IWATA, Y., KATANOSAKA, Y., ITO, T., OHYA, S., SHIGEKAWA, M. & IMAIZUMI, Y. (2003). TRPV2 is a component of osmotically sensitive cation channels in murine aortic myocytes. *Circ Res*, **93**, 829-38.

MUROHARA, T., KUGIYAMA, K., OHGUSHI, M., SUGIYAMA, S., OHTA, Y. & YASUE, H. (1996). Effects of sphingomyelinase and sphingosine on arterial vasomotor regulation. *J Lipid Res*, **37**, 1601-8.

MURPHY, M.P., PACKER, M.A., SCARLETT, J.L. & MARTIN, S.W. (1998). Peroxynitrite: a biologically significant oxidant. *Gen Pharmacol*, **31**, 179-86.

NADIF KASRI, N., BULTYNCK, G., SIENAERT, I., CALLEWAERT, G., ERNEUX, C., MISSIAEN, L., PARYS, J.B. & DE SMEDT, H. (2002). The role of calmodulin for inositol 1,4,5-trisphosphate receptor function. *Biochim Biophys Acta*, **1600,** 19-31.

NADLER, M.J., HERMOSURA, M.C., INABE, K., PERRAUD, A.L., ZHU, Q., STOKES, A.J., KUROSAKI, T., KINET, J.P., PENNER, R., SCHARENBERG, A.M. & FLEIG, A. (2001). LTRPC7 is a Mg.ATP-regulated divalent cation channel required for cell viability. *Nature*, **411,** 590-5.

NAGAMINE, K., KUDOH, J., MINOSHIMA, S., KAWASAKI, K., ASAKAWA, S., ITO, F. & SHIMIZU, N. (1998). Molecular cloning of a novel putative Ca^{2+} channel protein (TRPC7) highly expressed in brain. *Genomics*, **54,** 124-31.

NAGATA, K., DUGGAN, A., KUMAR, G. & GARCIA-ANOVEROS, J. (2005). Nociceptor and hair cell transducer properties of TRPA1, a channel for pain and hearing. *J Neurosci*, **25,** 4052-61.

NAZIROGLU, M., LUCKHOFF, A. & JUNGLING, E. (2007). Antagonist effect of flufenamic acid on TRPM2 cation channels activated by hydrogen peroxide. *Cell Biochem Funct*, **25,** 383-7.

NEWBY, A.C. (2007). Metalloproteinases and vulnerable atherosclerotic plaques. *Trends Cardiovasc Med*, **17,** 253-8.

NILIUS, B., PRENEN, J., JANSSENS, A., OWSIANIK, G., WANG, C., ZHU, M.X. & VOETS, T. (2005a). The selectivity filter of the cation channel TRPM4. *J Biol Chem*, **280,** 22899-906.

NILIUS, B., PRENEN, J., VENNEKENS, R., HOENDEROP, J.G., BINDELS, R.J. & DROOGMANS, G. (2001). Pharmacological modulation of monovalent cation currents through the epithelial Ca^{2+} channel ECaC1. *Br J Pharmacol*, **134,** 453-62.

NILIUS, B., PRENEN, J., VOETS, T. & DROOGMANS, G. (2004a). Intracellular nucleotides and polyamines inhibit the Ca^{2+}-activated cation channel TRPM4b. *Pflugers Arch*, **448,** 70-5.

NILIUS, B., TALAVERA, K., OWSIANIK, G., PRENEN, J., DROOGMANS, G. & VOETS, T. (2005b). Gating of TRP channels: a voltage connection? *J Physiol*, **567,** 35-44.

NILIUS, B., VRIENS, J., PRENEN, J., DROOGMANS, G. & VOETS, T. (2004b). TRPV4 calcium entry channel: a paradigm for gating diversity. *Am J Physiol Cell Physiol*, **286,** C195-205.

NORTH, R.A. (2002). Molecular Physiology of P2X Receptors. *Physiol. Rev.*, **82,** 1013-1067.

OANCEA, E., WOLFE, J.T. & CLAPHAM, D.E. (2006). Functional TRPM7 channels accumulate at the plasma membrane in response to fluid flow. *Circ Res*, **98,** 245-53.

OBERWINKLER, J., LIS, A., GIEHL, K.M., FLOCKERZI, V. & PHILIPP, S.E. (2005). Alternative splicing switches the divalent cation selectivity of TRPM3 channels. *J Biol Chem*, **280,** 22540-8.

OLA, M.S., MOORE, P., EL-SHERBENY, A., ROON, P., AGARWAL, N., SARTHY, V.P., CASELLAS, P., GANAPATHY, V. & SMITH, S.B. (2001). Expression pattern of sigma receptor 1 mRNA and protein in mammalian retina. *Brain Res Mol Brain Res*, **95,** 86-95.

OWENS, G.K., KUMAR, M.S. & WAMHOFF, B.R. (2004). Molecular regulation of vascular smooth muscle cell differentiation in development and disease. *Physiol Rev*, **84,** 767-801.

PAREKH, A.B. (2003). Mitochondrial regulation of intracellular Ca^{2+} signaling: more than just simple Ca^{2+} buffers. *News Physiol Sci*, **18,** 252-6.

PARK-CHUNG, M., MALAYEV, A., PURDY, R.H., GIBBS, T.T. & FARB, D.H. (1999). Sulfated and unsulfated steroids modulate gamma-aminobutyric acidA receptor function through distinct sites. *Brain Res*, **830,** 72-87.

PARK-CHUNG, M., WU, F.S., PURDY, R.H., MALAYEV, A.A., GIBBS, T.T. & FARB, D.H. (1997). Distinct sites for inverse modulation of N-methyl-D-aspartate receptors by sulfated steroids. *Mol Pharmacol*, **52,** 1113-23.

PEDERSEN, S.F. & NILIUS, B. (2007). Transient receptor potential channels in mechanosensing and cell volume regulation. *Methods Enzymol*, **428,** 183-207.

PEIER, A.M., MOQRICH, A., HERGARDEN, A.C., REEVE, A.J., ANDERSSON, D.A., STORY, G.M., EARLEY, T.J., DRAGONI, I., MCINTYRE, P., BEVAN, S. & PATAPOUTIAN, A. (2002). A TRP channel that senses cold stimuli and menthol. *Cell*, **108,** 705-15.

PEREIRA, D.A. & WILLIAMS, J.A. (2007). Origin and evolution of high throughput screening. *Br J Pharmacol*, **152,** 53-61.

PERIASAMY, M. & KALYANASUNDARAM, A. (2007). SERCA pump isoforms: their role in calcium transport and disease. *Muscle Nerve*, **35,** 430-42.

PERRAUD, A.L., FLEIG, A., DUNN, C.A., BAGLEY, L.A., LAUNAY, P., SCHMITZ, C., STOKES, A.J., ZHU, Q., BESSMAN, M.J., PENNER, R., KINET, J.P. &

SCHARENBERG, A.M. (2001). ADP-ribose gating of the calcium-permeable LTRPC2 channel revealed by Nudix motif homology. *Nature*, **411**, 595-9.

PORTER, K.E., LOFTUS, I.M., PETERSON, M., BELL, P.R., LONDON, N.J. & THOMPSON, M.M. (1998). Marimastat inhibits neointimal thickening in a model of human vein graft stenosis. *Br J Surg*, **85**, 1373-7.

PORTER, K.E. & TURNER, N.A. (2002). Statins for the prevention of vein graft stenosis: a role for inhibition of matrix metalloproteinase-9. *Biochem Soc Trans*, **30**, 120-6.

PORTER, K.E., VARTY, K., JONES, L., BELL, P.R. & LONDON, N.J. (1996). Human saphenous vein organ culture: a useful model of intimal hyperplasia? *Eur J Vasc Endovasc Surg*, **11**, 48-58.

PRESCOTT, E.D. & JULIUS, D. (2003). A modular PIP_2 binding site as a determinant of capsaicin receptor sensitivity. *Science*, **300**, 1284-8.

QIAN, F. & NOBEN-TRAUTH, K. (2005). Cellular and molecular function of mucolipins (TRPML) and polycystin 2 (TRPP2). *Pflugers Arch*, **451**, 277-85.

QIAN, Q., LI, M., CAI, Y., WARD, C.J., SOMLO, S., HARRIS, P.C. & TORRES, V.E. (2003). Analysis of the polycystins in aortic vascular smooth muscle cells. *J Am Soc Nephrol*, **14**, 2280-7.

QUIGNARD, J.F., FRAPIER, J.M., HARRICANE, M.C., ALBAT, B., NARGEOT, J. & RICHARD, S. (1997). Voltage-gated calcium channel currents in human coronary myocytes. Regulation by cyclic GMP and nitric oxide. *J Clin Invest*, **99**, 185-93.

REVETS, H., DE BAETSELIER, P. & MUYLDERMANS, S. (2005). Nanobodies as novel agents for cancer therapy. *Expert Opin Biol Ther*, **5**, 111-24.

ROBERTS, J.A., VIAL, C., DIGBY, H.R., AGBOH, K.C., WEN, H., ATTERBURY-THOMAS, A. & EVANS, R.J. (2006). Molecular properties of P2X receptors. *Pflugers Arch*, **452**, 486-500.

RODAL, S.K., SKRETTING, G., GARRED, O., VILHARDT, F., VAN DEURS, B. & SANDVIG, K. (1999). Extraction of cholesterol with methyl-beta-cyclodextrin perturbs formation of clathrin-coated endocytic vesicles. *Mol Biol Cell*, **10**, 961-74.

ROHACS, T., LOPES, C.M., MICHAILIDIS, I. & LOGOTHETIS, D.E. (2005). PI(4,5)P2 regulates the activation and desensitization of TRPM8 channels through the TRP domain. *Nat Neurosci*, **8**, 626-34.

ROSADO, J.A., BROWNLOW, S.L. & SAGE, S.O. (2002). Endogenously Expressed Trp1 Is Involved in Store-mediated Ca^{2+} Entry by Conformational Coupling in Human Platelets. *J. Biol. Chem.*, **277**, 42157-42163.

ROSADO, J.A., REDONDO, P.C., SAGE, S.O., PARIENTE, J.A. & SALIDO, G.M. (2005). Store-operated Ca^{2+} entry: vesicle fusion or reversible trafficking and de novo conformational coupling? *J Cell Physiol*, **205,** 262-9.

RUNNELS, L.W., YUE, L. & CLAPHAM, D.E. (2002). The TRPM7 channel is inactivated by PIP(2) hydrolysis. *Nat Cell Biol*, **4,** 329-36.

RUPPRECHT, R. & HOLSBOER, F. (1999). Neuroactive steroids: mechanisms of action and neuropsychopharmacological perspectives. *Trends Neurosci*, **22,** 410-6.

RUS, H.G., VLAICU, R. & NICULESCU, F. (1996). Interleukin-6 and interleukin-8 protein and gene expression in human arterial atherosclerotic wall. *Atherosclerosis*, **127,** 263-71.

RUSCH, A., KROS, C.J. & RICHARDSON, G.P. (1994). Block by amiloride and its derivatives of mechano-electrical transduction in outer hair cells of mouse cochlear cultures. *J Physiol*, **474,** 75-86.

SCHELLER, M., BLOBNER, M., VON LOEWENICH, C., SCHNECK, H., STADLER, J., FRANKE, C. & KOCHS, E. (1998). The NO synthase inhibitors L-Name and L-NMMA, but not L-arginine, block the mammalian nicotinic acetylcholine receptor channel. *Toxicol Lett*, **100-101,** 109-13.

SHARMA, M.R., JEYAKUMAR, L.H., FLEISCHER, S. & WAGENKNECHT, T. (2000). Three-dimensional structure of ryanodine receptor isoform three in two conformational states as visualized by cryo-electron microscopy. *J Biol Chem*, **275,** 9485-91.

SHIGEKAWA, M. & IWAMOTO, T. (2001). Cardiac $Na(^{+})$-$Ca(^{2+})$ exchange: molecular and pharmacological aspects. *Circ Res*, **88,** 864-76.

SHIMIZU, S., YOSHIDA, T., WAKAMORI, M., ISHII, M., OKADA, T., TAKAHASHI, M., SETO, M., SAKURADA, K., KIUCHI, Y. & MORI, Y. (2006). Ca^{2+}-calmodulin-dependent myosin light chain kinase is essential for activation of TRPC5 channels expressed in HEK293 cells. *J Physiol*, **570,** 219-35.

SIESS, W. (2002). Athero- and thrombogenic actions of lysophosphatidic acid and sphingosine-1-phosphate. *Biochim Biophys Acta*, **1582,** 204-15.

SOMLYO, A.P. & SOMLYO, A.V. (2000). Signal transduction by G-proteins, rho-kinase and protein phosphatase to smooth muscle and non-muscle myosin II. *J Physiol*, **522 Pt 2,** 177-85.

SPECTOR, A.A. & YOREK, M.A. (1985). Membrane lipid composition and cellular function. *J Lipid Res*, **26,** 1015-35.

STREHLER, E.E. & ZACHARIAS, D.A. (2001). Role of alternative splicing in generating isoform diversity among plasma membrane calcium pumps. *Physiol Rev*, **81**, 21-50.

STRUBING, C., KRAPIVINSKY, G., KRAPIVINSKY, L. & CLAPHAM, D.E. (2001). TRPC1 and TRPC5 form a novel cation channel in mammalian brain. *Neuron*, **29**, 645-55.

STUTZIN, A. & HOFFMANN, E.K. (2006). Swelling-activated ion channels: functional regulation in cell-swelling, proliferation and apoptosis. *Acta Physiol (Oxf)*, **187**, 27-42.

SUESSBRICH, H., SCHONHERR, R., HEINEMANN, S.H., ATTALI, B., LANG, F. & BUSCH, A.E. (1997). The inhibitory effect of the antipsychotic drug haloperidol on HERG potassium channels expressed in Xenopus oocytes. *Br J Pharmacol*, **120**, 968-74.

TAGAWA, N., TAMANAKA, J., FUJINAMI, A., KOBAYASHI, Y., TAKANO, T., FUKATA, S., KUMA, K., TADA, H. & AMINO, N. (2000). Serum dehydroepiandrosterone, dehydroepiandrosterone sulfate, and pregnenolone sulfate concentrations in patients with hyperthyroidism and hypothyroidism. *Clin Chem*, **46**, 523-8.

TAHA, T.A., MULLEN, T.D. & OBEID, L.M. (2006). A house divided: ceramide, sphingosine, and sphingosine-1-phosphate in programmed cell death. *Biochim Biophys Acta*, **1758**, 2027-36.

TAKAOKA, M., UEMURA, S., KAWATA, H., IMAGAWA, K., TAKEDA, Y., NAKATANI, K., NAYA, N., HORII, M., YAMANO, S., MIYAMOTO, Y., YOSHIMASA, Y. & SAITO, Y. (2006). Inflammatory response to acute myocardial infarction augments neointimal hyperplasia after vascular injury in a remote artery. *Arterioscler Thromb Vasc Biol*, **26**, 2083-9.

TALAVERA, K., YASUMATSU, K., VOETS, T., DROOGMANS, G., SHIGEMURA, N., NINOMIYA, Y., MARGOLSKEE, R.F. & NILIUS, B. (2005). Heat activation of TRPM5 underlies thermal sensitivity of sweet taste. *Nature*, **438**, 1022-5.

TANI, M., ITO, M. & IGARASHI, Y. (2007). Ceramide/sphingosine/sphingosine 1-phosphate metabolism on the cell surface and in the extracellular space. *Cell Signal*, **19**, 229-37.

TESFAI, Y., BRERETON, H.M. & BARRITT, G.J. (2001). A diacylglycerol-activated Ca^{2+} channel in PC12 cells (an adrenal chromaffin cell line) correlates with expression of the TRP-6 (transient receptor potential) protein. *Biochem J*, **358**, 717-26.

THASTRUP, O., DAWSON, A.P., SCHARFF, O., FODER, B., CULLEN, P.J., DROBAK, B.K., BJERRUM, P.J., CHRISTENSEN, S.B. & HANLEY, M.R. (1989). Thapsigargin, a novel molecular probe for studying intracellular calcium release and storage. *Agents Actions*, **27,** 17-23.

THUMMLER, S., DUPRAT, F. & LAZDUNSKI, M. (2007). Antipsychotics inhibit TREK but not TRAAK channels. *Biochem Biophys Res Commun*, **354,** 284-9.

TOGASHI, K., HARA, Y., TOMINAGA, T., HIGASHI, T., KONISHI, Y., MORI, Y. & TOMINAGA, M. (2006). TRPM2 activation by cyclic ADP-ribose at body temperature is involved in insulin secretion. *Embo J*, **25,** 1804-15.

TOMINAGA, M., CATERINA, M.J., MALMBERG, A.B., ROSEN, T.A., GILBERT, H., SKINNER, K., RAUMANN, B.E., BASBAUM, A.I. & JULIUS, D. (1998). The cloned capsaicin receptor integrates multiple pain-producing stimuli. *Neuron*, **21,** 531-43.

TSAVALER, L., SHAPERO, M.H., MORKOWSKI, S. & LAUS, R. (2001). Trp-p8, a novel prostate-specific gene, is up-regulated in prostate cancer and other malignancies and shares high homology with transient receptor potential calcium channel proteins. *Cancer Res*, **61,** 3760-9.

TSIOKAS, L., ARNOULD, T., ZHU, C., KIM, E., WALZ, G. & SUKHATME, V.P. (1999). Specific association of the gene product of PKD2 with the TRPC1 channel. *Proc Natl Acad Sci U S A*, **96,** 3934-9.

TURNER, N.A., O'REGAN, D.J., BALL, S.G. & PORTER, K.E. (2005). Simvastatin inhibits MMP-9 secretion from human saphenous vein smooth muscle cells by inhibiting the RhoA/ROCK pathway and reducing MMP-9 mRNA levels. *Faseb J*, **19,** 804-6.

UETA, K., SUZUKI, T., UCHIDA, I. & MASHIMO, T. (2004). In vitro inhibition of recombinant ligand-gated ion channels by high concentrations of milnacipran. *Psychopharmacology (Berl)*, **175,** 241-6.

ULLRICH, N.D., VOETS, T., PRENEN, J., VENNEKENS, R., TALAVERA, K., DROOGMANS, G. & NILIUS, B. (2005). Comparison of functional properties of the Ca^{2+}-activated cation channels TRPM4 and TRPM5 from mice. *Cell Calcium*, **37,** 267-78.

UPPU, R.M., NOSSAMAN, B.D., GRECO, A.J., FOKIN, A., MURTHY, S.N., FONSECA, V.A. & KADOWITZ, P.J. (2007). Cardiovascular effects of peroxynitrite. *Clin Exp Pharmacol Physiol*, **34,** 933-7.

VALENZANO, K.J., GRANT, E.R., WU, G., HACHICHA, M., SCHMID, L., TAFESSE, L., SUN, Q., ROTSHTEYN, Y., FRANCIS, J., LIMBERIS, J., MALIK, S., WHITTEMORE, E.R. & HODGES, D. (2003). N-(4-tertiarybutylphenyl)-4-(3-chloropyridin-2-yl)tetrahydropyrazine -1(2H)-carbox-amide (BCTC), a novel, orally effective vanilloid receptor 1 antagonist with analgesic properties: I. in vitro characterization and pharmacokinetic properties. *J Pharmacol Exp Ther*, **306,** 377-86.

VALLEE, M., MAYO, W., DARNAUDERY, M., CORPECHOT, C., YOUNG, J., KOEHL, M., LE MOAL, M., BAULIEU, E.E., ROBEL, P. & SIMON, H. (1997). Neurosteroids: deficient cognitive performance in aged rats depends on low pregnenolone sulfate levels in the hippocampus. *Proc Natl Acad Sci U S A*, **94,** 14865-70.

VAN BREEMEN, C., AARONSON, P. & LOUTZENHISER, R. (1978). Sodium-calcium interactions in mammalian smooth muscle. *Pharmacol Rev*, **30,** 167-208.

VANNIER, B., PEYTON, M., BOULAY, G., BROWN, D., QIN, N., JIANG, M., ZHU, X. & BIRNBAUMER, L. (1999). Mouse trp2, the homologue of the human trpc2 pseudogene, encodes mTrp2, a store depletion-activated capacitative Ca^{2+} entry channel. *Proc Natl Acad Sci U S A*, **96,** 2060-4.

VENKATACHALAM, K. & MONTELL, C. (2007). TRP channels. *Annu Rev Biochem*, **76,** 387-417.

VENKATACHALAM, K., ZHENG, F. & GILL, D.L. (2003). Regulation of canonical transient receptor potential (TRPC) channel function by diacylglycerol and protein kinase C. *J Biol Chem*, **278,** 29031-40.

VOETS, T., DROOGMANS, G., WISSENBACH, U., JANSSENS, A., FLOCKERZI, V. & NILIUS, B. (2004a). The principle of temperature-dependent gating in cold- and heat-sensitive TRP channels. *Nature*, **430,** 748-54.

VOETS, T., NILIUS, B., HOEFS, S., VAN DER KEMP, A.W., DROOGMANS, G., BINDELS, R.J. & HOENDEROP, J.G. (2004b). TRPM6 forms the Mg^{2+} influx channel involved in intestinal and renal Mg^{2+} absorption. *J Biol Chem*, **279,** 19-25.

WALDER, R.Y., LANDAU, D., MEYER, P., SHALEV, H., TSOLIA, M., BOROCHOWITZ, Z., BOETTGER, M.B., BECK, G.E., ENGLEHARDT, R.K., CARMI, R. & SHEFFIELD, V.C. (2002). Mutation of TRPM6 causes familial hypomagnesemia with secondary hypocalcemia. *Nat Genet*, **31,** 171-4.

WALKER, R.G., WILLINGHAM, A.T. & ZUKER, C.S. (2000). A Drosophila mechanosensory transduction channel. *Science*, **287,** 2229-34.

WALKER, R.L., HUME, J.R. & HOROWITZ, B. (2001). Differential expression and alternative splicing of TRP channel genes in smooth muscles. *Am J Physiol Cell Physiol*, **280,** C1184-92.

WALKER, R.L., KOH, S.D., SERGEANT, G.P., SANDERS, K.M. & HOROWITZ, B. (2002). TRPC4 currents have properties similar to the pacemaker current in interstitial cells of Cajal. *Am J Physiol Cell Physiol*, **283,** C1637-45.

WARDELL, B., MARIK, P.S., PIPER, D., RUTAR, T., JORGENSEN, E.M. & BAMBER, B.A. (2006). Residues in the first transmembrane domain of the Caenorhabditis elegans GABA(A) receptor confer sensitivity to the neurosteroid pregnenolone sulfate. *Br J Pharmacol*, **148,** 162-72.

WATANABE, H., DAVIS, J.B., SMART, D., JERMAN, J.C., SMITH, G.D., HAYES, P., VRIENS, J., CAIRNS, W., WISSENBACH, U., PRENEN, J., FLOCKERZI, V., DROOGMANS, G., BENHAM, C.D. & NILIUS, B. (2002). Activation of TRPV4 channels (hVRL-2/mTRP12) by phorbol derivatives. *J Biol Chem*, **277,** 13569-77.

WATANABE, H., VRIENS, J., PRENEN, J., DROOGMANS, G., VOETS, T. & NILIUS, B. (2003). Anandamide and arachidonic acid use epoxyeicosatrienoic acids to activate TRPV4 channels. **424,** 434-438.

WEHAGE, E., EISFELD, J., HEINER, I., JUNGLING, E., ZITT, C. & LUCKHOFF, A. (2002). Activation of the cation channel long transient receptor potential channel 2 (LTRPC2) by hydrogen peroxide. A splice variant reveals a mode of activation independent of ADP-ribose. *J Biol Chem*, **277,** 23150-6.

WEILL-ENGERER, S., DAVID, J.P., SAZDOVITCH, V., LIERE, P., EYCHENNE, B., PIANOS, A., SCHUMACHER, M., DELACOURTE, A., BAULIEU, E.E. & AKWA, Y. (2002). Neurosteroid quantification in human brain regions: comparison between Alzheimer's and nondemented patients. *J Clin Endocrinol Metab*, **87,** 5138-43.

WELSH, D.G., MORIELLI, A.D., NELSON, M.T. & BRAYDEN, J.E. (2002). Transient receptor potential channels regulate myogenic tone of resistance arteries. *Circ Res*, **90,** 248-50.

WILSON, P.W.F., D'AGOSTINO, R.B., LEVY, D., BELANGER, A.M., SILBERSHATZ, H. & KANNEL, W.B. (1998). Prediction of Coronary Heart Disease Using Risk Factor Categories. *Circulation*, **97,** 1837-1847.

WISSENBACH, U., NIEMEYER, B., HIMMERKUS, N., FIXEMER, T., BONKHOFF, H. & FLOCKERZI, V. (2004). TRPV6 and prostate cancer: cancer growth beyond the

prostate correlates with increased TRPV6 Ca^{2+} channel expression. *Biochem Biophys Res Commun*, **322,** 1359-63.

WU, S.N., JAN, C.R. & LI, H.F. (1999). Ruthenium red-mediated inhibition of large-conductance Ca^{2+}-activated K^+ channels in rat pituitary GH3 cells. *J Pharmacol Exp Ther*, **290,** 998-1005.

WU, X. & DAVIS, M.J. (2001). Characterization of stretch-activated cation current in coronary smooth muscle cells. *Am J Physiol Heart Circ Physiol*, **280,** H1751-61.

XU, S.Z. & BEECH, D.J. (2001). TrpC1 is a membrane-spanning subunit of store-operated $Ca(^{2+})$ channels in native vascular smooth muscle cells. *Circ Res*, **88,** 84-7.

XU, S.-Z., BOULAY, G., FLEMMING, R. & BEECH, D.J. (2006a). E3-targeted anti-TRPC5 antibody inhibits store-operated calcium entry in freshly isolated pial arterioles. *Am J Physiol Heart Circ Physiol*, **291,** H2653-2659.

XU, S.Z., MURAKI, K., ZENG, F., LI, J., SUKUMAR, P., SHAH, S., DEDMAN, A.M., FLEMMING, P.K., MCHUGH, D., NAYLOR, J., CHEONG, A., BATESON, A.N., MUNSCH, C.M., PORTER, K.E. & BEECH, D.J. (2006b). A sphingosine-1-phosphate-activated calcium channel controlling vascular smooth muscle cell motility. *Circ Res*, **98,** 1381-9.

XU, S.Z., ZENG, F., BOULAY, G., GRIMM, C., HARTENECK, C. & BEECH, D.J. (2005a). Block of TRPC5 channels by 2-aminoethoxydiphenyl borate: a differential, extracellular and voltage-dependent effect. *Br J Pharmacol*, **145,** 405-14.

XU, S.Z., ZENG, F., LEI, M., LI, J., GAO, B., XIONG, C., SIVAPRASADARAO, A. & BEECH, D.J. (2005b). Generation of functional ion-channel tools by E3 targeting. *Nat Biotechnol*, **23,** 1289-93.

YAMAMOTO, K., SOKABE, T., MATSUMOTO, T., YOSHIMURA, K., SHIBATA, M., OHURA, N., FUKUDA, T., SATO, T., SEKINE, K., KATO, S., ISSHIKI, M., FUJITA, T., KOBAYASHI, M., KAWAMURA, K., MASUDA, H., KAMIYA, A. & ANDO, J. (2006). Impaired flow-dependent control of vascular tone and remodeling in P2X4-deficient mice. *Nat Med*, **12,** 133-7.

YANG, X.R., LIN, M.J., MCINTOSH, L.S. & SHAM, J.S. (2006). Functional expression of transient receptor potential melastatin- and vanilloid-related channels in pulmonary arterial and aortic smooth muscle. *Am J Physiol Lung Cell Mol Physiol*, **290,** L1267-76.

ZAMPETAKI, A., ZHANG, Z., HU, Y. & XU, Q. (2005). Biomechanical stress induces IL-6 expression in smooth muscle cells via Ras/Rac1-p38 MAPK-NF-kappaB signaling pathways. *Am J Physiol Heart Circ Physiol*, **288,** H2946-54.

ZENG, F., XU, S.Z., JACKSON, P.K., MCHUGH, D., KUMAR, B., FOUNTAIN, S.J. & BEECH, D.J. (2004). Human TRPC5 channel activated by a multiplicity of signals in a single cell. *J Physiol*, **559,** 739-50.

ZHANG, F. & LI, P.L. (2007). Reconstitution and characterization of a nicotinic acid adenine dinucleotide phosphate (NAADP)-sensitive Ca^{2+} release channel from liver lysosomes of rats. *J Biol Chem*, **282,** 25259-69.

ZHANG, H. & CUEVAS, J. (2002). Sigma receptors inhibit high-voltage-activated calcium channels in rat sympathetic and parasympathetic neurons. *J Neurophysiol*, **87,** 2867-79.

ZHANG, S., REMILLARD, C.V., FANTOZZI, I. & YUAN, J.X. (2004). ATP-induced mitogenesis is mediated by cyclic AMP response element-binding protein-enhanced TRPC4 expression and activity in human pulmonary artery smooth muscle cells. *Am J Physiol Cell Physiol*, **287,** C1192-201.

ZHOU, B.Y., MA, W. & HUANG, X.Y. (1998). Specific antibodies to the external vestibule of voltage-gated potassium channels block current. *J Gen Physiol*, **111,** 555-63.

ZHU, M.X. (2005). Multiple roles of calmodulin and other $Ca(^{2+})$-binding proteins in the functional regulation of TRP channels. *Pflugers Arch*, **451,** 105-15.